JUSTUS-LIEBIG-UNIVERSITÄT GIESSEN

JUSTUS-LIEBIG-UNIVERSITY GIESSEN

Development of a Mobile High-Resolution Multiple-Reflection Time-of-Flight Mass Spectrometer for In-situ Life Science Application

Inauguraldissertation zur Erlangung des Doktorgrades Dr. rer. nat. der Naturwissenschaftlichen Fakultät der Justus-Liebig-Universität Gießen

Johannes Sebastian LANG
born in Lauterbach

June, 2016

For The Little and Happy Ones

Reviewers and Examinants

Prof. Dr. Christoph SCHEIDENBERGER
Justus-Liebig-University Giessen, GSI Helmholtzzentrum für Schwerionenforschung
Prof. Dr. Dr. h.c. Hans GEISSEL
Justus-Liebig-University Giessen, GSI Helmholtzzentrum für Schwerionenforschung
Prof. Dr. Zoltán TAKÁTS
Imperial Collage London
Priv.-Doz. Dr. Sophia HEINZ
Justus-Liebig-University Giessen, GSI Helmholtzzentrum für Schwerionenforschung
Prof. Dr. Werner SCHEID
Justus-Liebig-University Giessen

Abstract

A compact and mobile high resolution and high accuracy Mutliple-Reflection Time-of-Flight Mass Spectrometer (MR-TOF-MS) has been designed, built, commissioned and characterized. A new method delivers the capability for isobar separation and is a prerequisite for possible subsequent mass measurements (MS^N) in future experiments. This work gives an introduction to the theoretical principles of high performance and in-situ mass spectrometry and describes the whole building chain of a powerful instrument – that has its origin in nuclear physics – and now features the application in in-situ analytics and in life science with high analytical value on a mobile platform.

The wide field of mass spectrometry offers complex and stationary instruments with outstanding performance (mass resolving power $R_m > 100000$, mass accuracy $\delta m/m < 1$ ppm) on one hand and portable, less powerful devices for in-situ investigation on the other hand. The concept of MR-TOF-MS offers high mass spectrometric performance in a compact and robust concept, offering high mass resolving power, high mass accuracy, short measurement cycles and lowest infrastructural needs. The MR-TOF-MS of this work has been designed with the goal to build a device, which combines the aspects of high performance and field deployment. It is capable of application in fundamental sciences for precision measurements, as well as for various life science analytics that can be performed directly at the investigation site. The mass resolving power of $R_m > 300000$ is independent on mass and enables the resolution of isobars and isotopes at even high molecular mass. The mass accuracy of $\delta m/m < 1$ ppm allows to determine the composition and structure of biomolecules. Time-dependent studies such as chromatography and high throughput measurements are supported by a repetition rate of up to 2000 Hz. A new method for a highly mass-resolved separation with a resolution of $R_s > 60000$ may enable distinct precursor selection for tandem experiments and fragmentation studies in future, as well as the removal of isobaric contaminants in nuclear physics experiments.

The mass spectrometer itself relies on an effective combination of radio frequency quadrupoles and a multiple-reflection time-of-flight analyzer. Ion optics and system supply have been shaped into a rugged and transportable format. An atmospheric pressure interface offers great flexibility in the choice of the ion source and provides an essential in-situ aspect. Most components are custom-made and specially developed. This prototype instrument is ruggedized, reliable, stable in operation with a start-up time of 20 min only and therefore ideally suited for in-situ application like in the field of medicine, civil safety and environmental research. There is no need for further infrastructure.

Zusammenfassung

Ein kompaktes, mobiles hochauflösendes und hochgenaues Multireflexions Flugzeit Massenspektrometer (MR-TOF-MS) wurde entworfen, konstruiert, gebaut, in Betrieb genommen und charakterisiert. Eine neue Methode eröffnet die Möglichkeit zur Isobaren Separation und ist ein Grundstein für etwaige nachlaufende Massenmessung (MS^N) in künftigen Experimenten. Diese Arbeit gibt eine Einführung in die theoretischen Grundlagen eines leistungsstarken Massenspektrometers, dessen Ursprung in der Kernphysik liegt. Es ermöglicht den Einsatz in Vor-Ort-Analytik und in in Lebenswissenschaften durch hohe analytische Aussagekraft auf mobiler Basis.

Es gibt Massenspektrometer mit höchstem Massenauflösungsvermögen ($R_m > 100000$) und präziser Massenbestimmung ($\delta m/m < 1\,$ppm). Diese sind jedoch sehr gross, empfindlich und laborgebunden. Existierende portable Instrumente für Vor-Ort Analysen haben im Gegenzug ein eingeschränktes Leistungsvermögen. Die Idee eines Multireflexions-Flugzeit-Massenspektrometers erlaubt einen kompakten und robusten Aufbau mit enormer Massenauflösung und Massengenauigkeiten, kurzen Analysezeiten und geringsten Anforderungen an benötigte Infrastruktur. Das Gerät dieser Arbeit wurde entwickelt um Hochleistungs-Massenspektrometrie und Feldtauglichkeit zu kombinieren. Es ermöglicht den Einsatz in der Grundlagenforschung mit hochgenauer Massenmessung und vielfältige Anwendung in Vor-Ort Analysen der Lebenswissenschaften. Das erreichte Massenauflösungsvermögen von $R_m > 300000$ ist massenunabhängig und erlaubt es, isobare und isotope Moleküle mit hohen Massen zu unterscheiden. Die Massengenauigkeit von $\delta m/m < 1\,$ppm erlaubt die Bestimmung von Zusammensetzung und Struktur von Biomolekülen. Die Kombination mit zeitabhängigen Methoden wie Chromatographie und Messungen mit hohem Durchsatz sind durch eine hohe Repetitionsrate von bis zu $2000\,$Hz gewährleistet. Eine neue Mehtode zur hoch massenaufgelösten Separation ($R_s > 60000$) von beliebigen Ionenspezies kann künftig exakt ausgewählte Vorläufer-Ionen für Tandem Experimente und Fragmentations Untersuchungen liefern, sowie die Unterdrückung von isobaren Kontaminationen bei kernphysikalischen Experimenten ermöglichen.

Das Massenspektrometer beruht auf der nachhaltigen Kombination von Radiofrequenz Quadrupolen und einem Multireflexions-Flugzeit-Analysator. Die Ionenoptik und alle benötigten Systemkomponenten sind in einen robusten und transportablen Rahmen eingebaut. Ein atmosphärisches Einlasssytem stellt die Kopplung mit verschiedenstartigen Ionenquellen sicher und ist wesentlicher Bestandteil der Vor-Ort Analyse Möglichkeit. Die speziellen Komponenten sind eigens entwickelt und gefertigt. Dieses Prototyp-Instrument ist robust ausgelegt, zuverlässig, mit stabiler Messgenauigkeit und einer vollständigen Einsatzbereitschaft nach schon $20\,$min und somit ideal geeignet für Vor-Ort Analysen in Bereichen wie Medizin, ziviler Sicherheit und Umweltforschung. Eine zusätzliche Infrastruktur ist dabei nicht von Nöten.

Contents

1. Introduction

Mass spectrometry was founded a hundred years ago [Thomson, 1913] – it led to the discovery of isotopes and enabled various fundamental studies [Blaum and Litvinov, 2013]. It is an analytical tool to measure the mass of elements, molecules and particles. This is achieved by separation of individual masses-to-charge ratios in space or in time [Münzenberg, 2013]. Many types of Mass Spectrometry (MS) have been developed during years. Each has special features and limits – often dedicated for special application. Mass spectrometers instruments range from storage rings at accelerator facilities for relativistic ions [Bosch and Litvinov, 2013], dedicated accelerators [Kutschera, 2013], precision experiments of exotic nuclei [Ringle et al., 2013], mobile and hand-held instruments for analytical applications [Ouyang, 2014] and mass spectrometers in a mirco-chip format [Syms, 2016].

The targeted mass ranges from those of elementary particles to those of complex biomolecules (see figure 1.1).
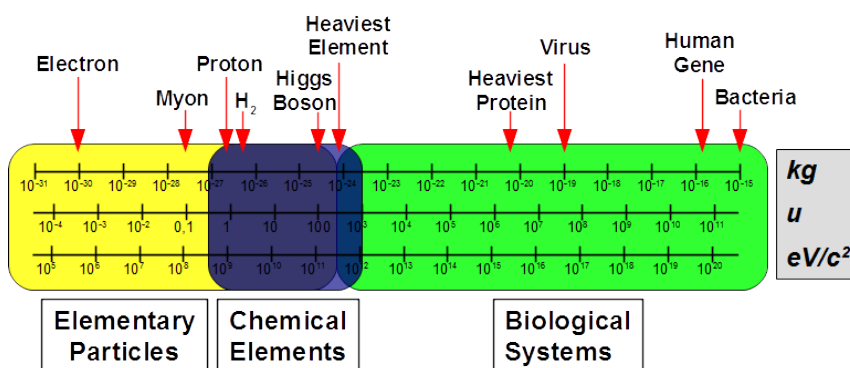
Figure 1.1.: Relevant mass scales of subjects to mass spectrometry: mass regions of elementary particles, of chemical elements and of molecular and biological systems. Depending on the field of application the masses can be expressed in units kg, u or eV/c^2.

The mass measurement – depending on its accuracy – can be used to determine the constituents and the formation of investigated species or to allow the identification and quantification of complex samples. The mass gives information on the binding energies B of a nucleus [Weizsäcker, 1935], an atom or molecule, as the mass-energy-equivalence $E = mc^2$ imposes [Cakirli and Casten, 2013].

For the mass of a nucleon m_{nuc}, the mass of an atom m_{atom} and the mass of a molecule m_{mol} follows:

$$m_{nuc} = N \cdot m_n + Z \cdot m_p - \frac{B_{nuc}}{c^2}$$
$$m_{atom} = m_{nuc} + Z \cdot m_e - \frac{B_{atom}}{c^2}$$
$$m_{mol} = \sum X_i m_{atom_i} - \frac{B_{mol}}{c^2}$$

with the neutron number N and mass m_N of neutrons, the atomic number (proton number) Z and mass m_p of protons, the mass of an electron m_e, as well as the amount of different atoms X_i.

Mass Spectrometry is a widely used technique in various fields from laboratory environment to in-situ locations and is a stand-alone analytical technique. Further, it is often combined with complementary techniques to increase analytic information, for selective experiments or as reference measurement [Turner et al., 2015, Chouinard et al., 2016, Strathmann and Hoofnagle, 2011].

Mass Spectrometry has become an indispensable tool in science and routine applications. Unfortunately, there is a discrepancy between high mass spectrometric performance and in-situ ability. The multiple-reflection time-of-flight mass spectrometer of this work is bridging this gap by providing highest mass resolution and accuracy and potential MS/MS capability on a mobile and robust platform.

2. Mass Spectrometric Basis

This chapter introduces to the basics of mass spectrometry related to this work. The physical foundation, general mass spectrometric techniques, ion generation, different approaches of high performance and in-situ mass spectrometers and the fields of application are explained.

The compartments of functionality of any mass spectrometer are depicted in figure 2.1. The sample or the analytes of interest needs to be fed into the vacuum vessel of the mass spectrometer. This may be done with or without preceding sample preparation. The atoms and molecules of interest have to be ionized for the investigation by the mass analyzer. A detection technique then delivers information to the data acquisition. Computation of the raw data finally delivers a mass spectrum.
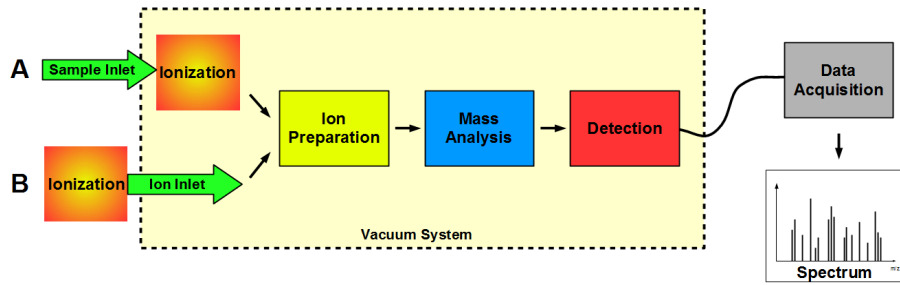
Figure 2.1.: What all mass spectrometers have in common: inlet and ionization (in order A or B), mass analyzer, detection, data acquisition and the resulting mass spectrum.

2.1. Parameters in Mass Spectrometry

Mass Resolving Power

The mass resolving power tells what fraction Δm of a given mass m of an atom or molecule can be resolved into an individual signal:

$$\text{Mass Resolving Power } R_m := \frac{m}{\Delta m} \left(= \frac{\frac{m}{Q}}{\Delta \frac{m}{Q}} \right). \tag{2.1}$$

In fact, the mass-to-charge ratio is considered, since mass spectrometers rely on the manipulation of ions. The according width of the signal for a definite mass resolution is commonly chosen as Full Width Half Maximum (FWHM). Values of typical mass resolving power range from some tenths to few 10^6. For masses with differing intensities A the resolving power drops, as the example of two neighboring masses with uneven intensity illustrates in figure 2.2.
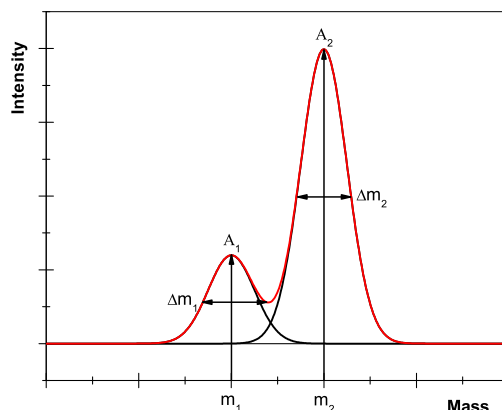
Figure 2.2.: Two mass signals with uneven intensity A_1 and A_2 resolved at FWHM; the width Δm_1 of the smaller signal of mass m_1 is close to the bottom of the more intense signal of mass m_2 and is barely resolved, since the width of m_2 at the half amplitude of m_1 is much broader than its FWHM Δm_2.

Mass Accuracy

The accuracy of a mass measurement is given by:

$$\text{Mass Accuracy } \frac{\delta m}{m} := \frac{m_{exp} - m_{lit}}{m_{exp}}. \tag{2.2}$$

This represents the deviation from the experimental value m_{exp} obtained to an accurate and preferably well-known mass literature value m_{lit} scaled by the measured mass m_{exp}. The higher the accuracy, the better a chemical composition or even an inner excitation state may be clearly identified. Common accuracy numbers range from single integer values to 10^{-9}. Mass accuracy below the ppm level can be considered as threshold for many high performance application [Liu et al., 2009].

Sensitivity

Sensitivity of a mass spectrometer either refers to an absolute amount of the desired species in mole or gram, or it refers to a necessary concentration in a sample, such as mol/l or similar. Sensitivity is reduced when contaminants are present in a sample and lead to misidentification or cross-response. A limit of sensitivity is an accurate measurement with only a single ion – referred to as single ion sensitivity. The sensitivity is closely related to the transmission factor for ions when passing the instrument, which is itself composed of the product of individual transmissions of the subsystems:

$$\text{Transmission} := \eta_{\text{total}} = \eta_{\text{sub}_1} \cdot \eta_{\text{sub}_2} \cdots . \tag{2.3}$$

The sensitivity may be defined by the product of the ion source efficiency, the transmission through single mass spectrometer stages and the efficiency of detection and connected data acquisition. The sensitivity is also related to the duty cycle – the proportion of time when the instrument or the subsystems are operated and accumulate ions for measurement. During the status of not accepting ions (e.g. recovery phase, blocked system during ongoing measurement, dead time,...) the incoming ions may be skipped and the overall sensitivity may be decreased.

Mass Range

The range of mass an MS can measure at the same time is usually restricted. The mass range is the span of mass that is covered within one single spectrum. With scanning mode one may cover a larger mass range by subsequent measurements of individual mass slots and integration of them into a single spectrum. Generally the mass range refers to a single measurement and can be defined as the ratio between the maximal mass m_{max} and the minimal mass m_{min} that is considered:

$$\text{Mass Range} := \frac{m_{max}}{m_{min}}. \tag{2.4}$$

The mass range can be principally limited by either light and/or heavy masses and may also be used to tell the absolute regime of mass that can be processed, e.g. from lighter elements to very heavy biomelecules. Absolute values of measured masses start from those of elementary particles to those of ultra-large molecules with $m > 10^6$u.

Selectivity and Specificity

Analytical selectivity expresses how good a certain species can be selected and measured among others – without any disturbance stemming from them. Specificity is a measure how good and reliable such a selection is and can be treated by statistical means.

Speed of Analysis

The speed of analysis describes how fast measurements can be done. Often, this is related to the time for measuring a certain span of mass. That is why it is also called scan speed – expressed in u/s. In case of non-scanning mass spectrometers the masses of the whole range can be covered simultaneously. Oftentimes the repetition rate of the system in s^{-1} is of interest.

Separation Power

Some mass spectrometers rely on the separation of mass species. The capability of choosing only a selected range of m/Q ratio or even single species of mass for further experiments is determined by the separation power, which may be defined similar to mass resolving power by

$$\text{Mass Separation Power } R_s := \frac{m}{\Delta m}, \tag{2.5}$$

which expresses the proportion Δm of a given mass m that can be separated or isolated. The maximal separation power offered by current instruments is in the order of few 10^4.

2.2. Physical Background

All mass spectrometers rely on fundamental physical phenomena. A constricted assortment of explanations focused on the methods used in this work is presented. A proper knowledge of these fundamentals enables a reasonable design and helps in commissioning an instrument.

2.2.1. Ion Movement in Radio Frequency Fields

The instrument in this work heavily relies on Radio Frequency (RF) quadrupoles and their quite universal capability of handling of ions. This has been decisively described by [Dawson, 1976] and is also found in [March and Todd, 2005]. An introduction is given below – with the intellectual approach predominantly based on the text book [Yavor, 2009], which is also suggested for further reading.

2.2.1.1. Multipole Field

To understand and describe the behavior of charged particles in RF fields, the field formation is important. A general multipole potential of order m in a 2D plane with unlimited depth in the z-direction can be expressed in cylindrical coordinates ($r = \sqrt{x^2 + y^2}, \varphi = \arctan(y/x)$) as

$$U_m(r, \varphi) = V_m \left(\frac{r}{r_0} \right)^m \cos\left[m\left(\varphi - \varphi_0 \right) \right] \tag{2.6}$$

with the inner radius r_0 between electrodes and φ as the azimuthal angle.

The order of $m = 2$ for a quadrupolar field results in

$$U_2(r, \varphi) = V_2 \left(\frac{r}{r_0} \right)^2 \cos(2\varphi) = V_2 \frac{x^2 + y^2}{r_0^2} \tag{2.7}$$

with constant $\varphi_0 = 0$. Such an ideal quadrupole field is possible only with exact hyperbolic electrode shapes. Cylindrical electrode rods are much easier to produce and are commonly used - taking into account their higher order field distribution. To mimic a similar character of the hyperbolic shape, it is recommended to use a cylindrical rod diameter of $r_c = 1.14511 r_0$ and a cylindrical shield electrode on ground potential at $4r_0$ [Reuben et al., 1996].

2.2.1.2. Ion Movement in RF Pseudopotential

To get a handle on movement of charged particles in an RF field – here emphasized on quadrupole arrangement – the following considerations are widely in use.
Applying the Lorentz equation for a 1D RF electric field $E(x,t) = \hat{E}\cos(\omega t + \varphi)$ with radio frequency $\omega = f_{RF}/2\pi$ and expressing a Taylor expansion of the same as $\hat{E} = \hat{E}(0) + \hat{E}'(0)x + \dots$ with $\hat{E}' = d\hat{E}/dx$ provides the equation of motion

$$m\ddot{x} = Q\{\hat{E}(0) + \hat{E}'(0)x + \dots\}\cos(\omega t + \varphi). \tag{2.8}$$

This can be solved by successive approximation for $x^{(i)}$ corresponding to single Taylor orders i. With this solution (with neglected average velocity $\bar{v}$ during one RF period) and small steps in x, equation 2.8 can be written as

$$m\ddot{x} \approx m\ddot{x}^{(1)} + m\ddot{x}^{(2)} \tag{2.9}$$

$$\approx Q\hat{E}(0)\cos(\omega t + \varphi) - \frac{Q^2\hat{E}'(0)\hat{E}}{m\omega^2}\cos(\omega t + \varphi)\left[\cos(\omega t + \varphi) - \cos\varphi\right]. \tag{2.10}$$

This force results in

$$\bar{F} = -\frac{Q^2}{4m\omega^2}\left(\frac{d\hat{E}^2}{dx}\right)_{x=0} \tag{2.11}$$

averaged over one RF period. This force can be considered as created by a so-called pseudopotential

$$U^{(ps)} = \frac{Q\hat{E}^2}{4m\omega^2} \tag{2.12}$$

and

$$U^{(ps)}(\mathbf{r}) = \frac{Q\hat{\mathbf{E}}^2(\mathbf{r})}{4m\omega^2} \tag{2.13}$$

in the more general 3D case. The particle motion averaged over the RF period amounts to the so-called secular motion and presents the motion in the pseudo potential. This holds true only if the secular motion is slow compared to the direct RF oscillation of the particle [Miller, 1958, Dehmelt, 1967]. $QU^{(ps)}$ is always positive and is directed from higher to lower field amplitude region. This allows the confinement of positive and/or negative charged particles in two or three dimensions. The adjustment of the pseudopotential for the application depends on the the mass-to-charge ratio of the particle, the amplitude of electric field and the frequency. This adjustment for a given mass is limited by too low frequencies (where ions may escape before confined) or too high amplitudes (where ions are dragged towards the electrodes within a single cycle).
With the quadrupolar field distribution (2.7) of the RF signal and $r^2 = x^2 + y^2$, the field strength reads

$$\hat{\mathbf{E}}^2 = \hat{E}_x^2 + \hat{E}_y^2 = \frac{4V^2}{r_0^2}\left(\frac{r^2}{r_0^2}\right). \tag{2.14}$$

Thus, the pseudopotential for the quadrupolar RF field can be written as

$$U_q^{ps}(r) = \frac{QV^2}{m\omega^2 r_0^2}\left(\frac{r^2}{r_0^2}\right).$$

(2.15)

Finally, the x- and y-coordinate of particle motion in a quadrupolar pseudopotential field can be written as

$$x = x_0\cos(\Omega t) + (\dot{x}_0/\Omega)\sin(\Omega t)$$

(2.16)

$$y = y_0\cos(\Omega t) + (\dot{y}_0/\Omega)\sin(\Omega t)$$

(2.17)

with Ω as the angular frequency of the secular motion

$$\Omega = \frac{\sqrt{2}QV}{m\omega_0^2}.$$

(2.18)

Since trajectories are only stable for a certain set of parameters, the Mathieu parameters [Dawson, 1976] turned out quite useful to describe the particle motion in a pure RF field with

$$\frac{d^2x}{d\eta^2} + 2q\cos(2\eta)x = 0$$

(2.19)

$$\frac{d^2x}{d\eta^2} + 2q\cos(2\eta)x = 0.$$

(2.20)

where $\eta = \omega t/2$ is the scaled time parameter and q the stability parameter

$$q = \frac{4QV}{m\omega^2 r_0^2}.$$

(2.21)

Equations 2.19 and 2.20 are independent and belong to the class of Mathieu differential equations. Solutions for those do exist [McLachlan, 1947] and are stable for an infinite number of stability zones, where the particle is confined in the RF field. The first and commonly used zone is given by $0 < q < q_c$ with $q_c \approx 0.908$ as the low mass cut-off where the mass-to-charge ratio becomes too small to confine the ion.

The pseudopotential (section 2.15) can be expressed using q as

$$U_q^{(ps)}(r) = \frac{qV}{4}\left(\frac{r^2}{r_0^2}\right).$$

(2.22)

and the angular frequency as

$$\Omega = \frac{q}{2\sqrt{2}}\omega.$$

(2.23)

2.2.1.3. Buffer Gas Cooling

Neutral gas inside ion traps leads to collisions between the neutral gas and desired charged particles, which results in a gradual loss of energy. This can be applied for a systematic kinetic energy

damping and spatial shrinking of ion clouds [Dehmelt, 1967, Douglas et al., 2005, Stafford et al., 1984]. The process can be simply referred to as collisional ion cooling.

In an ideal gas the ion tends to reach thermodynamic equilibrium with the gas. The components v_i of particle velocity is then given by a normal distribution and the probability density $F(v_i)$

$$f(v_i) = \sqrt{\frac{m}{2\pi k_B T}} \exp\left(-\frac{mv_i^2}{2kT}\right) \tag{2.24}$$

with k_B the Boltzmann constant and the temperature T. The absolute velocity is given by the Maxwell-Boltzmann law

$$f(x) = 4\pi \left(\frac{m}{2\pi kT}\right)^{2/3} v^2 \exp\left(\frac{m\omega^2}{2KT}\right) \tag{2.25}$$

and the kinetic energy distribution with $< K > = (3/2)kT$ by

$$f(K) = \sqrt{\frac{K}{\pi(kT)^3}} \exp\left(-\frac{K}{kT}\right). \tag{2.26}$$

Ions in reasonable pressure cooling gas – without any applied RF field – follow the equilibrium energy distribution of 2.26. However, in an RF field, a certain energy is always fed into the thermalized ion cloud by the RF driving force. This depends on the phase in which a dampening collision occurs and on the mass of the particle (or rather its particular q-value). Particles close to the cut-off mass are heated much stronger, as intuitively expected. For lower masses the energy of the secular motion can be assumed close to the kinetic energy of the cooling gas, like a secular motion cooled to thermal equilibrium.

A dependence on the neutral gas mass compared to the charged particle mass is obvious; when the the cooling gas becomes comparable or even larger, the single-collision energy transfer becomes bigger and raises the average kinetic energy of the ions.

The lower the pressure, the lower the rate of collisions and the longer the time for the same cooling effect. On the other hand, too high pressure relativists the confining force of the pseudopotential. As a side effect it also requires stronger pumping for higher vacuum regions and causes unwanted collisions of higher energetic ion clouds that pass into regions without buffer gas.

2.2.1.4. Transport and Storage

In many mass spectrometers ions are stored and transported within RF structures. Very common are linear structures of a Radio Frequency Quadrupole (RFQ). The validity of the introduced model of pseudopotential drops for pressures higher than $100 \, \text{mbar}$, since the RF driving force has to dominate the gas collisions. Transmission at higher pressures does work with a slightly different behavior. An RF confinement is also present in e.g. an atmospheric pressure interface and stopping cells. Typical structures are multiple electrode arrangements [Dodonov et al., 1997], stacked-ring arrangements (e.g. ion funnels) [Kim et al., 2000, Ibrahim et al., 2006] and RF carpets [Bollen, 2004, Schwarz et al., 2003, Wada et al., 2003]. To transport ions along the beam direction, in general an additional axial electrostatic field is required. Common approaches for RFQs are shown in figure 2.3, with single segmented RFQs, an inclined additional electrode or RFQ rods from resistive material with an applied potential gradient [Takamine et al., 2007].
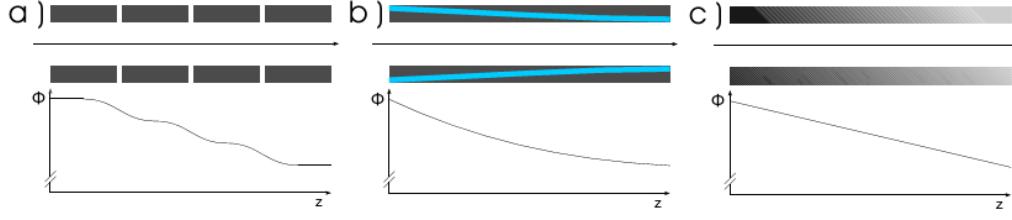
Figure 2.3.: Illustration of on-axis linear potential gradient of a) a segmented RFQ, b) a Linac RFQ and c) an RFQ made from resistive material. [Becker et al., 2009]

A qualitative theory of the ion confinement at an intermediate pressure regime uses a model of quasi-continuous viscous matter [Tolmachev et al., 1997]. The averaged change of velocity in x-direction by isotropic ion collision can be calculated to

$$< \Delta v_x > = -\frac{M}{m+M} v_x.$$ (2.27)

Treating the buffer gas as quasi-continuous viscous matter, the average variation per unit time can be expressed as

$$\frac{dv_x}{dt} = -\frac{v_x}{\tau}$$ (2.28)

with $\tau = m\tilde{\tau}/\mu$ as characteristic damping time and $\tilde{\tau}$ the mean time between collisions. With an electric field in x-direction the equation of motion becomes

$$\ddot{x} + \frac{\dot{x}}{\tau} = \frac{1}{m}QE_x(x,t).$$ (2.29)

With the polarization model (Langevin) the damping constant is not depended on velocity, thus, with $\tilde{\tau} = \bar{\tau} = \text{const}$ presenting

$$\tau = \sqrt{\frac{\varepsilon_0}{\pi}} \frac{m}{nQ\sqrt{\alpha\mu}}.$$ (2.30)

In the case of regular motion in an constant electric field the time constant 2.30 describes the general ion mobility law $v = \kappa E$ with the mobility coefficient

$$\kappa = \sqrt{\frac{\varepsilon_0}{\pi}} \frac{1}{n\sqrt{\alpha\mu}}.$$ (2.31)

2.2.1.5. Mass Analyzing

Time-varying fields can make trajectories depending on particles mass-to-charge ratio. An elegant and common way is the exertion of quadrupole mass filtering with RF fields as proposed by [Paul and Steinwedel, 1953].

RFQs create a rotational symmetric pseudopotential well along their linear axis (see equation 2.15). With a given geometry, the confinement is lower for an increasing mass. Ions follow an harmonic

oscillation (secular motion) superimposed by RF oscillation of smaller amplitudes. The secular frequency needs to be lower than the RF frequency for stable trajectories. The lower the mass is, the steeper is the pseudopotential and the higher the is secular motion. Up to the low mass cutoff, where the RF transfers too much energy into the secular motion creating a resonance instability. With a superposition of RF and an additional DC quadrupole field

$$U(x,y,t) = \frac{x^2 - y^2}{r_0^2}\left[V_0\cos(\omega t) + U_0\right] \tag{2.32}$$

a potential hill in the x-direction and a potential well in the y-direction for positively charged particles is set up. Each increases and decreases respectively the confinement in addition to the pure RF pseudopotential. The steeper potential in x-direction lifts the secular frequency, thus shifting the resonance instability to higher mass. In the y-direction the counteracting of DC potential and RF pseudopotential shifts the vanishing confinement to comparably lower mass. That means by applying a DC field the transmitted mass is limited from both, lower and higher side.

Ions positioned exactly at $x = 0$ and $y = 0$ experience no net confinement nor force. That is why many RF cycles are needed to increase their radii, so that the filtering for unstable trajectories is established. This is taken into account for a certain mass resolution (see 2.1). The number of required RF cycles n for a desired mass resolution R_m is given by [Paul et al., 1958] as

$$n \geq 3.5\sqrt{R_m}. \tag{2.33}$$

The number of cycles experienced by an ion depends on the length of the system L, the kinetic energy in z-direction E_{kin}^z and the RF frequency $\omega = 2\pi f$:

$$n = t \cdot f = \frac{L}{v_z} \cdot f = \frac{Lf}{\sqrt{\frac{2E_{kin}^z}{m}}}. \tag{2.34}$$

The mass resolving power can therefore be written as:

$$R_m \leq \frac{\omega^2 L^2 m}{98\pi^2 E_{kin}^z}. \tag{2.35}$$

Note that the resolving power is limited by geometrical misalignment, field imperfections of any kind and unstable or distorted RF amplitudes.

The ion motion can be calculated similar to those in section 2.2.1.4 by solution of the Mathieu equation [McLachlan, 1947] and setting up the equations of motion with $\eta = \omega t/2$

$$\ddot{x} + [a + 2q\cos(2\eta)]x = 0 \tag{2.36}$$
$$\ddot{y} + [a + 2q\cos(2\eta)]y = 0 \tag{2.37}$$

where $\ddot{x} = \frac{d^2x}{d\eta^2}$. The parameters (similar as in section 2.2.1.2)

$$a = \frac{8QU_0}{m\omega^2 r_0^2} \tag{2.38}$$

$$q = \frac{4QV_0}{m\omega^2 r_0^2} \tag{2.39}$$

are here expressed for a mass analyzing mode. The solutions can be stable, depending on the parameters a and q. A parameter $\beta(a,b)$ can be defined and approximated for small q-values ($q < 0,4$) to

$$\beta \approx \sqrt{a + \frac{q^2}{2}}. \tag{2.40}$$

Solutions are stable for a real and not imaginary β. For stability in both direction, the intersection region of stable solution for a and q is required. An infinite number of solutions exist, quite often the first zone closest to $a = q = 0$ is chosen for instrument operation (see figure 2.4). Its apex and
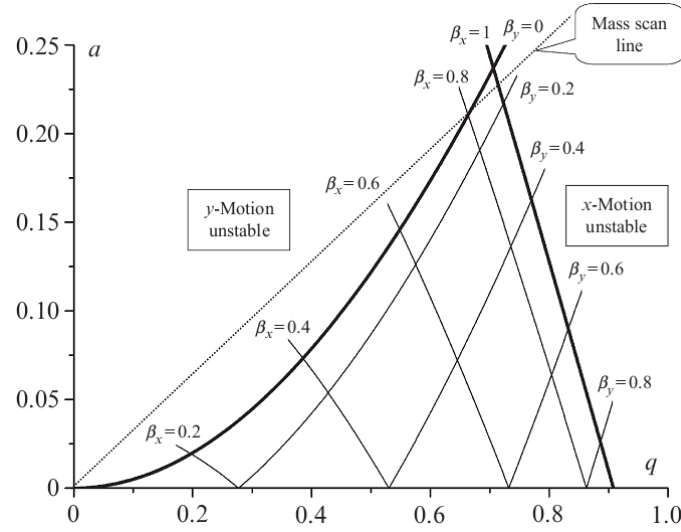

Figure 2.4.: First stability zone with equilines of the parameters β_x, β_y and mass scan line [Yavor, 2009].

point of best R_m corresponds to $\beta_x = \beta(a,q) = 1, \beta_y = \beta(-a,-q) = \beta(-a,q) = 0$ and is located at $a \approx 0.23699, q \approx 0.706$.

With fixed frequency and amplitudes, different masses describe a mass scan line passing through $q = a = 0$ with an inclination of $\tan(\lambda) = a/q = 2U_0/V_0$. Heavier masses are the ones closer to the origin. For fixed λ only masses at the intersection of mass scan line and stability region are transmitted. Highest R_m is observed with a tiny intersection in the apex vicinity with $\tan \lambda = 2U_0/V_0 \approx 0.33568$. The according mass with stable trajectory is given by $m \approx 4QV/(q_m\omega^2 r_0^2)$. Trajectories should be kept narrow when injecting into an RFQ mass filter. The acceptance is typically smaller in y-direction, given the introduced polarity of the quadrupole and positively charged particles that are dragged towards the y-direction electrodes. In an entrance fringing field both RF and DC potential are weakened, so that a and q for an ion start from 0 to the desired working point in the stability zone of an ideal field. If this path is out of the stability zone, the particle will experience bigger amplitudes in movement and is likely to get lost. This effect is stronger for heavier ions with equal kinetic energy in z-direction ions, since they are slower and spend more cycles in that region. This problem can be overcome with a delayed DC ramp by additional RFQ segments without applied DC field [Brubaker, 1968]. The RF confinement is then established before the discriminating DC potential is applied as shown in figure 2.5. Note, that
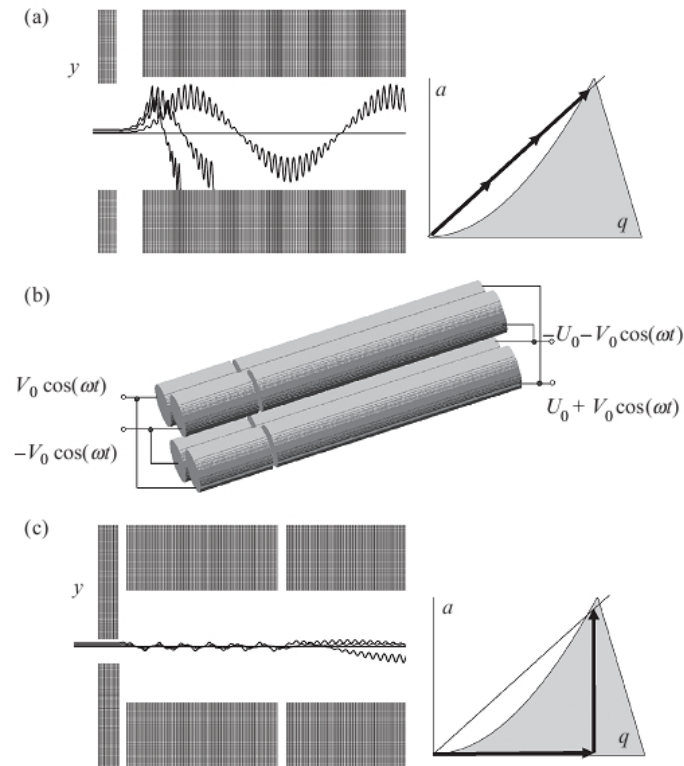
Figure 2.5.: (a) Unstable ions in y-direction in an entrance fringing field of a quadrupole mass filter; (b) delayed DC ramp in entrance fringing field by additional RFQ segments; (c) Enhanced acceptance by delayed DC ramp as parameters a and q always remain in stable region up to the desired working point at the apex of the stability zone. [Yavor, 2009]

same effect is true at the exit of the RFQ, so that these so-called Brubaker lenses may be placed also at the end of the filter.

When round shaped RFQ rods are applied, a reasonable ratio for the rod radius r_c and open space between rods radius r_0 of $r_c/r_0 \cong 1.14511$ has been calculated [Reuben et al., 1996]. A better performance however has been shown for a lower ratio of $r_c/r_0 \cong 1.13$ [Yavor, 2009].

2.2.2. Time-of-Flight Mass Analysis

The RF structures as described in the earlier section are (within this work) applied for ion transport and preparation only. The mass spectrometric principle itself is the time-of-flight method.

Time-of-Flight (TOF) mass spectrometry is used to temporally separate ion species according to the mass-to-charge ratio m/Q [Stephens, 1946, Wollnik, 1993, Cotter, 1999, Wollnik, 2013]. These ion are provided equal kinetic energy and pass a static electric field. It is intuitive, that ions of same energy but different mass travel a certain distance with different velocity v and in a different time, as the relation $v = \sqrt{2mE_{kin}} \propto mv = p$ for momentum p and kinetic energy E_{kin} imposes (see figure 2.6 a)). This approach was originally meant as an ion 'Velocitron' [Cameron and Eggers, 1948]. The time required for a flight path s can be written as

$$t = \int_{z_{start}}^{z_{stop}} \frac{1}{\sqrt{v(z)}} dz = \sqrt{\frac{m}{Q}} \int_{z_{start}}^{z_{stop}} \frac{1}{\sqrt{2U(z)}} dz \quad \rightarrow \quad t = \frac{l}{v} = \sqrt{\frac{m}{2E_{kin}Q}}, \tag{2.41}$$

which is simplified to the right expression in case of a field free drift region. This states a clear relation between the mass-to-charge ratio m/Q and the flight time $t \propto \sqrt{m/Q}$. This can be simply measured from the time of extraction from the ion source to the time of detection.

This technique is non-scanning and allows multiplexed detection of each m/Q-species. Depending on detection efficiency and the data acquisition, even single ions can be sufficient to determine a mass-to-charge ratio. A time-of-flight analyzer principally offers a simultaneous transmission of the entire mass range. The absolute mass ranges from light masses of elementary particles in high energy physics with $m \ll 1\,\mathrm{MeV}/c^2$ to huge mass biomolecules with $m \gg 100000\,\mathrm{u}$. This work concentrates on non-relativistic particles with elementary or molecular mass.

The resolving power for the quadratic relation between time and mass and a minimal resolved time difference Δt between the flight time of two different masses, can be formed to

$$R_m = \frac{m}{\Delta m} = \frac{t}{2\Delta t}, \tag{2.42}$$

which is directly expressed by mass in case of singly charged ions ($Q = 1$). Longer flight path with longer flight time improves the mass resolving power whenever the ion-optical contribution to the time error by the flight path is small compared to the initial time error. For practical reasons, the total flight path is limited by the size of the system.

Decisive is the determination of time, which is influenced by the detection and acquisition. Mostly, the mass resolving power is dominated by the time spread of the ion bunch of each species [Wiley and McLaren, 1955]

$$\Delta t^2 = \Delta t_{initial}^2 + \Delta t_{io}^2 \tag{2.43}$$

consisting of an initial time spread $\Delta t_{initial}$ and ion-optical time spread Δt_{io} induced by ion-optical aberrations. The initial time spread is itself dominated by the turn-around time Δt_{ta} of the ions in gas phase. This time is needed to turn around ions with non-vanishing thermal velocities v_{therm} during the extraction from the start point. This is a substantial contribution of the width of a peak, given by [Guilhaus, 1995]

$$\Delta t_{ta} = \frac{2mv_{therm}}{QE_{ex}}. \tag{2.44}$$

The thermal velocities are normally distributed and create Gaussian shapes of the time-of-flight signals. Another substantial error in time is due to a kinetic energy spread δ, which is mainly caused by an initial spatial distribution at the moment of extraction in the electric field E_{ex} that translates to

$$\Delta E_{kin} = \Delta z Q E_{ex}. \tag{2.45}$$

These energy deviations of ions with same mass cause different velocities and thus different flight times. At the time point of extraction either ions are pseudo-instantaneously generated (e.g. by Laser ionization) and extracted by a prevailing electric field or ions are trapped in an source region and extracted by a switched electric field. Also a combination of both may be used with a delayed extraction by an electric field.

The spatial dispersion according to the initial thermal velocities prior extraction translates into different starting points in the electric field. This essentially results in different kinetic energies after extraction. That ideally compensates in the so-called time-energy focus, where ions with different energies arrive at this focus plane at the same time. Ions with higher energy start at positions farther away from the detection plane and therefore have longer flight paths, while lower energetic ions have a shorter flight path (see figure 2.6 b)).

The mentioned aberrations cause the following time width $\Delta t_{initial}$ at FWHM at a time-energy focus [Plass, 1997]:

$$\Delta t_{ta}^{FWHM} = \frac{\sqrt{8\ln(2)mk_BT}}{QE_{ex}}. \tag{2.46}$$

To gain smallest peak shapes it is important to have a low thermal and spatial distribution prior to extraction. This may be achieved by collisional buffer gas cooling in an RFQ ion trap [Tolmachev et al., 1997, Plass et al., 2007a] or an orthogonal extraction of a focused ion beam, or a combination of both [Coles and Guilhaus, 1993, Dodonov et al., 2000, Raznikov et al., 2001]. A subsequent RFQ arrangement also enables an additional focusing and pumping stage that may be used for atmospheric inlet systems [Tolmachev et al., 1997]. Historically, these arrangements came up to diagnose individual properties of the system [Brincourt et al., 1990].

As discussed above, a longer flight path is favorable for higher mass resolution. Still, the time-energy focus needs to lay on the detection plane. The mass resolving power is in first order dependent on the initial peak width, that itself is dominated by the turn-around time $\Delta t_{ta} \propto E_{ex}$ and the total time-of-flight $t \propto 1/\sqrt{E_{kin}}$. The kinetic energy is proportional to extraction field strength E_{ex} for a fixed time-energy focus position. That leads to the expression of mass resolving power
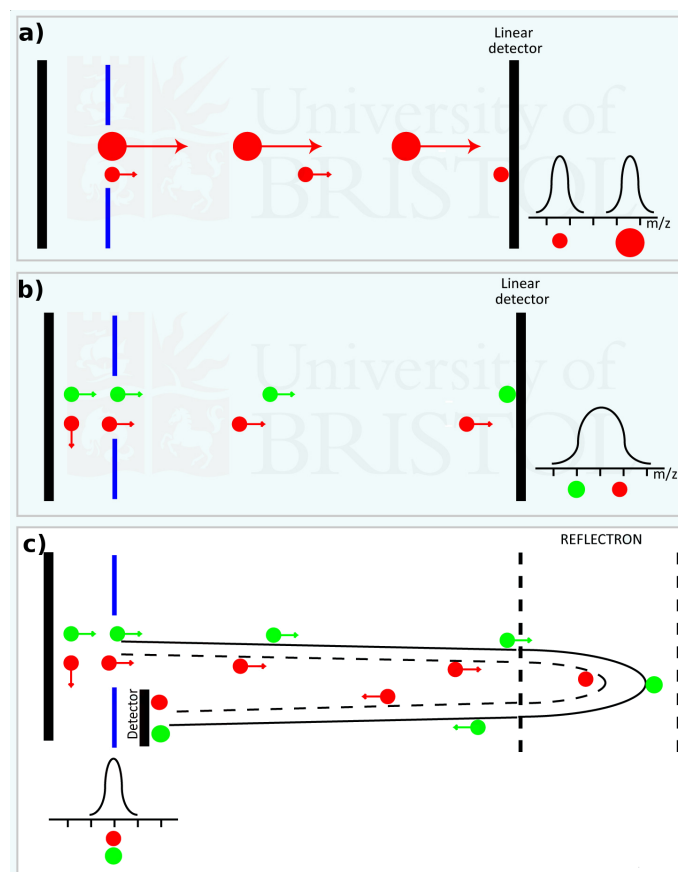
Figure 2.6.: Linear time-of-flight mass spectrometer a): two different mass-to-charge species tra-
verse at different velocities and are thus detected separately. Ions with same mass-
to-charge ratio, but different initial potential energies (indicated by the red and green
colors) b): ions arrive at the detector at slightly different times. Time-of-flight mass
spectrometer with reflectron c): the ions experience a detour depending on their en-
ergy and are refocused onto the detector plane. Adapted from [Gates, 2014].

of

$$R_m = t/2\Delta t \propto \frac{\frac{1}{\sqrt{E_{kin}}}}{\frac{1}{E_{kin}}} \propto \sqrt{E_{kin}} \tag{2.47}$$

and shows that higher kinetic energies result in higher mass resolving power. Experimentally, this is mostly restricted for technical reasons to several 10 keV.

As a milestone improvement, a reflector (also known as reflectron) was developed [Alikanov, 1957, Mamyrin, 1966] as ion optical mirror. It consists of several stacked electrodes as retarding field, that reflects ions into opposite direction. Higher energetic ions dive deeper into the field and experience an according detour compared to lower energetic ones (see figure 2.6 c)). This behavior raises the option to position the time-energy focus independent on the extraction field. Reflectors thereby extend the flight path on the one hand and transfer the primary time-energy focus towards the detector plane. This allows for a higher extraction field strength and smaller resulting turn-around time.

For longer flight paths the momentum p and the spatial component x as well as their product becomes more important. It can be considered as the phase space and defines the emittance of an ion beam. In electrostatic fields this product remains constant and is an important value to characterize the ion beam. One can distinguish transverse (or radial) emittance and longitudinal emittance along the beam axis. Ion optical systems have to cope with the realistic phase space of an ion beam, since minor deviations to the designed beam trace can lead to major aberrations with longer ion-optical pathway – or even cause ion losses. A small initial phase space for minimal ion optical aberrations is usually of advantage.

2.2.3. Vacuum Physics

Mass analysis takes place in intermediate or low pressure regimes to control the rate and kind of buffer gas collisions or exclude collisions at all. Thereby certain requirements on the vacuum system arise, such as reduction in neutral gas ballast from an atmospheric pressure interface, separation of pressure domains and complete suppression of residual gas to prevent any collision and potential charge transfer. The following gives a brief overview (well described in [Diels and Jaeckel, 1962, Jousten et al., 2006, Pfeiffer Vacuum GmbH, 2013]), which is important for the outlay of an instrument.

Pressure is defined as the quotient of a force F and an area A

$$p := F/A. \tag{2.48}$$

The pressure is a result of the summed force exerted by atoms or molecules upon the area. The mean velocity, given by the Maxwell-Boltzmann distribution, can be expressed as

$$\bar{c} = \sqrt{\frac{8k_B T}{\pi m}} \tag{2.49}$$

with temperature T and the mass of the particle m. Another important parameter is the mean free path length

$$\lambda = \frac{k_B T}{\sqrt{2}\pi p d_m^2}, \tag{2.50}$$

with the pressure p and the diameter d_m of one molecule species. The ratio of λ and the characteristic dimension d of the system

$$K_n = \frac{\lambda}{d} \tag{2.51}$$

is called Knudsen number. The characteristics of gas changes from higher pressures with viscous flow ($K_n < 0.01$, gas-gas interaction dominating) to lower pressures with molecular flow ($K_n > 0.5$, gas-gas interaction negligible). The intermediate range causes the Knudsen flow with a mixed characteristic, which is not as simple to estimate. Further, the Reynolds number [Reynolds, 1883]

$$R_e = \frac{\rho v l}{\eta} \tag{2.52}$$

relates inertial force and viscous force of a flow, with the length of the system l, the density of a fluid ρ and the specific dynamic viscosity η. It is a measure to distinguish laminar ($R_e < 2300$) and turbulent ($R_e > 4000$) flow. The regime of viscous (turbulent and laminar) flow is of special interest for an interface to atmospheric pressures. Therefore several models exist, but do only semi-empirically describe the flow characteristics.

Analog to electricity of direct current, a resistivity for flow can be defined as $W = 1/C$ with the flow conductance C. A total conductance can be composed of single conductances in parallel ($C_{par} = C_1 + C_2 + \cdots + C_n$) or in serial order ($\frac{1}{C_{ser}} = \frac{1}{C_1} + \frac{1}{C_2} + \cdots + \frac{1}{C_n}$). In an balanced system, the gas flow j_{flow} is then given by

$$j_{flow} = \Delta p_{1,2} \cdot C \tag{2.53}$$

and is proportional to the pressure difference of neighboring domains $\Delta p_{1,2} = p_1 - p_2$.

The conductance of molecular flow can be well described by simple formulas. The interaction is dominated by collisions of molecules with the wall of the recipient, rather than among molecules themselves. Thus, the conductance is independent of the pressure. Most relevant in this work is the conductance for short apertures ($l \leq r$) and longer geometries ($l >> r$):

$$C_{l \leq r} = A\frac{\bar{c}}{4} = \pi \left(\frac{d}{2}\right)^2 \sqrt{\frac{k_B T}{2\pi m}} \tag{2.54}$$

$$C_{l >> r} = \frac{\bar{c}\pi d^3}{12l}. \tag{2.55}$$

2.3. Ion Generation

Mass spectrometry is always relying on electro-magnetic manipulation of charged particles. Therefore, the process of ionization is essential to obtain a cumulative charge as handle for the atom or molecule. Numerous types of ion sources exist – with rising tendency. The ion sources implement a cumulative charge by their individual ionization mechanisms; either by adding or removing of an electron, or by adding or removing of a charged adduct. This can be done in a pulsed or continuous mode. The specific technique and its parameters influence the individual characteristics and

determine in large part the obtained ion species. The ionization technique further depends on the phase state of the sample and the desired information. Also of importance is the necessary amount of sample, the ionization efficiency, the reliability and the ease of operation. The result of each ion source is quite individual and also depends on the mass analyzer and its coupling. That is why a deeper understanding may be needed for a reliable interpretation of the data.

Nowadays, modern ambient ionization methods for chemical analysis are performed using samples in a raw or unprocessed 'ambient' state [Cooks et al., 2010]. This enables quick analysis and suppresses potential transformation during preparation and solvation of samples. The ambient ionization ensures an important in-situ aspect (see 2.6) and enables innovations in fields such as biomedicine, food safety, anti-terrorism, pharma-pharmaceuticals and environmental pollution [Ibanez et al., 2015, Huang et al., 2010]. Besides completely new-developed ambient techniques, there are also conservative ionization methods ported to ambient pressure by several modifications, combination and/or a second ionization step (post-ionization) [Huanga et al., 2011]. Generally, ambient sampling / ionization implies: possible ionization of large objects, direct ionization with minimal sample pretreatment, sampling at surfaces, possible interfacing to mass spectrometers with atmospheric pressure interface and soft ionization [Monge et al., 2013]. Also of interest in atmospheric ionization are ongoing reactions of the solvent under certain conditions. This can be studied for chemical analysis and even used for small-scale synthesis [Espy et al., 2014]. While atmospheric ionization seems contradictorily to the beliefs of the last decade, today's mass spectrometry studies realize ionization even at super-atmospheric pressure, which is a multiple of or atmospheric pressure, to select and enhance the ionization probability of individual species [Chen et al., 2013a]. Figure 2.7 gives exemplary an overview of ionization techniques for atmospheric and intermediate pressure depending on the molecular weight and polarity of the sample. The ion source means the medium to the desired sample – whether prepared or native –
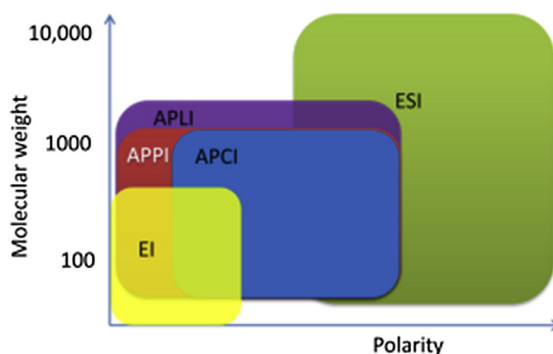
Figure 2.7.: Ionization ability of different ion sources at atmospheric and intermediate pressure – compatible to chromatographic methods [Li et al., 2015]: APCI [Hopmans et al., 2000], APPI [Robb et al., 2000], APLI [Constapel et al., 2005], ESI [Lee and Shiea, 1998] and the rather hard EI at low pressures [Cappiello, 2009].

and is thereby the key to many applications. Hence, a mass spectrometer becomes more universal by an increased compatibility to various ion sources. The presented techniques are used with the mobile high-performance MR-TOF-MS or may be applied in future.

Thermal Ion Source

In general, atoms can be ionized when in contact hot metal surfaces. This is referred to as thermal or contact ionization [Dobrezow, 1934]. A probability of ionization for ions in thermal equilibrium with the surface can be described by a special form of Langmuir-Saha equation [Langmuir and Kingdon, 1925]

$$p_{ion} = \left[1 + \frac{g_{neutral}}{g_{ion}} \exp \left(\frac{e(\Phi_{ion} - \Phi_w)}{k_B T_s ur} \right) \right]^{-1} \tag{2.56}$$

for a surface temperature $0\,\mathrm{K} < T_{sur} < \infty\,\mathrm{K}$, the ionization potential of the atom to be ionized Φ_{ion}, the work function of the metal surface Φ_w and $g = 2J + 1$ as the total angular momentum of the neutral atom and its ion. The evaporation rate also has to be considered and is given by the Hertz-Knudson-equation [Hertz, 1882, Knudsen, 1915]

$$R_{evap} = \frac{p_{vap} T_{sur}}{\sqrt{2\pi k_B m T_{sur}}} \tag{2.57}$$

with the mass m and the specific vapor pressure p_{vap} of the element to be evaporated. These sources are usually quite durable, reliable and easy to use. On the other hand they primarily offer only ions of elements with low ionization potential and destroy molecules at high temperatures.

Electrospray Ionization

ESI, as one default ionization method for macromolecules, has become a standard technique with various sub-versions. High voltage is applied to a sample in liquid solution and the solution is pumped through a glass or metal emitter [Yamashita and Fenn, 1984]. When a high electric potential is applied to the solution the interface between liquid and air is polarized with an excess ionic charge, that results in a quasi-conical shape. Once a sufficiently high voltage is supplied between the solution and the MS inlet, the solution is dispersed in fine droplets. These undergo a succession of solvent evaporation and coulombic fissions and create multi-charged molecular ions with intact analytes [T. C. Rohner and Girault, 2004]. This fission occurs when the Rayleigh limit is reached. This limit describes a surface charge density q_R, where the electrostatic force overcomes the surface tension at the surface of a droplet. With the pressure $p_R = 2\gamma/R$ (with the curvature R and surface tension γ) and the electrostatic pressure $p_E = \sigma^2/2\varepsilon_0$ (with surface charge density σ), the Rayleigh limit is given by

$$q_R = 4\pi R^2 \sigma_{(p_R = p_E)} = 8\pi (\varepsilon_o \gamma R^3)^{1/2}. \tag{2.58}$$

Two models are used to describe the distinct ionization process: (a) the ion evaporation model (IEM) [Iribarne and Thomson, 2004] assumes that, before the droplet reaches its ultimate stage, the field on its surface becomes strong enough to overcome solvation forces, thus releasing the solute ion form from the droplet surface. Supposed droplets have radii below 10 nm. (b) the charge residue model (CRM) [Dole et al., 2004, Schmelzeisen-Redeker et al., 1989] assumes a sequence of Rayleigh instabilities, that is caused by successive solvent evaporation and droplet fissions due to coulombic repulsion of charges on the surface of the droplet. Ultimate droplets
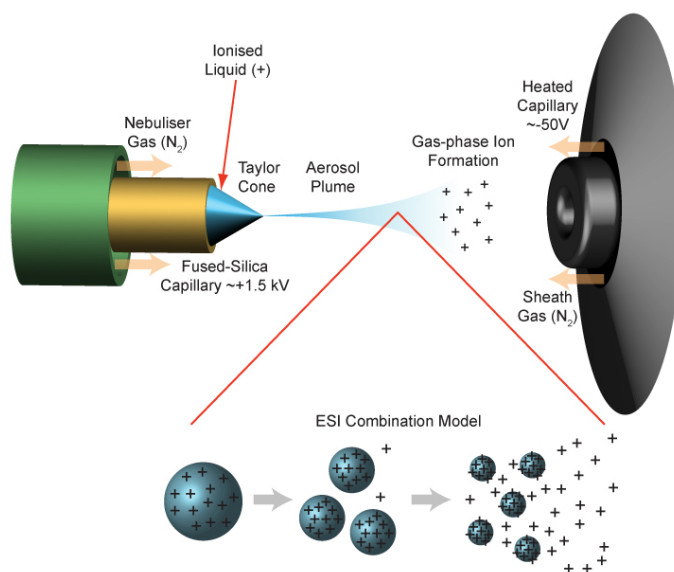
Figure 2.8.: Electrospray ionization process [LamondLab, 2014]; capillary with solvent forming
Taylor cone in electric field, optional nebulizer gas, aerosol plume with combined
model, gas-phase ion formation and MS inlet.

are created with each of them containing only one molecule of solute, which becomes a free gas-phase ion by retaining the charge of the droplet, when the solvent is evaporated. See figure 2.8 for a combined illustration.

ESI produces ions from macromolecules and causes only very little fragmentation. Therefore it is well-known as a soft ionization technique. It is routinely used at atmospheric pressures and produces multiply charged ions, which has the advantage of decreased mass-to-charge ratio for heavy ions. Commonly a sheath of nebulizing spray is implemented for shielding and supporting the ionization.

As a famed derivative Desorption Electrospray Ionization (DESI) is known, where the analyte is not solved and fed into an emitter, but desorbed from a surface by a pure solvent electrospray [Takats et al., 2004]. Analog with the DESI technique, imaging of biological tissue under ambient conditions with a single probe of solvent spray is possible and recently under investigation [Rao et al., 2015].
Another derivative is the paperspay method. There, an emitter is completely omitted and the analyte as well as the solvent are dropped onto a blank paper triangle as carrier. The sharp tip of the paper in front of a MS inlet yields a spray and ionization similar to ESI. This enables simple and prompt analysis like drug detection [Su et al., 2012]. Figure 2.9 demonstrates the simple ion source arrangement. Comparable results and with even greater ease can be achieved by leaf spray for the direct analysis of plant tissues and tissue spray for direct spray ionization from a biopsy needle for biological tissue diagnostics [Badu-Tawiah et al., 2013].
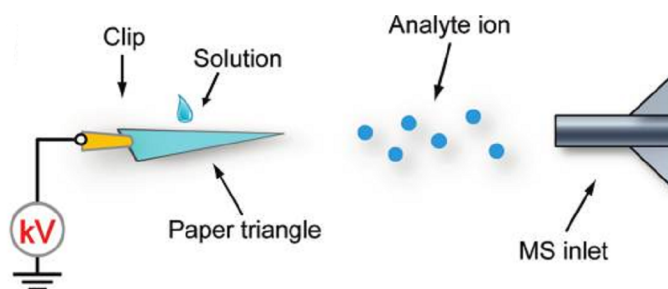
Figure 2.9.: Simple setup of paperspray ion source [Liu et al., 2010].

Further Compatible Ionization Techniques

Besides the implemented ionization techniques within the measurements in this work, further techniques are ideally suited for coupling to the MR-TOF-MS for in-situ and high-throughput application.

- Electron Impact Ion Source
  Ionization via EI is an universal and widely spread ionization technique by collision of accelerated electrons and the analyte [Dempster, 1921]. EI ionization is often used in combination with a direct gas inlet or as coupling to other techniques (e.g. for LC-MS coupling). It is a hard ionization method and not suited for very large or thermosensitive samples. The precursor ion is usually either of low intensity or not present any more. [Cappiello, 2009, Bhardwaj and Hanley, 2014]

- Photoionization
  The principle of photoionization is well known from the photoelectric effect of metals [Lossing and Tanaka, 1956]. The photons may be created by either Laser, a rare gas discharge lamp or a synchrotron light source. The common energy of the photons is $\approx 10eV$ and low enough to avoid fragmentation of the sample, where higher and specific energies can be used for targeted dissociation. [Brodbelt, 2014, Bhardwaj and Hanley, 2014]

- Laser Desorption
  Laser desorption is a method of choice for the ionization of macromolecules, bringing the molecules to gas phase and avoiding major decomposition of the same. In Matrix-Assisted Laser Desorption Ionization (MALDI) samples imbetted in a light absorbing matrix are mobilized by laser-induced ionization [Michael Karas, 1988, Trimpin, 2016, Karas et al., 2000]. MALDI-MS is nowadays also being used for spatial imaging at atmospheric pressures [Roempp et al., 2013]. Modern applications range from imaging to classification of tissue in native form [Nemes and Vertes, 2012, Cillero-Pastor and Heeren, 2014].

- Plasma Ionization
  As plasma ionization Inductivly-Coupled Plasma (ICP) [Fassel, 1977] is commonly used and created by applying an RF signal to a coil surrounding a recipient and an applied gas flow (e.g. Ar, He) [Niu and Houk, 1996]. A Low-Temperature Plasma (LTP) is realized in a similar way, but smaller and with comparably lower temperature. It is used to generate reactive species that are directed to an analyte surface where ambient ion/molecule reactions

take place with neutral molecules. [Benassi et al., 2013, Wiley et al., 2013b]

- Secondary Ion Mass Spectrometry
  In Secondary Ion Mass Spectromtery (SIMS) a sample is analyzed under ultrahigh vacuum conditions with bombardment of a primary ion beam [Benninghoven, 1971]. SIMS is an ideal tool to study surfaces and its interaction with its surroundings. This is particularly interesting for material sciences, molecular depth profiling, as well as the study of biomaterials [Yang and Gilmore, 2015, Henss et al., 2013]. Further, it was used as one of the first imaging techniques in mass spectrometry [Werner, 1972] and offers highest spatial resolution and therefore requires highest ion throughput.

2.4. Detection Techniques

Any mass spectrometer requires detection of the investigated ions. One can distinguish between destructive detection, where ions of interest are lost for further proceeding and non-destructive detection, where the ions are not affected by the detection mechanism (see section 2.7.1) and can be separated and/or used for further investigation.

Faraday Cup

The most simplest detector is an ordinary conductor to receive a positive or negative ion current. This is often build in a cup-shape known as Faraday Cup detector. It is easy and cheap to built and reliable. A quite sensitive charge or current measurement is needed for proper detection.

Micro-Channel Plate

Very common are electron multiplier or Secondary-Electron Multiplier (SEM), consisting of a series of discrete dynodes or a continuous channel [Goodrich and Wiley, 1962] with applied high voltage to convert impinging ions or electrons to an multiplied number of electrons. With a decreasing velocity of the incoming ion also the number of secondary electrons is reduced [Beuhler and Friedman, 1977]. That may be problematic when higher mass detection efficiency is required for slow ions. SEM are fast in response and very sensitive, but suffer from aging effects and mechanical and electric fragility. The amplification in general can be as high as 10^8 [Dass, 2007] and is usually sufficient to detect even single charges. By combination of the electric with a magnetic field isochronous SEM can be realized and produce more narrow time signal with less jitter [Stresau et al., 2006].
Micro-Channel Plate (MCP) can be described as an assembly of channel electron multiplier [Wiza, 1979] (see figure 2.10). Numerous of these channels with an inner diameter of a few μm are integrated into a thin plate. Since the amplification takes place along the whole area at the channel of an impinging particle, these plates can be also used for imaging purposes [Aberth, 1981]. Sophisticated designs of the charge collecting anode allow for a spatial information by clever segmentation or delay-line technique.
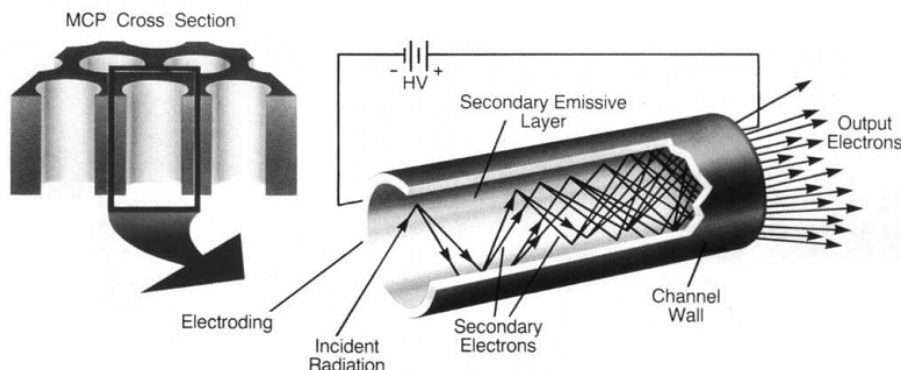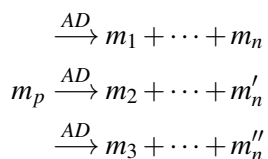
Figure 2.10.: Schematic insight into an MCP and the principle of secondary electron amplification [Plass, 1997].

2.5. Tandem Mass Spectrometry

The term tandem MS describes subsequent stages of single MS procedures – comprising the separation, as well as subsequent measurements, intermediate fragmentation or dissociation of an investigated sample. This is also referred to as MS/MS or, in case of the number of stages $N > 2$, it is called MS^N. The scheme of MS^N is depicted in figure 2.11. The idea of this procedure is to gain information on structure of molecules by the mass of single fragments and/or determine the location of cleaved bonds and the required energy to actually break them [Roussis, 2001]. Besides that, tandem MS enables the identification of complex species by identification of their fragments and their compounds [Jennings, 1968].

In general, a precursor ion m_p is chosen and isolated from a possibly complex mass spectrum. Which is nothing else than a non-destructive separation of an ion species. This precursor ion is then activated by feeding energy into its molecular system, which is then breaking up into the lighter products. This depends on the type of activation and the properties of the precursor ion. There may be only a single product arrangement or simultaneous dissociation into several product species (AD denotes activation and dissociation):

$$\begin{aligned} & \xrightarrow{AD} m_1 + \cdots + m_n \\ m_p \; & \xrightarrow{AD} m_2 + \cdots + m_n' \\ & \xrightarrow{AD} m_3 + \cdots + m_n'' \end{aligned}$$

In order to analyze and measure the daughter products a cumulative charge of these has to be involved. Neutral products are either not recognized or 'charged' by an additional ionization.

Two concepts do exist: 'in-space' and 'in-time' tandem mass spectrometry [de Hoffman and Strooband, 2007]. In the first case, the single stages are realized in different parts of the instrument, which can rely on completely different mass spectrometer types. In the second case, the precursor ions are selected, activated and analyzed in the very same part of the device. The operation of a tandem mass spectrometer can be done in four different ways which are product-ion scan, precursor-ion scan, neutral-loss scan and selected-reaction monitoring [Dass, 2007]. These
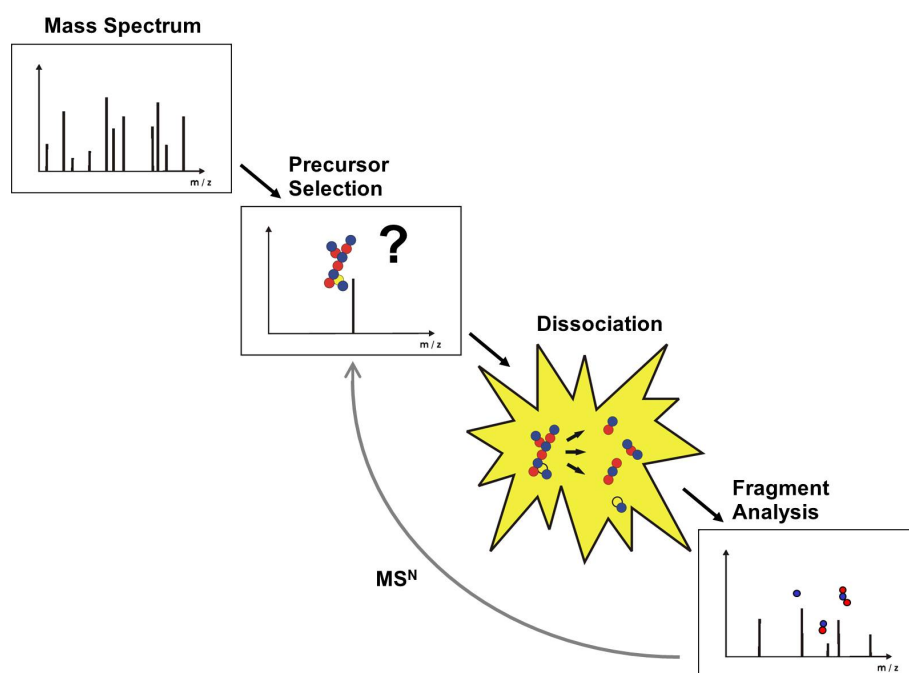
Figure 2.11.: Illustration of tandem mass spectrometry; selection of precursor from complex spectrum, dissociation of molecules and determination of fragments – optionally next stage of precursor selection.

depend on the required information and the state of the analysis. Most tandem mass spectrometers do not support all of these scan functions. Complex primary mass spectra with high mass multiplicity can require a very high separation power for neighboring mass lines to gain unambiguous results [Loo and Muenster, 1999]. Maximal available separation power for the precursor selection reaches few 10^4 [Dass, 2007], while still higher separation power could enable or simplify further studies. Quite relevant for practical reasons is the scan speed of tandem devices to have sufficient throughput and statistics [Schmidt et al., 2008]. A practical hassle arises from low separation and activation efficiencies that lead to pure statistics. Common tandem MS utilize RF traps or TOF devices (see later section 2.6). The nature of the RF confinement e.g. places a limit on the ratio between a precursor mass-to-charge ratio and the lowest trapped fragment ion, clearly causing restrictions in application, such as de novo sequencing of peptides. MS/MS is used in many fields, from fundamental research to clinical application [Leung and Fong, 2014].

To gain maximal information on the structure and composition of complex molecules, the dissociation of subgroups or the simple fragmentation at chemical bonds is used. Except the electron impact ionization, ionization techniques do not provide abundant structural information (see section 2.3). Therefore several techniques exist to purposely split the mother molecule into selected daughter molecules. The following methods are suitable for the MR-TOF-MS:

- Collision-Induced Dissociation
  The Collision-Induced Dissociation (CID) implies an activation by excitation to higher-energy states of the precursor ion by collisions with inert gas [Johnson et al., 1987, Medzihradszky and Chalkley, 2015]. This activation leads to an unimolecular dissociation into the products. The maximal transferred energy in the center-of-mass system E_{com} depends on the kinetic energy of the precursor ion E_{lab} and the ratio of precursor mass m_p and the mass of the neutral gas N:

$$E_{com} = \frac{N}{m_p + N} E_{lab} \tag{2.59}$$

  This energy drops for increasing precursor mass. The collision can be done at a high-energy (3 to 10 keV) and a low-energy regime. In high-energy collisions the ions are excited instantaneously at the moment of collision with their particular high kinetic energy, which results in vibrational energy stochastically distributed among the covalent bonds, where bonds are cleaved whenever the energy is sufficient [de Hoffman and Strooband, 2007]. The low-energy regime makes use of lower and multiple collisions [Yost et al., 1979]. Therefore the precursor ions can by heated e.g. by resonant RF excitation. The occurring fragmentation pattern is dominated by the low-activation-energy pathways. Usually only one of these methods is applied, depending on the instrument.

- Surface-Induced Dissociation
  With Surface-Induced Dissociation (SID) the precursor ions impinge with a certain kinetic energy on a devoted surface, leading to an internal excitation state and according fragmentation [Mabud et al., 1985, Wysocki et al., 2008]. The energy transfer is comparably higher than with CID, because of the higher mass of the collision surface. This is favorable for higher mass molecules.

- Absorption of Electro-Magnetic Radiation
  The absorption of electro-magnetic radiation can be used to activate precursor ions. There

are different regimes according to the absorbed wave length – from ultraviolet photodissociation [Nuwaysir and Wilkins, 1989] and infrared multiphoton dissociation [Little et al., 1994] to blackbody-induced radiative dissociation [Dunbar and McMahon, 1998].

- Electron-Capture Dissociation and Electron-Transfer Dissociation
  These dissociation techniques make use of a provoked instability by an additional charge brought into the precursor molecule. In Electron-Capture Dissociation (ECD) a low-energetic electron is captured by the molecule causing the same to break, most often at the site of capture without any prior randomization of the charge [Zubarev et al., 1998]. Electron-Transfer Dissociation (ETD) is similar to ECD but uses an ion-ion reaction to transfer an electron to for instance a multiply charged peptide [Sarbu et al., 2015].

2.6. In-Situ Compatible Mass Spectrometers

In-situ mass spectrometry means mass analysis directly in the situation, wherever this may be. There is no transport of sample into the laboratory – much more the analytical method is brought to the site of application. This leads to new insights into complex systems and transition effects due to a direct analysis during an exploration in the field. Prompt results can support decision making such as real-time recognition of cancerous tissue during surgery and allow for a deeper understanding of fast chemical transformation like metabolism sequences in biological environment. Generally, in-situ MS makes the chain of analytic investigation simpler and faster (see figure 2.12). [Careri and Mangia, 2011, Badu-Tawiah et al., 2013]
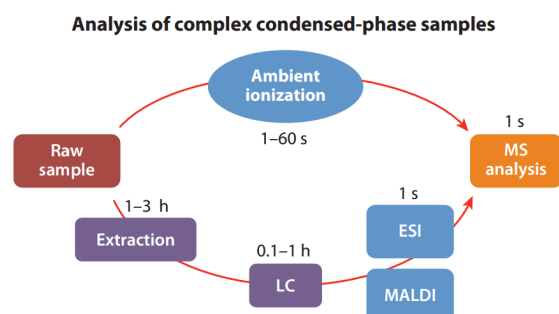

Figure 2.12.: Analysis of complex condensed-phase samples by the traditional extraction, chromatography and mass spectrometry sequence with typical timescales (bottom) contrasted with direct sampling and ionization by ambient ionization MS [Badu-Tawiah et al., 2013].

Therefore a mobile and robust instrumentation and/or miniaturization is required. The modern term miniature mass spectrometer describes self-contained mass analyzers with included vacuum pumping, ionization, mass analysis, instrument control and data acquisition [Ouyang, 2014]. The aim of in-situ mass spectrometry is a mobile stand-alone procedure to evolve an analytical outcome – without additional equipment for sample preparation, chromatographic separation.

Simple sample preparation is mandatory and often made selective to ease the mass spectrometric analysis. In the context of in-situ mass spectrometry, the ionization techniques play a major role [Huanga et al., 2011] (see section 2.3). Atmospheric pressure ionization can be a main aspect and in-situ mass spectrometry, for which reason the reduction of gas ballast and pumping capabilities have to be considered and implemented by an atmospheric pressure interface [Zhai et al., 2015, Chen et al., 2015]. Lower analyzer performance of mobile instruments may be compensated by the superior analytical power of the possibility of tandem mass spectrometry experiments [Careri and Mangia, 2011]. Micro-fabricated mass spectrometers employ mass analyzers build in sub-centimeter dimension for maximal mobility, simplicity and cost-reduction, while performance and output of analytical information is limited to lowest numbers. Infrastructure as pumping, control and supply are often not as miniaturized as the analyzer itself. Nevertheless these devices provide sufficient performance for special applications [Syms, 2016].

In-situ techniques are well established in medicine, security and the food industry. It is quite likely, that mass spectrometers will find their way into everybody's daily life and home [Cooks, 2012], which may actually create completely new aspects in life style. Only some of the overall mass spectrometer types can be reasonably employed to up-to-date scientific in-situ application – specific to requirements on analysis performance and mode, mobility, operation stability and ease of application. The following gives an overview of the available techniques.

2.6.1. Sector Field Mass Spectrometers

Sector field mass spectrometers have a long history and were the instruments with highest mass resolving power until the rise of FT-ICR. They usually consist of sectors of magnetic or electric fields or a combination of both [Thomson, 1913, Dass, 2007, Gross, 2013]. Ion trajectories are determined by the Lorentz force F_L and a magnetic sector field B can serve as momentum analyzer. With a characteristic magnetic radius r_m of ion flight path dictated by the centripetal force F_C:

$$F_L = qvB = \frac{mv^2}{r_m} = F_C \Rightarrow r_m = \frac{mv}{QB} \propto mv = p. \tag{2.60}$$

Given the velocity v and the kinetic energy $E_{kin} = \frac{mv^2}{2} = QU$ determined by an electric acceleration potential, the radius can be expressed as

$$r_m = \frac{1}{B}\sqrt{\frac{2QU}{m}} \tag{2.61}$$

and the mass-to-charge ratio becomes

$$\frac{m}{Q} = \frac{r_m^2 B^2}{2U}. \tag{2.62}$$

That implements, that the mass resolving power is restricted by the size of the instrument and the magnetic field B.
A radial electric field causes dispersion or focusing of the kinetic energy on a characteristic electric radius r_e:

$$F_e = QE = \frac{mv^2}{r_e} = F_C \Rightarrow r_e = \frac{mv^2}{QE}. \tag{2.63}$$

The sectors are typically arranged such, that they spatially focus an ion beam of certain mass-to-charge ratio onto a plane. Either the detection is along this plane for simultaneous mass measurement as in a mass spectrograph [Burgoyne and Hieftje, 1996] or only one species is allowed to pass a narrow slit for separation or detection in a scanning mode [Yavor, 1996]. Several geometries and arrangements exist with sub *ppm* mass accuracy and resolving power $> 10^4$ [Bateman, 2015]. Tandem experiments are typically realized by subsequent arrangement of several sectors. Because of their big footprint they are not common any more for standard high mass resolving applications, instead the are mainly used in Acellerator Mass Spectrometry (AMS) [Synal, 2013]. Besides that, there is an advent for miniaturized devices of sector field instruments limited to resolving powers of $R_m < 10000$ [Sinha and Wadsworth, 2005, Krachler et al., 2015]. Also sub-miniaturized sector field MS are being under investigation with accordingly limited performance [Diaz et al., 2001]. Recently a sector field instrument delivered data of the out-gassing of a comet within a space-borne application [Fuselier et al., 2015].

2.6.2. RFQ Mass Filters and Quadrupole Ion Traps

RFQ mass filters and quadrupole ion traps make use radio frequency electric fields to transport, trap and manipulate ions for analytical investigations. The theoretical background is provided in section 2.2.1.5. Where RFQ mass filters transport and filter, ion traps do trap ions and mass-selectively detect, store, fragment or eject ions [March and Todd, 2015].

RFQ mass filters provide a maximal mass resolving power of several 10^3, as can be calculated for reasonable boundary conditions. While the length of the RFQ could be increased, alignment of the electrodes and stability of the applied RF cause strict limits in performance. A certain mass range can be transmitted via stable trajectories to a detector, while any other masses are filtered out. There are two modes for scanning a complete mass range. Either transmission of isolated species with direct detection or transmission with a varied threshold of mass-to-charge ratios. In the latter case the increase of intensity with a certain threshold step denotes a quantity for that mass to-charge range. Scan rates of $3000\,\text{u/s}$ can be achieved [de Hoffman and Strooband, 2007]. RFQ mass filers are regularly applied to residual gas analyzers or to portable instruments [Urabe et al., 2014]. Despite their stand-alone application RFQ mass filters are often used for MS/MS experiments as first MS stage.

The trapping of ions in pure quadrupolar electric field with mass analyzing was proposed long time ago [Paul and Steinwedel, 1953]. This is still known as the concept of a Paul trap and one of the most common techniques. The usual geometry is composed of hyperbolic electrodes – one ring and two caps – which creates a perfect quadrupolar electric field. The ions are trapped by RF and DC potentials applied to the electrodes (see section 2.2.1.4 for storage and motion). The trajectories of ions are confined to a relatively small volume of $2\,\text{cm}^3$ to $3\,\text{cm}^3$. The theory of operation of an ion trap is similar to these of a mass filter. The two-dimensional quadrupole field is considered for a mass filter, while a three-dimensional quadrupole field is considered for an ion trap [March and Todd, 2005]. Typically a damping gas is also applied in combination with mass-selective instability by proper choice of parameters *a* and *q* [Stafford et al., 1984]. Ion Trap instruments often comprise MS/MS capability with distinct fragmentation techniques and range from big stand-alone devices with continuous atmospheric ion inlet and mass resolving powers of $R_m \approx 100000$ to hand-held or bench-top devices with low sensitivity and performance ($R_m \approx 10^3$) applicable for harsh environment [A.Contreras et al., 2008].

Besides the three-dimensional form described above, also a more simple linear form with of 4 rectangular electrodes is used with trapping potentials on both ends [Ouyang et al., 2004]. This form can also be used as RFQ mass filter and led to a series of miniaturized MS [Li et al., 2014a] and also miniature arrangements of ion traps for tandem mass spectrometry [Li et al., 2014b] (see figure 2.13).

A third variation is the cylindrical trap that is also used in miniaturized instruments [Patterson et al., 2002]. The mass resolving power of mobile devices unfortunately is still below few 10^3 [Kuerten et al., 2007]. A toroidal fabrication of an ion trap can be considered as a linear ion trap with infinite length [de Hoffman and Strooband, 2007, A.Contreras et al., 2008].

Tiniest devices are the so-called micromashined cylindrical ion traps in the sub-*mm* region [Chaudhary et al., 2014]. As curious example of application, ion traps in very robust format are used for planetary missions with unity mass resolution [Wong et al., 2013, Franz et al., 2014].
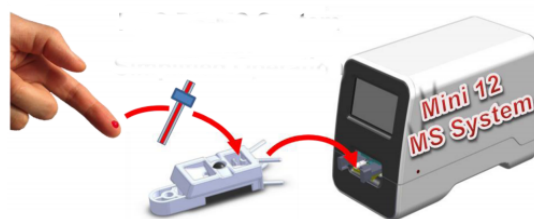

Figure 2.13.: A Mini 12 bench-top MS with automated operation for automated quantitative blood analysis [Li et al., 2014b]. The figure illustrates the size and ease of operation with automated prompt results.

2.6.3. Mobile Time-of-Flight Mass Spectrometers

The method of time-of-flight has been discussed in section 2.2.2 together with their advantages as simplicity, scalability, non-scanning operation with very short cycle times, mass range and mass accuracy. All in all, time-of-flight instruments are reliable and convince with simplicity in instrumentation and operation. The extremely high spectrum-acquisition rate, high duty cycles, high transmission rates and sensitivity, as well as the huge range of mass are the main advantages. The implementation of reflectors give access to higher resolving power and assures precise mass values. Time-of-flight mass spectrometers are nowadays used in heavy mass molecule diagnostics, nucleic acid investigation and proteomics [Khardori, 2014] as well as secondary ion mass spectrometry [Young-Pil et al., 2015]. Miniaturized instruments can be ideally suited for mobile application [Cotter et al., 1999], as well as ruggedized instruments can be used harsh environmental application, such as space missions e.g. [Riedo et al., 2013]. As a counterpart, in nuclear physics research with relativistic ions the time-of-flight method is used for stationary spectrometers and in storage rings [Geissel et al., 2006, Litvinov et al., 2005, Meisel and George, 2013].

Linear and single-reflecting TOF can be robust and compact for mobile application, but are restricted in performance by principle physical limits. Achieved parameters of transportable devices are $R_m \approx 10000$, repetition rates $f_{rr} > 1000\,\text{Hz}$ and mass accuracy $\delta m/m < 10^{-5}$ at maximum. Tandem experiments can be realized be subsequent time-of-flight analyzer stages. Usual parame-

ters are an order of magnitude lower for very mobile instruments [Junninen et al., 2010, Huanga et al., 2015]. The smaller and portable the instrument, the lower the performance.

With a long history of development, time-of-flight mass spectrometry is still en vogue and increasingly popular in mainstream analytical applications [Standing and Vestal, 2015]. Nevertheless, modern TOF instruments to meet highest analytical demands are yet to come.

2.6.4. Ion Mobility Spectrometers

Even though Ion Mobility Spectrometry (IMS) is not a pure mass spectrometric technique, it is important in the field of in-situ investigations – often even as stand-alone device. IMS delivers an ion current as a function of drift time $t_d = L/v_d = L/KE$ in a gas filled electric field E with a given length L and K as gas-phase mobility [Kanu et al., 2008]. The drift time is determined by the size-to-charge ratio depending on the collision cross-section σ. Analogue to the mobility κ (see equation 2.31), a mobility can be derived by the Mason equation:

$$K = \frac{1}{16}\sqrt{\frac{2\pi}{\mu k_B T}}\frac{Q}{n\sigma} \tag{2.64}$$

with the ion charge Q, the drift gas density n, the temperature T and the reduced mass μ [Davis et al., 2012]. This mobility can be considered as a characteristic velocity used for separation. This separation varies for different instruments and is not necessarily unambiguous, since there may be several species with same or similar drift time. Figure 2.14 demonstrates the principle of time wise separation according to the size-to-charge ratio.
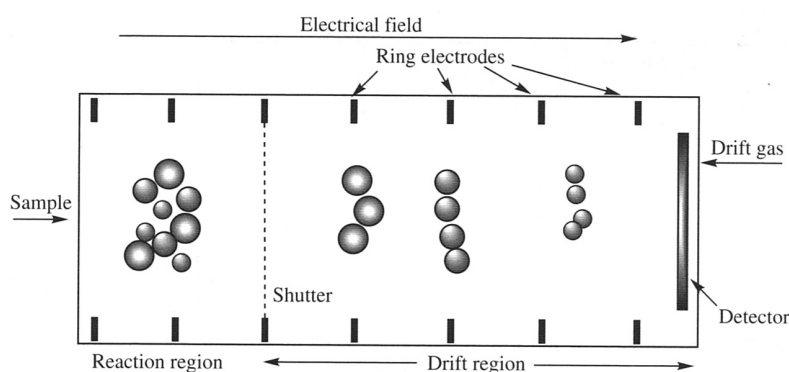

Figure 2.14.: Simple configuration of an IMS [Dass, 2007]: the sample is introduced into the reaction region and transported into the drift region at a given time, where the different species are separated according to their space-to-charge ratio by the electric field and the opposite direction drift gas. Instead of the direct detection the IMS may be attached to an MS and hence deliver the mobility and mass information.

MS may be used as next level analysis stage, where structure sizes and pressures in IMS are oftentimes such, that the time sequence for separated species is too fast for many MS [Tang et al., 2007]. For this reason time-of-flight mass spectrometers are a quite good choice for coupling to

IMS [Ibrahim et al., 2015]. IMS can be also operated in a scanning mode with a electric field pattern allowing only one species to pass, while others may be lost [Gaspar et al., 2009], or as filter in Field-Ion Spectrometry (FIS) with one type of ion transmitted continuously [Guevremont and Purves, 1999]. This is realized by a high-frequency asymmetric waveform as electric field. The instruments can be built compact and hand-held, ideally suited for field-application such as detection of of low traces of chemicals, e.g. explosives [Makinen et al., 2011], as well as clinical diagnostics [Chouinard et al., 2016].

2.7. High Performance Mass Spectrometers

High performance in mass spectrometry may refer to a single outstanding capability or to a collective strength of an instrument. In this work high performance is defined by a mass resolving power of $R_m > 100000$, a mass accuracy of $\delta m/m <$ ppm, a mass separation power of $R_s > 10000$, a repetition rate of $f_{rr} > 100\,\text{Hz}$, as well as a reproducible and stable operation for $> 1\,\text{h}$. These criteria may enable measurements with an enhanced level of identification, qualification and/or quantification and thus offer distinguished analytical information. The knowledge of a mass as exact as possible can promote e.g. the understanding in nuclear physics [Scheidenberger, 2005] or the clarification of biological compounds [Schober et al., 2011] (see figure 2.15). High mass resolution can help to distinguish isobaric species and isotopic patterns in high mass molecular isobars and may help for a clear identification of samples. This is relevant in many fields of application, such as clinical and forensic toxicology with drug screening [Ojanpera et al., 2012], identification of explosives [Makinen et al., 2011], as well as high spatial and mass resolved mapping of compounds in biological tissue [Roempp and Spengler, 2013].
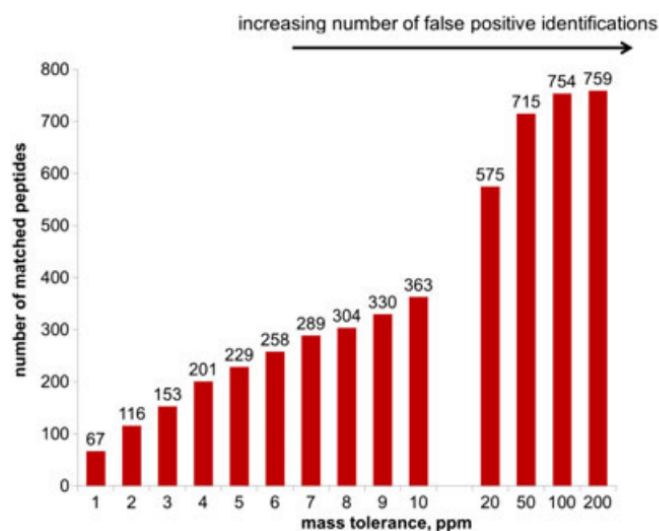Further, high performance mass spectrometry would be highly desirable for many in-situ application.

Figure 2.15.: Number of matched peptides of a complex sample versus the tolerance of the mass value used for matching. [Schober et al., 2011]

2.7.1. Ion Cyclotron Resonance Mass Spectrometry

Ion Cyclotron Resonance (ICR) mass spectrometry is the most often used high performance technique. It is based on a Penning trap, which is a combination of the geometry of a Paul trap with a constant magnetic field and offers two fundamental methods for precise mass measurement as described below [Kluge, 2013].

The ion movement in Penning traps is important for the understanding of the mass measurement. Ions with a velocity $v = \omega r$ experience a centrifugal force of $F_c = mrv^2$ equal to the Lorentz force of a pure magnetic field $F_L = QvB$. This causes the cyclotron frequency

$$\omega_c = \frac{Q}{m}B \tag{2.65}$$

with direct dependence on the mass-to-charge ratio. In a Penning trap the additional electrostatic field by cylindrical hyperbolic surfaces is superimposed and confines this movement in axial direction [Brown and Gabrielse, 1986] and describes harmonic oscillations with the following frequencies. The oscillation in the axial z-direction is given by

$$\omega_z = \sqrt{QU/md^2} \tag{2.66}$$

with the characteristic length of the trap d and the applied voltage U. The presence of quadrupolar fields causes the simple cyclotron motion to split into the reduced cyclotron frequency

$$\omega_+ = \frac{\omega_c}{2} + \sqrt{\frac{\omega_c^2}{4} - \frac{\omega_z^2}{2}} \tag{2.67}$$

and the reduced magnetron frequency

$$\omega_- = \frac{\omega_c}{2} - \sqrt{\frac{\omega_c^2}{4} - \frac{\omega_z^2}{2}} \tag{2.68}$$

For masses up to several thousand u is $\omega_+ >> \omega_-$ and thus the magnetron frequency independent on the mass-to-charge ratio.

In Fourier Transform Ion Cyclotron Mass Spectrometry (FT-ICR) the induced image charge [Comisarow and Marshall, 1974, Shubina et al., 2013, Marshall and Verdun, 1990] from the reduced cyclotron oscillation is detected from segmented cylindrical electrodes, amplified and Fourier transformed [Marshall et al., 1998]. This non-destructive technique does not affect or disturb the ions when passing the mass spectrometer. The effect of image charge can be enhanced by prior resonant dipole excitation [Chen and Marshall, 1987] to bring the charged ions closer to the electrodes and line up on resonance. Substitution of ω_c and ω_z into equation 2.68 prompts the mass-to-charge ratio

$$\frac{m}{Q} = \frac{B}{\omega_+} - \frac{U}{2d^2\omega_+^2}. \tag{2.69}$$

with FWHM of the measured frequency [Marshall and Verdun, 1990]

$$\Delta\omega_+ \approx 1.2\frac{2\pi}{t_{meas}}. \tag{2.70}$$

The resulting performance is quite outstanding: 3.5 million mass resolution has been achieved with a 14.5 Tesla superconducting magnet and typically 0.1 ppm mass accuracy. The time for acquisition varies from some tenths of seconds to around 1 s for an average performance [Marshall and Hendrickson, 2008, Hendrickson et al., 2015]. Measurement in a Penning trap with very close by masses can shift the resulting frequency [Easterling et al., 1999] due to an addition of their individual frequencies [Hofstadler et al., 1994]. Thus resulting in a wrongly measured mass-to-charge ratio. The large size, weight and sensitivity of the utilized magnets, as well as strong vacuum requirements for long measurement times hinder high performance FT-ICR to support any in-situ measurements outside of the laboratory. Nevertheless, heavy but mobile devices with permanent magnets have been developed with mass resolving power of $R_m > 70000$ [Mauclaire et al., 2004].

In Time-of-Flight Ion Cyclotron Resonance (TOF-ICR) mass spectrometry an excitation mode is used to increase the kinetic energy for an extraction process that leads to shorter extraction times in the case of perfect resonance. A clear elaboration is given for instance in [Bollen et al., 1990, König et al., 1995]: A resonant bipolar excitation of the magnetron motion is applied and followed by a quadrupolar excitation with cyclotron frequency so that the excitation is converted from magnetron to the reduced cyclotron oscillation. In case of the correct excitation resonance frequency, the energy is converted best possible and results in an increased magnetic momentum

$$\mu = \frac{K_r}{B} \qquad (2.71)$$

by the radial kinetic energy

$$K_r = \frac{mr^2\omega^2}{2}. \qquad (2.72)$$

During the extraction, the ions couple to the fringing field of the magnet ($\delta B \delta z$) and experience an acceleration force $F = \mu \cdot \delta B \delta z$ that minimizes the time-of-flight in dependence on the applied resonance frequency. The characteristic pattern allows to determine the excitation frequency with an FWHM of [König et al., 1995]

$$\Delta v \approx 1.1 \frac{1}{t_{meas}}, \qquad (2.73)$$

which shows the urge of a long measurement time for highest mass resolving power. Mass accuracy ranges to $\delta m/m \approx 10^{-8}$. For a correct determination of the mass only a single species is allowed in the trap to avoid systematic errors by ion-ion interaction. This is usually achieved with a second Penning trap dedicated for purification. Their working principle is similar, but an additional buffer gas cooling is applied. While the reduced cyclotron motion is damped faster than the magnetron motion, only ions meeting the conversion from magnetron to reduced cyclotron frequency are sufficiently cooled for the transport into the mass measurement trap. Even though TOF-ICR is very powerful, there are the same reasons like for FT-ICR why this technique is not suited for field deployment.

2.7.2. Orbitrap

Originally invented as a purely electrostatic ion trap [Kingdon, 1923], special electrode shapes allow to use such a trap as a mass analyzer as well [Makarov, 2000]. Therefore, the oscillation

frequency along the z-axis has to be independent of the velocity and position, which is realized by a special inner and outer electrode shape (see figure 2.16).
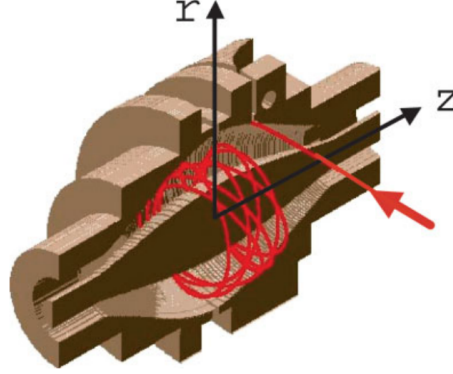

Figure 2.16.: Cutaway view of the Orbitrap mass analyzer [Hu et al., 2005]; injection into the Orbitrap with velocity perpendicular to z-axis indicated by red arrow and displacement from $z = 0$, that results in potential energy causing harmonic oscillation in z-direction.

The frequency along the axis is given by

$$\omega_z = \sqrt{k_{Orbi} \frac{Q}{m}} \tag{2.74}$$

with a geometric constant k_{Orbi} determined through r_1 and r_2 the maximal radii of the inner and outer electrode surfaces, as well as the radius of the electric field $r_m > r_2\sqrt{2}$:

$$k_{Orbi} = \frac{2U}{r_m^2 \ln \frac{r_1}{r_2} - \frac{1}{2}(r_2^2 - r_1^2)}. \tag{2.75}$$

An image current can be measured at the segmented outer electrode and a Fourier transformation leads to a frequency spectrum that can be converted into a mass-to-charge spectrum. The mass resolving power of

$$R_m = \frac{m/Q}{\Delta(m/Q)} = \frac{\omega_z}{\Delta\omega_z} \approx \frac{1}{4.8\pi}\sqrt{k\frac{Q}{m}}t_{meas} \tag{2.76}$$

with $\Delta\omega_z = \Delta\omega_+$ from equation 2.70 decreases with mass as shown in figure 2.18. Nevertheless, Orbitrap mass spectrometers are very powerful with an ultimate mass resolving power in excess of $R_m = 1000000$ and typical mass accuracy of $\approx$ ppm [Hu et al., 2005]. Orbitrap devices can be more compact than ICR, but they are mostly applied with a prior ion trap for filtering and injection. Also here, vacuum requirements, sensitivity and needed infrastructure do not allow for an in-situ measurement in non-laboratory fields.

2.7.3. Multiple-Reflection Time-of-Flight Mass Spectrometry

First time-of-flight instruments were developed many years ago [Cameron and Eggers, 1948] and are still state of the art, because of their fast, sensitive and precise measurement capabilities (see

section 2.2.2). While the early instruments offered only poor mass resolution, the improvement by two-stage ion sources [Wiley and McLaren, 1955] and reflectors [Mamyrin et al., 1973] or electric sectors [Poschenrieder, 1972] lead to competitive capabilities with rather simple technical requirements.

The hybrid combination of a quadrupole with buffer gas cooling as injection trap and a time-of-flight analyzer [Tolmachev et al., 1997, Plass et al., 2007a] offers an optimized initial phase space and a high duty cycle. A proper reduction of the temporal spread of the ions results in increased resolution and accuracy. The next level of performance enhancement is achieved by multiple-path time-of-flight mass spectrometers that make use of a folded flight path. Figure 2.17 illustrated different implementations of mass spectrometers. Closed path [Wollnik and Przewloka, 1990,
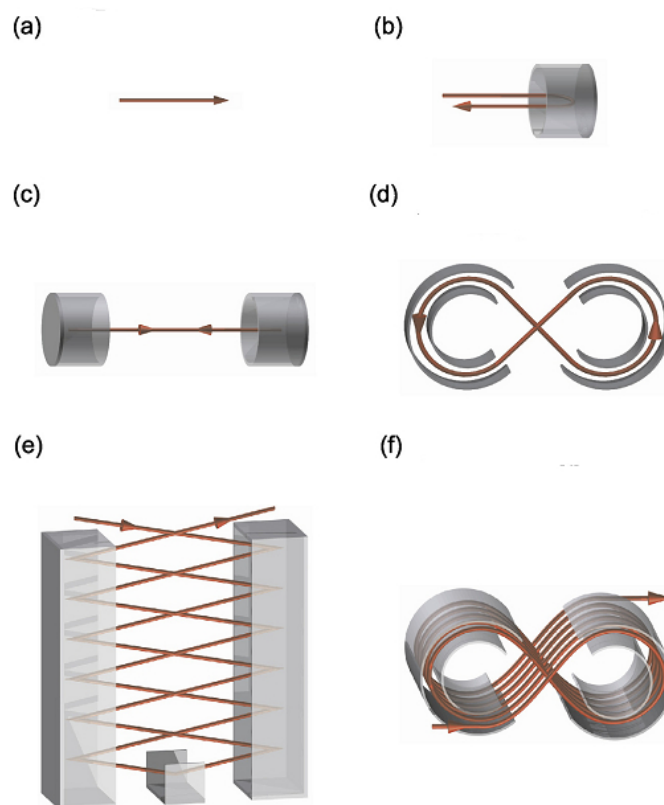

Figure 2.17.: Schematic view of different types of analyzers for time-of-flight mass spec-spectrometers (TOF-MS) [Plass et al., 2013b] : (a) linear TOF-MS [Cameron and Eggers, 1948], (b) single reflection TOF-MS [Mamyrin et al., 1973], (c) multiple-reflection TOF-MS with closed path [Wollnik and Przewloka, 1990], (d) multiple-turn TOF-MS with closed path [Okumura et al., 2004], (e) multiple-reflection TOF-MS with open path [Yavor et al., 2008a], (f) multiple-turn TOF-MS with open path [Satoh et al., 2005].

Okumura et al., 2004] and open path [Yavor et al., 2008a, Satoh et al., 2005] devices exist, while closed path designs require an electrical switching of potentials for injecting into and ejecting from the analyzer. They all differ in mass resolving power, mass accuracy, mass range, measurement

duration, complexity and reliability. In any case, the mass resolving power for a repetitive flight path MS can be described by

$$R_m = \frac{m}{\Delta m} = \frac{t}{2\Delta t} = \frac{t_0 + N \cdot t_{turn}}{2\sqrt{\Delta t_0^2 + (N \cdot \Delta t_{turn})^2}} = \frac{t_0/N + t_{turn}}{2\sqrt{\left(\frac{\Delta t_0}{N}\right)^2 + \Delta t_{turn}^2}}$$ (2.77)

with a default time-of-flight t_0 (without additional turns or reflections), the time t_{turn} for a single turn or reflection and the corresponding errors Δt_{turn}. N denotes the number of turns. For $N \to \infty$ the expression becomes independent on the initial time error Δt_0. The achieved mass resolving power for multiple-reflection devices is commonly $R_m > 10^5$ with a mass accuracy of $\delta m/m < 10^{-6}$ at typical measurement duration of $\approx 10\,\text{ms}$ [Dickel et al., 2015b, Wolf et al., 2013, Schury et al., 2014b]. The mass resolving power is not depending on mass, which is of great advantage especially for higher masses ($m >> 1000\,\text{u}$) compared to other high performance MS (see figure 2.18). As well, high transmission efficiency and high dynamic range ($\approx 10^6$) are common.

Open path instruments offer a higher simultaneous mass range, but are limited in mass resolution due to their complicated ion optical geometries and induced field aberrations. Nevertheless resolving powers $R_m > 30000$ have been recorded [Shimma et al., 2010]. Closed path devices on the other hand offer principally unlimited flight path, but have a limited mass range through necessary switching of fields. The unambiguous mass range is restricted to ions with the same number of turns in the first place. This leads to a the following estimation of mass range:

$$\frac{m_{max}}{m_{min}} < \left(\frac{N+1}{N}\right)^2 .$$ (2.78)

This mass range may be expanded by iterative or descriptive computation of resulting time spectra [Ishihara et al., 2005, Nishiguchi et al., 2009, Schury et al., 2014a]. Also, a subsequent scanning operation can provide full mass range by stringing together single spectra of neighboring mass range. A mass-selective scanned RF injection [Plass et al., 2007a] ensures thereby highest sensitivity.

In this work, a sweeping method for mass range extension and calculative disentanglement are proposed (see sections 3.4 and 3.5).

Applications of multiple-turn/reflection TOF-MS in nuclear physics are widely spread and lead from isobar separation [Wolf et al., 2012, Plass et al., 2007b, Dickel et al., 2015b, Jesch et al., 2015] to direct mass determination [Ishida et al., 2005, Dickel, 2010, Wienholtz et al., 2013, Plass et al., 2013a, Purushothaman et al., 2013] and also separation of isomeric states [Dickel et al., 2015a]. Analytical application of multiple-turn/reflection TOF-MS range from MALDI-MS [Okumura et al., 2004], imaging MS [Hazama et al., 2008], ESI-MS [Yavor et al., 2008b], environmental science [Shimma et al., 2012], tandem MS [Toyoda et al., 2007] as well as 2D tandem MS [Verentchikov et al., 2005]. Early developments of miniaturized multi-reflection TOF MS have been even engaged for space missions [Balsiger, 2007, Matsuo et al., 1999].

So far, there is no multiple-turn/reflection TOF-MS offering highest performance dedicated for in-situ analytical application. Up to now, there has been an incongruity of field-suitability and high performance. Highest mass accuracy and resolving power is gained by closed path devices only, especially by coaxial multi-reflection time-of-flight mass spectrometers. This geometry allows

for precise manufacturing and thereby rather ideal electrical fields. The injection and ejection is possible with comparably less deteriorating effects, the system is reliable, compact and can be easily scaled. Further, the short measurement cycle brings a low rate of collisions with residual gas, thus pumping power can be rather low. Enough reasons to claim a coaxial MR-TOF-MS as an excellent instrument for in-situ high performance mass spectrometry [Lang et al., 2012, Dickel et al., 2013, Plass et al., 2016].
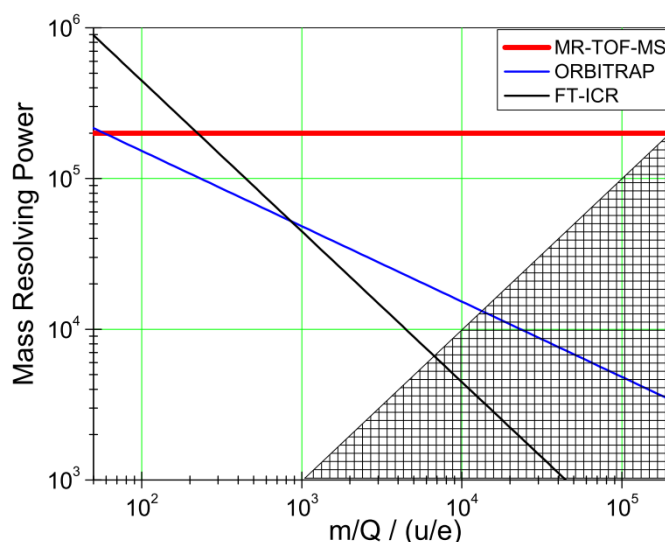

Figure 2.18.: Comparison of resolving power (FWHM) for $t = 1\,\text{s}$ measurement time as function of mass-to-charge ratio [Dickel, 2010]; multiple-turn/reflection time-of-flight mass spectrometer, standard Orbitrap and 7 Tesla FT-ICR mass spectrometer. In hatched region the mass resolving power is not sufficient to resolve equal intensity peaks with mass difference of 1 u.

2.8. Fields of Application

Mass spectrometry is employed by a multitude of scientific, industrial and life science applications. Originally developed for nuclear physics experiments, mass spectrometry became an essential tool for issues like security, nutrition, environment, as well as medicine and is a living example of important cross fertilization [Scheidenberger et al., 2014, Spengler, 2011].

Nuclear and Atomic Physics

Mass spectrometry contributes to many fundamental studies. These range from research of nuclear interactions and nuclear structure [Scheidenberger, 2005, Blaum, 2006, Lunney et al., 2003, Blaum et al., 2013], to nuclear astrophysics with production and abundance of nuclides in our solar system [Mathews, 2008, Schatz, 2013, Block, 2013], as well as fundamental studies testing the Standard Model [Eronen and Jokinen, 2013, Alanssari et al., 2015] and investigation of properties of exotic

nuclei [Walker et al., 2013]. Figure 2.19 illustrates aspects of fundamental nuclear research, which includes the genesis and organization of the universe from elemental particle to galaxy, as well as the existence and production mechanisms of nuclear species. These studies are oftentimes

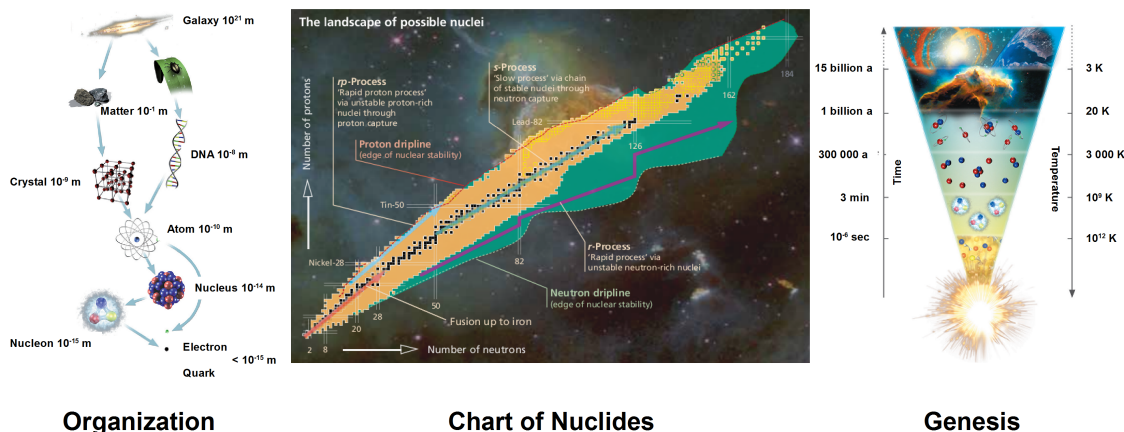**Organization**   **Chart of Nuclides**   **Genesis**

Figure 2.19.: Fundamental aims of nuclear research (adapted from [KHuK, 2012] and [FAIR, 2013]): organization, scales and interaction from elemental constituent to galaxy, chart of nuclides with production and decay pathways, as well as development of the universe and prevailing conditions. Mass spectrometry is a driving force to answer these fundamental questions.

performed in conjunction with exotic nuclides produced by nuclear production mechanisms and handled at accelerator facilities [Langanke and Schatz, 2013, Blumenfeld et al., 2013]. Mass measurements of relativistic ions are usually carried out in ion storage rings as fairly large mass spectrometers [Geissel et al., 2006, Franzke et al., 2008, Chen et al., 2010, Litvinov et al., 2013] or slowed down by a dedicated stopping of the ion beam in matter for further investigation [Geissel and Scheidenberger, 1998, Winfield et al., 2013, Purushothaman et al., 2013, Reiter et al., 2015]. Highest mass precision measurements enable also application in atomic and molecular physics, where slightest variations of the mass give even access to the low energy regimes of ionization and binding of atoms and molecules. Main challenges in this field are short lifetimes of unstable nuclides, small production yield and contamination by more abundant species. This needs to be addressed by new separation and fast mass measurement techniques.

Inorganic Mass Spectrometry

The inorganic mass spectrometry is applied for multielemental determination and isotope ratio measurements at trace and ultratrace level, as well as surface analysis by means of depth profiling and imaging for a variety of materials. Samples may stem from technical, environmental, biological or geological areas, as well as space missions. Detection limits may be below ng/g for solid and below pg/L for aqueous samples [Becker and Dietze, 2000, Synal, 2013, Bhardwaj and Hanley, 2014]. Sensitive and mobile techniques can improve studies by immediate results at the place of investigation.

Organic Mass Spectrometry

Organic mass spectrometry is oftentimes devoted to structure elucidation, de novo structure determination by accurate mass and reference spectra, the identification of unknown compounds, molecular formula from accurate mass values, as well as characteristic fragmentation for the classes of compounds [Gross, 1994, Dass, 2007]. In conjunction with the mass value, also elemental composition and fragmentation patterns are used. Typical fragmentation finger prints by MS/MS can reveal many classes of organic molecules.

Petroleomics

Petroleomics is the study of geographical origin, distillation and extraction methods, as well as the chemical composition of crude oil [Marshall and Rodgers, 2004, Rodgers et al., 2005]. For an identification of complex high mass molecules with multiple mass lines a high performance (often in conjunction with selective ionization) is indispensable. A mass resolving power of $R_m >$ 300000 e.g. offers the identification of more than 10000 elemental compositions [YunjuCho et al., 2015, Marshall and Hendrickson, 2008].

Forensic and Security

Many analytical techniques are applied to forensic and security application [Urabe et al., 2014, Makinen et al., 2011, Roennfeldt and Koenig, 2010]. The challenge is the quantification, the determination of trace substances and the identification of unknown substances. While the preparation and extraction of the sample is of great importance, recent methods even allow direct sampling from surfaces, e.g. to sample directly from the skin of individuals [Kabir et al., 2013, Wiley et al., 2013b]. The identification of targeted substances is regularly needed, such as drugs [Ojanpera et al., 2012, Menga et al., 2015, Tominagaa et al., 2015], explosives and hazardous compounds [A.Contreras et al., 2008, Chen et al., 2013b, Patel and Ahmed, 2015, Makinen et al., 2011]. Portable devices are thereby the key for prevention and counter-terrorism [A.Contreras et al., 2008, Urabe et al., 2014].

Mass Spectrometry Environmental Application

Environmental application of mass spectrometry involves basic research studies and daily use for monitoring issues like the screening for hazardous substances in food and other goods [Turner et al., 2015, Bottoni and Caroli, 2015, Ibanez et al., 2015], the search for environmental and climate agents [Young et al., 2011, Petrie et al., 2015], as well as tracing the flow of pollutants, fluids and gases over large geographical scales, leading to conclusions of anthropogenic influence to environment and climate change [Lindahl et al., 2010, Levin and Aeschbach-Hertig, 2004, Ghosh and Brand, 2003, Oxburgh et al., 2007]. Investigations of e.g. aerosols by high resolution MS allow a simultaneous elemental analysis of a multitude of constituents and can be used to map the composition for each location of probing [Wozniak et al., 2008, Kuerten et al., 2007]. Mass spectrometry helps to understand the 'environmental digestion', transition of substances and the

influences on biology [Gavina et al., 2014] or the remnants of drugs and their metabolites in environment [Bottoni and Caroli, 2015, Petrie et al., 2015].

High performance MS so far is only provided in laboratories – with the circumstance that samples have to be delivered there. Portable and robust instruments with atmospheric ion sources provide immediate results and less risk of sample transition.

Biological Mass Spectrometry

With increasing performance and mass accuracy even more complex systems of molecules, elemental composition and the structure and reaction pathways can be studied, as well as biological processes and metabolism of organisms (Metabolomics) [Iliuk et al., 2014, Crick and Guan, 2016, Marshall and Hendrickson, 2008]. Figure 2.20 shows the main columns of biological existence from the atomic and molecular level to complex macromolecules.
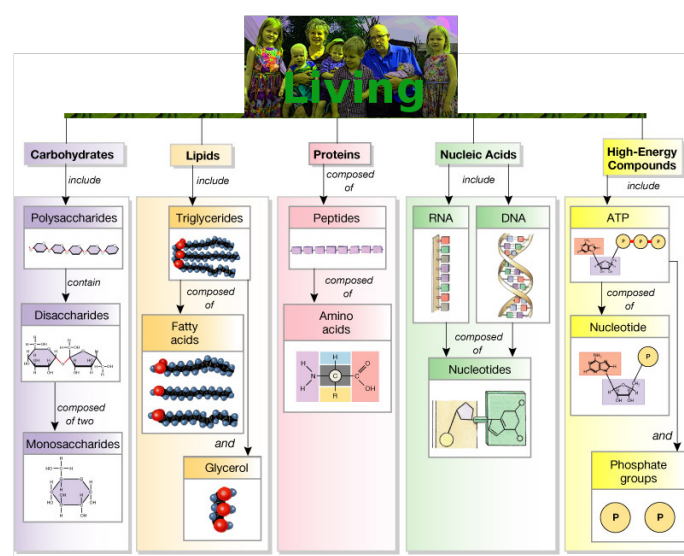

Figure 2.20.: Hierarchy of (macro)molecules that dominate our living (adapted from [Criticals, 2015]): carbohydrates, lipids, proteins, nucleic acids and high-energy compounds, as well as the composition they are made of.

Proteomics

Proteomics is the study of proteins, their expression, functions and changes under biological perturbation [Hauser et al., 2012]. Mass spectrometry has become a pivotal tool, with highest mass accuracy to identify proteins in complex mixtures and determine their structure and composition [Liu et al., 2009], as well as MS/MS studies are sensitive to their formation [Zhou and Wysock, 2014]. Proteomics may follow the bottom-up approach by mass spectrometric investigation of sequences from a prior tryptic digestion, or it may follow the top-down approach with high-resolution MS or MS/MS of intact protein molecules. In case of the study of unknown proteins, the so-called de

novo protein sequencing relies on the interpretation of MS/MS spectra. Mass spectrometry is also engaged in quantitative proteomics, that can help to estimate the state of biomarkers in clinical diagnostics. [Wilkins et al., 1996, Anderson and Anderson, 1998, Aebersold and Mann, 2003, Nelson and Cox, 2005, Biemann, 2014]

Lipidomics

The research of the entire cellular lipidome, the expression and functionality is called lipidomics [Hauser et al., 2012]. Mass spectrometry is, besides Nuclear Magnetic Resonance (NMR) the driving force in lipidomics, similar to proteomics, enabling high quality and high throughput results to categorize lipids, understand their presence and functionality and to discover structural information. Mass spectral data and MS/MS experiments can reveal information that is not accessible in other techniques. E.g. the position of double bonds in unsaturated fatty acids, that may not be determined by chromatographic methods alone. [Wang et al., 2015, Teo et al., 2015, Nelson and Cox, 2005, Vekey et al., 2008]

Characterization of Oligonucleotides and Oligosaccarides

Oligonucleotides and oligosaccarides arrange in higher order structures often in conjunction with other biomolecules (see figure 2.20) [Nelson and Cox, 2005, Dass, 2007]. Mass spectrometry is used to determine their composition and structure by means of accurate mass values, database comparison, directed cleavage of bonds and analysis of residues. MS is one key tool and strongly combined with other analytical techniques (as gel-electrophoresis and chromatography) and dedicated extraction and preparation (as physical processing and enzymatic digestion) [Zaia, 2004, Gavina et al., 2014]. A flexible coupling and high compatibility of the MS makes it an universal tool for these studies.

Medical Mass Spectrometry

Manifold medical applications originate from biological research and mass spectrometry [Chouinard et al., 2016] and there are numerous for the established clinical diagnosis and treatment [Khardori, 2014, Patel and Ahmed, 2015].// Cancer research is one main stream of modern clinical mass spectrometry application [Roboz, 2002, Vekey et al., 2008]. MS is used in the whole chain in cancer research, from diagnostics to its genesis, understanding and treatment. So it is involved in the synthesis of pharmaceuticals, metabolomics with cancer biomarker identification, in-vitro experiments, as well as histological, imaging and biopsy studies [Patel and Ahmed, 2015, Roempp and Spengler, 2013]. Further, there are intra-operative diagnostics based on mass spectrometry [Takats et al., 2012] with surgical tools serving as source of mass spectrometric samples. Note, that these investigations are done in-vivo, without any dedicated preparation of tissue. Thus, it MS avoids any time overhead, mistreatment or additional stress to the patient. Figure 2.21 demonstrates the application during a tumor resection. // Further fields of medical mass spectrometry are: diagnostic microbiology for infectious diseases [Khardori, 2014]; identification and quantification of biomarkers [Teo et al., 2015, Iliuk et al., 2014, Calderon-Santiago et al., 2014]; neona-
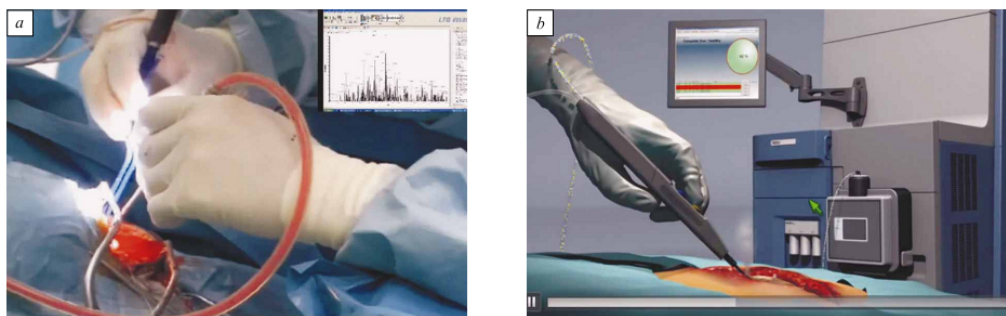
Figure 2.21.: Rapid evaporation ionization mass spectrometry as tool to guide through a surgical intervention for the removal of a tumor [Takatz, 2013, Lebedev, 2015]; with a conventional electro-surgical instrument ions can be transferred to the MS via a flexible tube resulting in a mass spectrum (a), which can be processed within a few seconds to distinguish the state of the tissue (tumor or intact) and prompt this information to the surgeon (b).

tal research [Denes et al., 2012, Oliveira et al., 2014]; Lipidomics to study tuberculosis and leprosy [Crick and Guan, 2016]; breath analysis for the detection of disease biomarkers and potential hazardous exposure [Kapishon et al., 2013, Kurada et al., 2015]; in-vivo local analysis and tissue imaging [Nemes and Vertes, 2012, Wu et al., 2013, Cillero-Pastor and Heeren, 2014]; mapping of e.g. calcium content in bones [Henss et al., 2013]; toxicology and endocrinology [Strathmann and Hoofnagle, 2011].

Generally, MS is often combined with complementary techniques. This also opens many clinical application like coupling capillary electrophoresis to mass spectrometry to detect bladder cancer [Latosinska et al., 2013] or the combination of liquid chromatography to tandem MS for routine clinical diagnostics [Leung and Fong, 2014].

While powerful stationary systems can be established for ex-vivo and laboratory measurements, in-vivo studies e.g. during surgeries do not allow for bigger mass spectrometers in the room of treatment. That is why in-situ suitable, mobile and hygienic MS are necessary.

3. Concepts for In-situ High Performance MR-TOF-MS

This chapter describes the concept of the mobile high performance multiple-reflection time-of-flight mass spectrometer for in-situ application, the role of the individual subsystems, as well as aspects of their design.

3.1. In-situ High Performance Mass Spectrometry

In the previous chapter in-situ mass spectrometric methods, as well as high performance mass spectrometry have been introduced. High performance mass spectrometers are usually stationary, have a long set up time, are sensitive to environmental conditions and most often need laboratory infrastructures. In-situ mass spectrometers are hand-held or portable and easy to use, but offer only low performance and can be restricted to specific application. The combination of both – high performance and in-situ capability – means an outstanding innovation.

The mobile MR-TOF-MS offers high mass resolved and high accurate mass determination and makes therefore valuable information on constituents and structure of in-situ generated samples available [Lang et al., 2013]. In addition, it offers information with unprecedented selectivity by means of high mass-resolved precursor selection for MS/MS experiments. Highest performance parameters enable non-targeted studies and may even overcome analytical sample preparation or complementary methods, thus enhancing the in-situ aspect of the instrument.

3.2. Mass Spectrometer

The instrument is based on the combination of linear RFQ traps with applied buffer gas cooling and a multiple-reflection time-of-flight analyzer. The synergy of ion trap and time-of-flight ensures highest duty cycle, high transmission and an optimal formation of a compact initial ion cloud phase space for the time-of-flight dispersion. The multiple-reflection time-of-flight analyzer provides an enormous enlargement of the mass-dispersive flight path (> 1000 m) in a compact format. The concept of this compact MR-TOF-MS is depicted in figure 3.1. Coaxially aligned are the ion inlet capillary, several linear RFQ ion traps, the symmetric multiple-reflection time-of-flight analyzer and the detector.
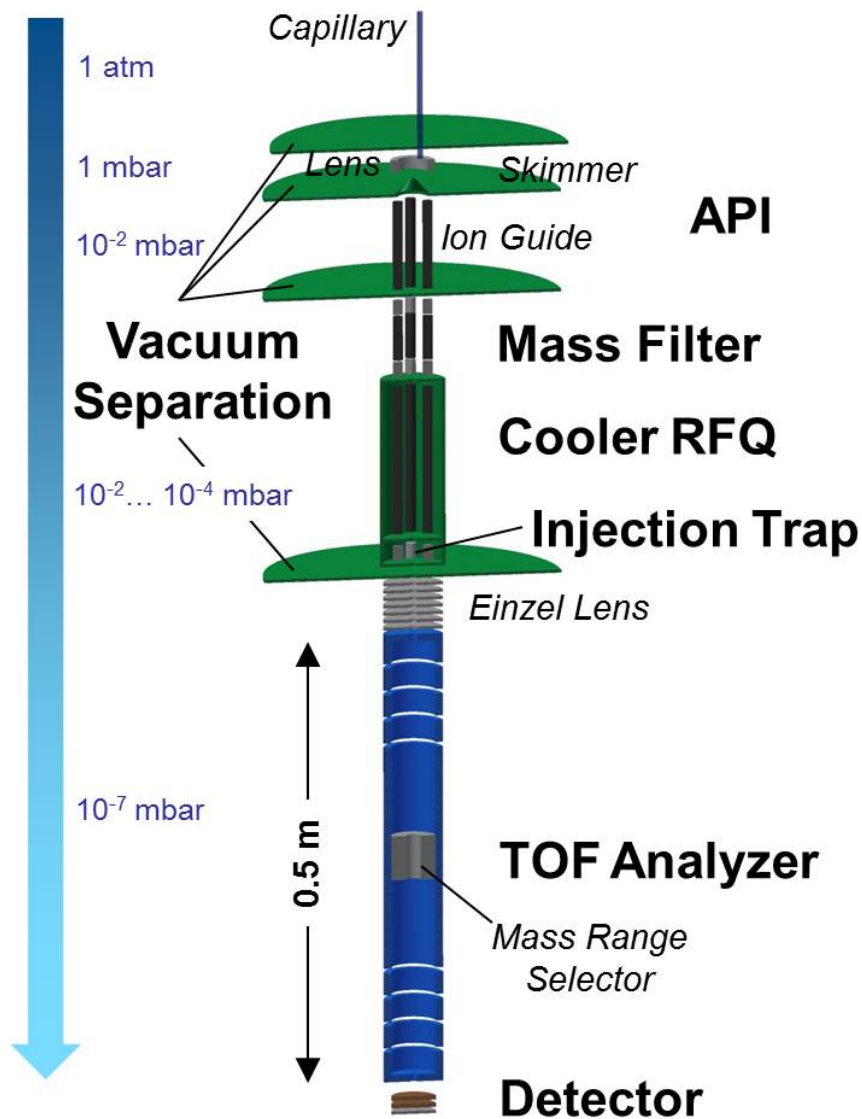
Figure 3.1.: Scheme of the ion-optical setup of the mobile high performance MR-TOF-MS; vacuum separation and according pressures are illustrated, as well as key systems and important units: atmospheric pressure interface (API) to introduce the sample from ambient ion sources, differential pumping, RFQ mass filter, cooler RFQ with attached RFQ injection trap, MR-TOF analyzer with two symmetric coaxial reflectors and time-of-flight detector.

3.2.1. Atmospheric Pressure Interface

The atmospheric pressure interface is the first subsystem of the instrument (see figure 3.1) and introduces ions and aerosols from atmospheric ions sources. Its central function is the transmission of sample into the mass spectrometer and reduction of the load of neutrals from ambient environment (e.g. ambient gas and solvent). A common assembly [Whitehouse et al., 1985, Takats, 2012] has been chosen (see figure 3.2).
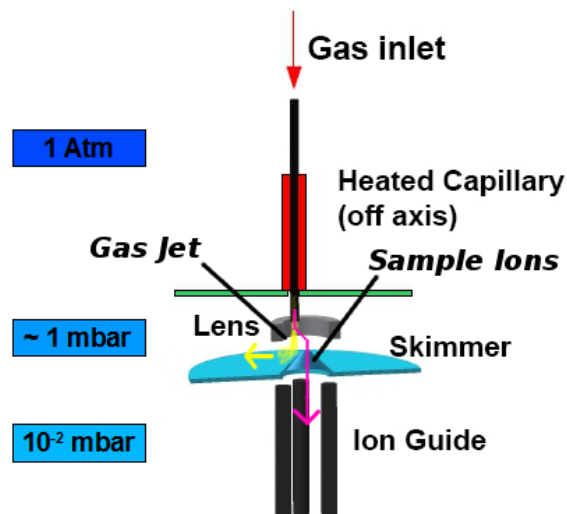

Figure 3.2.: Schematic illustration of the atmospheric pressure interface with prevailing pressures and the heated capillary; the off axis arrangement to the skimmer diverts the incoming gas jet and the lens focuses the sample ions into the open skimmer bore.

A heated stainless-steel inlet capillary functions as first stage of pressure reduction. Heating of this capillary helps to reduce clogging effects and increases ion transmission. Reasonable values for the temperature are $50\,°C$ to $150\,°C$ to reduce depositions and also to prevent thermal reaction on the inner surface at higher temperatures [Page et al., 2007, Guo et al., 2008, Page et al., 2009, Krutchinsky et al., 2015]. The straight forward calculation of the pressure gradient and the resulting gas flow is not feasible, because the mean free path length drastically changes and the pressure regime strikes right through the viscous to molecular flow and according Reynolds numbers (see section 2.2.3). Sophisticated predictions are only possible by simulation studies using Computaional Fluid Dynamics (CFD).

The first vacuum chamber is used as pre-evacuation stage with a direct connection to a roughing-pump. A cone-shaped skimmer with a bore of $1\,mm$ guides sample species into the next vacuum stage and skims unwanted gas load and neutrals sideways to be pumped away. The capillary is arranged with a certain offset perpendicular to beam direction to direct a created gas jet on the skimmer flank, rather than into the open bore. A concentric tube lens compensates for this offset and ensures the ion optical focusing into the next stage.

The following next vacuum chamber is equipped with a turbo-molecular pump and an RFQ-based ion guide confines ions for further transmission. Residual gas load is pumped at this stage to reach

compatible pressures for the remaining mass spectrometer and desired cleanliness. The dimensioning and aspect ratio of the quadrupolar assembly realizes a good flow conductance. Preliminary tests have determined, that typical pressures in that region are low enough to ensure proper operation of the analyzer and turbo molecular pump, as well as provide buffer gas cooling for the transportation in the ion guide.

3.2.2. Beam Preparation System

The beam preparation system is designed to transmit the wanted ion species, to filter unwanted species, to cool the ions and to form compact ion bunches matched for the time-of-flight analyzer (see figure 3.3). In addition, it may serve for first MS/MS experiments and as activation stage of mass-selected species in future experiments [Lippert, 2016]. It comprises an RFQ ion guide, an RFQ mass filter, a cooler RFQ and an RFQ trap. Further, diaphragms and encapsulation provide vacuum separation for the single compartments.

The radio-frequency quadrupole dimension is derived from the ratio $r_c = 1.14511 r_0$ and desired q-values (see section 2.2.1). This depends on the diameter, the applied RF amplitudes and the mass to be transmitted. Since this instrument aims for bioanalytical application, higher masses $m > 200\,\text{u}$ have to be considered. A dimension of $r_c = 8\,\text{mm}$ and $r_0 = 7\,\text{mm}$ is found to be favorable for high transmission of ions in the desired mass range and compatible to technical boundary conditions, such as discharge in moderate vacuum. Figure 3.4 demonstrates the peak-to-peak voltage for the given geometry (see equation 2.21) and the resulting effective pseudopotential (see equation 2.22) for the two different frequencies of the system in order to obtain a stability parameter of $q = 0.15$. The pseudopotentials are similar and both RFQ systems provide transmission of masses $m > 2000\,\text{u}$.

The ion guide RFQ is operated in a standard transmission mode with stable ion trajectories for optimal transmission. A shallow linear potential gradient can be established by conductive RFQ material (compare figure 3.3). The length is determined to have sufficient cooling effect for atmospherically created ions and large gas flow conductance for the pressure reduction.

The mass filter is equipped with two Brubaker lenses to stabilize ion trajectories prior and after the optional mass filtering by an additional DC offset (refer to section 2.2.1.5). The length, the frequency of the RF field, the mass and the kinetic energy limit the maximal achievable mass resolving power (see equation 2.33). The realistic mass resolving power is estimated to $R_m^{RFQ} \approx 100$ and expected to be dominantly restricted by geometric deviations. A characterization of the mass filter is part of a different work [Lippert, 2016]. An arrangement of two subsequent diaphragms prior the filter section is designed to focus the radial distribution of the desired mass and thus provide best initial conditions for filter operation [Dickel and Yavor, 2012]. Simulation studies presented in figure 3.5 show the advantage of this double aperture arrangement [Lippert, 2012a]. A focusing effect is achieved by a more negative potential on the second diaphragm. A slightly enhanced pressure reduction with same transmission values is an additional beneficial side effect for mass filtering, where residual or buffer gas collisions needs to be prohibited. No axial gradient is applied along the mass filter and ions travel unhindered with their kinetic energy obtained by applied DC potentials.

The cooler RFQ is encapsulated and equipped with a buffer gas inlet. The axial dimension is
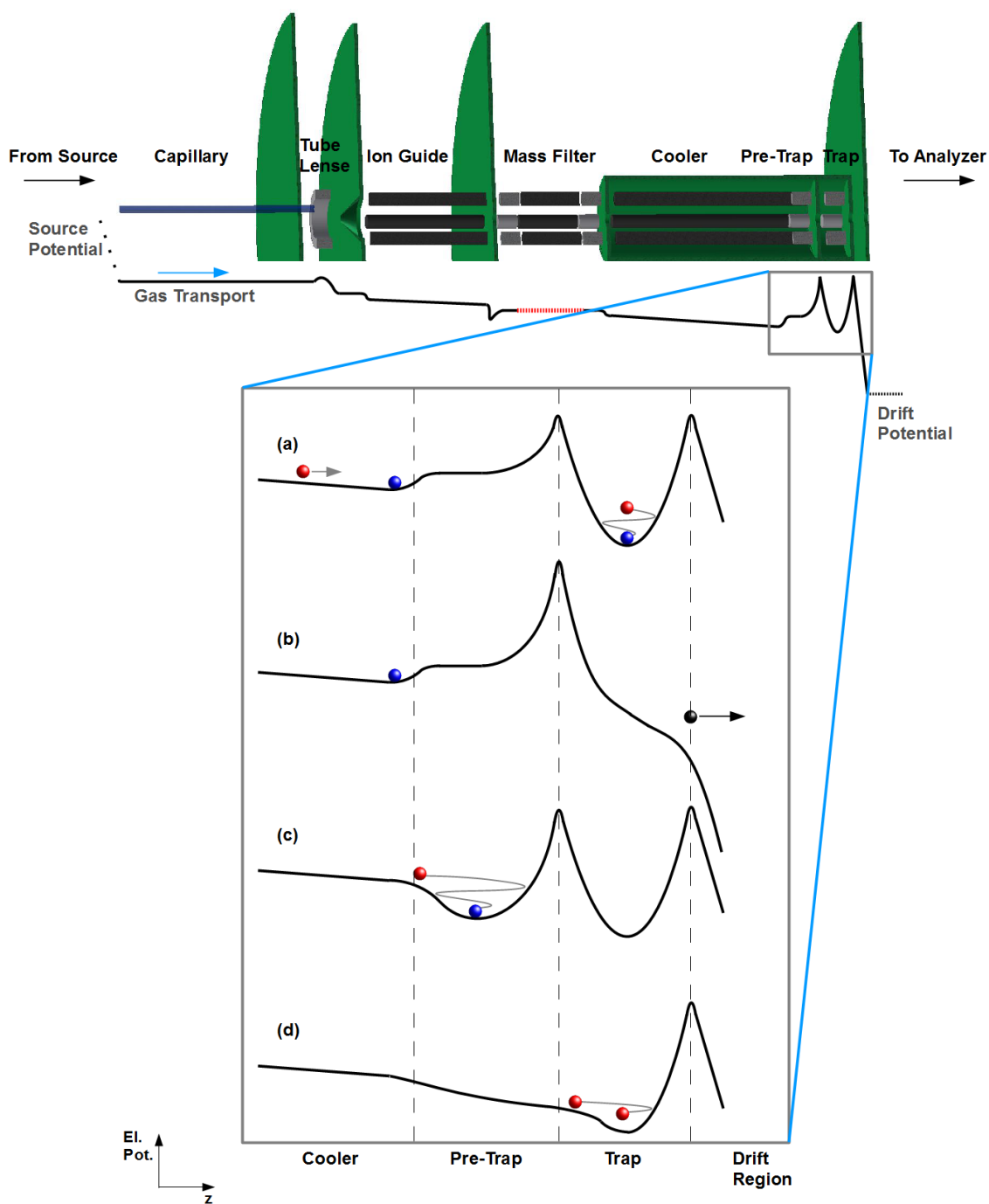
Figure 3.3.: Schematic view of RFQ beam preparation system with illustrated electric axial potentials; (a) to (d) describes individual states in the trap region of one cycle of operation: (a) simultaneous accumulation of ions passing the cooler RFQ and final cooling and bunching in the injection trap, (b) injection of compact ion bunch into the analyzer, (c) formation of accumulated ion packet in pre-trap before transport to trap, (d) transport from pre-trap to trap. The color indicates the level of cooling.
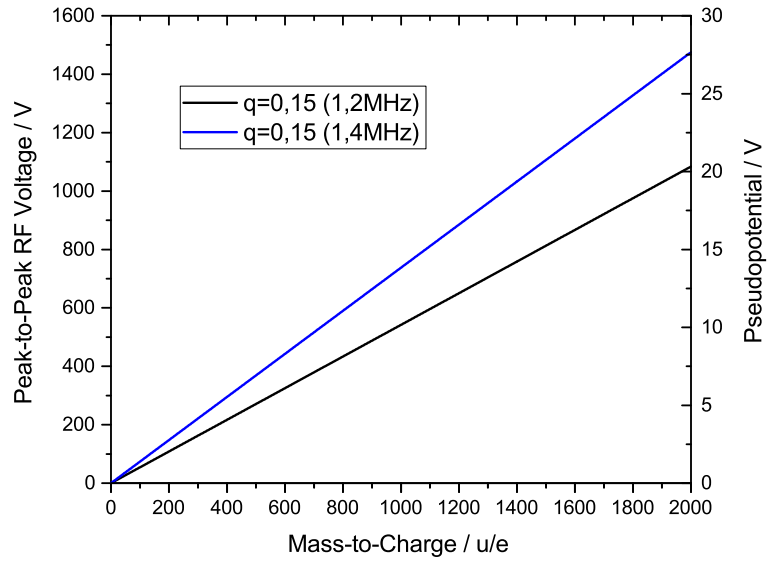
Figure 3.4.: Peak-to-peak voltage and effective pseudopotential to obtain a stability parameter of $q = 0.15$ with an RFQ of $r_0 = 7\,\mathrm{mm}$; the frequencies are chosen according to the resonance frequencies of the real RF voltage setup.
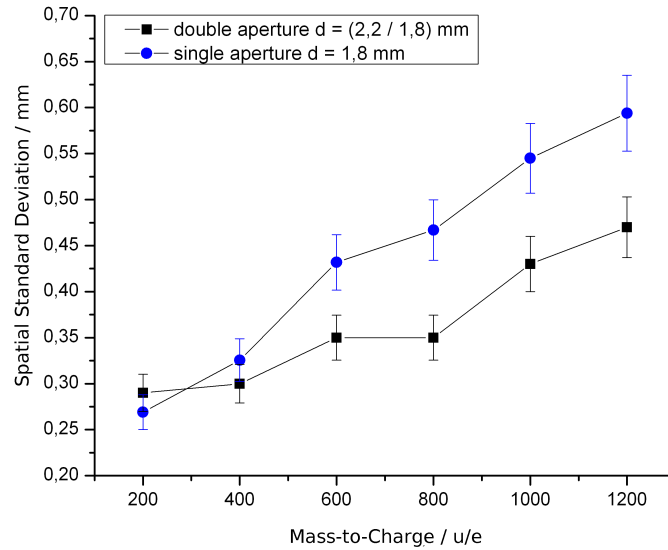

Figure 3.5.: Radial emission into mass filter with an arrangement of two apertures ($2.2\,\mathrm{mm}$ and $1.8\,\mathrm{mm}$ open diameter) arranged in $1\,\mathrm{mm}$ distance and with single aperture $1.8\,\mathrm{mm}$ [Lippert, 2012a]; the radial emission is clearly reduced as highly favorable condition for mass filtering operation.

designed to provide sufficient buffer gas collisions to reduce ion momenta such, that ions lose their kinetic energy and are trapped within the linear potential gradient and accumulated for further processing. This accumulation ensures a duty cycle of 100% for the entire operation cycle.

A short RFQ prior the injection trap (in the following named pre-trap) is a dedicated segment of the cooler RFQ with an individual DC potential (see figure 3.3). The potential of the pre-trap is first used as a potential barrier for continuous ion accumulation and shielding from switched electric fields of the injection trap potential. It is then switched to a lower potential to accumulate ions close to the next aperture and to form an ion packet that is finally transmitted into the trap. The length is long enough to provide shielding and short enough to transmit a broad mass range during the transfer from pre-trap to trap. This pulsed extraction of a quasi mono-energetic ion bunch causes a mass-time-dispersion up to the moment of applying the axial trap confinement. This causes some restrictions in mass range and has been considered in the design and has been extensively investigated by simulation studies shown in figure 3.6 [Wohlfahrt, 2011]. A transmission close to 100% for a mass range of a factor 4 at the transfer from pre-trap to trap is observed.
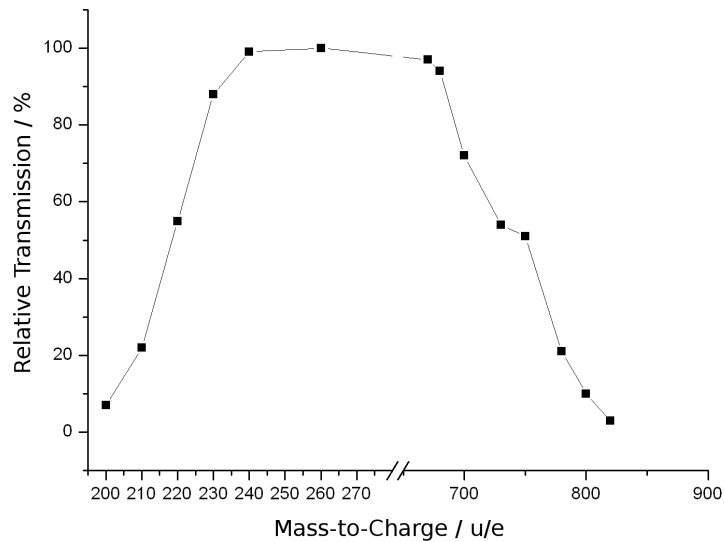

Figure 3.6.: Simulated relative transmission from pre-trap to trap with fixed operation parameters; a mass range as broad as 4 is possible to be transmitted simultaneously [Wohlfahrt, 2011].

The RFQ injection trap is a single linear quadrupole segment between two diaphragms. Such a linear Paul trap arrangement has been used in previous instruments [Plass et al., 2008] to serve as cooling and bunching instance for the delivery of a compact ion cloud into the analyzer. Confinement is provided by axial potentials on the neighboring diaphragms (see figure 3.3) and the radial pseudopotential field. The confinement in axial and radial direction are to some extent competitive. Strong confinement is principally desired, but whenever confinement in one direction is too strong, ions are pushed into the direction of weaker confinement and the ion cloud is formed to a disad-

vantageous phase space. Since the field of axially confining potential penetrates into the mid of the trap, higher voltages also create an additional DC offset of the trapped ions, which determines the kinetic energy in the drift region. The RF voltage which is applied for the cooling process can be switched off during the moment of injection as demonstrated in previous work [Haettner, 2011]. This prevents ions to experience changing electric fields when leaving the trap region, which may lead to errors in the mass calibration.

3.2.3. MR-TOF Analyzer

The multiple-reflection time-of-flight analyzer consists of two identical reflectors (with 4 independent electrodes each) and a drift region in between (compare to figure 3.7 with a single reflector). The principal design is based on [Verentchikov et al., 2005]. Ideally spoken, it provides an isochronous infinite drift length by a folded flight path, ensures periodic focusing of the beam and restores the time-energy focus on the very same position after every turn.

The analyzer of the present work is scaled by a factor of 0.6 from a former instrument [Dickel, 2010, Yavor et al., 2015]. Some loss in performance due to higher relative mechanical as well as ion optical aberrations is accepted in order to realize a more compact instrument. The drift potential is chosen to a negative voltage to leave the ion source at about ground potential. The design kinetic energy is $E_{kin} = 1300\,\text{eV}$. Exact values of geometry and electrode potentials are
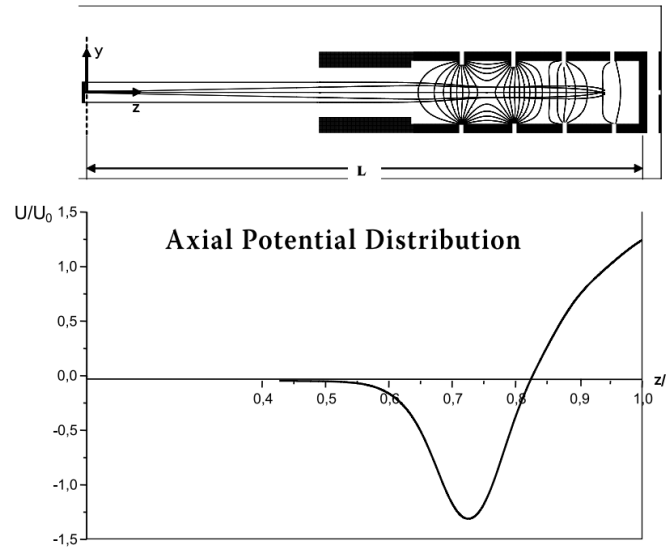

Figure 3.7.: Scheme of four-electrode grid-less mirror with sample ion trajectories, equipotential lines and axial potential distribution [Verentchikov et al., 2005]; U_0 denotes the drift potential of the beam, L the length of the reflector.

derived by a dedicated optimization algorithm [Yavor, 2011].Thereby an iterative process varies either potentials or geometric measures to bring resulting aberration on a requested level.

Ion-optical aberrations can be conveniently described by the 'Giessen notation' [Wollnik, 1986]. A coefficient is generated for each particle beam parameter (*x*, *y*, *a* and *b* as angles in *x*- and *y*-

direction, δ as relative energy spread) according to a deviation of those. These coefficients are denoted by parenthesis. The first term describes the measure the aberrations has effect on, the second term gives the order of contributing parameters. The design of the MR-TOF analyzer is optimized for the following set of aberrations after every reflection:

$$(x|x) = (t|xx) = (t|xa) = (T|aa) = (t|yy) = (t|yb) = (T|bb) = (t|\delta) = (t|\delta\delta) = 0 \qquad (3.1)$$

This implies parallel-to-point focusing from the middle of the analyzer back to the middle after each reflection ($(x|x) = 0$), second order focusing in energy from the primary to the final time focus $(t|\delta) = (t|\delta\delta) = 0$ and second-order time focusing with respect to the spatial coordinates from the middle of the analyzer back to the middle after one full turn (two reflections):

$$(t|xx) = (t|xa) = (t|aa) = (t|yy) = (t|yb) = (t|bb) = 0. \qquad (3.2)$$

3.2.4. Injection Lens and Steerer

An Einzel lens is placed right in front of the analyzer to provide focusing of the injected ion beam. A quadrupolar arrangement of electrodes next to the injection lens can be used to steer the beam in case of possible misalignment in *x*- and *y*-direction. A similar quadrupolar assembly of electrodes is placed in the field free drift region in the middle of the analyzer for the selection of the mass range (see section 3.4), which also has a steering capabilities.
Both together can be used for a two point beam alignment correction [Yavor, 2012]. With a single steering instance the beam may only be sent to a certain point by variation of the angle – or an angle is compensated by an additional offset. The combination of two deflectors however can compensate for a spatial offset and an angle introduced by mutual tilt or shift of the trap, lens and/or the analyzer. Thus, an ideal initial position and angle can be restored in spite of mechanical misalignment. The instance within the analyzer can be used as diagnostic tool for exactly this beam alignment. A measurement scheme has been developed to measure the misalignment and to correct for it. Therefore the lower half of the analyzer is switched off to drift potential, while the beam alignment is studied by the observed transmission during sweeping the ion beam in *x* and *y* direction.

3.3. Operation Modes

The combination of RFQ beam preparation unit and MR-TOF analyzer offers several operation modes. They are illustrated in figure 3.8 and listed below:

a) Broadband Mode; ions can be bunched, ejected into the analyzer and traverse it directly without reflection.

b) Medium Resolution Mode; ions can be reflected twice (one turn).

c) High Resolution Mode; ions can be reflected within the electrostatic reflectors for a given number of turns.
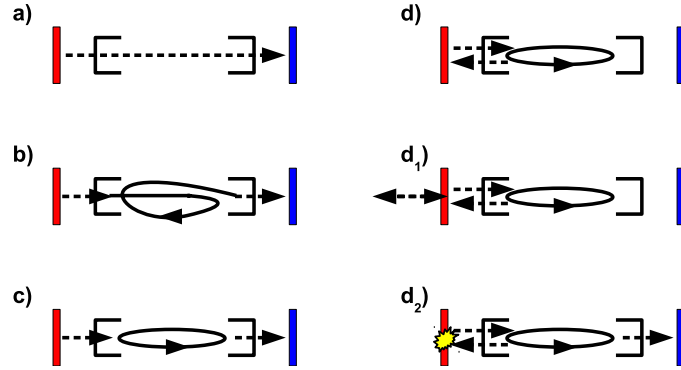
Figure 3.8.: Operation modes of the Multiple-Reflection Time-of-Flight analyzer; schematic ion trajectories indicated by arrows, reflectors by simple brackets, ion trap in red and detector in blue.

d) Re-Trapping; ions can be ejected into the analyzer, reflected multiple times and injected back to the RFQ trap, where they are mass selectively recaptured. Two options are available:

d_1) Isobar Separation Mode; ions can be dispersed in time in the analyzer and re-trapped with high mass selectivity.

d_2) MS/MS Mode; a certain ion species can be isolated by re-trapping, and may be dissociated and analyzed.

3.3.1. Broadband Mode

The analyzer can be passed directly without any reflection and is considered as a conventional linear TOF. The mode is often referred to as Pass-Through mode. The time focus needs to be formed at the detector surface to gain best mass resolution [McLachlan, 1947], which requires a comparably weak extraction field strength. Since there is no closed loop, the mass range of the analyzer is unlimited. The turn-around time and total flight time are not so much favorable by a mass resolving power amounting to $R_m^{PT} \approx 300$.

3.3.2. Medium Resolution Mode

In many existing MR-TOF-MS the optimized tuning depends on the number of reflections [Plass et al., 2013b]. The primary time focus can be formed for optimal extraction conditions and shifted by every reflection to an intermediate position away from the TOF detector towards the injection trap. The whole system then is tuned to place a final time focus on the detector surface, thus providing the same arrival time for the same masses with deviating energies. A change in the number of reflections then requires a dedicated tuning of the analyzer.

To create a final time focus independent of the number of turns, the analyzer can be tuned such, that each time focus occurs at the very same position for every turn. This mode is referred to as Multi Turn (MT) mode. An additional post-analyzer reflector can provide the necessary shift of final time focus to the detector surface (compare [Plass et al., 2008]).

As a new approach within this work, a single turn (two single reflections) is tuned to provide a shift of time focus from primary position to a final position on the detector surface (see figure 3.9). This mode of operation is referred to as Time Focus Shift (TFS) [Yavor, 2014b, Dickel et al., 2016]. The extraction field strength can be freely chosen for the compromise of small turn-around time t_{ta} and acceptable energy spread δ for higher numbers of turns. This method offers a new degree of freedom for the extraction field strength and the general tuning for an arbitrary number of turns without any additional ion optical instance.

Operation with a single time focus shift Turn only, meaning two reflections, offers enhanced mass resolving power of $R_m^{TFS} \approx 3000$ and a broad mass range of $\frac{m_{max}}{m_{min}} \approx 4$ (as described in section 3.4).
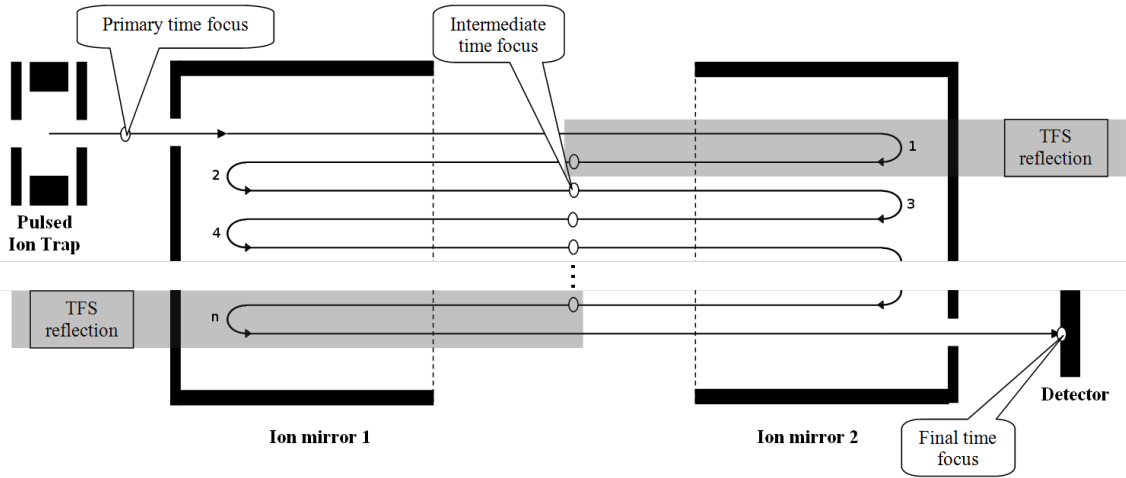

Figure 3.9.: Shift of the time energy focus by special tuning of the reflectors for 2 reflections (1 turn) [Yavor, 2014b]; the primary time focus is close to the trap due to a higher extraction field strength and is shifted twice into the detector direction during the reflection, thus placing the final time focus onto the detector plane. This is independent of the number of turns in between. For illustration reasons the time focus shift turn is split into the first and last reflection.

3.3.3. High Resolution Mode

The high resolution mode is based on a preceding time focus shift Turn and an arbitrary number of multi turns. These provide fewest aberrations and allow for a high number of turns ($N \gg 100$). The phase space of the ion bunches can be preserved as far as possible. Thus, the more turns, the longer the flight time, the higher the mass resolving power. Which is constant for every mass and only depends on the initial phase space. The time-energy focus can be preserved after every turn. Further, the fine tuning and placement of the time-energy focus may be done only once and can be left untouched during the operation with varying turn numbers.

An adjustment of kinetic energy to the reasonable acceptance of the analyzer can be done with an unsymmetrical storage potential of the trapping electrodes. The location of the cooled ion bunch can be shifted spatially, thus resulting in a different starting potential and kinetic energy. This

shift in kinetic energy translates into different peak shapes and peak tails. The option to adjust the trap potential is a perfect tool for energy adjustment and also very useful for investigation of contributing TOF aberrations.

Limitation of the multi turn mode arise for very high numbers of turns ($N > 1000$). Smallest spatial and energetic deviations from desired initial phase space of the ions, as well as slightest misalignment of analyzer electrodes and/or tiny electrical in-continuities can lead to a saturation effect in mass resolving power and mean an upper limit of performance.

The combination of time focus shift and multi turn is illustrated in figure 3.9. Injection of ions into the analyzer is done irrespective to the primary time focus, which is typically not far from the trap. Ions enter the analyzer through the lowered potential of the 'opened' reflector and experience a time focus shift in the first reflection. This virtual time focus remains at the same position during multi turn mode and is finally moved to the detector by the final reflection with time focus shift. In the experiment the two time focus shift reflections are done subsequent within the first turn, which has the same effect.

3.3.4. Re-Trapping

MR-TOF-MS provide very high mass resolving power via time dispersion after a folded flight path. Exactly this dispersion in time can be used to separate different species of m/q. Earlier approaches make use of a Bradbury-Nielson gate as mass selector [Plass et al., 2008, Wolf et al., 2011]. In this work a dynamic energy bunching used to decelerate and capture ions in an RFQ is demonstrated as a new method [Yavor et al., 2014, T. Dickel and J. Lang et al., 2016, Dickel, 2012]. The theoretical assertion is based on [Yavor, 2014a].

A non-destructive separation is realized via the inverse process of injecting ions from the trap into the TOF analyzer. Figure 3.10 illustrates the analog procedure of injection (stage 1) and dispersion (stage 2) for mass measurement and re-trapping operation. After the desired flight time in the analyzer, as mass dispersive stage, the reflector next to the trap is switched to open mode to prompt ions back to the trap (stage 3). Ions are retarded by exactly the same fields as for the initial injection. Note, that no selection of ion species is done yet. At a certain time moment t_r, when ions of desired mass are stopped in the center of the trap, the retarding field is switched to a shallow axial trapping field. Ions of different mass arrive at different time and are not at rest at the same time moment t_r. Either they are too early (lighter ions) and re-accelerated into direction of the analyzer or they are too late (heavier ions) and not yet stopped. Thus, only the desired mass is stopped, consequently re-trapped and cooled via applied buffer gas, while others escape the trapping region. This way, the same ion optical system can serve for high-resolution mass measurement and for mass-selective re-trapping.

When the retarding field in the trap is switched to a field creating an axial potential well at the right moment, the considered ions that are just at rest are re-trapped. At the same time, ions of a different mass m_2 can be also spatially located inside the trapping region – but since they arrive at a different time they are completely stopped only at a different time moment t_2 and have non-zero energies at t_1. Then, if the re-trapping potential well is shallow enough, the ions of the mass m_2 will not be trapped (see figure 3.11). Their potential energy adds to the remaining kinetic energy and is well above the trap energy depth QU_r.
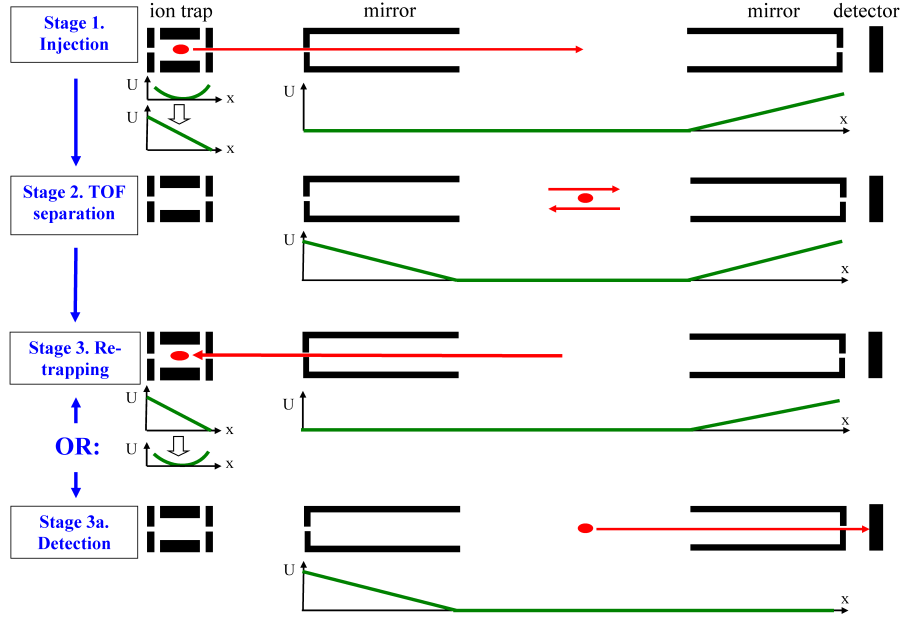
Figure 3.10.: Initial injection into and separation in the time-of-flight analyzer, with either re-trapping or detection [Yavor, 2014a].
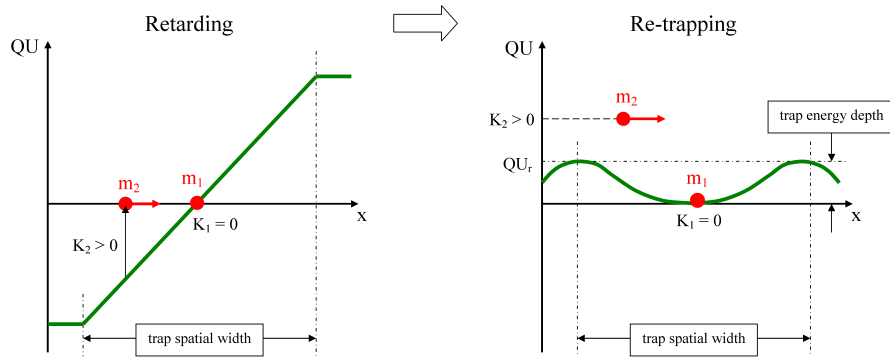

Figure 3.11.: Separation of ions due to kinetic energy difference at the time moment of switching the axial electrostatic field from the retarding to the re-trapping one [Yavor, 2014a].

The ion mass separation in the re-trapping mode is not based on the difference of the flight time, like it is for a Bradbury-Nielsen gate. It relies much more on the conversion of the time spread into the kinetic energy spread and the separation of ions according to their kinetic energy difference. The resulting mass resolution is therefore dependent of the time-of-flight mass separation of ions in the MR TOF analyzer. The flight time of an ion of the mass m from the moment of extraction t_e to the moment of re-trapping can be written as t_r $t_f = t_r - t_e$. The theory of TOF mass analyzers shows that $dt_f/dm = t_f/(2m)$ [Yavor, 2009]. At the time of re-trapping time the ion velocity time gradient is $dv/dt = -QE_r/m$, whith Q the ion charge and E_r the retarding electrostatic field strength at the point where ions are stopped. The velocity mass dispersion at the re-trapping process can be calculated to

$$D_v = \frac{dv}{dm} = \frac{-t_f Q E_r}{2m^2}.$$
(3.3)

With realistic conditions the ions of a single mass approach the retarding trap field with a time spread of $\Delta t = \Delta t_0 + \Delta t_A$ with the turn-around time $\Delta t_0 = m\Delta v_0/(QE_i)$ (compare section 2.2.2). E_i is the acceleration field strength during injection, and Δt_A is an aberration time spread induced in the MR-TOF analyzer. This time spread leads to a velocity spread of ions of a single ion mass at the re-trapping time t_r

$$\Delta v = \frac{QE_r}{m}\Delta t.$$
(3.4)

With a velocity depth of the trap (derived from the energetic acceptance)

$$S_v = \sqrt{\frac{2QU_r}{m}}$$
(3.5)

with the depth U_r of the recapturing axial potential well, the minimally resolved ion mass difference Δm_{min} is given by the relation

$$|D_v|\Delta m_{min} = \Delta v + S_v.$$
(3.6)

The mass separation power $R_s = m/\Delta m$ can be formed by subsequent replacement of Δm by equation 3.6, D_v by 3.3, Δv by 3.4 and S_v by 3.5 to

$$R_s = \frac{m}{\Delta m} = \frac{t_f}{2(\Delta t_0 + \Delta t_A) + \frac{2}{E_r}\sqrt{\frac{2mU_r}{Q}}}.$$
(3.7)

For a very shallow recapture potential $U_r \to 0$ the mass separation power tends to the principle value of mass resolving power of a time-of-flight mass spectrometer

$$\hat{R}_m = \frac{t_f}{2(\Delta t_0 + \Delta t_A)}.$$
(3.8)

In case of a large number of ion turns in the MR-TOF, the difference t_{12} between times of arrival of the ion packets of two different, but close masses m_1 and m_2, to the last time focal plane almost coincides with the difference of the flight times t_f for ions of these two masses. The time width of ion packets is again $\Delta t = \Delta t_0 + \Delta t_A$. Assuming a homogeneous axial retarding field in the trap

at the re-trapping time t_r, defined as stopping time for ions of the mass m_1, the average velocity of the ions of the mass m_2 is $v_2 \approx QE_r t_{12}/m$ and thus the average kinetic energy of the these ions is

$$K_2 = \frac{t_{12}^2 Q^2 E_r^2}{2m_2}. \tag{3.9}$$

With an average velocity equal to zero, Δv from equation 3.4 is the velocity spread around velocity $v = 0$. The corresponding total energy width for mass m_1 is

$$\Delta K = \frac{m_1}{2}\left(\frac{\Delta v}{2}\right)^2 = \frac{Q^2 E_r^2 (\Delta t)^2}{8m_1} \tag{3.10}$$

accounting for the maximal velocity as half of Δv. This shows that the flight time dispersion at the last time focus determines the energy difference (or velocity dispersion) at the re-trapping time and the time width of the ion packets at this focus determines the energy width of the re-trapped ion bunch. If this energy width is smaller than the energy depth of the axial potential well of the trap ($\Delta K < QU_r$), the whole ion packet is captured in the trap.

The time-of-flight dispersion t_{12} can be compared to the spatial dispersion in a magnetic separator, the energy width of the re-trapped ion bunch is analog to the such an ion beam width, and the ion trap energy depth is similar to the slit width in the magnetic separator.

The energy width and the energy dispersion both can be changed by varying the retarding field strength E_r. This does not change the relative separation of the individual energy dispersion and the individual energy width and has therefor no effect on the 'spectrometric' resolving power (see equation 3.8). But, it allows to match the energy width of the bunch and the energy width of the trap to optimize the re-trapping separation power (see equation 3.7). A stronger retarding field E_r rises ΔK and also the energy dispersion K_2 of the neighboring mass m_2 (compare figure 3.11). That is ideally adjusted to fill ΔK_1 to the full ion trap energy depth for, while K_2 is lifted above.

3.3.5. Isobar Separation Mode

Isobaric separation of ion species is a common challenge for MR-TOF instruments in nuclear physics experiments (e.g. [Plass et al., 2008, Wolf et al., 2012]). There, one has to clean for later high precision experiments, while contamination with isobaric species drastically reduces measurement capabilities. The new method of re-trapping allows for very high separation power and high efficiency in a single process with the default infrastructure of an MR-TOF-MS. Thus, the compact setup and the low need of infrastructure can be maintained [T. Dickel and J. Lang et al., 2016].

Ions from different production mechanisms such as Isotope Separation OnLine (ISOL) and In-flight may be introduced into an MR-TOF-MS via individual stopping and selection systems [Purushothaman et al., 2013, Heinz et al., 2013] and common RFQ transport. The mass-selective re-trapping may ensure pure species for the delivery to further experiments (see figure 3.12). Ions may be re-trapped, cooled and transported in backward direction in the beam preparation system. Intermediate broad-band measurements for diagnosis or high accurate mass determination are possibly done at any time by an automated change of operation settings.
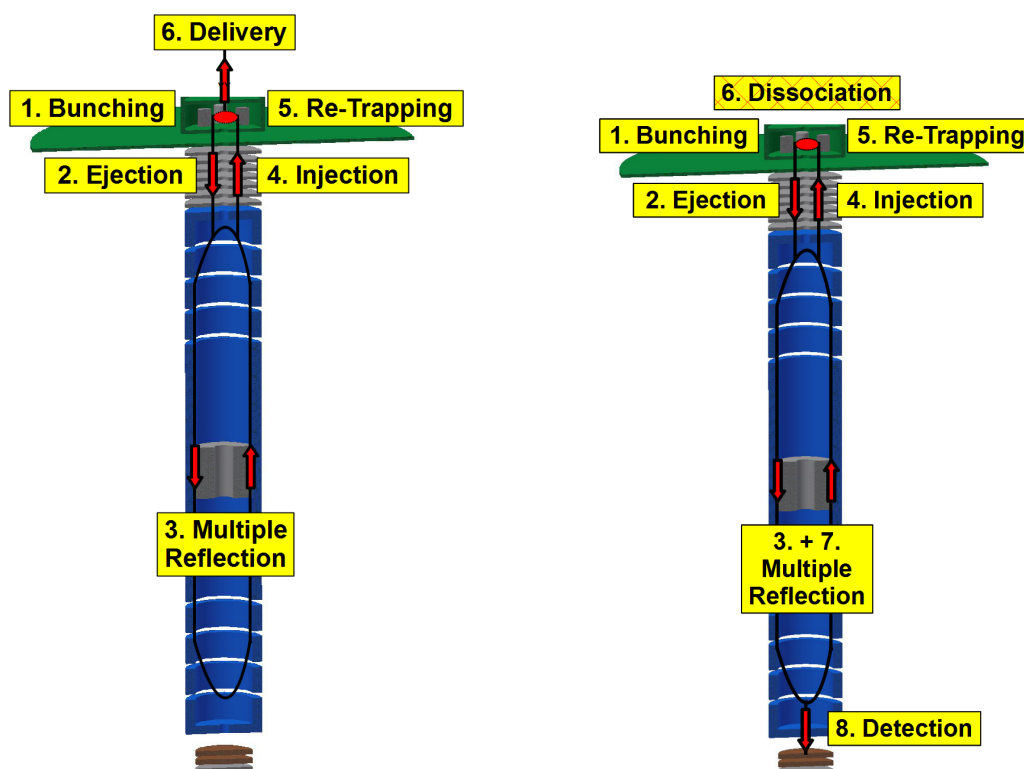
3.3.6. MS/MS Mode

Figure 3.12.: Separation mode with subsequent bunching, mass-selective re-trapping, delivery of isobaric clean beam to further experimental stage (left) or dissociation of the chosen analyte and final accurate mass determination of the fragments (right).

The re-trapping process may be utilized to isolate individual species from an analytical spectrum (see figure 3.12), where a provoked fragmentation or dissociation would be necessary. This may provide further information on structure and composition of molecules as well as molecular bonds by mass spectrometric examination of the fragments. The possibility of such highly mass-resolved and selected precursors suppresses ambiguous fragments from neighboring species and provides a basis for future MS/MS experiments. In addition, delivery of those fragments to other analytical instrumentation like ion-mobility spectrometers, spectrometric experiments or chromatographic methods may be possible and generate again an unprecedented level of information.

Different fragmentation and dissociation techniques (see section 2.5) in conjunction with the presented instrument are foreseen for future development.
One technique is SID, where selected species are directed to a surface with ion energies from few to thousands eV. The massive deformation leads to formation of fragments of the molecules, which are recaptured for a mass spectrometric examination. While the fragmentation probability is quite high, typical recapture efficiencies are expected to be very low.
The next technique is CID with either low or high energetic collisions with buffer gas. The latter one is typically realized in a dedicated collision cell (e.g. [Hilger et al., 2013]) which can be implemented by directing a high energetic ($E_{kin} \approx 1000\,\text{eV}$) ion beam through the trap into the cooler

RFQ. Due to inelastic collisions molecules can fragment and the constituents can be investigated. First simulation studies show sufficient stopping capabilities for ions in that energy regime [Lippert, 2016].

Lower energetic buffer gas collisions can be realized by excitation in the injection trap, e.g. with bipolar direct current (DDC) [Webb et al., 2013] or bipolar AC applied in addition to the native RF amplitudes. The trajectories of ion species with the particular resonance frequency are enlarged with an increase of the average kinetic energy. Steady buffer gas collisions lead to inner excitation of the molecules and a rise of effective temperature. Figure 3.13 presents exemplary the rise of this temperature in dependence on the applied AC amplitude of a particular resonance amplitude (which is in the order of $f_{res}^{AC} \approx 1/10 f_{RF}$). The application of this method with the MR-TOF-MS is subject of recent studies [Lippert, 2016].
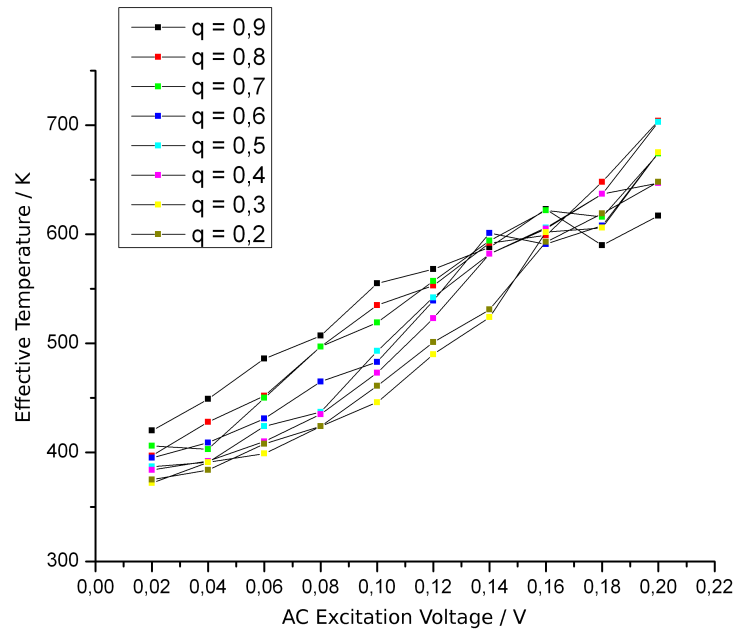
Figure 3.13.: Effective temperature of ions after AC excitation versus applied resonance AC amplitude plotted for different q-values [Lippert, 2012a].

3.4. Mass Range

The correct timing for the switching of the analyzer electrodes is essential to realize individual operation modes. So it is to realize a proper mass range. In the following, a consideration of mass range and the proper timing is given.

In an electrostatic field the time-of-flight of an ion with the general kinetic energy E_k is proportional to the square root of its mass m: $t \propto \sqrt{m}$. This allows to scale the switching times for individual masses. To do so, one has to know when to switch the electrodes of the analyzer for in-

and ejection for a given mass, in order to avoid that the ions experience any pulsed electric field. Since there is a certain time window in which a single mass is not affected by switching, one can consider this single mass as the lightest or heaviest mass in the desired mass range. This way, the minimal and maximal time can be determined.

3.4.1. Mass Range and Scaling

The following considerations are made for quadratic relation of mass and time without any additional time offset. To derive the maximal or analogously the minimal mass $m_{max/min}$ (*max* for maximal or *min* for minimal) relative to a known 'probing ion' with mass m_p (with $m_{p\_max/min}$ as maximal or minimal mass of the given mass range of the device), the following equation of ratios can be used:

$$\frac{m_{max/min}}{(t_{max/min})^2} = \frac{m_{p\_max/min}}{(t_{p\_max/min})^2} \tag{3.11}$$

$$m_{max/min} = \frac{(t_{max/min})^2}{(t_{p\_max/min})^2} \cdot m_{p\_max/min}. \tag{3.12}$$

Where $t_{max/min}$ is the time of switching for the considered mass and $t_{p\_max/min}$ the same for the probe ion as the maximal or minimal mass in the spectrum. This assumption can be used to set up the timing for a desired mass and to ensure that this mass is right within the mass range. That is particularly true, whenever there is no inert time offset of the instrument t_0.

The time for the the switching can be arbitrarily chosen, e.g. the time of the probing ion may be defined with the probing mass as maximal or minimal mass of the mass range - dictating the time for switching. Thereby the respectively minimal or maximal mass can be observed. Note that indices are now altered:

$$t_{max/min} := t_{p\_min/max} \tag{3.13}$$

The resulting maximal or minimal mass is then given by

$$m_{max/min} = \frac{(t_{p\_min/max})^2}{(t_{p\_max/min})^2} \cdot m_{p\_max/min} = \frac{(t_{p\_min/max})^2}{(t_{p\_max/min})^2} \cdot m_p, \tag{3.14}$$

where $m_{p\_max} = m_{p\_min} = m_p$. This is true even though the ions with minimal and maximal mass are at different positions in the analyzer at the time of switching.

The mass range from the time-of-flight point-of-view of a multiple-reflection time-of-flight mass spectrometer is given by the squared ratio of the usable time span and the total time-of-flight for the moment of the last and most restrictive switching of electrodes. One can define t_{inj}, the time from the injection trap to the location in the anaylzer, where the ion is influenced by the switching field

$$t_{inj} = \lambda_{inj} t_{turn} = \lambda_{inj} A \sqrt{m/Q} \tag{3.15}$$

and the time t_{mir} in the analyzer, for which the ions are influenced by the switching

$$t_{mir} = \lambda_{mir} t_{turn} = \lambda_{mir} A \sqrt{m/Q}, \tag{3.16}$$

that are both independent on mass for fixed voltages. For $Q = 1$ this leads to

$$\frac{m_{max}}{m_{min}} = \left(\frac{N + \lambda_{inj}}{N + \lambda_{inj} - (1 - \lambda_{mir})} \right)^2 \tag{3.17}$$

for the mass range of ions with equal number of turns N [Yavor et al., 2015]. With a given approximation of a completely usable range in the analyzer ($\lambda_{mir} = 0$) and a comparable time for the injection and the turn ($\lambda_{inj} = 1$), one obtains an ideal mass ratio [Yavor et al., 2015]:

$$\frac{m_{max}}{m_{min}} = \left(\frac{N + 1}{N} \right)^2 . \tag{3.18}$$

The reasonable timing to adjust the instrument can be derived analogously from this behavior of the probing ion. Again, with the assumption of $t_0 = 0$, the proper timing for any other mass can be extracted by scaling following the ratio

$$\frac{m}{t^2} = \frac{m_p}{t_p^2} \tag{3.19}$$

with m the desired mass, t the according time, m_p the mass of the probe ion and its time t_p. By transposing

$$t = \sqrt{\frac{m}{m_p} \cdot t_p^2} \tag{3.20}$$

is obtained and can be used to get the necessary values for the particular mass m.

3.4.2. Mass Selection

A quadrupolar arrangement of electrodes in the analyzer offers selective deflection of unwanted species and can be used as Mass Range Selector (MRS) [Dickel, 2010, Toker et al., 2009]. It is primarily used to purify a spectrum and to avoid any ambiguity of turn number for different masses. Typically the mass selection for a particular time-of-flight and mass range is done during the first turns in the analyzer. This provides an unambiguous mass range (without any uncertainty of turn number) for even highest time-of-flight and reduces the amount of species (and charge) in the analyzer.

A new approach to enlarge the quasi-simultaneous mass range $m_{range} = \frac{m_{max}}{m_{min}}$ of an MR-TOF-MS is the scanning usage of the mass range selector. Different species can be allocated to a certain turn number by a variation of the MRS settings. This can allow for an unambiguous identification of all ions even in complex spectra. Therefore, the behavior of the MRS needs to be well-known (see section 5.1.5).

For high accurate studies of single masses, the RFQ mass filter may deliver in future aplications a pre-filtered ion beam to the trap system and hence prohibit potential space charge effects in trap and analyzer, as well as simplify the obtained mass spectra.

3.5. Calibration

High mass resolving power is delivered by proper operation of the device in high resolution mode and sufficient voltage stabilization (refer to 4.3). Mass accuracy on the other hand comes along with mass resolving power and predictable behavior within the ion-optical system. But, to actually have absolute mass values with high accuracy a calibration with calibrants as comparison is essential.

3.5.1. General Time-of-Flight Calibration

For an ideal time-of-flight mass spectrum the following describes a valid calibration method

$$m = A \cdot t^2 \tag{3.21}$$

with mass m, total time-of-flight t and the calibration factor A, which can be obtained by using one calibrant with known mass and clear identification. In reality an additional time delay t_0 occurs (through electronics and cable length, etc.) and leads to

$$m = A \cdot (t - t_0)^2 \tag{3.22}$$

as calibration. With a saddle point fit and two known and identified masses the determination of A and t_0 is here possible. The time offset can be determined as constant in time for $t_{TOF} >> t_0$. A calibration and determination of t_0 with a single reference mass is possible [Ito et al., 2013].

3.5.2. Calibration for MR-TOF-MS

Since the way of ions through an MR-TOF-MS is consisting of differing flight paths, a separate consideration of those is advantageous. According to section 3.3 different operation modes exist. The total time-of-flight may be divided in t_{PT} as the time of an ion species from the source to the detector without any reflection (pass-through mode), t_{TFS} as the time for a time focus shift turn, t_{MT} as the time for a multi turn and N as the number of those turns. A certain t_0 as offset still remains.

$$t_{meas} = t_0 + t_{PT} + t_{TFS} + N \cdot t_{MT} \tag{3.23}$$

presents the measured time t_{meas}. The single times are dependent on the kinetic energy E_{kin} and the mass of the ion m. The time of the multi turn is in addition also dependent on the turn number N (precisely spoken on the time after switching of potentials):

$$t_{meas} = t_0 + t_{PT}(E, m) + t_{TFS}(E, m) + N \cdot t_{MT}(E, m, N). \tag{3.24}$$

The mass m can be expressed as

$$m = A \cdot (t_{PT} + t_{TFS} + N \cdot t_{MT})^2. \tag{3.25}$$

To make things little easier one can combine t_{TFS} and t_{PT} to t_{TFS+PT} and neglect t_0 for the ideal case:

$$m = A \cdot (t_{PT+TFS} + N \cdot t_{MT})^2, \tag{3.26}$$

while the term in parentheses is nothing more than the time-of-flight t_{TOF} – or in the real case $t_{meas} - t_0$. By varying the number of turns N the multi-reflection time t_{MT} can be obtained directly. Only t_{PT+TFS} is now left unknown, but can be determined by changing the mass m or the kinetic energy E_{kin} and a calculative scaling of $t_{MT} \propto \sqrt{m} \propto \sqrt{E}$.

An alternative approach to the one above is to make use of two independent calibration parameters B and C:

$$t_{TOF} = t_{PT+TFS} + N \cdot t_{MT} \tag{3.27}$$
$$= C \cdot \sqrt{m} + N \cdot B \cdot \sqrt{m} \tag{3.28}$$
$$= (C + N \cdot B) \cdot \sqrt{m}. \tag{3.29}$$

The mass is then determined to

$$m = \left(\frac{t_{TOF}}{C + N \cdot B} \right)^2 = \left(\frac{t_{PT+TFS} + N \cdot t_{MT}}{C + N \cdot B} \right)^2. \tag{3.30}$$

C can be obtained be omitting any multiple-reflection having $t_{TOF} = t_{PT+TFS}$:

$$t_{TOF} = t_{PT+TFS} = C \cdot \sqrt{m} \Rightarrow C = \frac{t_{PT+TFS}}{\sqrt{m}}. \tag{3.31}$$

Parameter B is derived by the following transposing

$$\sqrt{m} = \frac{t_{PT+TFS} + N \cdot t_{MT}}{C + N \cdot B}$$
$$C + N \cdot B = \frac{t_{PT+TFS} + N \cdot t_{MT}}{\sqrt{m}}$$
$$B = \frac{\frac{t_{PT+TFS} + N \cdot t_{MT}}{\sqrt{m}} - C}{N}$$
$$B = \frac{\frac{t_{PT+TFS}}{N} + t_{MT}}{\sqrt{m}} - \frac{C}{N} \tag{3.32}$$

with a certain number of turns N. Thereby the calibration with parameters C and B for an ideal case with constant behavior of the electronics is complete.

The more realistic scenario includes also the general fixed time delay t_0 into the expression for the mass (according to equation 3.30):

$$m = \left(\frac{t_{TOF}}{C + N \cdot B} \right)^2 = \left(\frac{t_{meas} - t_0}{C + N \cdot B} \right)^2 = \left(\frac{t_{PT+TFS} + N \cdot t_{MT} - t_0}{C + N \cdot B(N, \sqrt{m})} \right)^2. \tag{3.33}$$

Equation 3.28 with $t_{meas} = t_{TOF} - t_0$ becomes

$$t_{meas} = C \cdot \sqrt{m} + N \cdot B \cdot \sqrt{m} - t_0. \tag{3.34}$$

B is intentionally displayed in dependence of N and $\sqrt{m}$ and should be treated as a function of N to gain a high accurate calibration. Imagine, that for high mass resolving measurements with $N > 100$ the influence of B is much larger than C with only a single turn. The function $B(N, \sqrt{m})$ is steadily changing for lower N and becomes asymptotic for higher N.

To elaborate the calibration one can start again by an TFS and omitting any multi turn. Parameter C can be measured by having at least two different masses m:

$$t_{meas} = C \cdot \sqrt{m} + t_0 \Rightarrow t_0 = t_{meas} - C \cdot \sqrt{m} \tag{3.35}$$

Applying two different known masses with the still unknown t_0 brings

$$t_0 = t_{meas\_1} - C \cdot \sqrt{m_1} = t_{meas\_2} - C \cdot \sqrt{m_2} \tag{3.36}$$

$$C \cdot \sqrt{m_2} - C \cdot \sqrt{m_1} = t_{meas\_2} - t_{meas\_1} \tag{3.37}$$

$$C \cdot (\sqrt{m_2} - \sqrt{m_1}) = t_{meas\_2} - t_{meas\_1} \tag{3.38}$$

$$C = \frac{t_{meas\_2} - t_{meas\_1}}{(\sqrt{m_2} - \sqrt{m_1})} . \tag{3.39}$$

With the obtained parameter C it is easy to have t_0 by use of equation 3.35.

Determination of B is done by variation of N. The time-of-flight contribution of the multiple-reflections is

$$t_{MT} = B \cdot \sqrt{m} \tag{3.40}$$

and prompts parameter B with equation 3.23 as

$$B = \frac{t_{MT}}{\sqrt{m}} = \frac{t_{meas} - t_0 - t_{PT\_TFS}}{N \cdot \sqrt{m}} = \frac{t_{meas} - t_0 - C \cdot \sqrt{m}}{N \cdot \sqrt{m}} . \tag{3.41}$$

3.5.3. Disentanglement

Besides the calibration for known species, a new approach for an ambiguous mass range with a single reference mass is explained in the following. Only a single known-mass reference ion is required to identify completely unknown masses with an unknown and differing number of turns. Therefore, the time distances to reference peaks in the spectrum can be evaluated for different numbers of turns (see figure 3.14). With a known species as calibrant, one can determine its time-of-flight t_{MT}^{cal} for a single turn with the time-of-flight t^{cal} for two different turn numbers N_1^{cal} and N_2^{cal}:

$$t_{MT}^{cal} = \left| \frac{t_{N\_2}^{cal} - t_{N\_1}^{cal}}{\Delta N} \right| \tag{3.42}$$

The time for one turn of the unknown species m_x can be calculated respectively to the calibrant by

$$t_{MT}^x = \left| \frac{(t_{N\_2}^{cal} - t_{N\_2}^x) - (t_{N\_1}^{cal} - t_{N\_1}^x)}{\Delta N} \right| = \left| \frac{\Delta t}{\Delta N} \right| \tag{3.43}$$

with $\Delta N_{cal} = N_2^{cal} - N_1^{cal} = \Delta N_x$.

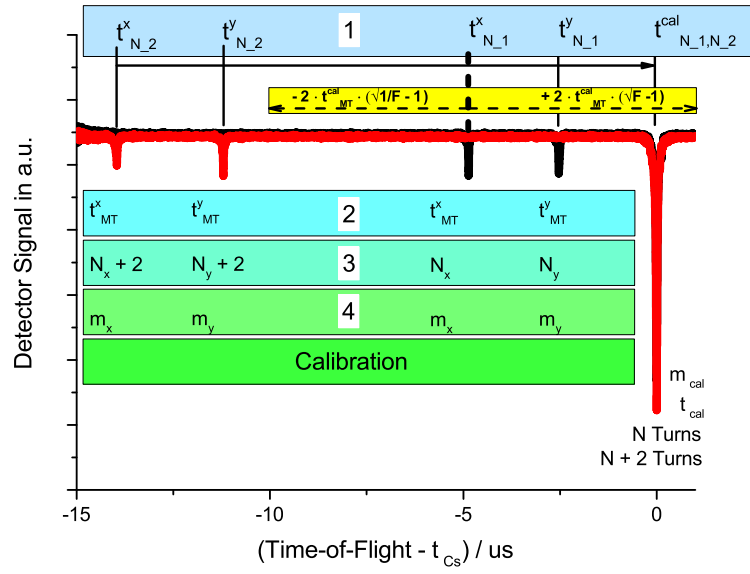Figure 3.14.: Time spectrum for 2 unknown species (m_x and m_y) in an ambiguous mass range with a reference mass for calibration (m_{cal}); within few steps a disentanglement can be done. 1: Acquisition of spectra of different turn numbers (in this case N (black) and $N + 2$ (red)) and asignment of peaks in the accepted mass range (yellow indicator for an $\Delta N = 1$); 2: Calculation of the individual time for a single turn; 3: Derivation of the absolute turn number; 4: Identification of the unknown species. With these parameters an accurate calibration of the previously unknown species is now possible.

For a mass range with lighter and heavier species as the calibrant it is reasonable to choose the timing such, that the calibrant is right in the center of the investigated mass range $\frac{m_{max}}{m_{min}}$. Further, to ensure an identical ΔN for the single species, the difference in time for these varied number of turns $N + \Delta N$ has to be smaller than the time for one turn t_{MT}^{cal} of the calibrant itself:

$$\Delta t_{MT}^{x} < t_{cal\_MT} \tag{3.44}$$

When the calibrant is chosen as the mid of the mass range the following conditions with an equal factor F can be defined:

$$m_{max} = F \cdot m_{cal}, \quad m_{min} = \frac{1}{F} \cdot m_{cal} \tag{3.45}$$

The difference in the time for the varied number of turns for each mass then amounts to

$$\Delta t_{max} < \Delta N \cdot (t_{max}^{x} - t_{MT}^{cal}) = \Delta N \cdot (t_{MT}^{cal} \cdot \sqrt{F} - t_{MT}^{cal}) \tag{3.46}$$

$$= +\Delta N \cdot t_{MT}^{cal} \cdot (\sqrt{F} - 1) \tag{3.47}$$

and

$$\Delta t_{min} > \Delta N \cdot (t_{min}^{x} - t_{MT}^{cal}) = \Delta N \cdot (t_{MT}^{cal} \cdot \sqrt{\frac{1}{F}} - t_{MT}^{cal}) \tag{3.48}$$

$$= -\Delta N \cdot t_{MT}^{cal} \cdot (\sqrt{\frac{1}{F}} - 1). \tag{3.49}$$

The mass range may be intensionally restricted within the beam preparation system to allow for the above conditions. E.g. for the mass range of $\frac{m_{max}}{m_{min}} \approx 4$ with $F = 2$ the time difference for every species Δt_{MT}^{x} is resticted to

$$-0.3 \cdot t_{MT}^{cal} \approx t_{MT}^{cal} \cdot (\sqrt{\frac{1}{F}} - 1) < \Delta t_{MT}^{x} < t_{MT}^{cal} \cdot (\sqrt{F} - 1) \approx +0.4 \cdot t_{MT}^{cal}. \tag{3.50}$$

The difference for a variation of one turn is thereby smaller than a factor of 2, which guarantees that the difference in turn numbers for the identification is not a multiple of that of the calibrant. Still, possibly a signal may disappear for the alternative turn number when the ions are eliminated by the switching field of the analyzer. In this case, the timing can be shifted ($m_{cal} \neq F \cdot m_{min} = \frac{1}{F} \cdot m_{max}$) to restore the intact comparison of the calibrant and unknown mass.

When the time for a single turn is known, the number of turns for the unknown mass for different times of the multiple-reflection t_{MR} can be directly derived by

$$N_x = \frac{t_{MR}}{t_{x\_MT}}. \tag{3.51}$$

Finally, all necessary parameters have been identified from the unknown and ambigous mass spectrum to do a highly accurate mass measurement by the known system with the time-of-flight calibration of the previous section 3.41. For few peak signals, this evaluation can be done manually, taking into account intensity and peak width of each species. A post-experimental calibration of data seems to be most reliable. One reason is the human ability to recognize the individual characteristics and patterns. An automated evaluation by the DAQ software on the other hand may

identify and accurately determine the mass in real-time. For plenty of peak signals in a crowded spectrum a control sequence by a dedicated DAQ software may be used together with a variation to additional turn numbers.// An important prerequisite for this calibration with disentanglement is the fact that the time-of-flight for the single turns in the instrument is constant and proportional to the square root of mass. Which is particularly the case with sufficiently high accuracy for turn numbers $N > 2$.

Further techniques to achieve unambiguous mass spectra are:

- Survey and Zoom Mode
  A medium resolution mass spectrum can be acquired and the interesting mass range may be zoomed in then for higher mass resolution and accuracy.

- Width of Peak
  The mass resolving power in a time-of-flight mass spectrometer is constant over the mass range (compare section 2.2.2). Accordingly, the Δt is proportional to the time-of-flight. This is a useful fact to sort single peaks and coarsely assign to a mass.

The automated computational deconvolution and calibration is enhancing mass range, analysis time, sensitivity and operation comfort. As well, such an automation is quite specific for each individual instrument and settings. Many features for this instrument have been developed and are subject of recent work [Bergmann, 2015a].

4. Instrumental Setup

This chapter shows how the theoretical concepts in chapter 3 are brought to a concrete design and how the instrument is set up.

4.1. Vacuum System

Calculations, requirements and preceding tests for the vacuum system have been realized in agreement with available vacuum system components. Weight, size and power consumption has been minimized as possible. A scheme of the vacuum setup is depicted in figure 4.1. The main recipients are 3 standard DIN 160 CF crosses in stacked arrangement and provide a dense housing of the ion optical assembly. The atmospheric pressure interfacing recipient is custom made. Flanges are designed and manufactured according to individual interfaces for electrical feed-throughs and buffer gas inlet. The single components are chosen for the ease of assembling and interchangeability during commissioning. A future version of a mobile MR-TOF-MS may be equipped solely with custom made recipients with integrated feed-throughs and further decrease in size and weight. The typical resulting pressures during atmospheric ion source measurements are listed in table 4.1.

From $1\,atm \approx 1032\,mbar$, the pressure is reduced to $p_{pre} \approx 2\,mbar$ in the first chamber with a direct roughing pump connection ($430\,l/m$ pumping capability). The second chamber, which is dedicated for an enhanced pressure reduction containing the ion guide RFQ, is evacuated to $p_{API} \approx 10^{-2}\,mbar$ ($71\,l/s$ pumping capability for N_2). In the following chamber, containing the complete beam preparation system, the pressure is further reduced to $p_{up} \approx 10^{-4}\,mbar$ in spite of the buffer gas inlet (again $71\,l/s$ pumping capability for N_2) and allows for reasonably low collision rate during injection and suppressed collision rate in the analyzer region with $p_{low} \approx 10^{-7}\,mbar$ ($260\,l/s$ pumping capability for N_2).

Compartment	Label	Pressure / mbar
(I)	p_{pre}	2
(II)	p_{API}	$2.7 \cdot 10^{-2}$
(III)	p_{up}	$1.2 \cdot 10^{-4}$ (regulated)
(IV)	p_{cool}	$1.2 \cdot 10^{-2}$ (calculated)
(V)	p_{trap}	$8 \cdot 10^{-3}$ (calculated)
(VI)	p_{low}	$1.3 \cdot 10^{-7}$

Table 4.1.: Table of compartments and according pressures during atmospheric ion inlet operation with N_2 as buffer gas.
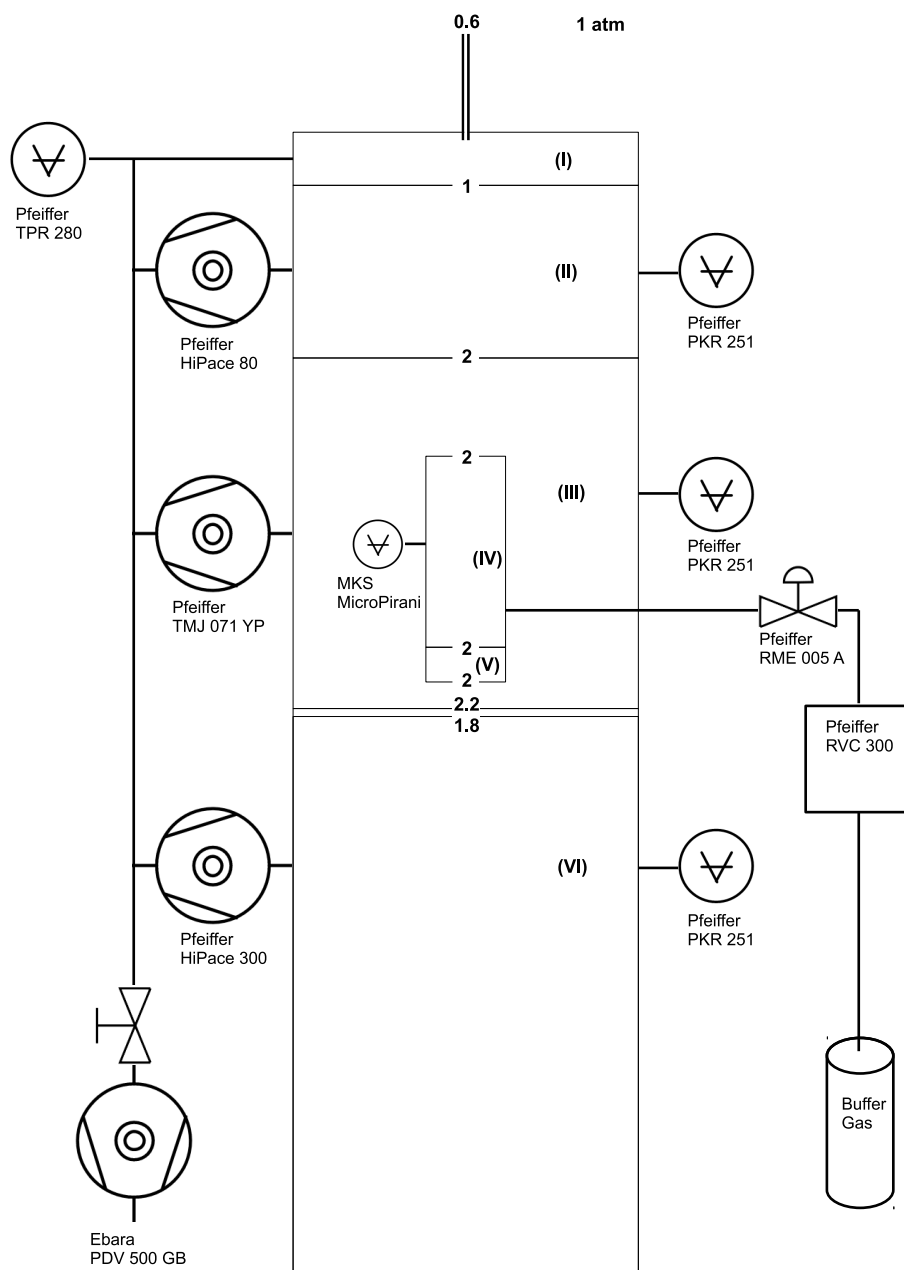
Figure 4.1.: Schematic view of the vacuum system; aperture diameters are presented in mm, compartments are enumerated in roman numbers.

4.2. Timing

This section describes the temporal switching of potentials to allow for the single operation modes of section 3.3. This switching of (even high) voltages on a short time scale with necessary stable voltage at the electrodes (refer to 4.3) is the key to use the multiple-reflection analyzer as a 'pseudo-electrostatic' analyzer. It is of great importance that traversing ions neither experience the actual switching of potentials nor a steady variation of them, in order to obtain an accurate and unambiguous spectrum. The timing schemes for the mass spectrometric operation and the ReTrapping operation are depicted in figure 4.2.
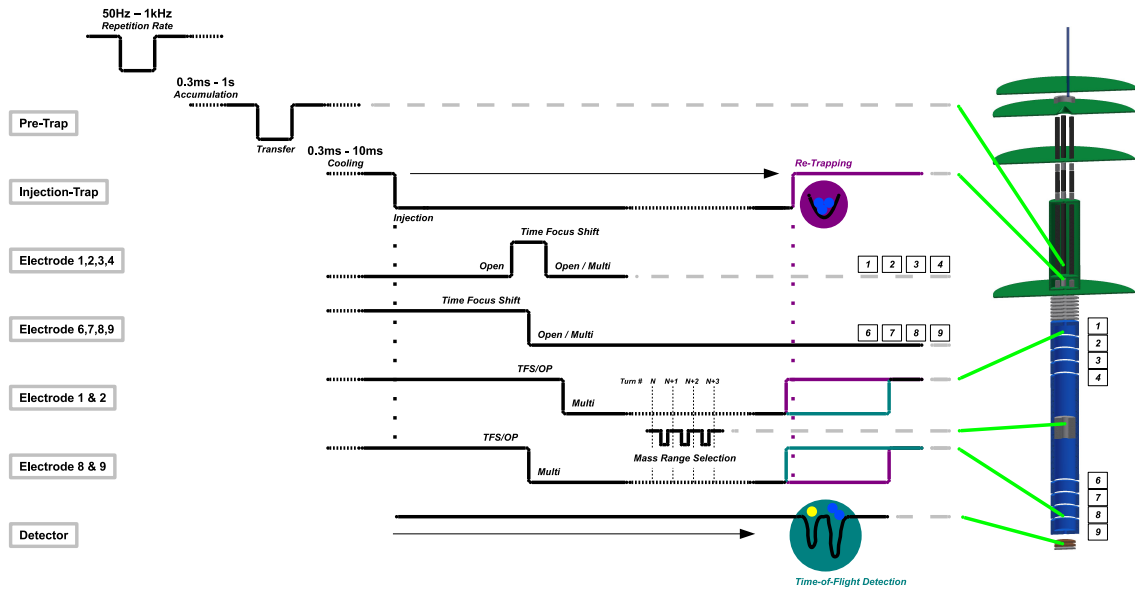
Figure 4.2.: Timing diagram with a preceding TFS, the multi turn mode and the mass range selector for either mass detection (Turquois) or Retrapping (Magenta). For the TFS every of the 4 electrodes of the two mirrors have to be switched.

4.3. Electronics

Time Signal Generator

The timing signals for the control and acquisition are kept in Transistor-Transisor Logic (TTL) format. For the different modes of operation, the fundamental sequence is created by two PCI cards (National Instruments PCI-6602) in the mounted lab PC with 8 timing channels each. These are controlled by a custom-made software [Jesch, 2009] and distributed with an amplifier break-out box [Kinsel, 2010] equipped with Metal-Oxide-Semiconductor Field-Effect Transistor (MOSFET)

drivers and Bayonet Neill-Concelman Connector (BNC) sockets for wiring. In addition, the complex timing scheme for individual operation modes and optional ReTrapping of ions requires a dedicated TTL manipulator to connect individual timings with AND, OR and inversion gates. A dedicated stand-alone box has been designed and built to enable necessary flexibility for full functionality of the instrument.

RF System

The instrument is equipped with two custom-made resonant circuit RF generators. The resonance circuits of two coupled air-core coils and capacities (dominated by cable capacities) are therefore fed by rectangular shaped voltage pulses produced by an RF driver circuit [Konradi, 2012] (see figure 4.3). With an RF resonance frequency $\omega = \frac{1}{\sqrt{LC}}$ optimized for desired pseudopotential and q-value (refer to 2.2.1) and given capacity of the cabling and the electrode system C_{tot}, the inductance L can be adapted by the dimension of the air-core coils. For moderate capacitive load this system delivers up to $5000V_{pp}$.
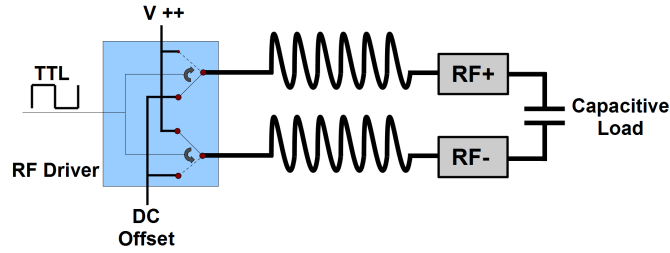
Figure 4.3.: RF Generator system with an RF driver box, two air-core coils and provided with supply voltage as well as RF timing.

The distribution of the RF to the RFQ electrodes is realized on a dedicated Printed Circuit Board (PCB) for each RF circuit. The mixing with an according DC potential is applied by a coupling inductance. Those are chosen to transmit the DC potential (with a resistance of $R_{DC} \approx 10\,\Omega$) and suppress a short cut effect between the high voltage of the radio frequency with the DC by a resistance $R_{RF} = 2\pi f L >> k\Omega$. To decrease parasitic capacities of longer cables, electrical noise and the amount of needed feed-throughs, a part of the distribution system is place into the vacuum recipient. Resistances are designed high enough to maintain necessary amplitudes and potentials, but low enough to withstand electric power deposited in the single components. This is of increased importance for the RF distribution board mounted in vacuum, because of the absence of convectional cooling.

The RF generation system is stable even during longer operation and is quite power efficient. The resonance frequency depends strongly on the capacitive load and varies already with an attached HV probe. The load of the system is dominated by capacities of cables, less of the actual RF electrodes. Mass shielded and twisted pair cabling for noise reduction also mean higher load. The typical values are several $100\,\text{pF}$, that enable amplification factors of up to 100 of the primary switched input voltage.

A reasonable method to reduce the produced noise by the generation and to minimize the electric

Electrical Supply	WORK WPD 163 STUV Power Distribution
	WIENER MPod Crate
	WIENER LV MPod Modules
	ISEG HV MPod Modules
	RIGOL DG1012 Function Generator
	National Instruments PCI-6602 Timer/Counter PCI Cards

Table 4.2.: Collection of commercial electronics components.

power necessary, is to tune the applied frequency in dependence of the drawn power instead of the amplification factor.

High Voltage Switching

Since every measurement requires altered electrode potentials, the HV switches are a very important tool. First efforts to custom build those switches were made many years before and are still ongoing ([Petrick, 2010, Kinsel, 2011, Ayet, 2014a]). The principle idea is to switch between a (more) positive and a (more) negative by means of a TTL signal. That can be done by two semi-conducting sequential switches with input potentials on the outer side and output on the connected inner side.

Passive Stabilization

For high performance of an MR-TOF-MS, stable and correct voltages are essential. In this work, a low-pass filter in fourths order provides a noise cut-off frequency $f_{co} \approx 2\,\text{s}$ (noise reduced to $-3\,\text{dB}$) [Ayet, 2014b]. Therefore, the latest version of HV switches and low-pass filters are condensed into a single box. These boxes each provide switching and stabilization for one reflector (4 electrodes). For the analyzer electrodes 1 and 2, as well as electrodes 8 and 9 three different potentials are required, though resulting in cascaded switches.

If mass range is not an issue, the upper and lower reflector may be combined and switched simultaneously with a single instance of theses boxes, in order to safe necessary infrastructure.

4.4. Infrastructure and Supply

The entire instrument is mounted into a single frame made by aluminum profiles. The construction is robust and fits into an average van. All components are integrated. The system is totally autonomous and requires only the common 220 V or 380 V net supply. The total power consumption is determined to below 1.3 kW during operation. Main consumers are the roughing pump (with gas ballast from API), the commercial voltage supply crate with HV and LV modules, as well as the PC. A list of commercial electrical components is given in table 4.2. Buffer gas is provided by an integrated gas tank – alternatively also air can be applied as buffer gas. The overall size of the instrument is $0.8\,\text{m} \cdot 0.8\,\text{m} \cdot 1.2\,\text{m} \approx 0.8\,\text{m}^3$. The weight amounts to $\approx 230\,\text{kg}$ and is

dominated by the stainless steel vacuum recipient and flanges, the voltage supply crate, the robust frame and the roughing pump.

Easy and automated operation is a definite design goal and requires the option to remotely and electrically control every single instance of the instrument. That has been entirely considered during the design process. Any parameter with influence on the ions can be controlled and adjusted. Feedback values for each parameters are displayed as well. The operation of the entire instrument is possible via LAN or WLAN via a remote desktop connection.

Figure 4.4 demonstrates the setup of this compact, mobile and robust high performance MR-TOF-MS. The presented instrument is an operational in-situ device and development platform at the same time. Many commercial components have been chosen for practical reasons and interchangeability with other experimental setups. It is obvious that size, footprint, weight, power consumption and reliability can be further improved by dedicated engineering of those components.// The ion optics system is vertically arranged in one line and thereby dictates the minimum measure of the instrument (length of ion optics ≈ 1.1 m). Folding of the system to 0.7 m would be possible by a curved RFQ providing a $180°$ redirection of the ion path. A dedicated and fabricated recipient can allow for smaller form factor and lower weight. Dedicated power supply channels as well as voltage dividers can also decrease size and weight.

4.5. Mechanical Design and Manufacturing

The construction of the mounting frame, electronic circuits, housing, as well as the ion optical system are developed with Computer-Aided Design (CAD). This ensures enhanced visualization and flexibility during the design process and the quality of technical drawings for manufacturing. Requirements on the model arise from several aspects; the component has to be mechanically stable and needs to be compatible with the process of manufacturing, the geometric boundaries and availability of raw material, the material needs to cling to thermal, mechanical and electrical requirements, electric discharge and noise effects, and, of course the demanded precision for the ion optical concept.

Figure 4.5 shows the CAD model of the ion optics and enclosing vacuum recipient. The manufacturing has been done with primary scope on tolerances and has been monitored and adapted throughout the whole process chain, as well as finally revised during assembling and commissioning. For this design of an in-situ compatible device, special care was taken for robustness, ruggedization, transportability and stable operation in harsh environments. That causes an overhead of design work, material layout and safety margin. Therefore thermal expansion of the analyzer, stress on components during transportation and a safe and economic operation have been considered.
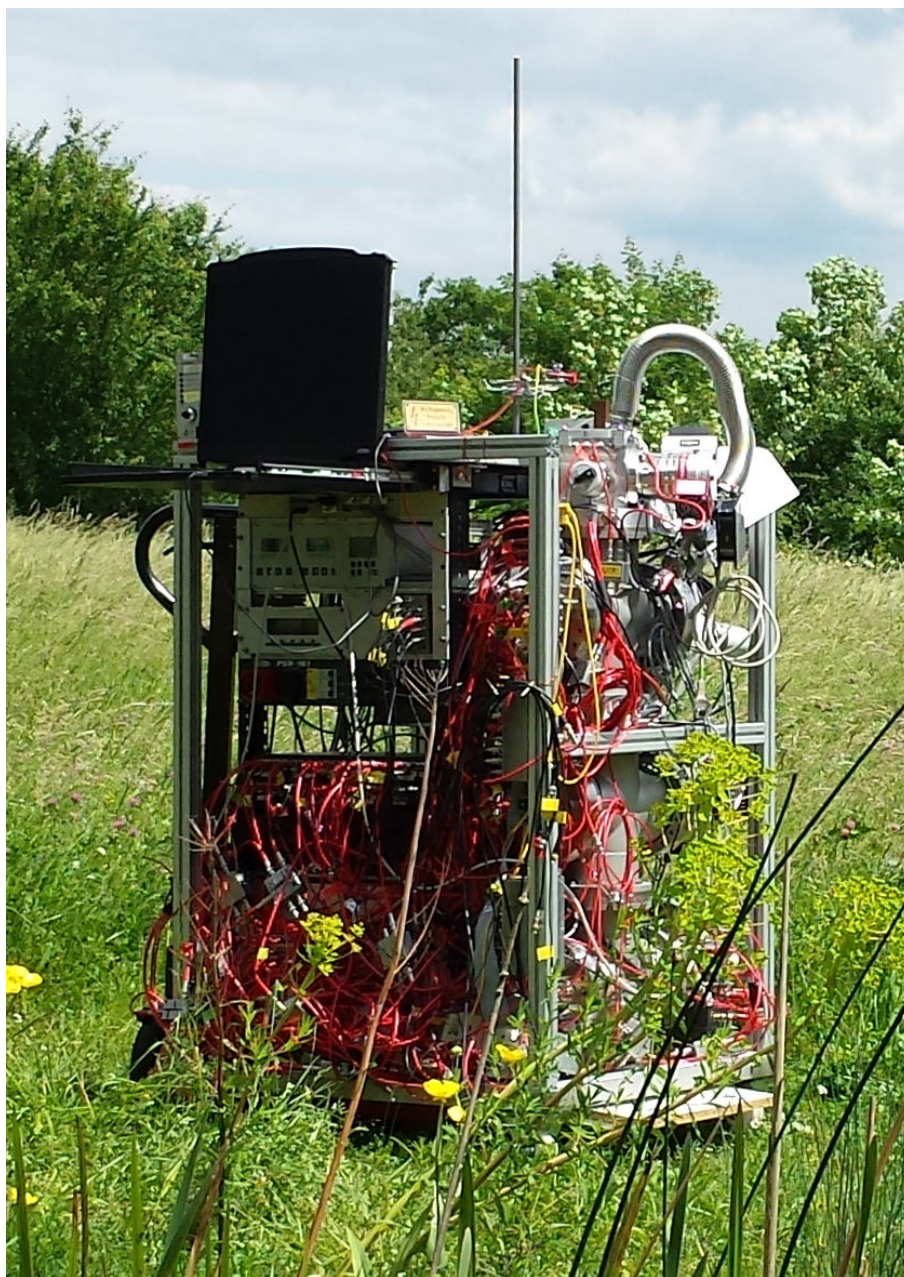
Figure 4.4.: Photograph of the mobile MR-TOF-MS during transportation outside the laboratory.
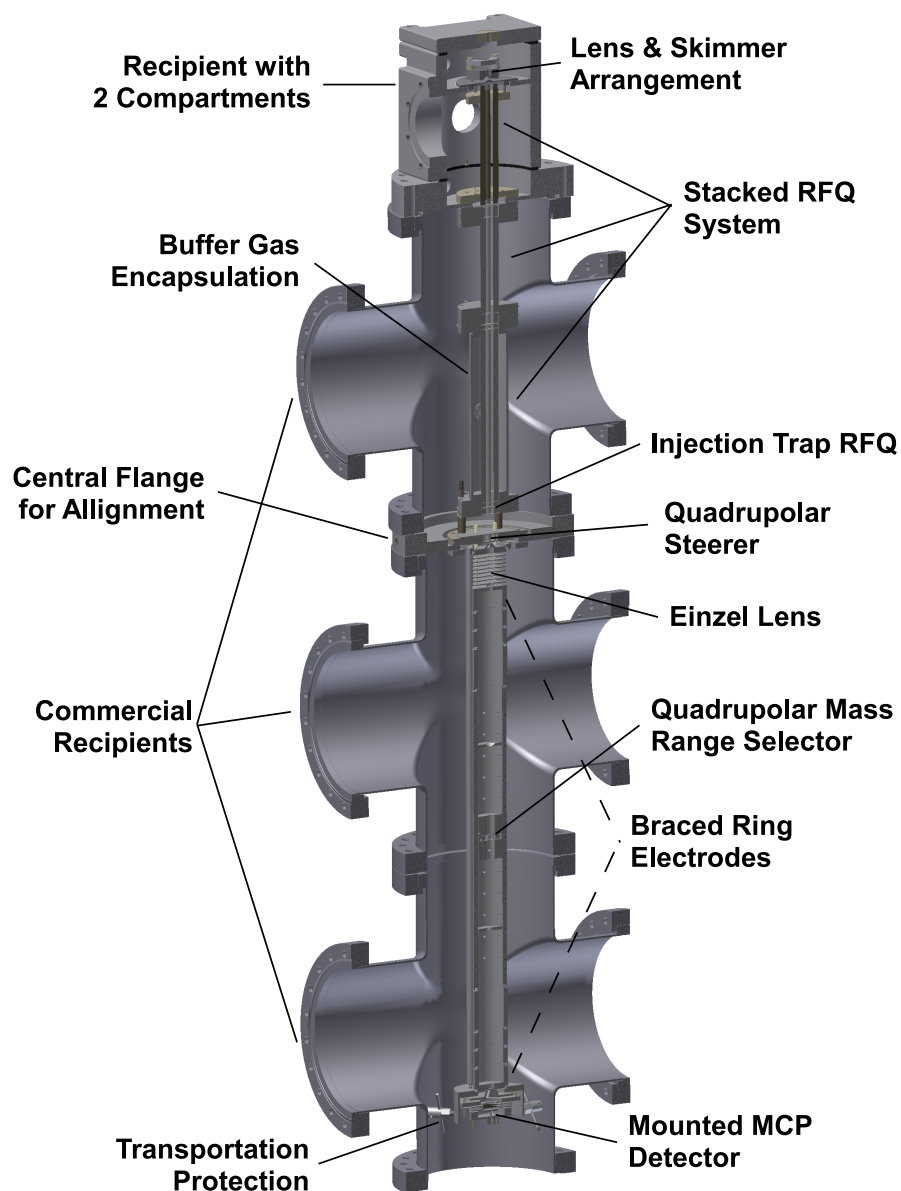
Figure 4.5.: CAD model of the entire ion optical system with surrounding vacuum recipients (cutted view on central axis); besides commercial vacuum recipients all components have been drafted, designed and manufactured. Available materials are restricted by the vacuum requirements; dominantly used are stainless steel, ceramics, PEEK, Polyimide and PTFE.

4.6. Ion Sources

^{133}Cs Surface Ionization Source

A ^{133}Cs surface ion source is applied as easy-to-use and very stable source of ions to commission and investigate most important characteristics of the instrument – apart from the atmospheric inlet. The ion rate can be easily adjusted by the applied current (ranging from 1 to 1.8 A) and is stable to few percent.

To generate broad mass spectra with an internal source for commissioning reasons, a charge transfer ionization has been developed. The source is therefore used to deliver an initial high current ion beam, that is stored in the injection trap for > 4 s under delivery of unfiltered ambient air. Ionization of species different to CS^+ are produced amounting to several percent of the initial Cs intensity. That happens with a broad mass distribution as found in figure 4.6. The burden of this
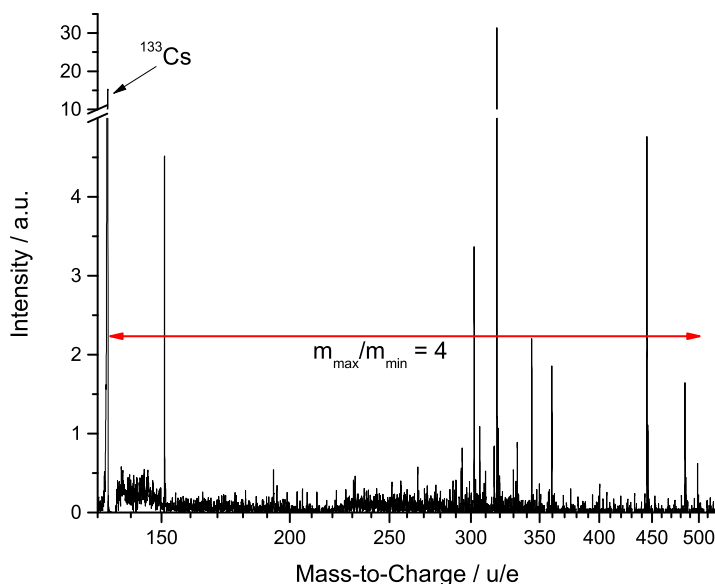
Figure 4.6.: Charge transfer spectrum by high current long time storage of ^{133}Cs and ambient air inlet.

method are very long acquisition times, since the cycle time is dominated by the long storage time. For that reason, a TDC has been chosen as DAQ hardware. In this case, the dominating Cs peak is affected by dead time and single ion hit capability of the TDC.

nano Electrospray Ionization

The very versatile and effective ionization with nano electrospray is used as default atmospheric ion source. Different distances and orientations from glass emitter to the inlet capillary are possible

– as default arrangement an orthogonal orientation and an equidistant offset of the mid point of the emitter and the inlet of about $\approx 2\,mm$ in horizontal and vertical direction is applied. The applied voltage to establish a constant spray with stable ion current differs with the exact distance, micro shape of emitter, solvent and its corrosive properties, as well as atmospheric temperature and humidity. To ignite the spraying, a voltage of $1300\,V$ to $2000\,V$ is necessary, while a later reduction of up to 30% delivers the same ion current.

As solvent a $1:1$ mixture of H_2O and methanol with 1% formic acid is used as proton deliverer. Analytes are added with individual concentration. The solution is injected into the emitter by a pipette with micro loader pipette tips in amounts of $10\,\mu l$ to $25\,\mu l$. Typical operation conditions offer more than $1\,h$ ion current from a single glass emitter. Sparking effects typically occur with applied voltages $> 3300\,V$ and possibly ultimately affect the tip of the glass emitter. The typical setup is shown in figure 4.7.

Paperspray Ionization

Another simple and effective ionization source is given by paperspray. A triangle is cutted out of ordinary printer paper sheets with scissors. The very tip is preferably created by crossing cuts with an angel of $40°$. The paper triangle is oriented straight to the inlet capillary, both inclined by $\approx 45°$. That causes the sample load (a positioned drop of solution) to move towards the tip. The necessary voltage of $3000\,V$ to $4500\,V$ is not exactly reproducible and changes with addition of solvent and re-usage of a single tip with constant orientation.

The solution is prepared same as in 4.6 and is typically applied in amounts of $30\,\mu l$. The comparably huge open surface causes a fast evaporation and drying out of the solution. To compensate for that, the tip may be covered with pure solvent in advance and an addition of solvent may be applied at intermediate operation. In general, this setup (see figure 4.7) is easy to realize, but is found to be less reliable and reproducible than nESI.
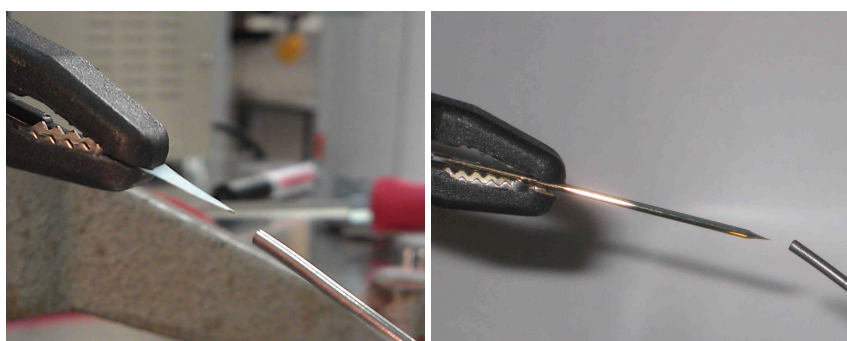

Figure 4.7.: Left: typical paperspray setup; cutted paper tip with solvent and analyte on top, inlet capillary in single mm distance and applied voltage $U \approx 3.5\,kV$. Right: typical nESI setup; filled glass emitter with inner tip diameter of $\sim 5\,\mu m$ and gold coating to establish electrical contact to the voltage supply $U \approx 1.2\,kV$.

4.7. Detector

For the studies of this work, two MCP with Chevron arrangement (zick-zack order) are used. The MCPs have a pore size of $12\,\mu\text{m}$ and an approximate amplification of 10^4 for a single MCP. The maximal amplification can be estimated by the released electrons of the first MCP illuminating 1000 channels of the second MCP, with again an amplification of 10^4. That leads to 10^7 produced secondary electrons for detection. This amplification is limited in rate by a non-vanishing recharge time. The activated channels in the second plate amount to $6 \cdot 10^{-7}$ of the total number of channels. The spatial distribution of the any incoming ions covers only 2 to 3% of the active area. That translates in ≈ 350 simultaneously detectable ions.// A resistive voltage divider serves as voltage supply and bias between the first and second MCP, as well as between the second MCP and the anode. It is designed for a compromise of delivering enough current for short recover times and low power dissipation at the resistors. The detection efficiency is restricted due to the open area ratio of the channels of 60%. The anode potential is kept on ground for the ease of direct coupling. The detector voltages is set between $1.8\,\text{kV}$ and $2.4\,\text{kV}$ with according level of amplification of several 10^7. A dedicated AC coupler can be applied, to float the detector and provide additional post-acceleration. This increases the heavy mass detection efficiency by higher kinetic energy of molecules at the surface of the detector.

A pulse height distribution of the detector has been taken for a lower and a medium ion rate. Therefore the applied voltage of the MCP assembly has been set to the maximum limit for highest amplification. As a consequence, the discharge of the channels is also at maximum. Thus, a decrease in pulse height is observed for higher rates. The amplification for single ion events and low ion rates ($\approx 50\,\text{ions/s}$) is in the same order and tends to higher peak amplitudes. With an increased count rate ($\gg 100\,\text{ions/s}$) the peak amplitudes are much lower leading to a lower mean amplification. This is a limitation of the linear dynamic range and has to be considered for qualitative studies.

As an alternative to the Chevron MCP a cost-intensive commercial available isochronous MagneTOF detector can be installed to provide higher detection efficiency and higher maximal count rate.

4.8. Data Acquisition

Data Acquisition (DAQ) is one of the key tasks in any experiment. It is obvious, that the best instrument delivers only poor data if the DAQ system is not adopted correctly [Kuehn, 2005, Lang, 2008]. Every application and even single measurement modes have own requirements and make a proper use of DAQ system essential. In case of the MR-TOF-MS, the following criteria should be met:

- Sufficient time resolution and accuracy for time-of-flight peaks

- Sufficient amplitude resolution where required

- Repetition rate sufficiently high for according measurement mode

- Compatibility of number of ions per spectrum

- Data transfer capable for continuous measurement

The detector signals are transmitted via an SMA cable and terminated with 50 Ohm to ground potential. As acquisition devices several digital oscilloscopes have been utilized. Despite handy oscilloscopes with integrated Analog-to-Digital-Converter (ADC), several Time-to-Digital-Converter (TDC) have been applied in order to obtain correct intensities for a low rate of events. In case of an TDC, a precedent discriminator is necessary. Ringing of the detector, reflections and electric noise pickup is automatically suppressed by an appropriate threshold. For application of an ADC (including oscilloscopes), the bandwidth of the signal transmission and sampling plays an important role and can affect the measurement. An insufficient bandwidth leads to broadening of the acquired single ion signals and an averaged peak. A loss in mass resolution is the direct consequence. On the other hand, high bandwidth in transmission and sampling may allow unwanted spikes in the analog signal and requires higher processing power of the ADC, that may be a limiting factor for continuous acquisition. The number of averaged spectra is another important criteria to compromise between measurement duration and vanishing signals for low intensities.//
Analysis and data evaluation can be considered as the last part of a DAQ chain. Within this work ADC and TDC data is evaluated with Origin®or with a dedicated mass analyzer control software (see section 4.9). The following hardware has been used within this work.

Time-to-Digital-Converter

The important value in TOF-MS is obviously the time. Using an TDC to measure the time suggests itself. TDCs are built to measure the time between a start signal and a stop signal, which is given in an MR-TOF-MS by the extraction from the trap and impinging of the interesting ion on the detector. Time measurements well below 100 ps with low jitter are possible, though not limiting mass resolution and accuracy. Time data can be collected in a list of times when events occurred or in an histogram with a bin size bigger or equal the time resolution of the device. The amount of data is comparably smaller than for continuous sampling methods. When the event rate becomes higher, which means multiple ions in one cycle impinging on the detector and even several ions with same mass arriving at the same time, the usage of an TDC becomes critical. After each event, there is a certain dead time for most TDC electronics to recover the idle state again. Events may be suppressed by this feature and the spectrum is not reflected correctly any more. Also the quantity of ions is not valid whenever multiple ion signals form a joint pulse shape, as this will be counted as single event. Important parameters of an TDC are maximal time resolution, dead time, compatible input values, maximal time span measurable, possible jitter, repetition rates and data format as output.
In this work two kinds of TDC have been used: ORTEC 9353 100 ps analyzer and IONWORKS TDCx4.

Analog-to-Digital-Converter

An ADC samples continuously the amplitude of an arbitrary signal and puts it into a digital format. There is a variety of resolution in amplitude (vertical) and in time (horizontal) direction. In general, higher resolution is of advantage. So there is ideally no discrimination of events and usually no interpretation of the input signal is being done. The analysis for mass spectrometry is

being done later on, when peaks are identified in averaged spectra. Advantages of ADCs is the continuous visualization of the signal, which may imply additional information for optimization and interpretation. Back draw is the bigger amount of data and restrictions in the amount of taken data. E.g. the maximal time span t_{span} to cover for an individual measurement is given by the sample rate f_s and the available fast memory for data points N_{mem} and amounts to

$$t_{span} = \frac{N_{mem}}{f_s}.$$ (4.1)

This can be an important limiting criteria for a broad mass range application. Other important characteristics are resolution in time (to properly describe also fast signals), resolution in amplitude (which is important for the averaging of small and rare signal), possible repetition rate, possible real-time averaging and data output.

In this work two kinds of ADC have been used: ORTEC FastFlight2 and SPDevice ADQ412. The latter one is based on Field-Programmable Gate Array (FPGA), that allows a customized treatment of the acquired date. In collaboration with the vendor, a hardware-based averaging has been realized as well as a parallel TDC-like discrimination for highest detection efficiency has been proposed.

Oscilloscope

Nowadays oscilloscopes are usually digital ones, which combine an ADC chip, an pre-amplifier, trigger logic, adjustable time and voltage range, visualization and control of the system. An oscilloscope is the common tool for testing, diagnostic and commissioning issues. Depending on the performance of the scope, it may be even sufficient for an accurate DAQ. While more elaborate scopes usually are bigger in size and weight, the in-situ application requires the correct choice of DAQ hardware.

In this work several oscilloscopes have been used; LeCroy WaveRunner 6100A for acquisition and the mixed signal scope Rigol DS1102D for surveillance and commissioning.

4.9. Software

Within the framework of this thesis, several software projects have been created and refined for data acquisition and control of the system. Custom software always means severe effort in development, but also severe advantage in realizing individual needs.

Vacuum System Control

A LabView®based software for control and supervising of the vacuum system has been implemented [Siebring, 2013]. It allows to set, adjust and supervise pressures, as well as the status and the temperatures of the turbo pumps.

Voltage Control

A dedicated software for voltage control has been developed based on C++ [Lotze, 2014, Schaefer, 2011]. It offers principle access to HV and LV voltage and current, delivers steady feedback of voltages and currents, highlights any deviation, routes software to hardware channels, as well as provides grouped control and individual visualization of the of the necessary channels.

MAc Data Acquistition

The Mass Analyzer control software (MAc) has been refined in last years [Pikhtelev, 2015, Bergmann, 2015b], adapted to single DAQ hardware and special need for MR-TOF-MS. It offers individual real-time processing of data, automated storage of data for long-term or automated measurements, calibration, visualization and export of the results.

For commercial DAQ devices usually no according software is provided. If it is provided, this software may be only for general or very special purpose and is not dedicated to and compatible with a custom instrument or experiment. MAc features application specific adaption and makes use of individual advantages of DAQ devices and guarantees operation and format interchangeability. During years of development, necessary features for analytical and nuclear physics application of MR-TOF-MS have been implemented, tested and optimized. This custom-made software provides full flexibility in data handling, evaluation and export, thus allows to integrate with other studies and experiments. In future, compatibility to common data standards (such as [Martens et al., 2011]) may be realized to ease the evaluation with data from commercial MS devices.

5. Measurements and Results

This chapter presents commissioning measurements of each individual subsystem as well as overall performance results.

5.1. Commissioning

The system has been set up and commissioned along with the conceptual and design aspects of chapters 3 and 4. The instrument has been optimized to highest performance and combines the requested mobility and robustness, as well as several modes of operation [Lang et al., 2011, Lang et al., 2012, Lang et al., 2013, Plass et al., 2014]. A default set of operation parameters has been identified for the majority of measurements and the determination of performance characteristics. The most important parameters are presented in tabular 5.1. The default operation of the TOF analyzer is performed with a preceding TFS (refer to section 3.3.2) followed by a desired number of multi turns (refer to section 3.3.3).

5.1.1. Atmospheric Pressure Interface

The aim of the API as inlet system is the transmission of ions as well as the reduction of the atmospheric pressure. As proof of concept, a first prototype of the API has successfully been applied for a miniature rectilinear ion trap [Schaefer et al., 2011a, Ouyang et al., 2009]. A duplicate has been installed at the MR-TOF-MS. The resulting pressures are shown in table 4.1 and reflect the design calculations. The length of the capillary has been varied between 90 mm and 140 mm and has been found to have a minor influence on transmission. The inner diameter of the capillary is chosen to $r_i = 1/16$ inch ≈ 0.57 mm. An improvement in transmission has been achieved by heating via a copper body, including heating cartridge and temperature sensor; the default applied temperature is set to $70°$C and regulated by control electronics.

5.1.2. Atmospheric Ion Sources

For the in-situ investigations the coupling to atmospheric ion sources by the API is important. During commissioning of the MR-TOF-MS, different ion sources and analytes have been used.

Ion Source		
nESI Voltage	Capillary Temperature	^{133}Cs Thermal Ion Source
$1600 - 3500\,\text{V}$	$70°\text{C}$	$1.1 - 1.9\,\text{A}$

Beam Preparation System		
RF1 Supply	RF3 Supply	Axial Trapping Potential
$255\,V_{pp}$ at $1.2\,\text{MHz}$	$340\,V_{pp}$ at $1.44\,\text{MHz}$	$30\,\text{V}$
Trap Depth	Extraction Voltage (Field Strength)	N_2 Pressure in Upper Recipient
$0\,\text{V}$	$\pm 347\,\text{V}\,(74\,\text{V/mm})$	$1.2 \cdot 10^{-4}\,\text{mbar}$

TOF Analyzer (Values in V)		
Einzel Lens	E1/9 (OP / TFS / MT)	E2/8 (OP / TFS / MT)
-4600	$-870/+239/+410$	$-1310/0/-85$
E3/7 (TFS / MT)	E4/6 (TFS / MT)	E5 (Drift)
$-474/-869$	$-3327/-4599$	-1300

Detector	Characteristics of Cooled Ion Bunch	
HV Supply	Axial $\Delta z \approx 0.4\,\text{mm}$ (FWHM)	$\delta \approx 25\,\text{eV}$ (FWHM)
$1800 - 2400\,\text{V}$	Radial $\Delta x, \Delta y \approx 1.5\,\text{mm}$ (FWHM)	

Table 5.1.: Operation parameters as default settings for the majority of measurements with $50\,\text{Hz}$ operation rate and adjusted for ^{133}Cs. The ions start on a potential of $0\,\text{V}$ and gain a kinetic energy of $1300\,\text{eV}$ in the drift region. The geometric distribution after cooling is Gaussian and amounts to an energy distribution of $\delta_{FWHM} \approx 25\,\text{eV}$ [Yavor, 2014c] with the applied extraction field strength. The electrodes E1 to E9 of the analyzer have two and three states: open (OP), time focus shift (TFS) and multi turn (MT).

Nano-Electrospray

Electrospray has been used as reliable and stable ion source. Figure 5.1 shows a spectrum of Caffeine obtained with the MR-TOF-MS. The mass resolving power in this mode of operation
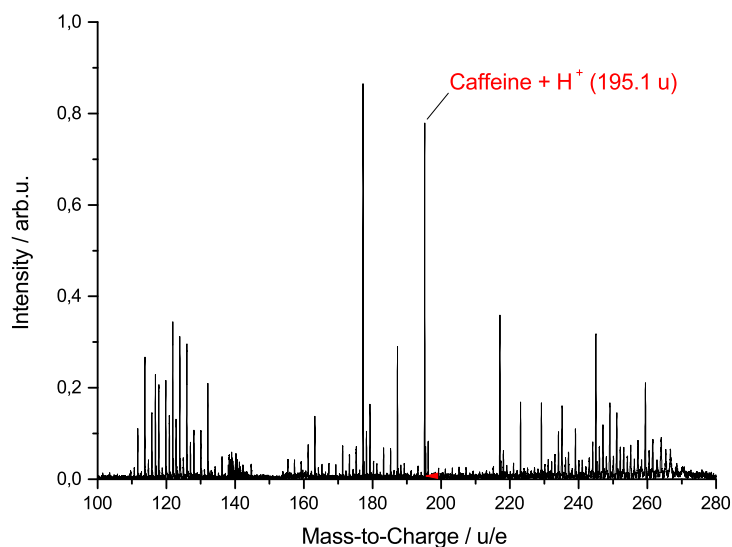
Figure 5.1.: Mass spectrum of Caffeine with nano-electrospray measured with the MR-TOF-MS at a mass resolving power of ≈ 3000 (single TFS, see sections 3.3.2 and 5.2.1). The Caffeine has been solved in H_2O / methanol 1 : 1 with 1% formic acid in 10^{-5} molar concentration. A glass emitter with an applied voltage of $U = 1250$ V is used to spray and ionize.

is determined to $R_m = 3080$ and applies for the whole mass range. The peak structure for the protonated Caffeine ion is Gaussian shaped with a peak width $\Delta t = 7.5$ ns only. The same species measured with high resolving power is depicted in figure 5.2. The concentration of Caffeine in solution of 10^{-5} mol/l produces sufficient statistic for a smooth peak shape and mass resolving power $R_m > 100000$.

A native biological sample can be rather complex, containing many different groups of elements ranging from light to heavy species. Figure 5.3 shows such a native spectrum of porcine brain in TFS mode and demonstrates its complexity and a wide range of masses. This spectrum is obtained by summation of 1000 single spectra for improved statistics and permits a good overview, as well as possible evaluation of the presence of meaningful species. The reliability and reproducibility is quite high with even such complex analytes.
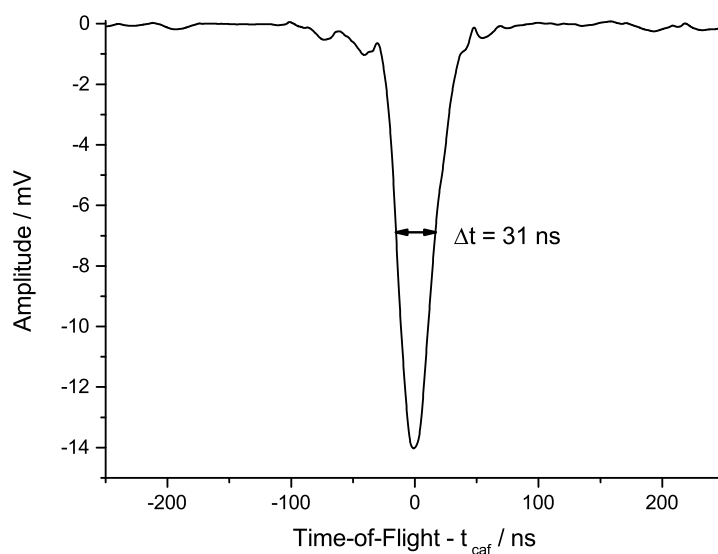
Figure 5.2.: High resolved mass spectrum of protonated Caffeine by nESI. A mass resolving power of $R_m > 110000$ has been obtained with a flight time of $t_{\mathrm{caf}} \approx 7\,\mathrm{ms}$.
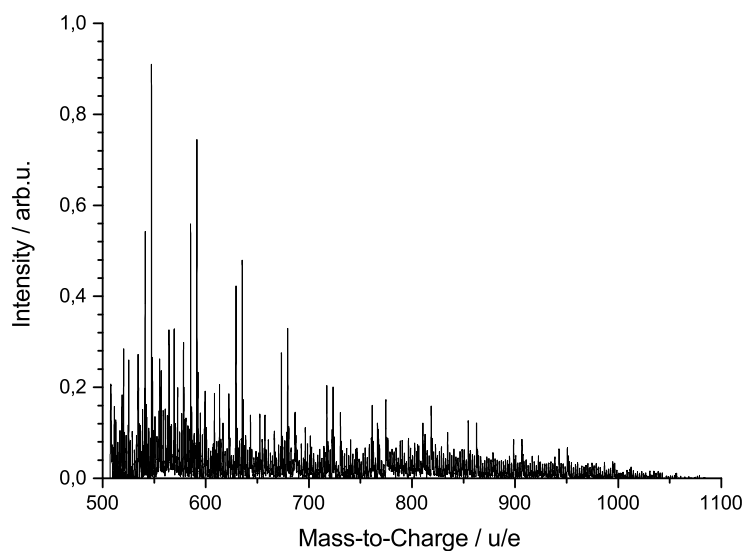
Figure 5.3.: Single porcine brain mass spectrum by the MR-TOF-MS with nESI; porcine brain has been homogenized, centrifuged and solved in methanol and H_2O $(1:1)$ [Roempp, 2014].

Paperspray Ionization

Figure 5.4 illustrates a spectrum generated by paperspray ionization – an ion source that is simple, cheap and versatile. The duration for a stable measurement varies with that ionization technique. Also the applied voltage has to be steadily adjusted. As pleasant analyte, the important neural
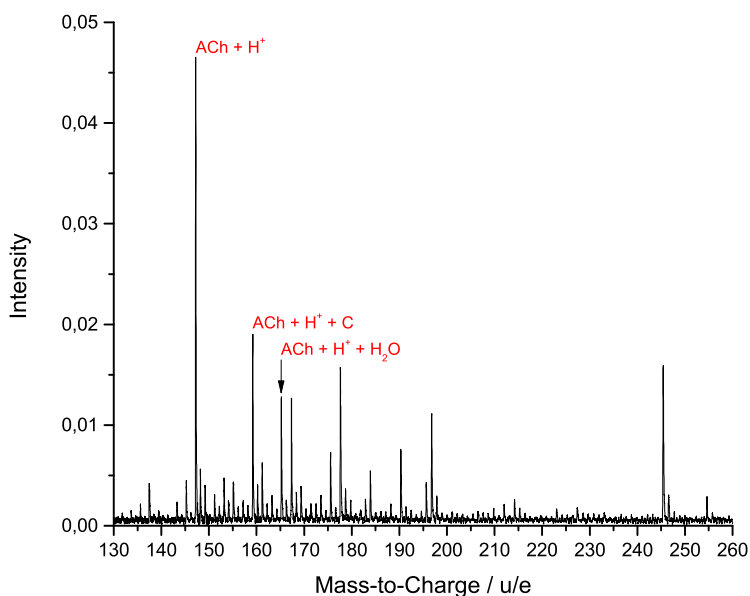
Figure 5.4.: Mass spectrum of Acetylcholine obtained with paperspray ionization with H_2O and methanol as solvent (H_2O / methanol 1 : 1 with 1% formic acid).

transmitter Acetylcholine has extensively used, which has been devoted a lot of research efforts [Lips et al., 2007]. While it is easily ionized by ESI, nESI or paperspray, it is challenging to identify Acetylcholine in complex spectra by in-situ ionization from native biological tissue, where the high mass resolving power of the MR-TOF-MS substantially may enhance the identification of Acetylcholine and connected species in measurements of native tissues – even with large intensity ratios and overlapping isobaric contamination.

5.1.3. Beam Preparation System

The beam preparation system has been designed, simulated, dimensioned, built, assembled and commissioned. The commissioning and optimization is an iterative process, that relies on transmitted ions as indicator for transmission and as probe of the initial phase space before the injection into the TOF analyzer. As main parameter, the buffer gas pressure is adjusted for a proper operation of the RFQ system. For default operation of the instrument (1 kHz compatible) the collision rate during injection is validated as low enough to provide compatiobility with the time-of-flight analysis.

Single potentials and timings have been experimentally validated and optimized. A beneficial aspect of buffer gas cooling is that ion manipulation in preceding subsystems is not maintained in the next stage. This enables a more independent optimization of the individual stages.

The storage behavior of the trap system is described by an exponential decrease of ion intensity with long storage times t_s: $I_{\text{ion}} = A \exp(-t_s/\tau_s)$. With ^{133}Cs ions and N_2 buffer gas the time constant for the pre-trap has been determined to $\tau_s = (6.6 \pm 2.7)\,\text{s}$ and for the trap to $\tau_s = (4.6 \pm 2.2)\,\text{s}$ [Lippert, 2012b]. Thus, the fraction of lost ions is negligible for a typical cooling duration of 10 ms, even for a storage time of 1 s an efficiency $> 80\%$ is provided.

The buffer gas cooling is a major prerequisite for the injection of a bunched ion cloud into the analyzer. The resulting initial peak width of the buffer gas cooling can be written as [Reinheimer, 2008]

$$\Delta t^2 = \Delta t_{ta}^2 + \Delta t_{io}^2 = (C/E_{ex})^2 + \Delta t_{const}^2. \tag{5.1}$$

The turn-around time Δt_{ta} depends on the extraction field strength E_{ex} and a constant C, that includes the thermal kinetic energy K_{therm}. By plotting the squared observed peak widths Δt^2 versus $1/E_{ex}^2$, the intercept of a linear fit can be read as Δt_{const}^2 and the linear slope reflects $(C/E_{ex})^2$, which can be processed to yield the thermal energy of $K_{therm} = (0.0357 \pm 0.0066)\,\text{eV}$ and an ion temperature of $T = 2/3 K_{therm}/k_B = (276 \pm 51)\,\text{K}$ [Lippert, 2012b].

The exponential decrease of peak width $\Delta t = A \exp(t_c/\tau_c) + \Delta t_{\text{cooled}}$ delivers the cooling constant τ_c, that represents the time of cooling t_c (above the time for storage t_s) after which collisional cooling reduces the peak width to $1/e \approx 0.368$. Cooling constants for ^{133}Cs at different pressures in the RFQ cooler and RFQ trap have been determined and are presented in figure 5.5 for He and N_2 as buffer gas. For the standard operation, a cooling capacity allowing for 1 kHz repetition rate is desired. An acceptable cooling constant therefore is any with $\tau_c < 0.2\,\text{ms}$.

In spite of the high repetition rate capability with higher applied cooling gas pressures, the gas ballast that stems from the trapping region affects the transmission in the time-of-flight analyzer and the resulting peak shape. A peak broadening through a loss of energy by ion-gas collision can occur in the region close to the injection trap, when the ions leave the middle recipient into the lower pressure regime of the analyzer. The lower left N_2 data point in the green region can satisfy either of them. This enables a repetition rate as high as 1 kHz without increasing the base pressure that is determined by the gas ballast of the API. The necessary pressure with He is one order of magnitude higher compared to N_2. This is a considerable effect for the transmission inside the analyzer.

Figure 5.6 demonstrates the measured transmission within the TOF analyzer for different buffer gas pressures of N_2 and He. Therefore, different pressures and resulting cooling constants have been correlated to the transmission in the analyzer for 257 turns. At comparable cooling time, the transmission is much higher with N_2 as buffer gas. That is in agreement with the higher cooling power of N_2 by its relatively higher collisional momentum transfer, as well as with the lower gas flow conductance from the cooling trap into the analyzer region. Further, the asymptotic behavior of the transmission for higher cooling constants indicates, that losses are not dominated by the prevailing pressure any more. For those reasons N_2 has been chosen as default buffer gas – providing a cooling constant $\tau_c < 200\,\mu\text{s}$ with maximal transmission.

The straight transport through the RFQ system provides highest transmission efficiency in agreement with the simulation studies. The transfer through the separating diaphragms is most critical,
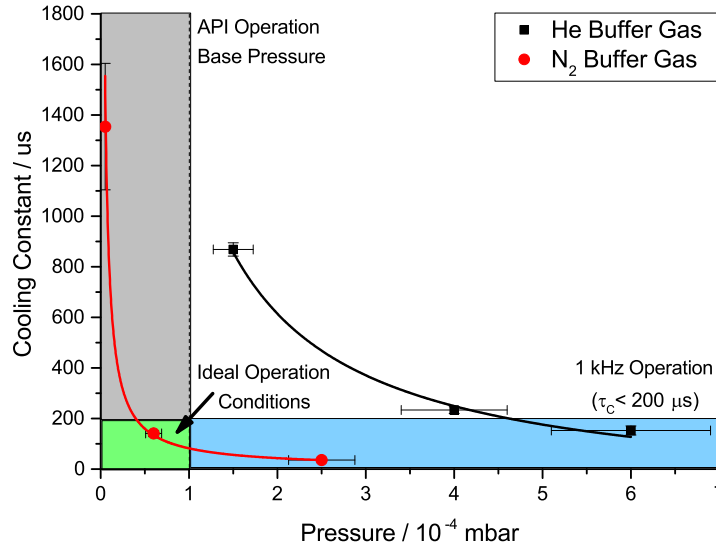
Figure 5.5.: Cooling constants for *He* and *N₂* as buffer gas versus adjusted and calibrated pressure in recipient (III) (compare figure 4.1). A base pressure of 10^{-4} mbar is present during operation with the API. For 1 kHz operation a cooling constant of $\tau_c < 200\,\mu$s is sufficient. The data points are fitted with a $1/p$ dependence. (Measurement for ^{133}Cs. The pressure inside the RFQ system is related to the pressure in the recipient, which is higher by a factor of $\approx 10^2$.)

especially the transfer of the cooled ion bunch from pre-trap to trap. Besides a typical heating effect, it bears an additional time-of-flight selective behavior because of its pulsed operation (as studied in 3.2.2). Nevertheless, a transmission for an ion cloud of a single species moved from pre-trap to trap has been determined higher than 95%.

For time-dependent measurements a quick transition through the beam preparation system is required. For ^{133}Cs ions the transport from the ion source to the injection trap is predominantly done within one cycle in the RFQ system. The mean time required for the transmission through the whole beam preparation system into the trap is below 100μs. This enables a high duty cycle, high efficiency and allows to separate any incoming ion intensity by at least 1 ms time resolution.
That is ideal for chromatography. (Where one can distinguish between Liquid Chromatography (LC) [Parks et al., 2007] and Gaseous Chromatography (GC) [Szulejko and Solouki, 2002] depending on the phase of the sample. The difference is the utilized column and in the time required for passing it.) The separated species can be transmitted through the column as close as 100 ms next to each other [Bicchi et al., 2005] and need sufficient temporal resolution of the following technique. This is quite challenging for most other high resolution MS.

The mass range provided by the beam preparation system (exemplary shown in figure 4.6) is determined to $\frac{m_{mas}}{m_{min}} > 4$. This is also in agreement with the studies presented in section 3.2.2. The transmission in an RFQ system strongly depends on the Matthieu parameter q and on the
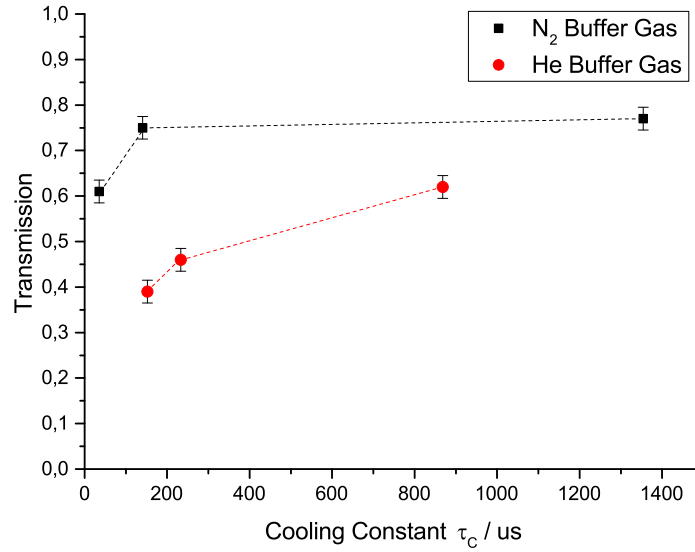
Figure 5.6.: Transmission for ^{133}Cs ions in the analyzer for 1 TFS and 256 MT for different cooling constants with N_2 and He as buffer gas; for both buffer gases the pressure has been varied resulting in different cooling constants and according cooling time.

pseudopotential. For strong suppression of interesting species or too high current of the ion source the RF amplitudes of RF1 and RF3 can be set to intentionally remove a certain mass range. Since ions below the Low Mass Cut-Off (LMCO) (see section 2.2.1.2) are not transmitted, one can take advantage of this and suppress unwanted species. A dedicated filtering with additional DC offset at the RF mass filter (RF-DC apex isolation) is subject of future work [Lippert, 2016].

The intensity of ions passing through the beam preparation system has been varied with scope on deteriorating effects for pure ^{133}Cs and a mixture of ^{133}Cs, ^{85}Rb and ^{87}Rb. A good indicator is the peak width for low numbers of turns, because it reflects the initial phase space. The analyzer aberrations are then less dominant. For high ion intensities (higher than 10^4 ions per cylce), no trend for the peak width or the flight time has been observed, whose onset is expected at much greater intensities [Tolmachev et al., 2000].

5.1.4. Time-of-Flight Analyzer

The analyzer, as the heart of the instrument, has been thoroughly investigated and optimized. New supply electronics and operation modes have been developed to enhance the performance and reliability.

An important role for the transmission efficiency plays the initial focusing by the injection Einzel lens and the self focusing behavior of the analyzer by the lens electrodes $E4$ and $E6$. Systematic studies show an advantage of high (negative) voltages of the injection lens compared to simulations. For the analyzer lenses, an optimization with good transmission by proper self focusing and

minimized time-of-flight aberrations has been found in accordance to the values from simulation studies [Yavor, 2011].

The second influence on transmission is the prevailing pressure in the analyzer region. It is most likely, that an ion is kicked out of the acceptance of the analyzer whenever it is affected by residual gas in the analyzer (due to high average kinetic energy and high momentum transfer). Due to effective vacuum separation and N_2 as buffer gas for cooling, these collisions are minimized (see figure 5.6). The electrical optimal tuning of the analyzer has been derived by a priori values from simulation studies and measured with best care for the stabilized and switched potentials (see section 4.3). Since the adjustable potentials create a rather complex parameter space, a systematic procedure, estimations from the peak shape and a certain amount of experience is essential. Once a good optimization is found, it is stable over a long period (weeks). Already tenths of Volts have a wide effect for most delicate electrodes, especially the end-cap electrodes E1 and E2.

5.1.5. Mass Range Selector

The temporal behavior of the MRS is studied in figure 5.7. The time of unhindered passing through the analyzer has been measured for ^{133}Cs ions with an active MRS. For each reflection there is a time interval when ions are not affected by an applied deflection voltage. And, as can be seen from the fact, that the total time-of-flight is constant over the whole interval, there is also no effect of possible electric noise from the MRS switching. A time wise sharp and effective operation is important to maintain a maximum of mass range and to avoid any effects on the time-of-flight, e.g. by a slight modification in drift energy by the MRS. Figure 5.7 demonstrates, that within a change of the activation time of $\Delta t_{MRS} = 150$ ns the mass selection of close species can be done for $1 ppm$ accuracy. The investigated species is thereby left totally unaffected. This observed time resolution of the MRS for cleaning from unwanted species enables a mass resolution of $R_{MRS} = \frac{t_{16turns}}{2 \cdot \Delta t_{MRS}} > 1000$ for a high resolution spectrum with activation of the MRS at the first 16 turns. It can even be reasonable to select species at a dispersed stage for higher turn numbers for even higher MRS mass resolution. As a consequence, the MRS can be employed as initial mass selector for low turn numbers to keep the total charge inside the analyzer low, and clean from neighboring masses for a narrow mass range at higher turn numbers.

The characterization of the MRS can further be used to study the unambiguous mass range. Therefore it is important to understand that the MRS affects at a certain time always several ion species with different turn numbers. When the MRS is applied at the latest turns, it is essential to skip unwanted species for sufficiently enough reflections, to guarantee that possible overlapping of species with different turn numbers $N \pm x$ are eliminated. Figure 5.8 illustrates the activation of the MRS for different time offsets. The peak positions are not affected, if the species is not eliminated. This behavior can be readily utilized for the determination of turn numbers. The timing of the MRS can be swept; whenever a species disappears/appears for an active MRS at time t_{MRS}, it is an indicator that one more reflection has been made by this species. The time difference between two of these events of disappearing/appearing is proportional to $\sqrt{m}$. If the behavior of the MRS is known for a probing ion, the constant factor of this proportion is known and the unknown mass can be determined, hence the number of turns can be derived for high accurate mass determination. When the disappearing/appearing signals are locked in dependence of the turn number, a crowded and unambiguous spectrum can be even automatically disentangled and the accepted mass range widely
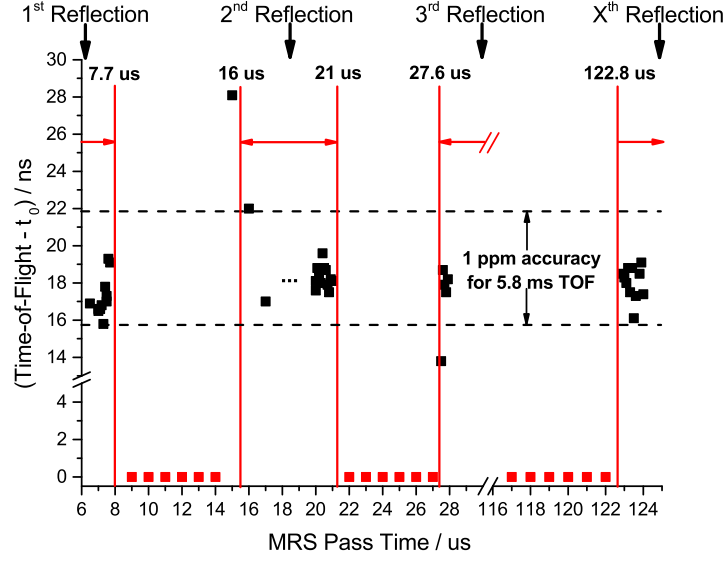
Figure 5.7.: Total time-of-flight versus the time period of ^{133}Cs ions to pass through the mass range selector; red squares indicate the ions are eliminated by the MRS, black squares represent the time-of-flight with unhindered transmission. The red arrows show the free transmission time range, the dashed line represents the allowed time-of-flight deviation for 1 ppm accuracy at 5.8 ms flight time.

enlarged. Even highly accurate measurements of unknown species with different turn numbers are thereby principally possible.

Besides the usage as purification tool for an ambiguous mass range, the MRS can also be employed as deflector for probing or adjusting the ion beam alignment in the analyzer (as explained in section 3.2.4). There has been no crucial misalignment been detected for the trap-analyzer axis. The optimum of the transmitted intensity for a broad ion beam is highest for a MRS deflection voltage of 10 V.

5.2. Characterization

5.2.1. Mass Resolving Power

Multi Turn Mode

The conventional operation with the the so-called multi turn (MT) mode of the analyzer and the principle concept is already validated in a previous work [Dickel, 2010]. Compared to that, the drift energy is increased by a factor of 1.7: $E_{kin} : 750\,\text{eV} \rightarrow 1300\,\text{eV}$. The initial peak width has been thereby decreased by a factor of 0.7, which matches perfectly with the expected value of $1/\sqrt{1.7}$ derived by the turn-around time Δt_{ta} [Plass et al., 2016] ($\propto 1/E_{kin}$). The energy dependence of the mass resolving power is increased accordingly (compare to equation 2.47).
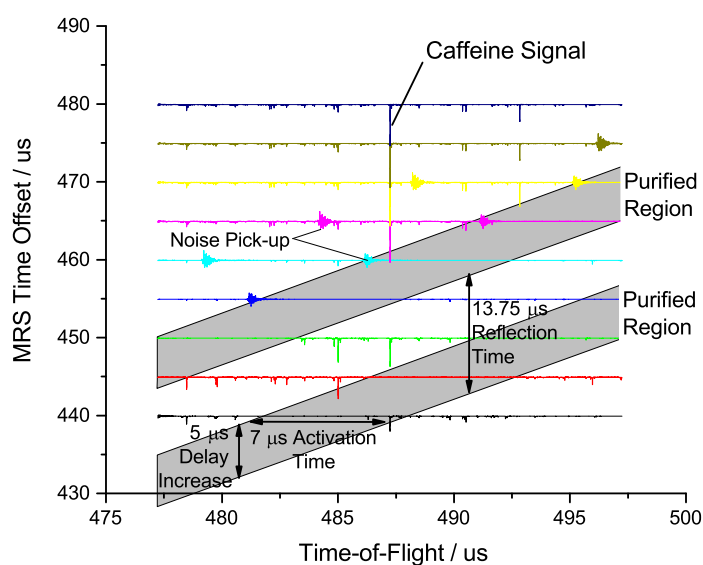
Figure 5.8.: Individual time-of-flight spectra of Caffeine by nESI with variation of the offset (in steps of $5\,\mu$s) of the MRS activation time ($7\,\mu$s); the eliminating effect of the MRS can be seen for multiples of the time of one reflection ($13.75\,\mu$s) as purified regions. The Caffeine signal is present at a constant time position, even for a late switching of the MRS shortly after the last transition through the analyzer. Distortions by the swept MRS pulsing for an invalid timing can occur within the spectrum.

Time Focus Shift

The turn-around time has major influence on the mass resolving power. It is inversely proportional to the extraction field strength (see equation 2.44). Thus, its contribution for the initial peak width $\Delta t_{initial}$ can be decreased by increase of extraction voltages. Since the time-energy focus has to occur on the detector plane for narrow peak widths, either the extraction field strength has to be adapted or a shift of the time-energy focus has to be realized. The latter is achieved by the time focus shift as described in 3.3.2. In figure 5.9 peak shapes measured with two extraction field strengths are displayed. For the multi turn mode with low extraction field strength the focus
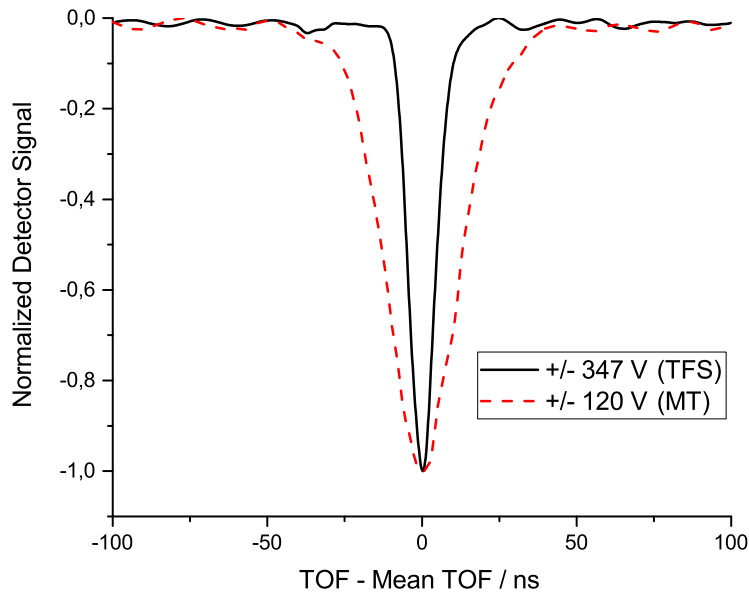
Figure 5.9.: Initial peak shape with time-energy focus on the detector plane for two applied extraction voltages: with normal multi turn mode only and an adjusted extraction field strength of $25\,\mathrm{V/mm}$ as well as with an time focus shift and higher extraction field strength of $74\,\mathrm{V/mm}$. (Measurement with ^{133}Cs.)

position is preserved on the detector and results in a peak width of $\Delta t_{\mathrm{initial}} \approx 27\,\mathrm{ns}$. The time focus shift with higher extraction field strength shifts the focus position to the detector (within this turn) and results in a much smaller peak width of $\Delta t_{initial} \approx 9.6\,\mathrm{ns}$. The ratio of voltages $347\,\mathrm{V}/120\,\mathrm{V} \approx 2.9$ is in good agreement with the ratio of the peak widths $27\,\mathrm{ns}/9.6\,\mathrm{ns} \approx 2.8$. This ratio increases the mass resolving power for lower turn numbers by the same factor. Besides that, the same charge (peak area) of the detected signal leads to a higher amplitude, which results in an improved signal-to-noise ratio. That is beneficial for the DAQ, sensitivity and accuracy.

Figure 5.10 demonstrates the advantage of a preceding time focus shift turn in terms of mass resolving power. For low turn numbers a drastic increase is observed. For higher turn numbers the relative contribution of initial energy spread $\delta \propto E_{kin}$ becomes more dominant for the operation
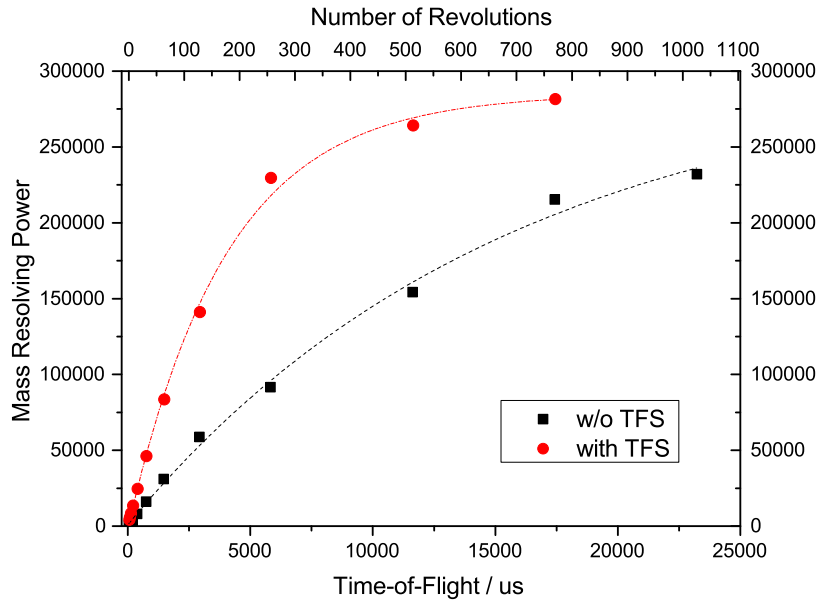
Figure 5.10.: Mass resolving power evolved by the total number of turns and corresponding total time-of-flight for ^{133}Cs for multi turn mode with and without a preceding time focus shift turn. The data points are fitted according to the equation for mass resolution 2.77 with $t_{PT\_TFS} \approx 40\,\mu s$ and $\Delta t_{initial}^{TFS} \approx 9.6\,ns$ as well as with $t_{PT} \approx 18\,\mu s$ and $\Delta t_{initial}^{MT} \approx 27\,ns$. That prompts a value of $\Delta t_{turn} \approx 40\,ps$ for both operation modes.

with TFS. For both operation modes higher turn numbers lead to an asymptotic behavior with some difference in maximal mass resolving power. The asymptotic trend can be explained by ion optical aberrations (due to mechanical and ion optical imperfections of the analyzer). The effect of time-of-flight aberrations accumulates with turn numbers, resulting in a maximum mass resolving power. Deviation of the ideal initial conditions of the injected ions enhance the contribution of higher orders aberration (refer to section 3.2.3). The non-vanishing mixed third order aberrations seem to dominate the total time-of-flight aberration, which is also predicted by simulation. The fitting of both mass resolving power evolvements according to equation 2.77 prompt a similar time aberration contribution for each single turn of $\Delta t_{turn} \approx 40$ ps.

The slope in the linear region for operation with and without time focus shift reflects the peak width $\Delta t = t_{\text{TOF}}/2 \cdot R_m$, which actually determines the resolving power. This width is growing slower for pure MT compared to that with TFS. This is compliant with the lower energy spread δ from the initial spatial distribution in the trap, since the extraction field strength is lower by a factor of 3, where the aberrations $(t|\delta^N)$ take less effect.

For a fixed mass resolving power, the smaller initial peak width through the TFS provides comparably faster analysis time by smaller required total time-of-flight. That implies a shorter measurement time and therefore less accumulated aberrations and less transmission losses. This is beneficial for e.g. time time-dependent processes as chromatography, high throughput application as screening or imaging, as well as for time-critical application as measurement of species with short half-lives.

Behavior of Mass Resolving Power

The dependence of the time-of-flight, the corresponding number of turns and the resulting mass resolving power is presented in figure 5.11 together with the typical transmission efficiency. The resolving power increases with the number of turns. For ^{133}Cs a value of 100000 is achieved after 2 ms and a value of 200000 after 5 ms only. A mass resolving power of $R_m > 250000$ is achieved routinely. The mass resolving power with adapted cooling and bunching of the ions is principally the same for any mass for a given number of turns. The analyzing time is proportional to the square root of the analyzed mass.

The transmission efficiency decreases with higher flight time due to residual gas collisions. N_2 is used as buffer gas with a cooling time $t_{cool} < 1$ ms for repetition rates $f_{\text{rr}} = 1$ kHz. Still, for highest mass resolving power the transmission is well above 50%. Besides the depicted error bars, a variation of transmission with an alternating odd/even behavior during lower number of turns is observed. A maximal mass resolving power of $R_m = 415000$ has been achieved (see figure 5.12). These settings are however not favorable for a stable and reproducible operation, because the mass resolution is sensitive to every change in the system. More reliable settings (referred to as 'conservative' settings) are preferably used and result in a resolving power of more than 250000. Such settings are chosen throughout the dominant part of this studies.

The capability of an MR-TOF-MS analyzer for high ion intensities is important for an analytical measurement with a large total and/or mass specific ion rate. While space charge influences the mass resolution as well as the mass accuracy above certain onsets [Boldin and Nikolaev, 2009], the ion capacity of an MR-TOF-MS has been reported differently and is subject of recent investigations [Kozlov et al., 2006, Grinfeld et al., 2014]. Figure 5.13 gives an impression for the analyzer
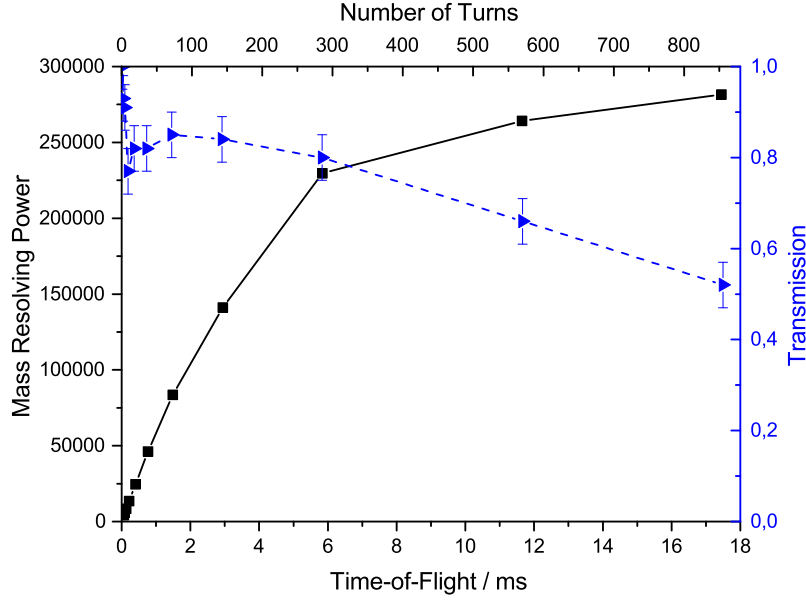
Figure 5.11.: Mass resolving power for stable settings and ^{133}Cs ions in dependence of total time-of-flight and total number of turns (black squares); transmission with N_2 as buffer gas capable of 1 kHz repetition rate (blue triangles).

of this instrument. The peak width for the default operation mode with time focus shift and 256 multi turns becomes 4 times larger with an increase of intensity by a factor of 100 and indicates some repelling of the ions by space-charge effects. The time-of-flight on the other hand has been monitored and is stable within statistical deviation. The broadening of peak width for the default operation (TFS + MT) is compared to pure multi turn Mode with 1536 turns without time focus shift. There, the energy spread δ is reduced by a factor 3 from lower extraction field strength and may cause the opposite effect – narrowing of the peak with rising intensity. That lifts the mass resolving power up to values of $R_m > 500000$, which is in this case not considered as a valid measurement. A self-bunching effect may give rise to that behavior, where (due to more dense energy phase space) faster ions push slower ions in front, resulting in a comparably narrow detected peak width [Zajfman et al., 2003]. The number of turns has been chosen to 1536 to be sensitive to the effect and for comparability, since the mass resolving power of both modes amounts to $R_m \approx 200000$. Further experiments show, that for pure multi turn mode – in contrast to the TFS and multi turn combined mode – an unreasonable behavior of the peak width with increasing total time-of-flight can be observed. This behavior is different with TFS and reflects the aberrations from simulation studies.

For the mentioned reasons the TFS is an ideal tool to minimize possible self-bunching for higher intensities and long flight times and to prevent any deterioration of mass resolving power for higher intensities. Further studies are underway to understand and circumvent the effect of space-charge for the MR-TOF-MS [Lippert, 2016, Lippert et al., 2015]. Generally, for the results of this work the intensity has been on levels (< 40 detected ions per species per shot), that do not implement any noticeable space charge effect.
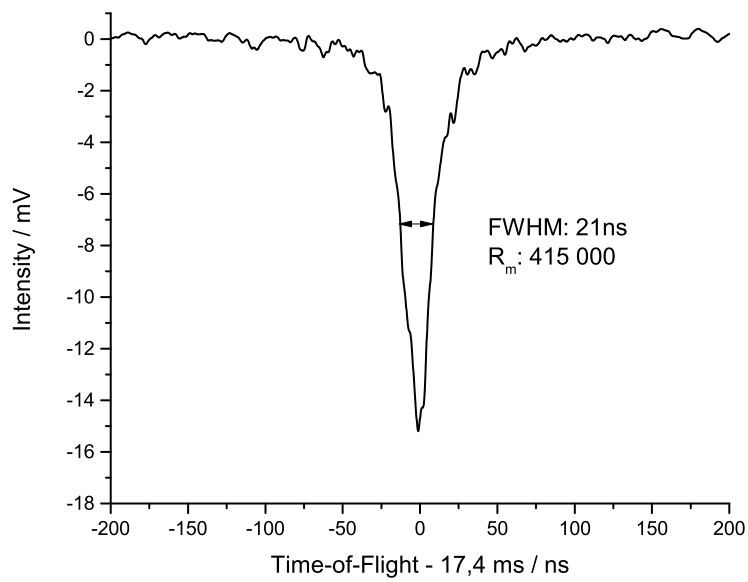
Figure 5.12.: Mass line of ^{133}Cs measured with the MR-TOF-MS. A mass resolving power of $R_m = 415000$ is achieved. The peak width at FWHM is determined to $\Delta t = 21\,\text{ns}$ with ^{133}Cs ions after 769 turns and $17462\,\mu$s total flight time.
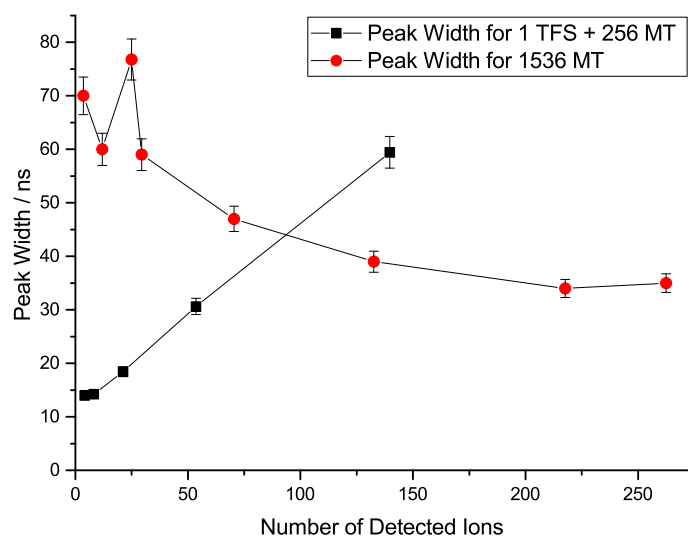
Figure 5.13.: Peak width after for ^{133}Cs for different numbers of detected ions 1 TFS + 256 MT (black squares) and 1536 MT (red dots); for comparability the mass resolving power of both modes corresponds to a similar mass resolving power of $R_m \approx 200000$. The number of ions is gained by the detected charge. Because of saturation effects of the detector, the number of ions is underestimated up to a factor of 50% for higher intensities.

5.2.2. Mass Accuracy

Mass accuracy is the decisive parameter for the determination of mass and composition of molecules. The potentially critical effects for highest mass accuracy have been exemplified and no systematic deterioration of ppm accuracy has been discovered. It has been shown that single negative effects on mass accuracy shown in the following amount to an influence of far below ppm values – even under unfortunate in-situ like conditions.

RF Influence

The RF field is likely to influence flight times depending on the RF phase during ejection. This has been investigated, while the RF was set to a non-optimal high Matthieu parameter (q>0.8) to artificially provoke unfortunate initial conditions of the ions and to emphasize the RF induced effects. In figure 5.14 the deviation in flight time in dependence of the RF phase is presented. Within the statistical deviation, no major deviation can be found. The error is below ±0.5ppm. High accuracy measurements seem not to be dominated by a possible RF influence. A switch-off procedure for the RF may nevertheless completely exclude such influence (see [Haettner, 2011]).
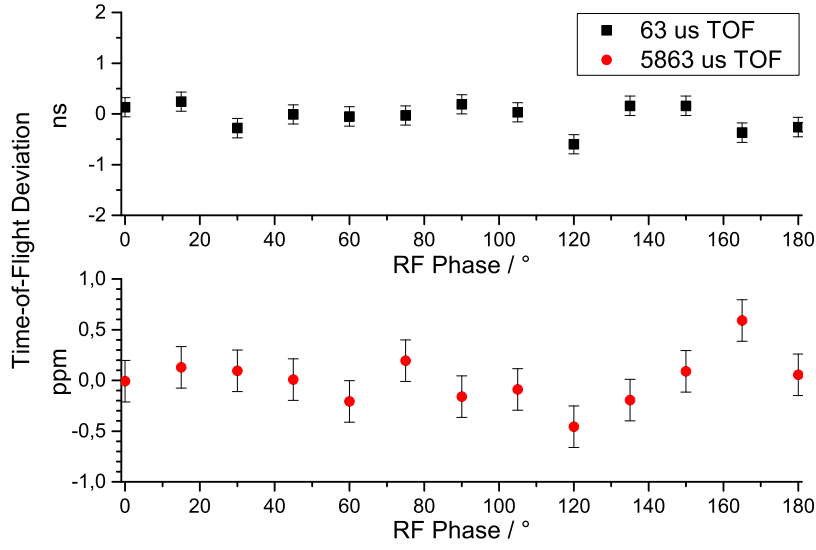
Figure 5.14.: Deviation of time-of-flight for ^{133}Cs ions versus RF phase during injection into analyzer for $63\,\mu s$ and $5863\,\mu s$ total flight time. The standard deviations of $\sigma = 0.25\,ns$ and $\sigma = 0.5\,ppm$, respectively. Intensity and peak widths stay well within the error of the measurement.

Electric Switching Influence

The correct timing for individual species and the switching behavior of the electronics is of highest importance and has been carefully explored. Switched potentials can potentially influence the energy and flight time of single species, that pass a varying electric field at different times, and negatively influence mass accuracy. This influence has been probed with ^{133}Cs ions for the time of closing the analyzer for the multiple-reflection mode. Figure 5.15 shows the resulting mass error in units of FWHM for different time moments of switching the analyzer electrodes. This time is translated into a scale of ions with different mass, that would experience the effects of electic switching at accordingly different times. In the considered scaled mass range of simultaneous measurement is no systematic shift of the time-of-flight (and the corresponding mass value) observed. In case of a flight time of $17\,ms$ and a temporal peak width at FWHM of $21\,ns$ (corresponding to figure 5.12) a maximal mass error of $0.05\,FWHM$ for the entire mass range results in an absolute mass error of $\frac{\delta m}{m} = \frac{2 \cdot 0.05 \cdot \Delta t_{FWHM}}{t_{TOF}} \approx 1.2 \cdot 10^{-7}$.

The next critical switching is at an enhanced stage of mass dispersion when switching the lower reflector from multi turn mode to open mode, the latest switching during measurement. In figure 5.16 the influence on flight time for ^{133}Cs ions during the whole principle time region of opening is shown. Translated into a flight time of $5.8\,ms$, the variation is below the relevant level for an 10^{-7} accuracy. Outside the usable time frame the ions experience a potential shift during the switching of potential and arrive at earlier time-of-flight.
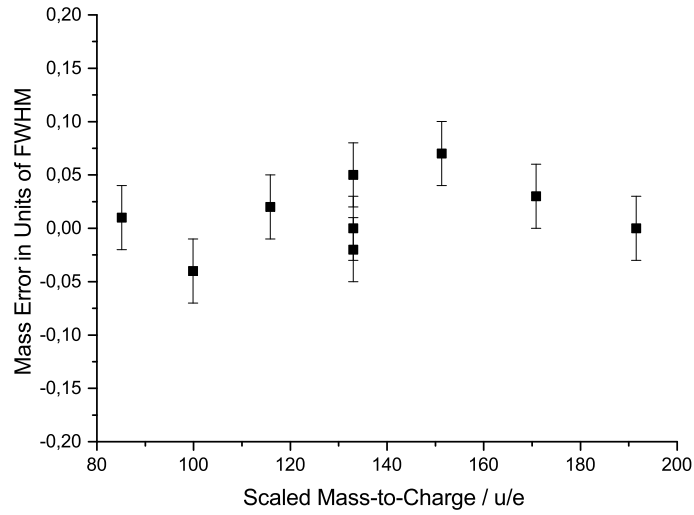
Figure 5.15.: Shown is the mass error in FWHM scaled for a range of masses. A time-of-flight variation for ^{133}Cs after 1 TFS and 1 MT is recorded in dependence on the time of closing the analyzer electrodes to a multiple-reflection potential. This is translated into the corresponding mass error of the considered range of ions with different mass – assuming these experience different electric fields.
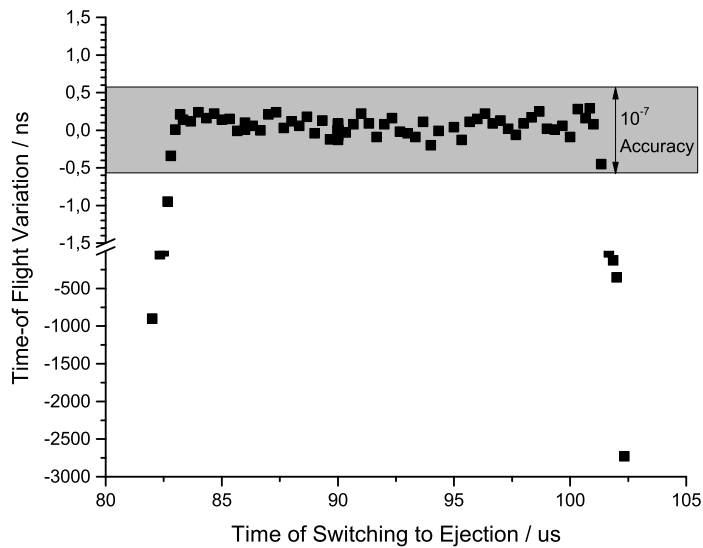

Figure 5.16.: Switching time for the ejection of ^{133}Cs ions to the detector and resulting deviation of Time-of-Flight; the gray region marks the tolerance region for $5,8\,\mathrm{ms}$ flight time to achieve a mass accuracy level of 10^{-7}.

Obtained Mass Accuracy

The resulting mass accuracy has been investigated with nESI of a peptide (MRFA) delivering mass lines at 524 u with isotopic contributions in the following mass numbers as seen in figure 5.17. The observed mass accuracy for the ion of interest at mass 525.2689 u in this case amounts to
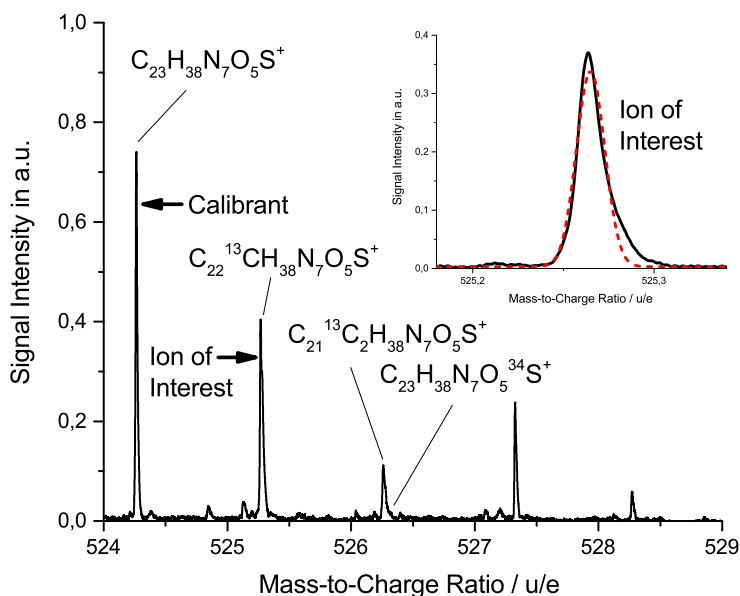
Figure 5.17.: Isotopic positive ion pattern of MRFA peptide with nESI recorded with the MR-TOF-MS with 1 TFS and 16 MT turns. A mass accuracy of $8.2 \pm 5.3 \cdot 10^{-7}$ has been observed for the ion of interest after a total time-of-flight of 795 μs only. The inset shows the detector signal and the Gauss fit curve for the ion of interest. The tail on the right hand side of the peak is in this measurement in the same proportion for all peaks due to ion optical aberrations. An isobaric overlap is observed at mass 526 u, which is caused by the integration of either $^{13}C_2$ or ^{34}S [Wilson and GlaxoSmithKline, 2006].

$8.2 \pm 5.3 \cdot 10^{-7}$ after a total time-of-flight of 795 μs only. These numbers can be underlined by the results of the systematic studies of potential error contributing factors that are mentioned above. A benefical effect on the mass accuracy is gained by the calibration with one of the detected species (internal calibration – see section 3.5.2). Any systematic influence on a single measurement should therefore affect the calibrant as well as the ion of interest and may be noted as a decrease in mass resolving power. The error contribution of the RF phase (see figure 5.14) in the ion trap during the ejection can be neglected, since the difference in mass is only $\approx 1/524$ and thus the time for leaving the trap region is very similar – as it is the RF phase. The error by the switching of the analyzer potentials to close and open can also not contribute, since both take effect on a sub-10^{-7} level only at tramendous mass differences (see figures 5.15 and 5.16). The mean total number of detected ions per spectrum of $N_{total} \approx 22$ is derived by comparison of the peak area of the mass peaks with a single peak area. A linear behavior of the detector can be presumed

for this low number of ion detections. The mean number per cycle of the ion of interest amounts to $N_{ioi} \approx 5$ respectively. The potential space charge effects may be excluded from prior studies, since the charge of the considered ions is far below the observed onset of space charge effects (compare figure 5.13). The number of real ions present in the analyzer with an estimated detection efficiency of 50% amounts to $N_{ioi}^{real} \approx 5/0.5 = 10$ and is below any expected effect [Grinfeld et al., 2014]. The considered Gauss peak distribution at mass 525 u is likely to be shifted due to isobaric contributions. The resulting deviation of the observed peak center has been evaluated to about $\approx 4 \cdot 10^{-7}$ by the estimation of a constant existence, ionization and transmission of the single isobaric species. The statistical error ($\Delta s = \sigma/\sqrt{N}$) is expected quite low, because of the sufficiently high number of detected ions of interest of $N_{ioi} \approx 2600$. Further studies of the mass accuracy [Dickel, 2010] for the mobile MR-TOF-MS is subject of future work.

The stability of the system provides *ppm* accuracy for several hours even without intermediate calibration (see section 5.2.6). The peak width and form for an accumulated spectrum does not obviously depend on the time of acquisition. Hence a constant mass accuracy is maintained for long measurement and acquisition times.
The effect on mass accuracy for higher ion intensities has been studied similar to the effect on mass resolving power in section 5.2.1. For ion intensities of up to 10^3 ions per cycle the time-of-flight has been was stable to sub-*ppm* level – for a single 1 TFS and also after several ms total time-of-flight.

5.2.3. Mass Range

The mass transmission for the RFQ beam preparation system varies slightly due to *q*-value and pseudopotential dependence (see section 5.1.3). This is different to the transmission mass range of the time-of-flight analyzer. There, by default any mass is transmitted and possibly cut by switched reflector electrodes. To prevent any deterioration the MSR is used to skip all species exceeding the valid mass range. Effects on TOF by switching the lower reflector of the analyzer to open state – this is the unambiguous mass range limiting instance – are shown in figure 5.16. Extrapolation of this time span to the moment of ejection from the analyzer delivers the mass range as plotted in figure 5.18. Higher mass resolution (and higher required time-of-flight) brings a more narrow mass range (compare equation 2.4 and section2.4). Nevertheless, the mass range is broad enough to resolve isobars of several neighboring masses.
In praxis, the mass range of the MR-TOF-MS can be extended by a larger mass window by subsequent measurments of sub-ranges of mass. As well, sophisticated methods to disentangle overlapping signals from different turn numbers are proposed and investigated (see section 3.4).

High masses with $m/Q > 2000$ can be accessed by the MR-TOF-MS as demonstrated in figure 5.19. A tuning solution, a mixture dedicated for calibration of ion traps [Thermo Fischer Scientific, 2015]. It delivers characteristic equidistant signals up to masses $m = 2122$ u. Single substances can be recognized and a typical distribution of Ultramark 1621® [Moini, 1994] is observed.
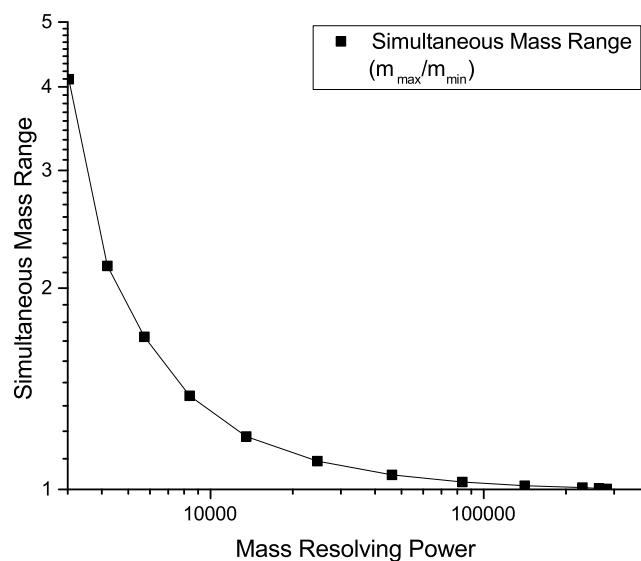
Figure 5.18.: Simultaneous mass range for a given mass plotted versus the observed mass resolving power (derived by ^{133}Cs measurement).
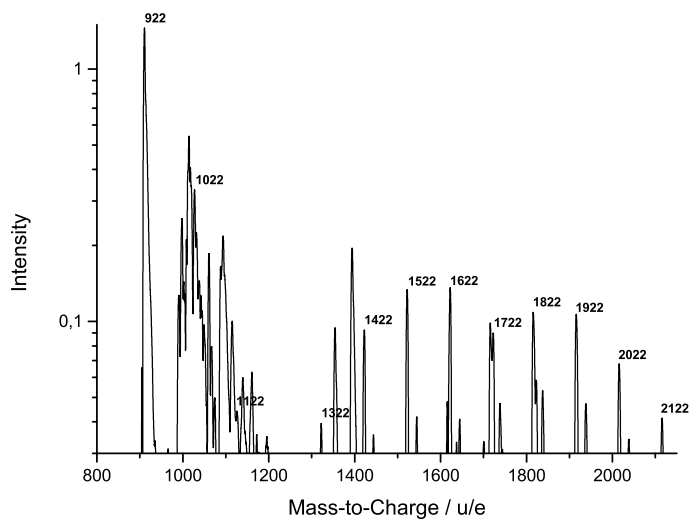

Figure 5.19.: Mass spectrum of Tuning solution by nESI demonstrates the measurement capability for masses $m > 2000u$. The typical intensity distribution of markers is observed [Moini, 1994]. Tuning solution comprises Caffeine ($20\,\mu g/ml$), MRFA ($1\,\mu g/ml$) and Ultramark 1621®[1] (0.001%) in an aqueous solution of Acetonitrile (50%), methanol (25%) and acetic acid (1%).

5.2.4. Repetition Rate

For applications with time-dependent processes the repetition rate and the corresponding acquisition time is relevant. The acquisition time t_{acq} is determined by the number of spectra n_{spec} required to gain sufficient statistics for high performance divided by the repetition rate f_{rr}:

$$t_{acq} = \frac{n_{spec}}{f_{rr}}. \tag{5.2}$$

The total time for complete ion processing is given by

$$t_{total} = t_{trans} + t_{cooling} + t_{tof} + t_{daq} \tag{5.3}$$

with the time for transport in the beam preparation system t_{trans}, the cooling time $t_{cooling}$, the time-of-flight t_{tof} and the time for the data acquisition t_{daq}. Note, that all processes are done in parallel, thus keeping the required time for one repetition very low, ideally suited for a multitude of transient and high through-put measurements. The repetition rate is limited by the transmission through the beam preparation system (determined to far below 1 ms in section 5.1.3), the necessary cooling time (also below 1 ms (see section 5.1.3)) and the required time-of-flight to gain the desired mass resolving power as depicted in figure 5.20. The repetition rate for the pure time-of-flight analysis can be considered as the inverse of the time-of-flight. A maximal repetition rate of 2 kHz has been realized.

For imaging MS such high-resolution and fast measurement cycles can greatly improve the total imaging time, where the typical scan speed can be in the order of one second per pixel [Roempp et al., 2015]. According to figure 5.20, the repetition rate for $R_m > 10^4$ at mass $u = 800$ is as high as 1000 Hz, thus accelerating the imaging time by a factor of 1000. For a $10 \mu m$ pixel size and an image dimension of $1\,mm^2$, this leads to a reduction from 10000 s to 10 s and helps to avoid any sample transformation and dry out effect for especially atmospheric imaging techniques [Roempp and Karst, 2015].

5.2.5. Sensitivity

The sensitivity is important for very low amounts of substance, high contamination ratios or simply few analyte ions. Principally, the instrument offers the sensitivity to measure individual ions. Therefore, the dark count rate needs to be low in order not to confuse dark counts with the investigated ions. In an relevant time window t_{rel} a validated dark count rate of $f_{dc} < 1/\min$ ensures sufficient chance of detecting a single ion without any disturbance. Considering an expected mass in a certain time window for this species $t_{ion} = 1/100 \cdot t_{rel}$ and a repetition rate of the instrument of 100 Hz, the probability of a false positive follows

$$p(fp) = f_{dc} \frac{1}{f_{rr}} \frac{t_{ion}}{t_{rel}} \tag{5.4}$$

and can be computed to $p(fp) = (600000)^{-1}$. This requires the absence of other close species and background signals from solvent, matrix or any other parasitic ionization.
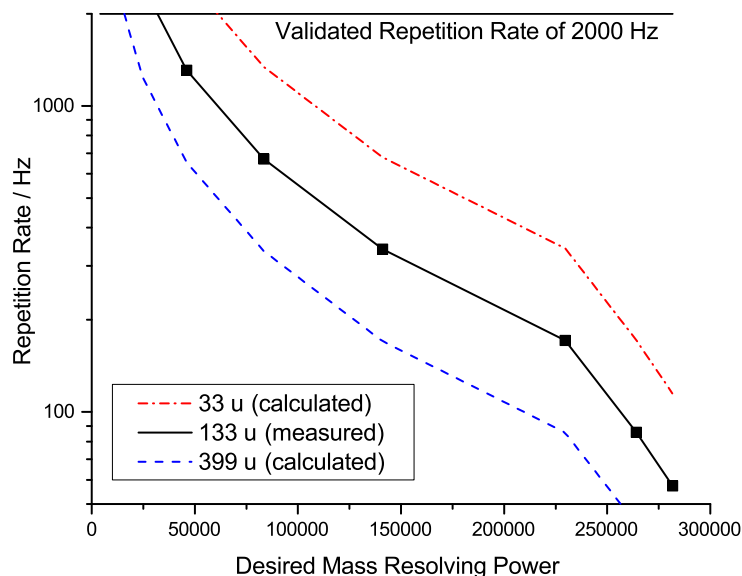
Figure 5.20.: Possible repetition rate according to desired mass resolving power and the required time-of-flight (this is the longest time contribution for high resolution spectra). The data is given by measurements with mass $m = 133$ u and scaled to masses 33 u and 399 u.

The individual subsystems of the MR-TOF-MS have been investigated concerning transmission efficiency, which is the decisive criteria for sensitivity. While all subsystems except the API principally provide transmission efficiencies up to 100%, the atmospheric pressure interface lacks of high efficiency, as initially expected as consequence of its concept. Also the choice of the ion source and according ionization efficiency determines the absolute sensitivity of the instruments.

The sensitivity of the MR-TOF-MS has been investigated, while a lower concentration of 10^{-7} mol/l requires a TDC for best identification, e.g. for the characteristic protonated Caffeine signal among multiple background signals originating from the solvent. A concentration of 10^{-5} mol/l on the other hand delivers such high intensity, that sensitive measurements of suppressed species require a selective transmission of these ions or high mass resolving power to guarantee their individual detection. Reliable measurements with intense signals have been obtained with nESI of Caffeine with a concentration of 10^{-6} mol/l. This is illustrated in figure 5.21. The population in the spectrum is similar to those of higher concentrations such as 10^{-5} mol/l. The gain of the detector has been adjusted for the individual concentration measurements to avoid any saturation effects. The total amount of substance n_{sub} can be calculated by

$$n_{sub} = n_{spec} \frac{1}{f_{rr}} r_{cons} c_{cons} \qquad (5.5)$$

with a required acquisition time of $t_{acq} = n_{spec}/f_{rr} = 100 * 1\,\text{s}/50 = 2\,\text{s}$ for 50 Hz operation and $n_{spec} = 100$ averaged spectra, a consumption rate of $r_{cons} = 30\,\mu\text{l}/3600\,\text{s}$ and an concentration
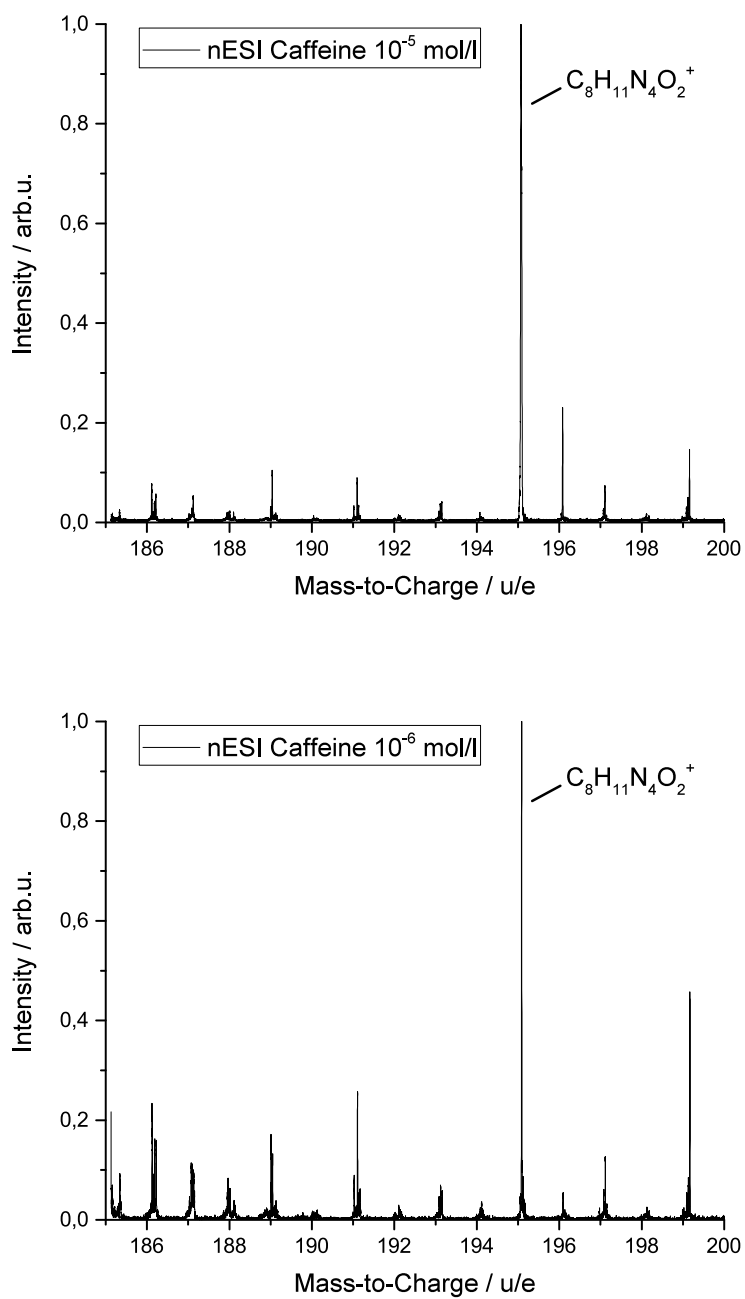
Figure 5.21.: nESI spectrum with Caffeine of 10^{-5} mol/l and 10^{-6} mol/lconcentration. The operation mode has been set to 1 TFS and 16 MT resulting in a mass resolving power of $R_m \approx 10000$. Same species are recognized at both concentrations.

of $c_{cons} = 10^{-6}$ mol/l, the absolute amount of necessary substance is $n_{sub} = 1.66 \cdot 10^{-14} mol$. This amount equals to $2.34 \cdot 10^{-12}$ g Caffeine.

5.2.6. Operational Stability and Ease of Operation

The stability of the overall system, especially the time-of-flight, is indispensable for obtaining high mass accuracy and mass resolution for any in-situ application. The stability of the overall flight time of $5843 \mu s$, corresponding to 257 turns, has been measured for ^{133}Cs over a time period of more than 5 hours with normal indoor conditions. No additional precaution, such as temperature control, has been taken. The resulting standard deviation in the time.of-flight is about $\sigma \approx 0.5 ppm$ for the whole period (figure 5.22) and assures sub-ppm accuracy with a single external calibration. In case of continuous calibration much higher stability of accuracy is reached (see section 5.2.2).
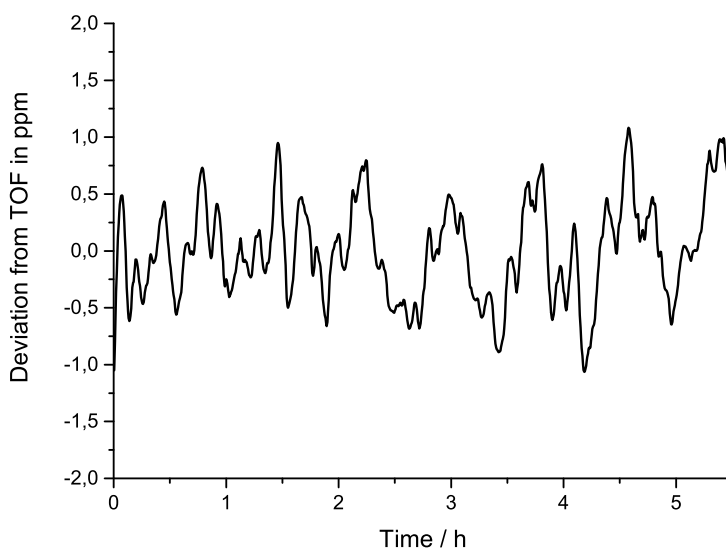
Figure 5.22.: Stability of the time-of-flight of ^{133}Cs for 257 turns and $5843 \mu s$ TOF respectively. The standard deviation is about $\sigma \approx 0.5 ppm$ and the related mass resolving power amounts to $R_m \approx 230000$. For better visualization a smoothing function of 30 neighboring data points has been applied.

Since the instrument is designed for in-situ applications, temperature and humidity regulated conditions are not fulfilled in most cases. The time-of-flight drift for a variation of temperature and an air flow through electronics assemblies from an open window at winter time is demonstrated in figure 5.23. The temperature sensitivity is found to be very low ($0.3 ppm/K$), ensuring high performance under unfavorable conditions. The temperature sensitivity rises, when the circulation within the instrument is changed by an external flow. When intermediate external calibration is possible (applied once per 10 minutes or once per hour), stability for sub-ppm accuracy is provided for even extremely changing conditions (e.g. wind fluctuations and sudden sunshine).
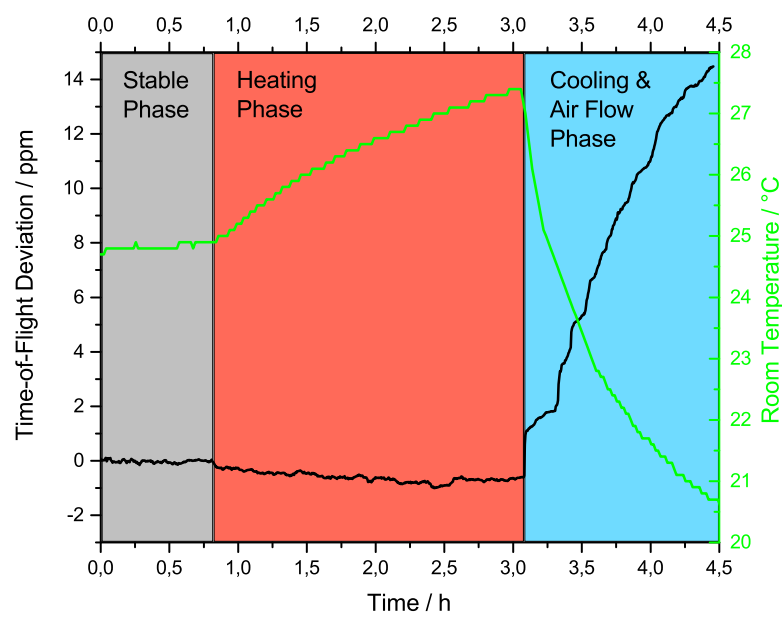
Figure 5.23.: Deviation of time-of-flight in ppm in accordance to room temperature change; for a slow change in the room temperature by heating the laboratory a deviation rate of $0.3\,ppm/K$ is observed and for a rapid change by open windows including an enhanced air flow a deviation rate of $2.1\,ppm/K$ is found.

In the future, a housing for the instrument may prevent any sudden wind blow and fast temperature change inside the instrument and minimize the dependence on environmental conditions. A steady cooling air flow through the system is therefore necessary to take away the heat ballast of the electronic components. Possible hygienic specifications for operation in a surgery room can be met, e.g. by a filter for the cooling air and the exhaust of the roughing pump.

Since the instrument is designed for universal application and optional coupling to complementary techniques, the time for a measurement may vary. Default acquisition times are rather short and perfectly suited for high throughput measurements, fast time-dependent processes in life science or studies of short-lived radioactive nuclides. The behavior for an even longer time of acquisition has been tested in terms of high performance parameters. It is possible to acquire a single measurement during a period longer than an quarter of an hour with a mass resolving power > 250000 with a single calibration – without any peak broadening or shifting of mass value. That goes along with a steady and stable operation of the device.

The settings for proper operation and highest performance of the device are usually found during adjustment for the individual measurement. This can be specific and dependent on the desired goal. The performance after switching on the device is close to maximal performance – even after weeks without intermediate optimization. Generally, the settings for single operation modes and masses are determined, documented and easily scaled with dedicated software calculations. A future and integrative system control may access these settings – derived from few input parameters – and automatically operate and control the system.

Operation of an in-situ instrument also includes some practical aspects in setting up the system. This is very promising for the mobile MR-TOF-MS. Transportation is guarantied by wheels and the compact architecture. It has been designed to fit into an ordinary van. Needed infrastructure in only a power supply below $1.5\,\mathrm{kW}$. Sufficient pumping and base pressure is achieved after $20\,\mathrm{min}$ only. Electronics are in operation in the same time without noticeable thermal drift.
The manual preparation of the system requires 2 minutes only – the operation of the ready for action system can be done automatically or remotely. Acoustic emission stems from the integrated roughing pump, which can also be separated for a more silent operation.

5.3. Mass Selective Ion Re-Trapping

The mass-selective re-trapping of ions with an RFQ trap is the inverse process of the injection into the analyzer. This procedure provides simultaneous highly mass-resolved separation and high efficient stopping and trapping of a single ion species. No principle change of the MR-TOF-MS in ion optics is necessary and no additional subsystems are needed. This method has not been reported elsewhere. Once implemented, the operation is reliable and reproducable.

5.3.1. Separation

The aim of mass-selective re-trapping is the separation or isolation of individual ion species for MS/MS experiments, collection of single species for other applications or high precision measurments without disturbing contamination. The re-trapping of ions from a multiple-reflection

time-of-flight analyzer has been done for the first time. It is based on a dynamic closing of the injection trap to catch a directed and time-dispersed ion bunch with extraordinary mass-selectivity. The capability of the mobile MR-TOF-MS is characterized concerning separation power and fundamental behavior. The underlying physical theory is described in section 3.3.5 and agrees with the results of the experimental data.

Figure 5.24 shows the time dependence for the re-trapping efficiency for different numbers of turns (1.5, 16.5 and 256.5 normal turns plus a preceding time focus shift turn). The ions are reflected
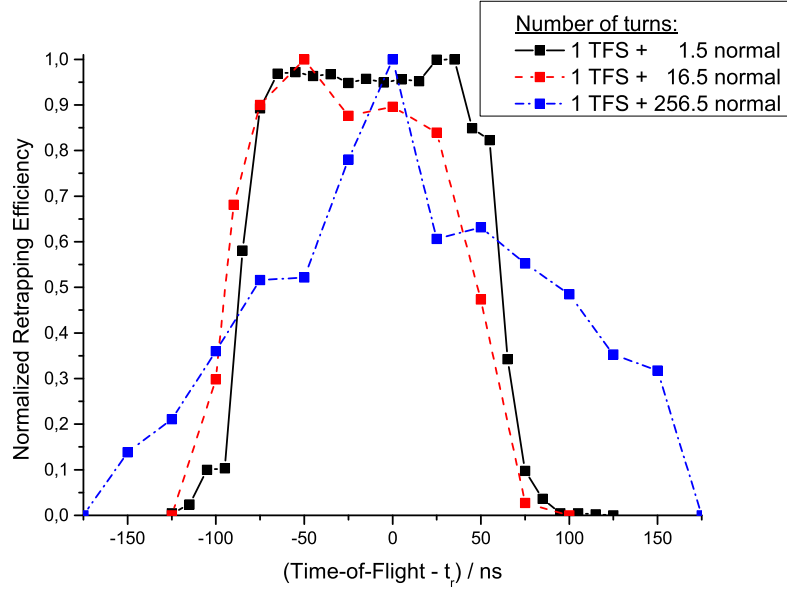
Figure 5.24.: Re-trapping efficiency for ^{133}Cs ions versus the medial time of re-trapping t_r for different turn numbers and a potential well depth of 12 V on the trap axis.

in the analyzer and transmitted back to the injection trap. That is switched to storage potentials at the time of re-trapping t_r, which is the time in the middle of the acceptance time range. Every ion that arrives at a time $t_{re-trapped} = t_r \pm \Delta t_r$ for a width of time-acceptance for each mass line of $2 \cdot \Delta t_r^0 > 2 \cdot \Delta t_r$ is re-trapped, cooled and stored in the injection trap. While ions with $\Delta t_r > \Delta t_r^0$ are not captured in the trap. The reason why they are not trapped is their remaining kinetic energy, since the potential is switched to trapping while they are not entirely at rest.

For a low number of turns a sharp rise of the acceptance guarantees for similar mass separation powers $R_s^{0.01}$ and R_s^{FWHM} (at 1% and 50% acceptance level). With higher flight time the shape of re-trapping efficiency broadens due to cumulative aberrations and an increased deviation from the initial phase space prior injection. For the ideal case with ion bunches remaining their initial phase space throughout the entire mass-dispersion an infinite mass separation power would be possible (same as applies to mass resolving power). For a higher flight-time and correspondingly higher time-dispersion for different masses, a higher mass separation power $R_s = t_{tof}/2\Delta t_r^{FWHM}$ can be accounted.

An overlapping time for the re-trapping acceptance of different species would defeat their sepa-

ration. In order to reduce the indivieual time acceptance for re-trapping, the energy acceptance of the trap can be lowered. This effect is shown in figure 5.25 with different depths of the axial trap potential well. The lower the well, the more selective the re-trapping process for species with
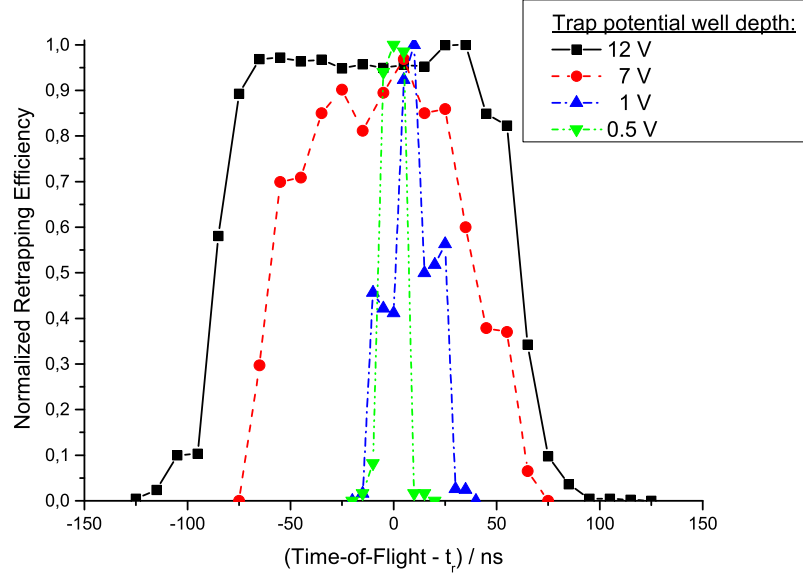

Figure 5.25.: Re-trapping acceptance for ^{133}Cs ions as function of the re-trapping time t_r ($\approx 50\,\mu$s) in case of different axial potential well depths in the trap for one TFS + 1.5 multi turns.

different arrival time. Their corresponding higher remaining kinetic energy at arrival times $\neq t_r$ is above the shallow trapping potential. So they are not trapped by the axially and radially confining field. The mass separation power increases with decreased arrival time acceptance Δt_r^0. Such a shallow trapping potential is favorable for separation power, but brings losses in efficiency. Further, it is also visible that the separation power is similar for FWHM and 10% in case of a deeper well and differs for a more shallow well. There, a plateau structure on the flank appears, that is not yet understood.

The evolvement of separation power in dependence of the number of turns is depicted in figure 5.26 for 2 different trap well potentials. A deeper storage potential well delivers lower separation power, a shallow well higher separation power. The re-trapping efficiency behaves vice versa (see figure 5.29). The narrow acceptance however is more sensitive for changes in beam profile caused by higher numbers of turns, thus resulting in a saturation effect in separation power.// In these experiments, a more shallow trapping well is only established for the re-trapping process. During cooling and injection into the analyzer for mass separation and mass measurement a default trap well potential is applied. When the shallow trapping potential is applied for a time $t_{shallow} > 10\mu$s, the ions are separated, efficiently stored and cooled.

The possible mass separation power is demonstrated in figure 5.27 and reaches $R_s > 60000$ at FWHM. At the 1 % level a separation of $R_s^{0.01} = 27000$ with nearly entire suppression for different
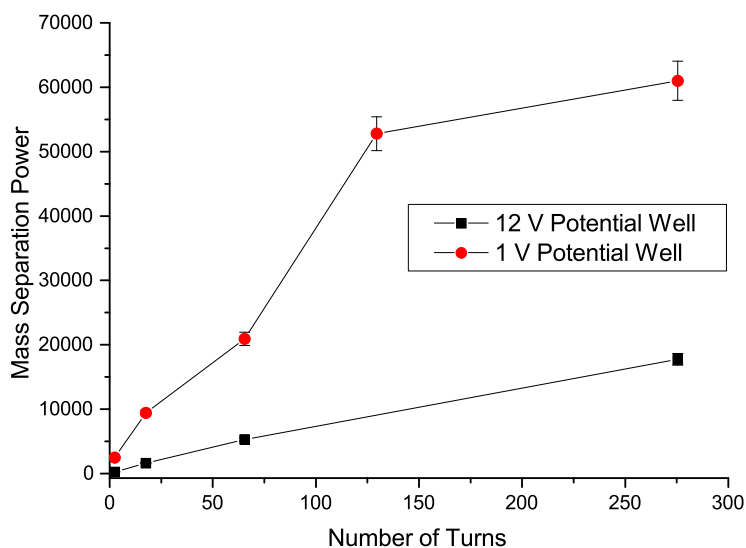
Figure 5.26.: Mass separation power (FWHM) for ^{133}Cs ions versus the number turns with a potential well depth on trap axis of 12 V and 1 V. The error for the shallow potential well is due to the heterogeneous plateau structure of the re-trapping acceptance (see figure 5.25).

species is achieved. If this is applied to future MS/MS experiments, the mass separation power can thereby be increased by a factor of 6 compared to existing, conventional TOF MS/MS instruments. That may allow for a much more specific precursor selection, which is absolutely beneficial for proteomics and other analytical disciplines [Liu et al., 2009].

For most separation cases, very close neighboring contaminants are either of the higher or lower mass side. This fact offers a separation by the rising or falling edge of the re-trapping acceptance shape. From figure 5.27 exemplary the mass separation power by the time for the rising or falling flank $t_{flank}(\approx 15\,\text{ns})$ of $R_s \approx 3000\,\mu\text{s}/(2 \cdot 15\,\text{ns}) = 100000$ can be derived.

A mass-selective separation within a spectrum is shown in figure 5.28. The separated species amounts to $\approx 2\%$ of the total intensity and is entirely isolated after re-trapping. This can be done with any species, while delivery to later experiments is possible through the high efficient RFQ storage. E.g. in-trap CID or higher energetic CID in the RFQ cooler can be used to fragment the isolated precursor and highly mass-resolved investigation of daughter ions can provide further information of structure and the character of chemical bonds.

5.3.2. Efficiency

The efficiency of mass-selective re-trapping is of great interest for applications with rare ion production rates and for application with high intensity demands for further experiments (e.g. MS/MS experiments). The efficiency of the MR-TOF-MS has been investigated and is rather high com-
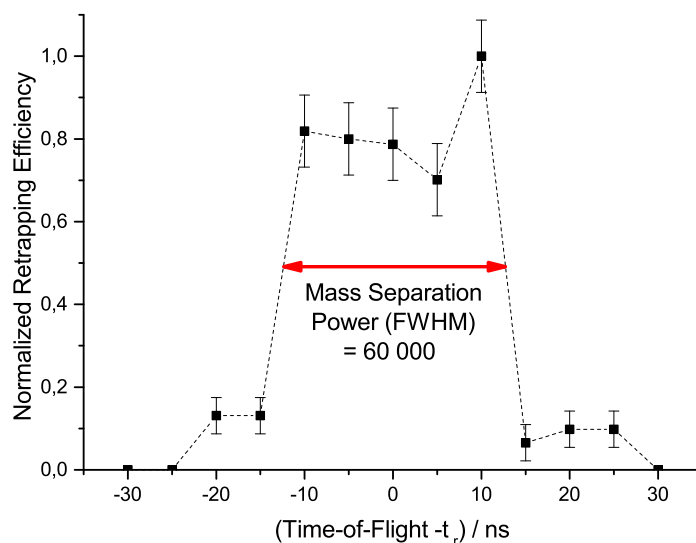
Figure 5.27.: Demonstrated mass separation power by probing the acceptance of re-trapping for ^{133}Cs by the time of switching the trap to re-trapping potential. With $1\,V$ trap well potential and $129,5$ turns (corresponding to $t_r = 2960\,\mu s$) a separation power at FWHM of $R_s^{FWHM} > 60000$ is achieved. The separation power for either lighter or heavier masses is is provided by the rising and falling flank and amounts to $R_s^{flank} \approx 100000$.
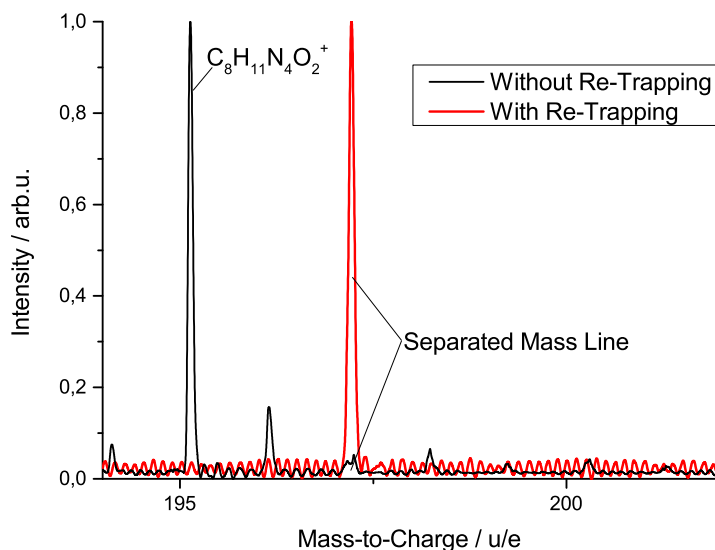

Figure 5.28.: Separation of low abundance mass line ($\approx 2\%$ of Caffeine intensity) by re-trapping in Caffeine nESI spectrum. The spectrum is cleaned from any other species.

pared to other very high resolving separation techniques. Figure 5.29 shows the obtained efficiency versus the number of turns for the very selective and medium selective potential well depths of 1 V and 12 V. An exponential drop is visible. This is predicted similarly by simulation studies [Yavor, 2014a], however with decreasing efficiency only for higher number of turns. Simulation and
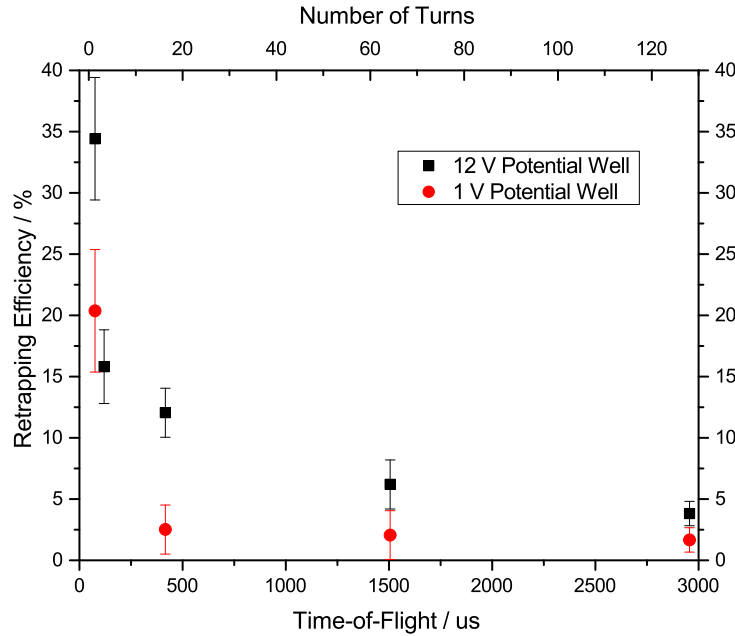
Figure 5.29.: Re-trapping efficiency for ^{133}Cs with 1 V and 12 V potential well depth versus time-of-flight and number of turns.

experiment both show a deficiency in focusing of the incoming beam, as well as field penetration from the high voltage drift potentials into the trap region. An additional lens has been designed to counter these effects and will be implemented in future.

Detailed studies show also an alternating efficiency for odd and even turns at low turn numbers and indicate a slight misalignment of beam profile in the analyzer. A two point deflection of injected and re-trapped ion cloud (see 3.2.4) may compensate for that effect and improve the efficiency as well. Expected values for efficiency exceed 90% even for higher turn numbers [Lippert et al., 2015].

6. Conclusion and Future Directions

6.1. Conclusion

A compact high performance multiple-reflection time-of-flight mass spectrometer on mobile basis for in-situ analytics has been designed, manufactured, assembled, commissioned and characterized. It combines for the first time high performance and the option of field deployment.

Performance parameters can be summarized as: mass resolving power larger than 300000, mass accuracy below 1 ppm, an atmospheric pressure interface for ambient ion sources, a mass separation power of exceeding 60000 and the potential for MS^N measurements, a repetition rate of more than 1 kHz for time-dependent processes, a duty cycle of 100% even for continuous ion sources, a high sensitivity of 10^{-7} mol/l or 10^{-12} g, single ion sensitivity, stable performance (≈ 0.5 ppm for hours and time-of-flight drift of only 0.3 ppm/K), a simultaneous mass range of higher than 4, as well as an analyzer transmission of 80% with a mass resolving power of $R_m = 200000$ for ^{133}Cs after 5 ms measurement time. All together on a robust and mobile platform perfectly suited for in-situ applications, with a set up time of ≈ 20 min, moderate power consumption, no need of additional infrastructure and optional remote control. Novel concepts have been elaborated: A time focus shift for a constant time-energy focusing, independent of extraction field strength and number of turns, without need of additional electrodes, a well as a highly mass-resolving re-trapping for an efficient isobar separation, which is an important pre-requisite for MS^N experiments.

This instrument is a vital connection of interdisciplinary research fields. It has been derived from a pre-existing high performance instrument developed for nuclear physics, while the underlying technique has now been made available for in-situ analytics and life sciences. Moreover, aspects and techniques developed in the course of this work are in turn going to be used in nuclear physics experiments. The analyzer design, according techniques, electronics, components in a rugged and compact format, as well as operation modes are also well suited for nuclear physics experiments such as the TRIUMF's Ion Trap for Nuclear and Atomic Science (TITAN) experiment at TRi University Meson Facility (TRIUMF) [Dilling et al., 2006, Chaudhuri et al., 2014]. There, an analog design of the mobile MR-TOF-MS analyzer and according electronics has been set up as diagnostic tool for the facility and as isobar separator to provide an isobarically clean beam for the highly accurate mass measurement in a Penning trap [Jesch et al., 2015]. The demonstrated mass separation power of some 10^4 will ensure to increase the number of accessible nuclides for precision experiments in comparison to the default separation techniques [Ettenauer et al., 2013].

First measurements with analytical samples verify the overall concept and demonstrate great application potential. The conduction of tandem MS experiments will further enhance the analytical significance [Lippert, 2016]. The capability and flexibility of the developed instrument enable a broad variety of analytical investigations, such as medicine, civil safety, environmental and climate research, bio science, as well as food and pharma industry, which are subject of future efforts.

6.2. Outlook and Future Direction

Clinical Mass Spectrometry

Higher capabilities of modern instruments and new ion generation methods allow for a prompt diagnosis even during medical examinations and interventions.

Since breath contains similar chemical composition to compounds present in blood, also many metabolites are expected in exhaled breath. This is used in diagnostic methods by means of high-resolution secondary electrospray mass-spectrometry [Berchtold et al., 2014]. Thereby one can discriminate between exhaled endogenous metabolites from an illness and exogenous contaminants that have been incorporated. The MR-TOF-MS offers fast measurements to pin the time-dependence of exhaled breath and resolve meaningful components. The compactness and mobility allows for an efficient operation in medical facilities.

Intra-operative tissue recognition by means of Rapid Evaporation Ionization Mass Spectrometry (REIMS) allows to differentiate between healthy and pathogenous tissue and immediate identification of cancer type [Takats et al., 2012]. Tissue specific mass patterns and compound levels are compared to a data base during application. That offers a so-called Computer-Assisted Surgical (CAS), where an alert may inform the surgeon during tumor resection when the tumor tissue is approached to adjust the resection line further from the bulk tumor tissue [Balog et al., 2010, Balog et al., 2013]. As well, a minimally invasive micro probing of suspicious tissue is possible to gain a histology-level identification. The mobile MR-TOF-MS can be utilized to provide for higher mass resolution and repetition rate compared to other MS with similar flexibility and footprint [Waters Corporation, 2014], thus an improvement in identification capability is most likely. Further, short measurement cycles guarantee for a quick response during incision movement. The API guarantees for the compatibility to sample delivery, which may be done by individual surgical tools [Schaefer et al., 2012, Schaefer et al., 2011b].

High Resolution Imaging

Mass spectrometry imaging with high resolution in mass and space requires first of all a good instrumentation for the spatial resolution. A high mass spectrometric performance on the other, as well as a fast processing is necessary to cope with the multiplicity of the single pixel measurements [Roempp and Spengler, 2013]. The MR-TOF-MS delivers both, shortest measurement cycles and highest mass resolution and accuracy as discussed in chapter 5.2. That is very much beneficial for ambient imaging to avoid sample transformation during the measurement period and still deliver a clear classification of the compounds [Roempp and Karst, 2015]. Further, the future option of MS/MS experiments may even extend the analytic significance.

Environmental Science

Environmental science relies increasingly on mass spectrometry as a qualitative and quantitative tool. Modern extraction techniques allow to concentrate chemical agents present in artificial or natural water reservoirs by many orders of magnitude [Ocana-Gonzalez et al., 2016]. A dedicated sample-pretreatment as well as the enrichment of analytes [Belardi and Pawliszyn, 1989, Eisert

and Pawliszyn, 1997] allow for an ambient analysis of the absorbent, [Deng et al., 2014], such as supervision of industrial processes, understanding and location of environmental metabolic trans-reactions, as well as for tracing and quantification of chemical pollution [Schrittmatter et al., 2012].

One targeted substance is the anti-inflammatory and antigenic drug Diclophenac, that is often insufficiently metabolized and occurs in waste water. Monitoring of such pharmacological residues on hot-spots (e.g. clinical institutions) is important for the conservation of our environment and possible intervention.

The MR-TOF-MS can be used therefore as analytical stage [Duering, 2012]. A direct detection of higher concentrated species without preparative extraction may be possible, as the sensitivity of the instrument promises (see section 5.2.5). For example, the MR-TOF-MS can measure and identify Diclophenac from bodies of water among many other constituents and provide a fast and time-resolved monitoring – not tied to a certain place.

Civil Protection

Analytical tools play a major role in modern anti-terror and civil security institutions. Ion scanner for instance are utilized on airports to detect explosives and drugs with wiped sampling from arbitrary surfaces from passengers baggage. In the civil security sector a variety of analytical methods identify or trace dangerous goods in case of miscellaneous incidents [BBK, 2010, Bruker GmbH, 2013]. They all have to be field-deployable, robust and easy to use. Even though a great range of chemicals can be detected, there is a lack of sensitivity and specificity for some substances. And, there is no instrument to cover several classes of chemicals. Mobile instruments so far lack of sufficient mass spectrometric performance to do so [Lange et al., 2011, Lange, 2011]. That is why there are recently new techniques and instruments under investigation [Koenig, 2014]. Higher mass resolving power could enable higher specificity and a broader range of application. The mobile MR-TOF-MS represents a good tool for an universal detection and identification and may overcome a supplemental chromatographic stage, as well as the limits in the detection of explosives, which are commonly conducted with IMS [Zalewska et al., 2013]. The ambient ionization enables immediate analytical results at the place of measurement and the accurate mass the high mass resolving power ensure sufficient specificity. The future option of tandem MS states an additional identification capability. With LTP as complementary ionization method to electrospray, both are ideal in-situ ion sources and readily applicable [Wiley et al., 2013a]. The low infrastructural needs, high analytical capability and the fast set up time is perfectly suited for civil security. Direct and broad band mass spectra offer the detection and quantitative comparison of leading substances and allow an unambiguous identification in high resolution mode. While the prerequisites are given in terms of performance and robustness, the operation of the instrument has to be simplified in future for the incidence application [Koenig, 2013].

For the first time an analytical instrument may target the detection of all dangerous goods, which are chemicals, explosives, biological material and radio nuclides on-site in a hazardous environment.

Re-Trapping Efficiency

The method of re-trapping has proven great potential with comparably high efficiency at low turn numbers. The efficiency drops for higher separation power and higher turn numbers. This is believed to be related to misalignment and field penetration at the re-trapping region. The implementation of an additional diaphragm next to the injection trap, an additional focusing as well as the two point steering will compensate for this effects and improve the efficiency.That leads to higher possible turn numbers at constant efficiency and thus increases the absolute separation power.

Instrument Automation

As a prototype instrument, operation and adjustment of settings is at best done by a trained person. Automation in terms of optimization and fine tuning, adjustment of measured mass range, choice of high or medium mass resolution, scanning of mass range at highest mass resolution, autonomous MS/MS experiments and complete calibration and mass evaluation is a fundamental goal for an all-round application. The underlying principles are understood and single software packages for the operation of the instrument are available. An integrative software platform combining all these aspects needs to be developed.

Ruggedization and Shrinking

Proof-of-principle experiments have been very successful. For coming applications, the reliability of the instrument is of increasing importance. The resistivity for environmental stress and transportation needs to be assured. While the current implementation is already robust and ready for most applications, it is still as flexible as a development platform needs to be. Dedicated engineering of individual subsystems will give rise to more extreme experiments. Power supplies with fixed high precision voltages, custom-made vacuum recipient and condensed electronics can drastically shrink size and weight of the instrument and make it more robust and directs into air-borne, under water and space mission applications.

A. Abbreviations

List of Figures

Bibliography

[Aberth, 1981] Aberth, W. (1981). An imaging detector system for mass spectrometry. *Int. J. Mass Spectrom. Ion Phys.*, 87:379–382.

[A.Contreras et al., 2008] A.Contreras, J., A.Murray, J., E.Tolley, S., L.Oliphant, J., Tolley, H., A.Lammert, S., D.Lee, E., W.Later, D., and L.Lee, M. (2008). Hand-portable gas chromatograph-toroidal iontrap mass spectrometer (gc-tms) for detection of hazardous compounds. *Journal of the American Society for Mass Spectrometry*, 19:1425–1434.

[Aebersold and Mann, 2003] Aebersold, R. and Mann, M. (2003). Mass spectrometry-based proteomics. *Nature*, 422:198–206.

[Alanssari et al., 2015] Alanssari, M., Frekers, D., Eronen, T., Canete, L., Dilling, J., Haaranen, M., Hakala, J., Holl, M., Jeskovsky, M., Jokinen, A., Kankainen, A., Koponen, J., Mayer, A., Moore, I., Nesterenko, D., Pohjalainen, I., Povinec, P., Reinikainen, J., Rinta-Antila, S., Srivastava, P., Suhonen, J., Thompson, R., Voss, A., and Wieser, M. (2015). Single and double beta-decay q values among the triplet ^{96}zr, ^{96}nb and ^{96}mo. *Phys. Rev. Lett.*, 116(072501).

[Alikanov, 1957] Alikanov, S. G. (1957). A new impulse technique for ion mass mearsurement. *Sov. Phys. JETP*, 4:452.

[Anderson and Anderson, 1998] Anderson, N. L. and Anderson, N. G. (1998). Proteome and proteomics: New technologies, new concepts, and new words. *Electrophoresis*, 19:1853–1861.

[Ayet, 2014a] Ayet, S. (2011-2014a). Fast high voltage switch. private communication.

[Ayet, 2014b] Ayet, S. (2012-2014b). Passive voltage stabilization for an mr-tof-ms. private communication.

[Badu-Tawiah et al., 2013] Badu-Tawiah, A. K., Eberlin, L. S., Ouyang, Z., and Cooks, R. G. (2013). Chemical aspects of the extractive methods of ambient ionization mass spectrometry. *Annu. Rev. Phys. Chem.*, 64:481–505.

[Balog et al., 2013] Balog, J., Sasi-Szabo, L., Kinross, J., Lewis, M. R., Muirhead, L. J., Veselkov, K., Mirnezami, R., Dezso, B., Damjanovich, L., Darzi, A., Nicholson, J. K., and Takats, Z. (2013). Intraoperative tissue identification using rapid evaporative ionization mass spectrometry. *Science Translational Medicine*, 5(194):194.

[Balog et al., 2010] Balog, J., Szaniszlo, T., Schaefer, K.-C., Denes, J., Lopata, A., Godorhazy, L., Szalay, D., Balogh, L., Sasi-Szabo, L., Toth, M., and Takats, Z. (2010). Identification of biological tissues by rapid evaporative ionization mass spectrometry. *Anal. Chem.*, 82:7343–7350.

[Balsiger, 2007] Balsiger, H. (2007). Rosina - rosetta orbiter spectrometer for ion and neutral analysis. *Space Science Reviews*, 128:745–801.

[Bateman, 2015] Bateman, R. (2015). Sector instruments for chemical analysis and research. *International Journal of Mass Spectrometry*, 377:281–294.

[BBK, 2010] BBK, B. (2010). ABC-erkundungskraftwagen.

[Becker et al., 2009] Becker, A., Dickel, T., Giessel, H., Petrick, M., Plass, W. R., Scheidenberger, C., and Simon, A. (2009). Simplified radio frequency quadrupoles with a linear axial field based on highly resistive electrodes. In *DPG Frühjahrstagung, Bochum*.

[Becker and Dietze, 2000] Becker, J. and Dietze, H.-J. (2000). Inorganic mass spectrometric methods for trace, ultratrace, isotope, and surface analysis. *International Journal of Mass Spectrometry*, 197(1-3).

[Belardi and Pawliszyn, 1989] Belardi, R. P. and Pawliszyn, J. (1989). *Water Pollut.Res. J. Can.*, 24:179–191.

[Benassi et al., 2013] Benassi, M., Garcia-Reyes, J. F., and Spengler, B. (2013). Ambient ion/molecule reactions in low-temperature plasmas (ltp): reactive ltp mass spectrometry. *Rapid Commun. Mass Spectrom.*, 27:795–804.

[Benninghoven, 1971] Benninghoven, A. (1971). Beobachtung von oberflchenreaktionen mit der statischen methode der sekundrionen-massenspektroskopie. i die methode. *Surface Science*, 28(2):541–562.

[Berchtold et al., 2014] Berchtold, C., Meier, L., Steinhoff, R., and Zenobi, R. (2014). A new strategy based on real-time secondary electrospray ionization and high-resolution mass spectrometry to discriminate endogenous and exogenous compounds in exhaled breath. *Metabolomics*, 10:291–301.

[Bergmann, 2015b] Bergmann, J. (2013-2015b). Mass analyzer control and daq software.

[Bergmann, 2015a] Bergmann, J. (2015a). *Datenaufnahme und Systemsteuerung eines Flugzeit-massenspektrometers mit Anwendungen*. Master thesis, Justus-Liebig-University Gießen.

[Beuhler and Friedman, 1977] Beuhler, R. J. and Friedman, L. (1977). Low noise, high voltage secondary emission ion detector for polyatomic ions. *Int. J. Mass Spectrom. Ion Phys.*, 23:81–97.

[Bhardwaj and Hanley, 2014] Bhardwaj, C. and Hanley, L. (2014). Ion sources for mass spectrometric identification and imaging of molecular species. *Nat. Prod. Rep.*, 31:756–767.

[Bicchi et al., 2005] Bicchi, C., Brunelli, C., Cordero, C., Rubiolo, P., Galli, M., and Sironi, A. (2005). High-speed gas chromatography with direct resistively heated column (ultra fast module-GC)-separation measure (S) and other chromatographic parameters under different analysis conditions for samples of different complexities and volatilities. *J. Chromatogr. A*, 1071:3–12.

[Biemann, 2014] Biemann, K. (2014). Laying the groundwork for proteomics: Mass spectrometry from 1958 to 1988. *JOURNAL OF PROTEOMICS*, 107:62–70.

[Blaum, 2006] Blaum, K. (2006). High-accuracy mass spectrometry with stored ions. *Physics Reports*, 425:1–78.

[Blaum et al., 2013] Blaum, K., Dilling, J., and Noertershaeuser, W. (2013). Precision atomic physics techniques for nuclear physics with radioactive beams. *PHYSICA SCRIPTA*.

[Blaum and Litvinov, 2013] Blaum, K. and Litvinov, Y. A. (2013). 100 years of mass spectrometry. *International Journal of Mass Spectrometry*, 349-350:1 – 2.

[Block, 2013] Block, M. (2013). Direct mass measurements of the heaviest elements with penning traps. *International Journal of Mass Spectrometry*, 349-350:94 – 101.

[Blumenfeld et al., 2013] Blumenfeld, Y., Nilsson, T., and Van Duppen, P. (2013). Facilities and methods for radioactive ion beam production. *PHYSICA SCRIPTA*, 152(1-3).

[Boldin and Nikolaev, 2009] Boldin, I. A. and Nikolaev, E. N. (2009). Theory of peak coalescence in Fourier transform ion cyclotron resonance mass spectrometry. *Rapid Commun. Mass Spectrom.*, 23:3213–3219.

[Bollen, 2004] Bollen, G. (2004). Traps for rare isotopes. *The Euroschool Lectures on Physics with Excotic Beams, Springer*, 1:169–210.

[Bollen et al., 1990] Bollen, G., Moore, R. B., Savard, G., and Stolzenberg, H. (1990). The accuracy of heavy-ion mass measurements using time of flight-ion cyclotron resonance in a Penning trap. *J. Appl. Phys.*, 68(9):4355–4374.

[Bosch and Litvinov, 2013] Bosch, F. and Litvinov, Y. A. (2013). Mass and lifetime measurements at the experimental storage ring of {GSI}. *International Journal of Mass Spectrometry*, 349-350:151 – 161.

[Bottoni and Caroli, 2015] Bottoni, P. and Caroli, S. (2015). Detection and quantification of residues and metabolites of medicinal products in environmental compartments, food commodities and workplaces. a review. *Journal of Pharmaceutical and Biomedical Analysis*, 106:3–24.

[Brincourt et al., 1990] Brincourt, G., Catella, R., Zerega, Y., and Andre, J. (1990). Time-of-flight detection of ions ejected from a radiofrequency quadrupole trap: experimental determination of their fi secular frequency. *Chem. Phys. Let.*, 174(6):626–630.

[Brodbelt, 2014] Brodbelt, J. S. (2014). Photodissociation mass spectrometry: new tools for characterization of biological molecules. *Chem. Soc. Rev.*, 43:2757.

[Brown and Gabrielse, 1986] Brown, L. S. and Gabrielse, G. (1986). Geonium theory: Physics of a single electron or ion in a Penning trap. *Rev. Mod. Phys.*, 58(1):233–311.

[Brubaker, 1968] Brubaker, W. M. (1968). An improved quadrupole mass analyser. *Advances in mass spectrometry*, 4:293–299.

[Bruker GmbH, 2013] Bruker GmbH (2013). Product overview: The cbrn detection specialists.

[Burgoyne and Hieftje, 1996] Burgoyne, T. W. and Hieftje, G. M. (1996). An introduction to ion optics for the mass spectrograph. *Mass Spectrometry Reviews*, 15:241–259.

[Cakirli and Casten, 2013] Cakirli, R. and Casten, R. (2013). Nuclear binding and nuclear structure. *International Journal of Mass Spectrometry*, 349-350:187 – 191.

[Calderon-Santiago et al., 2014] Calderon-Santiago, M., Priego-Capote, F., Galache-Osunac, J., and de Castro, M. L. (2014). Analysis of serum phospholipid profiles by liquid chromatography-tandem mass spectrometry in high resolution mode for evaluation of atherosclerotic patients. *Journal of Chromatography*, 1371:154–162.

[Cameron and Eggers, 1948] Cameron, A. E. and Eggers, D. F. (1948). An ion "velocitron". *Rev. Sci. Instrum.*, 19:605–607.

[Cappiello, 2009] Cappiello, A. (2009). The direct-ei interface.

[Careri and Mangia, 2011] Careri, M. and Mangia, A. (2011). Trends in analytical atomic and molecular mass spectrometry in biology and the life sciences. *Anal Bioanal Chem*, 399:2585–2595.

[Chaudhary et al., 2014] Chaudhary, A., van Amerom, F. H., and Short, R. T. (2014). Experimental evaluation of micro-ion trap mass spectrometer geometries. *International Journal of Mass Spectrometry*, 371:17–27.

[Chaudhuri et al., 2014] Chaudhuri, A., Andreoiu, C., Brodeur, M., Brunner, T., Chowdhury, U., Ettenauer, S., Gallant, A. T., Grossheim, A., Gwinner, G., Klawitter, R., Kwiatkowski, A. A., Leach, K. G., Lennarz, A., Lunney, D., Macdonald, T. D., Ringle, R., Schultz, B. E., Simon, V. V., Simon, M. C., and Dilling, J. (2014). Titan: an ion trap for accurate mass measurements of ms-half-life nuclides. *Appl. Phys. B*, 114:99–105.

[Chen et al., 2015] Chen, C.-H., Chen, T.-C., Zhou, X., Kline-Schoder, R., Sorensen, P., Cooks, R. G., and Ouyang, Z. (2015). Design of portable mass spectrometers with handheld probes: Aspects of the sampling and miniature pumping systems. *International Journal of Mass Spectrometry*, 26:240–247.

[Chen and Marshall, 1987] Chen, L. and Marshall, A. G. (1987). Stored waveform simultaneous mass-selective ejection/excitation for Fourier transform ion cyclotron resonance mass spectrometry. *Int. J. Mass Spectrom. Ion Proc.*, 79:115–125.

[Chen et al., 2010] Chen, L., Plass, W. R., Geissel, H., Knöbel, R., Kozhuharov, C., Litvinov, Y. A., Patyk, Z., Scheidenberger, C., Siegien-Iwaniuk, K., Sun, B., Weick, H., Beckert, K., Beller, P., Bosch, F., Boutin, D., Caceres, L., Carroll, J. J., Cullen, D. M., Cullen, I. J., Franzke, B., Gerl, J., Górska, M., Jones, G. A., Kishada, A., Kurcewicz, J., Litvinov, S. A., Liu, Z., Mandal, S., Montes, F., Münzenberg, G., Nolden, F., Ohtsubo, T., Podolyák, Z., Propri, R., Rigby, S., Saito, N., Saito, T., Shindo, M., Steck, M., Ugorowski, P., Walker, P. M., Williams, S., Winkler, M., Wollersheim, H.-J., and Yamaguchi, T. (2010). Discovery and investigation of heavy neutron-rich isotopes with time-resolved schottky spectrometry in the element range from thallium to actinium. *Phys. Lett. B*, 691:234–237.

[Chen et al., 2013a] Chen, L. C., Rahman, M. M., and Hiraoka, K. (2013a). Super-atmospheric pressure chemical ionization mass spectrometry. *J. Mass Spectrom.*, 48:392–398.

[Chen et al., 2013b] Chen, W., Hou, K., Xiong, X., Jiang, Y., Zhao, W., Hua, L., Chen, P., Xie, Y., Wang, Z., and Li, H. (2013b). Non-contact halogen lamp heating assisted LTP ionization miniature rectilinear ion trap: a platform for rapid, on-site explosives analysis. *Analyst*, 138:5068–5073.

[Chouinard et al., 2016] Chouinard, C. D., Wei, M. S., Beekman, C. R., Kemperman, R. H., , and Yost, R. A. (2016). Ion mobility in clinical analysis: Current progress and future perspectives. *Clinical Chemistry*, 62:124–133.

[Cillero-Pastor and Heeren, 2014] Cillero-Pastor, B. and Heeren, R. M. A. (2014). Matrix-assisted laser desorption ionization mass spectrometry imaging for peptide and protein analyses: A critical review of on-tissue digestion. *J. Proteome Res.*, 13:325–335.

[Coles and Guilhaus, 1993] Coles, J. and Guilhaus, M. (1993). Orthogonal acceleration - a new direction for time-of-flight mass spectrometry: fast, sensitive mass analysis for continuous ion sources. *Trends in Analytical Chemistry*, 12(5):203.

[Comisarow and Marshall, 1974] Comisarow, M. and Marshall, A. (1974). Fourier transform ion cyclotron resonance spectroscopy. *Chem. Phys. Lett.*, 25:282–283.

[Constapel et al., 2005] Constapel, M., Schellentraeger, M., Schmitz, O., Gaeb, S., Brockmann, K., Giese, R., and Benter, T. (2005). Atmospheric-pressure laser ionization: a novel ionization method for liquid chromatography/mass spectrometry. *Rapid Commun. Mass Spectrom.*, 19:326–336.

[Cooks, 2012] Cooks, R. G. (2012). Private communication.

[Cooks et al., 2010] Cooks, R. G., Ifa, D. R., Sharma, G., Kh., F., Tadjimukhamedova, and Ouyang, Z. (2010). Perspectives and retrospectives in mass spectrometry: one view. *European Journal of Mass Spectrometry*, 16 (3):283–300.

[Cotter, 1999] Cotter, R. J. (1999). The new time-of-flight mass spectrometry. *Anal. Chemi.*, 71:13.

[Cotter et al., 1999] Cotter, R. J., Fancher, C., and Cornish, T. J. (1999). Miniaturized time-of-flight mass spectrometer for peptide and oligonucleotide analysis. *J. Mass Spectrom.*, 34:1368–1372.

[Crick and Guan, 2016] Crick, P. J. and Guan, X. L. (2016). Lipid metabolism in mycobacteria – insights using mass spectrometry-based lipidomics. *Biochimica et Biophysica Acta*, 1861:60–67.

[Criticals, 2015] Criticals, N. (2015). Organic compounds.

[Dass, 2007] Dass, C. (2007). *Fundamentals of Contemporary Mass Spectrometry*. Wiley-Intercience.

[Davis et al., 2012] Davis, E. J., Grows, K. F., Siems, W. F., and Herbert H. Hill, J. (2012). Improved ion mobility resolving power with increased buffer gas pressure. *Anal. Chem.*, 84:4858–4865.

[Dawson, 1976] Dawson, P. H. (1976). *Quadrupole Mass Spectrometry and its applications*. Elsevier Scientific Publishing Company, Amsterdam-Oxford-New York.

[de Hoffman and Strooband, 2007] de Hoffman, E. and Strooband, V. (2007). *Mass Spectrometry: Principles and Application*. Wiley.

[Dehmelt, 1967] Dehmelt, H. G. (1967). Radiofrequency spectroscopy of stored ions I: Storage. *Adv. At. Mol. Phys.*, 3:53–72.

[Dempster, 1921] Dempster, A. (1921). *Phys. Rev.*, 18(398).

[Denes et al., 2012] Denes, J., Szabo, E., Szatmari, S. L. R. I., Szonyi, L., Kreuder, J. G., Rauterberg, E. W., and Takats, Z. (2012). Metabonomics of newborn screening dried blood spot samples: A novel approach in the screening and diagnostics of inborn errors of metabolism. *Anal. Chem.*, 84:10113–10120.

[Deng et al., 2014] Deng, J., Yang, Y., Wang, X., and Luan, T. (2014). Strategies for coupling solid-phase microextraction with mass spectrometry. *Trends in Analytical Chemistry*, 55:55–67.

[Diaz et al., 2001] Diaz, J. A., Giese, C. F., and Gentry, W. R. (2001). ROSINA/DFMS and IES observations of 67p: Ion-neutral chemistry in the coma of a weakly outgassing comet. *Journal of the American Society for Mass Spectrometry*, 12:619–632.

[Dickel, 2010] Dickel, T. (2010). *Design and Commissioning of an Ultra-High-Resolution Time-of-Flight Based Isobar Separator and Mass Spectrometer*. PhD thesis, Justus-Liebig-Universität Gießen.

[Dickel, 2012] Dickel, T. (2012). Recapture of ions with injection trap. private communication.

[Dickel et al., 2015a] Dickel, T., Plass, W., Andres, S. A. S., Ebert, J., Geissel, H., Haettner, E., Hornung, C., Miskun, I., Pietri, S., Purushothaman, S., Reiter, M., Rink, A.-K., Scheidenberger, C., Weick, H., Dendooven, P., Diwisch, M., Greiner, F., Heisse, F., Knbel, R., Lippert, W., Moore, I., Pohjalainen, I., Prochazka, A., Ranjan, M., Takechi, M., Winfield, J., and Xu, X. (2015a). First spatial separation of a heavy ion isomeric beam with a multiple-reflection time-of-flight mass spectrometer. *Physics Letters B*, 744:137–141.

[Dickel et al., 2015b] Dickel, T., Plass, W., Becker, A., Czok, U., Geissel, H., Haettner, E., Jesch, C., Kinsel, W., Petrick, M., Scheidenberger, C., Simon, A., and Yavor, M. (2015b). A high-performance multiple-reflection time-of-flight mass spectrometer and isobar separator for the research with exotic nuclei. *Nuclear Instruments and Methods in Physics Research A*, 77:172–188.

[Dickel et al., 2013] Dickel, T., Plass, W., Lang, J., Ebert, J., Geissel, H., Haettner, E., Jesch, C., Lippert, W., Petrick, M., Scheidenberger, C., and Yavor, M. (2013). Multiple-reflection time-of-flight mass spectrometry forin situ applications. *Nuclear Instruments and Methods in Physics Research B*, 317:779–784.

[Dickel and Yavor, 2012] Dickel, T. and Yavor, M. (2012). Double aperature arrangement for rfq mass filter. private communication.

[Dickel et al., 2016] Dickel, T., Yavor, M., Lang, J., Plass, W., H.Geissel, Lippert, W., and Scheidenberger, C. (2016). An independent time focus shift for multiple-reflection time-of-flight analyzer. *to be published*.

[Diels and Jaeckel, 1962] Diels, K. and Jaeckel, R. (1962). *Leybold Vakuum-Taschenbuch für Laboratorium amd Betrieb*. Springer-Verlag, Berlin/Göttingen/Heidelberg, 2 edition.

[Dilling et al., 2006] Dilling, J., Baartman, R., Bricault, P., Brodeur, M., Blomeley, L., Buchinger, F., Crawford, J., Lopez-Urrutia, J. R. C., Delheij, P., Froese, M., Gwinner, G. P., Ke, Z., Lee, J. K. P., Moore, R. B., Ryjkov, V., Sikler, G., Smith, M., Ullrich, J., and Vaz, J. (2006). Mass measurements on highly charged radioactive ions, a new approach to high precision with TITAN. *Int. J. Mass Spectrom.*, 251:198–203.

[Dobrezow, 1934] Dobrezow, L. (1934). Ionisation von Alkalimetallatomen auf Wolfram, Molybdän und thoriertem Wolfram. *Z. Phys. A*, 90:788–801.

[Dodonov et al., 1997] Dodonov, A., Kozlovsky, V., Loboda, A., Raznikov, V., Sulimenkov, I., Tolmachev, A., Kraft, A., and Wollnik, H. (1997). A new technique for decomposition of selected ions in molecule ion reactor coupled with ortho-time-of-flight mass spectrometry. *Rapid Commum. Mass Spectrom.*, 11:1649–1656.

[Dodonov et al., 2000] Dodonov, A. F., Kozlovski, V. I., Soulimenkov, I. V., Razinkov, V. V., Loboda, A. V., Zhen, Z., Horwath, T., and Wollnik, H. (2000). High-resolution electrospray ionization orthogonal-injection time-of-flight mass spectrometer. *Eur. J. Mass Spectrom.*, 6:481–490.

[Dole et al., 2004] Dole, M., Mack, L. L., Hines, R. L., Mobley, R. C., Ferguson, L. D., and Alice, M. B. (2004). Molecular beams of macroions. *Phys.Chem.Chem.Phys.*, 6:3056–3068.

[Douglas et al., 2005] Douglas, D. J., Frank, A. J., and Mao, D. (2005). Linear ion traps in mass spectrometry. *Mass Spectrom. Rev.*, 24:1–29.

[Duering, 2012] Duering, R. A. (2012). Im trueben fischen: Umweltanalytik mit massenspektrometrie vor ort. *GIT Labor-Fachzeitschrift*, 10/2012:740–741.

[Dunbar and McMahon, 1998] Dunbar, R. C. and McMahon, T. B. (1998). Activation of unimolecular reactions by ambient blackbody radiation. *Science*, 279(5348):194–197.

[Easterling et al., 1999] Easterling, M. L., Amster, I. J., van Rooij, G. J., and Heeren, R. M. A. (1999). Isotope beating effects in the analysis of polymer distributions by fourier transform mass spectrometry. *J. Am. Soc. Mass Spectrom.*, 10:1074–1082.

[Eisert and Pawliszyn, 1997] Eisert, R. and Pawliszyn, J. (1997). New trends in solid-phase microextraction. *Critical Reviews in Analytical Chemistry*, 27(2):103–135.

[Eronen and Jokinen, 2013] Eronen, T. and Jokinen, A. (2013). High-precision atomic mass measurements for a {CKM} unitarity test. *International Journal of Mass Spectrometry*, 349-50:69 – 73.

[Espy et al., 2014] Espy, R. D., Wleklinski, M., Yan, X., and Cooks, R. G. (2014). Beyond the flask: Reactions on the fly in ambient mass spectrometry. *Trends in Analytical Chemistry*, 57:135–146.

[Ettenauer et al., 2013] Ettenauer, S., Simon, M., Macdonald, T., and Dilling, J. (2013). Advances in precision, resolution, and separation techniques with radioactive, highly charged ions for penning trap mass measurements. *International Journal of Mass Spectrometry*, 349-350:74 – 80.

[FAIR, 2013] FAIR, F. (2013). FAIR - an international science centre in europe for studying the building blocks of matter and the evolution of the universe. pages 0–12.

[Fassel, 1977] Fassel, V. A. (1977). Current and potential applications of inductively coupled plasma (icp)-atomic emission spectroscopy (aes) in the exploration, mining, and processing of materials. *Pure and Appl. Chem.*, 49(10):1533–1545.

[Franz et al., 2014] Franz, H. B., Trainer, M. G., Wong, M. H., Manning, H. L., Stern, J. C., Mahaffy, P. R., Atreya, S. K., Benna, M., Conrad, P. G., Harpold, D. N., Leshin, L. A., Malespin, C. A., McKay, C. P., Nolan, J. T., and Raaen, E. (2014). Analytical techniques for retrieval of atmospheric composition with the quadrupole mass spectrometer of the sample analysis at mars instrument suite on mars science laboratory. *Planetary and Space Science*, 96:99–113.

[Franzke et al., 2008] Franzke, B., Geissel, H., and Münzenberg, G. (2008). Mass and lifetime measurements of exotic nuclei in storage rings. *Mass Spectrom. Rev.*, 27:428–469.

[Fuselier et al., 2015] Fuselier, S. A., Altwegg, K., Balsiger, H., Berthelier, J. J., Bieler, A., Briois, C., Broiles, T. W., Burch, J. L., Calmonte, U., Cessateur, G., Combi, M., Keyser, J. D., Fiethe, B., Galand, M., Gasc, S., Gombosi, T. I., Gunell, H., Hansen, K. C., Hässig, M., Jäckel, A., Korth, A., Roy, L. L., Mall, U., Mandt, K. E., Petrinec, S. M., Raghuram, S., Reme, H., Rinaldi, M., Rubin, M., Semon, T., Trattner, K. J., Tzou, C.-Y., Vigren, E., Waite, J. H., and Wurz, P. (2015). ROSINA/DFMS and IES observations of 67p: Ion-neutral chemistry in the coma of a weakly outgassing comet. *Astronomy and Astrophysics*, 583.

[Gaspar et al., 2009] Gaspar, A., Kunenkov, E. V., Lock, R., Desor, M., Perminova, I., and Schmitt-Kopplin, P. (2009). Combined utilization of ion mobility and ultra-high-resolution mass spectrometry to identify multiply charged constituents in natural organic matter. *Rapid Commun. Mass Spectrom.*, 23:683–688.

[Gates, 2014] Gates, P. J. (2014). Time-o-flight analysis.

[Gavina et al., 2014] Gavina, J. M., Yao, C., and Feng, Y.-L. (2014). Recent developments in dna adduct analysis by mass spectrometry: A tool for exposure biomonitoring and identification of hazard for environmental pollutants. *Talanta*, 130:475–494.

[Geissel et al., 2006] Geissel, H., Knöbel, R., Litvinov, Y. A., Sun, B., Beckert, K., Beller, P., Bosch, F., Boutin, D., Brandau, C., Chen, L., Fabian, B., Hausmann, M., Kozhuharov, C., Kurcewicz, J., Litvinov, S. A., Mazzocco, M., Montes, F., Münzenberg, G., Musumarra, A., Nociforo, C., Nolden, F., Plass, W. R., Scheidenberger, C., Steck, M., Weick, H., and Winkler, M. (2006). A new experimental approach for isochronous mass measurement of short-lived exotic nuclei with the FRS-ERS facility. *Hyperfine Interact.*, 173:49–54.

[Geissel and Scheidenberger, 1998] Geissel, H. and Scheidenberger, C. (1998). Slowing down of relativistic heavy ions and new applications. *Nuclear Instruments and Methods in Physics Research B*, 136-138:114–124.

[Ghosh and Brand, 2003] Ghosh, P. and Brand, W. A. (2003). Stable isotope ratio mass spectrometry in global climate change research. *International Journal of Mass Spectrometry*, 228:1–33.

[Goodrich and Wiley, 1962] Goodrich, G. W. and Wiley, W. C. (1962). Continuous channel electron multiplier. *Rev. Sci. Instrum.*, 33:761–762.

[Grinfeld et al., 2014] Grinfeld, D., Giannakopulos, A. E., Kopaev, I., Monastyrskiy, M., Skoblin,

M., and Makarov, A. (2014). Space charge effects in a coaxial two-mirror electrostatic multi-reflection mass analyzer. *Thermo Scientific*, pages 1–7.

[Gross, 2013] Gross, J. H. (2013). *Massenspektrometrie – Ein Lehrbuch*. Springer Spektrum.

[Gross, 1994] Gross, M. L. (1994). Accurate masses for structure confirmation. *Journal of the American Society for Mass Spectrometry*, 5(2).

[Guevremont and Purves, 1999] Guevremont, R. and Purves, R. W. (1999). High field asymmetric waveform ion mobility-mass spectrometry: an investigation of leucine enkephalin ions by electrospray ionization. *J. Am. Soc. Mass Spectrom.*, 10:492–501.

[Guilhaus, 1995] Guilhaus, M. (1995). Principles and instrumentation in time-of-flight mass spectrometry. *JOURNAL OF MASS SPECTROMETRY*, 30:1519–1532.

[Guo et al., 2008] Guo, C., Huang, Z., Gao, W., Nian, H., Chen, H., Dong, J., Shen, G., Fu, J., and Zhou, Z. (2008). A homemade high-resolution orthogonal-injection time-of-flight mass spectrometer with a heated capillary inlet. *Review of Scientific Instruments*, 79:013109.

[Haettner, 2011] Haettner, E. (2011). *A novel radio frequency quadrupole system for SHIPTRAP & New mass measurements of rp nuclides*. PhD thesis, Justus-Liebig-Universität Gießen.

[Hauser et al., 2012] Hauser, K., Deutzmann, R., Rassow, J., and Netzker, R. (2012). *Duale Reihe Biochemie*. Thieme.

[Hazama et al., 2008] Hazama, H., Aoki, J., Nagao, H., Suzuki, R., Tashima, T., Fujii, K. I., Masuda, K., Awazu, K., Toyoda, M., and Naito, Y. (2008). Construction of a novel stigmatic MALDI imaging mass spectrometer. *Applied Surface Science*, 255:1257–1263.

[Heinz et al., 2013] Heinz, S., , Barth, W., Franczak, B., Geissel, H., Gupta, M., Hofmann, S., Mickat, S., Mnzenberg, G., Plass, W., Scheidenberger, C., Weick, H., and Winkler, M. (2013). Design of a new in-flight separator for heavy and superheavy fusion and transfer products. *Nuclear Instruments and Methods in Physics Research B*, 317:354–356.

[Hendrickson et al., 2015] Hendrickson, C. L., Quinn, J. P., Kaiser, N. K., Smith, D. F., Blakney, G. T., Chen, T., Marshall, A. G., Weisbrod, C. R., and Beu, S. C. (2015). 21 tesla fourier transform ion cyclotron resonance mass spectrometer: A national resource for ultrahigh resolution mass analysis. *Journal of the American Society for Mass Spectrometry*, 26:1626–163.

[Henss et al., 2013] Henss, A., Rohnke, M., Knaack, S., Kleine-Boymann, M., Leichtweiss, T., Schmitz, P., Khassawna, T. E., Gelinsky, M., Heiss, C., and Janek, J. (2013). Quantification of calcium content in bone by using tof-sims-a first approach. *Biointerphases*, 8(31):8pp.

[Hertz, 1882] Hertz, H. (1882). über die Verdunstung der Flüssigkeiten, insbesondere des Quecksilbers, im luftleeren Raume. *Ann. d. Phys. u. Chem. N. F.*, 17(10):177–193.

[Hilger et al., 2013] Hilger, R. T., Santini, R. E., and McLuckey, S. A. (2013). Nondestructive tandem mass spectrometry using a linear quadrupole ion trap coupled to a linear electrostatic ion trap. *Anal. Chem.*, 85:5226–5232.

[Hofstadler et al., 1994] Hofstadler, S. A., Bruce, J. E., Rockwood, A. L., Anderson, G. A., Winger, B. E., and Smith, R. D. (1994). Isotopic beat patterns in Fourier transform ion cy-

clotron resonance mass spectrometery: implications for high resolution mass measurements of large biopolymers. *Int. J. Mass Spec. Ion Processes*, 132:109–127.

[Hopmans et al., 2000] Hopmans, E., Schouten, S., Pancost, R., van der Meer, M., and Damste, J. S. (2000). Analysis of intact tetraether lipids in archaeal cell material and sediments by high performance liquid chromatography/atmospheric pres-sure chemical ionization mass spectrom-etry. *Rapid Commun. Mass Spectrom.*, 14:585–589.

[Hu et al., 2005] Hu, Q., Noll, R. J., Li, H. Y., Makarov, A., Hardman, M., and Cooks, R. G. (2005). The orbitrap: A new mass spectrometer. *J. Mass Spectrom.*, 40:430–443.

[Huang et al., 2010] Huang, M.-Z., Yuan, C.-H., Cheng, S.-C., Cho, Y.-T., and Shiea, J. (2010). Ambient ionization mass spectrometry. *Annu. Rev. Anal. Chem.*, 3:43–65.

[Huanga et al., 2011] Huanga, M.-Z., Chenga, S.-C., Choa, Y.-T., and Shieaa, J. (2011). Ambient ionization mass spectrometry: A tutorial. *Analytica Chimica Acta*, 702(1):1–15.

[Huanga et al., 2015] Huanga, Z., Tan, G., Zhou, Z., Chen, L., Cheng, L., Jin, D., Tan, X., Xie, C., Li, L., Dongb, J., Fu, Z., , Cheng, P., and Gaoa, W. (2015). Development of a miniature time-of-flight mass/charge spectrometer for ion beam source analyzing. *International Journal of Mass Spectrometry*, 379:60–64.

[Ibanez et al., 2015] Ibanez, C., Simo, C., Garcia-Canas, V., Acunha, T., and Cifuentes, A. (2015). The role of direct high-resolution mass spectrometry in foodomics. *Anal Bioanal Chem*, 407:6275–6287.

[Ibrahim et al., 2006] Ibrahim, Y., Tang, K., Tolmachev, A. V., Shvartsburg, A. A., and Smith, R. D. (2006). Improving mass spectrometry sensitivity using a high-pressure electrodynamic ion funnel interface. *J. Am. Soc. Mass Spectrom.*, 17 (9):1299–1305.

[Ibrahim et al., 2015] Ibrahim, Y. M., Baker, E. S., DanielsonIII, W. F., Norheim, R. V., Prior, D. C., Anderson, G. A., Belov, M. E., and Smith, R. D. (2015). Development of anew ion mobility (quadrupole) time-of-flight mass spectrometer. *International Journal of Mass Spectrometry*, 377:655–662.

[Iliuk et al., 2014] Iliuk, A. B., Arrington, J. V., and Tao, W. A. (2014). Analytical challenges translating mass spectrometry-based phosphoproteomics from discovery to clinical applica-tions. *Electrophoresis*, 35:3430–3440.

[Iribarne and Thomson, 2004] Iribarne, J. V. and Thomson, B. A. (2004). On the evaporation of small ions from charged droplets. *Phys.Chem.Chem.Phys.*, 6:3056–3068.

[Ishida et al., 2005] Ishida, Y., Wada, M., and Wollnik, H. (2005). A multi-reflection time-of-flight mass spectrometer for mass measurements of short-lived nuclei. *Nucl. Instr. and Meth. in Phys. Res. B*, 241:983–985.

[Ishihara et al., 2005] Ishihara, M., Miyamura, T., Higashigaki, M., Okumura, D., Toyoda, M., and Katakuse, I. (2005). A new correlation function method for multi-turn TOF spectrum. In *Proceedings of the 53th ASMS Conference on Mass Spectrometry and Allied Topics*, San Antonio, USA.

[Ito et al., 2013] Ito, Y., Schury, P., Wada, M., Naimi, S., Sonoda, T., Mita, H., Arai, F., Takamine, A., Okada, K., Ozawa, A., and Wollnik, H. (2013). Single-reference high-precision mass measurement with a multi-reection time-of-ight mass spectrograph. *arXiv:1307.7373v1 [nucl-ex]*.

[Jennings, 1968] Jennings, K. R. (1968). Collision-induced decompositions of aromatic molecular ions. *Int. J. Mass Spetrom. Ion Phys.*, 1:227–235.

[Jesch, 2009] Jesch, C. (2009). User interface for pci trigger cards.

[Jesch et al., 2015] Jesch, C., Dickel, T., Plass, W. R., Short, D., Ayet, S., Dilling, J., Hans, Geissel, Greiner, F., Lang, J., Leach, K. G., Lippert, W., Scheidenberger, C., and Yavor, M. I. (2015). The mr-tof-ms isobar separator for the TITAN facility at TRIUMF. *Hyperfine Interactions*, submitted.

[Johnson et al., 1987] Johnson, R. S., Martin, S. A., and Biemann, K. (1987). Novel fragmentation process of peptides by collision- induced decomposition in a tandem mass spectrometer: Differentiation of leucine and isoleucine. *Anal. Chem.*, 59:2621–2625.

[Jousten et al., 2006] Jousten, K., Jitschin, W., Lachenmann, R., and Juenemann, A. (2006). *Wutz Handbuch Vakuumtechnik: Theorie und Praxis*. Vieweg Verlag.

[Junninen et al., 2010] Junninen, H., Ehn, M., Petäjä, T., Luosujärvi, L., Kotiaho, T., Kostiainen, R., Rohner, U., Gonin, M., Fuhrer, K., Kulmala, M., and Worsnop, D. R. (2010). A high-resolution mass spectrometer to measure atmospheric ion composition. *Atmos. Meas. Tech.*, 3:1039–1053.

[Kabir et al., 2013] Kabir, A., Holness, H., Furton, K. G., and Almirall, J. R. (2013). Recent advances in micro-sample preparation with forensic applications. *Trends in Analytical Chemistry*, 45:264–279.

[Kanu et al., 2008] Kanu, A. B., Dwivedi, P., Tam, M., Matz, L., and Hill, H. H. (2008). Ion mobility-mass spectrometry. *J. Mass Spectrom.*, 43:1–22.

[Kapishon et al., 2013] Kapishon, V., Koyanagi, G. K., Blagojevic, V., and Bohme, D. K. (2013). Atmospheric pressure chemical ionization mass spectrometry of pyridine and isoprene: potential breath exposure and disease biomarkers. *J. Breath Res.*, 7(026005):1–8.

[Karas et al., 2000] Karas, M., Glueckmann, M., and Schaefer, J. (2000). Ionization in matrix-assisted laser desorption/ionization: singly charged molecular ions are the lucky survivors. *J. Mass Spectrom.*, 35:1–12.

[Khardori, 2014] Khardori, N. (2014). Future of diagnostic microbiology. *Indian Journal of Medical Microbiology*, 32(4):371–377.

[KHuK, 2012] KHuK, K. f. H.-u. K. (2012). Forschen fr die zukunft hadronen- und kernphysik in deutschland. pages 0–35.

[Kim et al., 2000] Kim, T., Udseth, H. R., and D., S. R. (2000). Improved ion transmission fromatmospheric pressure to high vacuum using a multicapillary inlet and electrodynamic ion funnel interface. *Anal. Chem.*, 72 (20):5014–5019.

[Kingdon, 1923] Kingdon, K. H. (1923). A method for the neutralization of electron space charge by positive ionization at very low gas pressures. *Phys. Rev.*, 21:408–418.

[Kinsel, 2010] Kinsel, W. (2010). Break-out and driver box for ttl trigger system.

[Kinsel, 2011] Kinsel, W. (2010-2011). Fast high voltage switch.

[Kluge, 2013] Kluge, H.-J. (2013). Penning trap mass spectrometry of radionuclides. *International Journal of Mass Spectrometry*, 349-350:26 – 37.

[Knudsen, 1915] Knudsen, M. (1915). Die maximale Verdmpfungsgeschwindigkeit des Quecksilbers. *Ann. d. Phys.*, 352(13):697–708.

[Koenig, 2013] Koenig, M. (2013). Feldanalytik fr feuerwehr und analytische task force (private communication).

[Koenig, 2014] Koenig, M. (2014). Entwicklung moderner feldanalytik und ihre anwendung durch die analytische task force. Presentation.

[König et al., 1995] König, M., Bollen, G., Kluge, H.-J., Otto, T., and Szerypo, J. (1995). Quadrupole excitation of stored ion motion at the true cyclotron frequency. *Int. J. Mass Spectrom. Ion Proc.*, 142:95–116.

[Konradi, 2012] Konradi, M. (2012). Radio frequency driver documentation. Internal report, Justus-Liebig-University Gießen.

[Kozlov et al., 2006] Kozlov, B., Gavrik, M., Hasin, Y., Kirillov, S., Monakhov, A., Trufanov, A., Yavor, M., and Verentchikov, A. (2006). Space charge effects in multireflecting time-of-flight mass spectrometer. In *Proceedings of the 54th ASMS Conference on Mass Spectrometry and Allied Topics*, Seattle, USA.

[Krachler et al., 2015] Krachler, M., Alvarez-Sarandes, R., and Winckel, S. V. (2015). Challenges in the quality assurance of elemental and isotopic analyses in the nuclear domain benefitting from high resolution ICP-OES and sector field ICP-MS. *J Radioanal Nucl Chem*, 304:1201–1209.

[Krutchinsky et al., 2015] Krutchinsky, A. N., Padovan, J. C., Cohen, H., and Chait, B. T. (2015). Maximizing ion transmission from atmospheric pressure into the vacuum of mass spectrometers with a novel electrospray interface. *Journal of the American Society for Mass Spectrometry*, 26:649–658.

[Kuehn, 2005] Kuehn, W. (2005). *Modern data acquisition and trigger systems for hadron physics*. IOS Press. 657-677.

[Kuerten et al., 2007] Kuerten, A., Curtius, J., Helleis, F., Lovejoy, E. R., and Borrmann, S. (2007). Development and characterization of an ion trap mass spectrometer for the on-line chemical analysis of atmospheric aerosol particles. *International Journal of Mass Spectrometry*, 265:30–39.

[Kurada et al., 2015] Kurada, S., Alkhouri, N., Fiocchi, C., Dweik, R., and Rieder, F. (2015). Review article: breath analysis in inflammatory bowel diseases. *Aliment Pharmacol Ther*, 41:329–341.

[Kutschera, 2013] Kutschera, W. (2013). Applications of accelerator mass spectrometry. *International Journal of Mass Spectrometry*, 349-50:203 – 218.

[LamondLab, 2014] LamondLab (2014). Electrospray ionisation.

[Lang, 2008] Lang, J. (2008). *Control and Management Unit for ATCA conform Trigger and Data Acquisition Processors in the PANDA Experiment*. Diploma thesis, Justus-Liebig-University Gießen.

[Lang et al., 2012] Lang, J., Plass, W. R., Dickel, T., Ebert, J., Geissel, H., Haettner, E., Lippert, W., Petrick, M., Pikhtelev, A., Scheidenberger, C., and Yavor, M. (2012). Design and commissioning of a mobile multiple-reflection time-of-flight mass spectrometer for in-situ analytical mass spectrometry. *Annual Report 2012 – II. Physikalisches Institut*, pages 80–81.

[Lang et al., 2013] Lang, J., Plass, W. R., Dickel, T., Ebert, J., Geissel, H., Haettner, E., Lippert, W., Petrick, M., Pikhtelev, A., Scheidenberger, C., and Yavor, M. (2013). Design and commissioning of a mobile multiple-reflection time-of-flight mass spectrometer for in-situ analytical mass spectrometry. *GSI Report 2012*, 1:163.

[Lang et al., 2011] Lang, J., Plass, W. R., Dickel, T., Ebert, J., Geissel, H., Haettner, E., Scheidenberger, C., and Yavor, M. (2011). First performance results of a mobile high resolution multiple-reflection time-of-flight mass spectrometer for in-situ analytics. *Annual Report 2011 – II. Physikalisches Institut*, pages 80–81.

[Langanke and Schatz, 2013] Langanke, K. and Schatz, H. (2013). The role of radioactive ion beams in nuclear astrophysics. *Phys. Scr.*, 152:1–17.

[Lange, 2011] Lange, F. (2011). Mobile gc/ms for civil protection (private communication).

[Lange et al., 2011] Lange, F., Ludwig, T., and Bruker Daltonik GmbH (2011). Mobile mass spectrometer in daily use - experiences made by non-scientific operators.

[Langmuir and Kingdon, 1925] Langmuir, I. and Kingdon, K. H. (1925). Thermionic effects caused by vapours of alkali metals. *Proc. Roy. Soc. London (A)*, 107(741):61–79.

[Latosinska et al., 2013] Latosinska, A., Frantzi, M., Vlahou, A., and Mischak, H. (2013). Clinical applications of capillary electrophoresis coupled to mass spectrometry in biomarker discovery: Focus on bladder cancer. *Proteomics Clin. Appl.*, 7:779–793.

[Lebedev, 2015] Lebedev, A. T. (2015). Ambient ionization mass spectrometry. *Russ. Chem. Rev.*, 84(7):665–692.

[Lee and Shiea, 1998] Lee, C.-Y. and Shiea, J. (1998). Gas chromatography connected to multiple channel electrospray ionization mass spectrometry for the detection of volatile organic compounds. *Anal. Chem.*, 70:2757–2761.

[Leung and Fong, 2014] Leung, K. S.-Y. and Fong, B. M.-W. (2014). Lc-ms/ms in the routine clinical laboratory: has its time come? *Anal Bioanal Chem*, 406:2289–2301.

[Levin and Aeschbach-Hertig, 2004] Levin, I. and Aeschbach-Hertig, W. (2004). Umwelttracer in atmosphre und terrestrischen systemen.

[Li et al., 2015] Li, D.-X., Gan, L., Bronja, A., and Schmitz, O. J. (2015). Gas chromatography coupled to atmospheric pressure ionization mass spectrometry (gc-api-ms): Review. *Analytica Chimica Acta*, 891:43–61.

[Li et al., 2014a] Li, L., Chen, T.-C., an Paul I. Hendricks, Y. R., Cooks, R. G., , and Ouyang, Z. (2014a). Mini 12, miniature mass spectrometer for clinical and other applications-introduction and characterization. *Anal. Chem.*, 86 (6):2909–2916.

[Li et al., 2014b] Li, L., Zhou, X., Hager, J. W., and Ouyang, Z. (2014b). High efficiency tandem mass spectrometry analysis using dual linear ion traps. *Analyst*, 139:4779.

[Lindahl et al., 2010] Lindahl, P., Lee, S.-H., Worsfold, P., and Keith-Roach, M. (2010). Plutonium isotopes as tracers for ocean processes: A review. *Marine Environmental Research*, 69:73–84.

[Lippert et al., 2015] Lippert, M. Y. W., Dickel, T., and Lang, J. (2013-2015). Private communication.

[Lippert, 2012a] Lippert, W. (2012a). *Bearbeitung aktueller Fragestellungen und technischer Entwicklungen in der subatomaren Physik*. Spezialisierungsmodul, Justus-Liebig-University Gießen.

[Lippert, 2012b] Lippert, W. (2012b). *Setup, Commissioning and Characterization of a Trap System for a Mobile Multiple-Reflection Time-of-Flight Mass Spectrometer*. Master thesis, Justus-Liebig-University Gießen.

[Lippert, 2016] Lippert, W. (2016). *Weiterentwicklung und Anwendung eines Flugzeitmassenspektrometers (in preparation)*. Phd thesis, Justus-Liebig-University Gießen.

[Lips et al., 2007] Lips, K., J, W., S, Z., T, B., K, S., W, W., I, W., U, S., H, K., and W., K. (2007). Acetylcholine and molecular components of its synthesis and release machinery in the urothelium. *Eur Urol.*, 317:1042–1053.

[Little et al., 1994] Little, D. P., Speir, J. P., Senko, M. W., O'Connor, P. B., and McLafferty, F. W. (1994). Infrared multiphoton dissociation of large multiply charged ions for biomolecule sequencing. *Anal. Chem.*, 66(18):2809–2815.

[Litvinov et al., 2013] Litvinov, Y., Bishop, S., Blaum, K., Bosch, F., Brandau, C., Chen, L., Dillmann, I., Egelhof, P., Geissel, H., Grisenti, R., Hagmann, S., Heil, M., Heinz, A., Kalantar-Nayestanaki, N., Knbel, R., Kozhuharov, C., Lestinsky, M., Ma, X., Nilsson, T., Nolden, F., Ozawa, A., Raabe, R., Reed, M., Reifarth, R., Sanjari, M., Schneider, D., Simon, H., Steck, M., Sthlker, T., Sun, B., Tu, X., Uesaka, T., Walker, P., Wakasugi, M., Weick, H., Winckler, N., Woods, P., Xu, H., Yamaguchi, T., Yamaguchi, Y., and Zhang, Y. (2013). Nuclear physics experiments with ion storage rings. *Nuclear Instruments and Methods in Physics Research Section B: Beam Interactions with Materials and Atoms*, 317 B(0):603–616.

[Litvinov et al., 2005] Litvinov, Y. A., Geissel, H., Radon, T., Attallah, F., Audi, G., Beckert, K., Bosch, F., Falch, M., Franzke, B., Hausmann, M., Hellström, M., Kerscher, T., Klepper, O., Kluge, H.-J., Kozhuharov, C., Löbner, K. E. G., Münzenberg, G., Nolden, F., Novikov, Y. N., Quint, W., Patyk, Z., Reich, H., Scheidenberger, C., Schlitt, B., Steck, M., Sümmerer, K., Vermeeren, L., Winkler, M., Winkler, T., and Wollnik, H. (2005). Mass measurement of cooled neutron-deficient bismuth projectile fragments with time-resolved schottky mass spectrometry at the FRS-ESR facility. *Nucl. Phys. A*, 756:3–38.

[Liu et al., 2010] Liu, J., Wang, H., Manicke, N. E., Lin, J.-M., Cooks, R. G., and Ouyang, Z.

(2010). Development, characterization, and application of paper spray ionization. *Anal. Chem.*, 82:2463–2471.

[Liu et al., 2009] Liu, T., Belov, M. E., Jaitly, N., Qian, W.-J., and Smith, R. D. (2009). Accurate mass measurements in proteomics. *Chem Rev.*, Author manuscript; available in PMC:1–63.

[Loo and Muenster, 1999] Loo, J. A. and Muenster, H. (1999). Magnetic sector-ion trap mass spectrometry with electrospray ionization for high sensitivity peptide sequencing. *Rapid Commun. Mass Spectrom.*, 13:54–60.

[Lossing and Tanaka, 1956] Lossing, F. P. and Tanaka, I. (1956). Photoionization as a source of ions for mass spectrometry. *J. Chem. Phys.*, 25(103):1031–1034.

[Lotze, 2014] Lotze, C. (2012-2014). Voltage control software for mr-tof-ms.

[Lunney et al., 2003] Lunney, D., Pearson, J. M., and Thibault, C. (2003). Recent trends in the determination of nuclear masses. *Rev. Mod. Phys.*, 75(3):1021–1062.

[Mabud et al., 1985] Mabud, M. D. A., Dekrey, M. J., and Cooks, R. G. (1985). Surface-induced dissociation ofmolecular-ions. *Int. J. Mass Spectrom.*, 67:285–294.

[Makarov, 2000] Makarov, A. (2000). Electrostatic axially harmonic orbital trapping: a high performance nique of mass analysis. *Anal. Chem.*, 72:1156–1162.

[Makinen et al., 2011] Makinen, M., Nousiainen, M., and Sillanpaa, M. (2011). Ion spectrometric detection technologies for ultra-traces of explosives: A review. *Mass Spectrometry Reviews*, 30:940–973.

[Mamyrin, 1966] Mamyrin, B. A. (1966). Author's abstract of doctorate. *A. F. Ioffe Physio-Technical Institute, Leningrad.*

[Mamyrin et al., 1973] Mamyrin, B. A., Karataev, V. I., Shmikk, D. V., and Zagulin, V. A. (1973). The mass-reflectron, a new nonmagnetic time-of-flight mass spectrometer with high resolution. *Sov. Phys. JETP*, 37(1):45.

[March and Todd, 2005] March, R. E. and Todd, J. F. (2005). *Quadrupole ion trap mass spectrometry*. John Wiley & Sons, Inc., Hoboken, New Jersey.

[March and Todd, 2015] March, R. E. and Todd, J. F. (2015). Design of portable mass spectrometers with handheld probes: Aspects of the sampling and miniature pumping systems. *International Journal of Mass Spectrometry*, 377:316–328.

[Marshall and Hendrickson, 2008] Marshall, A. G. and Hendrickson, C. L. (2008). High-resolution mass spectrometers. *Annu. Rev. Anal. Chem.*, 1:579–599.

[Marshall et al., 1998] Marshall, A. G., Hendrickson, C. L., and Jackson, G. S. (1998). Fourier transform ion cyclotron resonance mass spectrometry: A primer. *Mass Spectrom. Rev.*, 17:1–35.

[Marshall and Rodgers, 2004] Marshall, A. G. and Rodgers, R. P. (2004). Petroleomics: The next grand challenge for chemical analysis. *Acc. Chem. Res.*, 37:53–59.

[Marshall and Verdun, 1990] Marshall, A. G. and Verdun, F. R. (1990). *Fourier Transforms in NMR, Optical and Mass Spectrometry: A Users Handbook.* Elsevier Science Ltd.

[Martens et al., 2011] Martens, L., Chambers, M., Sturm, M., Kessner, D., Levander, F., Shofstahl, J., Tang, W. H., Roempp, A., Neumann, S., Pizarro, A. D., Montecchi-Palazzi, L., Tasman, N., Coleman, M., Reisinger, F., Souda, P., Hermjakob, H., Binz, P.-A., and Deutsch, E. W. (2011). mzml - a community standard for mass spectrometry data. *Mol Cell Proteomics.*, 10 (1).

[Mathews, 2008] Mathews, G. (2008). Frontiers of nuclear astrophysics. *NUCLEAR PHYSICS A*, 805:303C–312C.

[Matsuo et al., 1999] Matsuo, T., Ishihara, M., Toyoda, M., Ito, H., Yamaguchi, S., Roll2, R., and Rosenbauer, H. (1999). A space time-of-flight mass spectrometer for exobiologically-oriented applications. *Adv. Space Res.*, 23(2):341–348.

[Mauclaire et al., 2004] Mauclaire, G., Lemaire, J., Boissel, P., Bellec, G., and Heninger, M. (2004). Micra: A compact permanent magnet fourier transform ion cyclotron resonance mass spectrometer. *EJMS*, 10 (2):155–162.

[McLachlan, 1947] McLachlan, N. W. (1947). *Theory and Application of Mathieu Functions*. Oxford University Press, Oxford.

[Medzihradszky and Chalkley, 2015] Medzihradszky, K. F. and Chalkley, R. J. (2015). Lessons inde novopeptide sequencing by tandem mass spectrometry. *Mass Spectrometry Reviews*, 34:43–63.

[Meisel and George, 2013] Meisel, Z. and George, S. (2013). Time-of-flight mass spectrometry of very exotic systems. *International Journal of Mass Spectrometry*, 349-350:145–150.

[Menga et al., 2015] Menga, L., Zhang, W., Mengc, P., Zhu, B., and Zheng, K. (2015). Comparison of hollow fiber liquid-phase microextraction and ultrasound-assisted low-density solvent dispersive liquid-liquid microextraction for the determination of drugs of abuse in biological samples by gas chromatography-mass spectrometry. *Journal of Chromatography B*, 989:46–53.

[Michael Karas, 1988] Michael Karas, F. H. (1988). Laser desorption ionization of proteins with molecular masses exceeding 10 000 daltons. *Anal. Chem.*, 60:2299–2301.

[Miller, 1958] Miller, M. A. (1958). *Motion of charged particles in high-frequency electromagnetic fields.*

[Moini, 1994] Moini, M. (1994). Ultramark 1621 as a calibrationireference compound for mass spectrometry ii. positive- and negative-ion electrospray ionization. *RAPID COMMUNICATIONS IN MASS SPECTROMETRY*, 8:711–714.

[Monge et al., 2013] Monge, M. E., Harris, G. A., Dwivedi, P., and Fernandez, F. M. (2013). Mass spectrometry: Recent advances in direct open air surface sampling/ionization. *Chem. Rev.*, 113:2269–2308.

[Münzenberg, 2013] Münzenberg, G. (2013). Development of mass spectrometers from thomson and aston to present. *International Journal of Mass Spectrometry*, 349-350:9 – 18.

[Nelson and Cox, 2005] Nelson, D. L. and Cox, M. M. (2005). *Principles of Biochemistry*. W. H. Freeman and Company.

[Nemes and Vertes, 2012] Nemes, P. and Vertes, A. (2012). Ambient mass spectrometry for in vivo local analysis and in situ molecular tissue imaging. *Trends in Analytical Chemistry*, 34:22–34.

[Nishiguchi et al., 2009] Nishiguchi, M., Ueno, Y., Toyoda, M., and Setou, M. (2009). Design of a new multi-turn ion optical system 'IRIS' for a time-of-flight mass spectrometer. *J. Mass Spectrom.*, 44:594–604.

[Niu and Houk, 1996] Niu, H. and Houk, R. (1996). Fundamental aspects of ion extraction in inductively coupled plasma mass spectrometry. *Spectrochimica Acta Part B*, 51:779–815.

[Nuwaysir and Wilkins, 1989] Nuwaysir, L. M. and Wilkins, C. L. (1989). Photodissociation of laser-desorbed ions as a structure determination tool. *Anal. Chem.*, 61(7):689–693.

[Ocana-Gonzalez et al., 2016] Ocana-Gonzalez, J. A., Fernandez-Torres, R., Bello-Lopez, M. A., and Ramos-Payan, M. (2016). New developments in microextraction techniques in bioanalysis. a review. *Analytica Chimica Acta*, 905:8–23.

[Ojanpera et al., 2012] Ojanpera, I., Kolmonen, M., and Pelander, A. (2012). Current use of high-resolution mass spectrometry in drug screening relevant to clinical and forensic toxicology and doping control. *Anal Bioanal Chem*, 403:1203–1220.

[Okumura et al., 2004] Okumura, D., Toyoda, M., Ishihara, M., and Katakuse, I. (2004). Application of a multi-turn time-of-flight mass spectrometer, MULTUM II, to organic compounds ionized by matrix assisted laser desorption/ionaziation. *J. Mass Spectrom.*, 39:86–90.

[Oliveira et al., 2014] Oliveira, R. V., Henion, J., and Wickremsinhe, E. R. (2014). Automated high-capacity on-line extraction and bioanalysis of dried blood spot samples using liquid chromatography/high-resolution accurate mass spectrometry. *Rapid Commun. Mass Spectrom.*, 28:2415–2426.

[Ouyang, 2014] Ouyang, Z. (2014). The future of miniature mass spectrometers and a path forward: A few thoughts from an academic researcher. *Chromatographyonline*, 32(2):104–112.

[Ouyang et al., 2009] Ouyang, Z., Noll, R. J., and Cooks, R. G. (2009). Handheld miniature ion trap mass spectrometers. *Anal. Chem.*, 81:2421–2425.

[Ouyang et al., 2004] Ouyang, Z., Wu, G., Song, Y., Li, H., Plass, W., and Cooks, R. (2004). Rectilinear ion trap: concepts, calculations, and analytical performance of a new mass analyzer. *Anal. Chem.*, 76 (16):4595–605.

[Oxburgh et al., 2007] Oxburgh, R., Pierson-Wickmann, A.-C., Reisberg, L., and Hemming, S. (2007). Climate-correlated variations in seawater ^{187}os/^{188}os over the past 200,000 yr: Evidence from the cariaco basin, venezuela. *Earth and Planetary Science Letters*, 263:246–258.

[Page et al., 2007] Page, J. S., Kelly, R. T., Tang, K., and Smith, R. D. (2007). Ionization and transmission efficiency in an electrospray ionization mass spectrometry interface. *Journal of the American Society for Mass Spectrometry*, 18:1582–1590.

[Page et al., 2009] Page, J. S., Marginean, I., Baker, E. S., Kelly, R. T., Tang, K., and Smith, R. D. (2009). Biases in ion transmission through an electrospray ionization-mass spectrometry capillary inlet. *Journal of the American Society for Mass Spectrometry*, 20:2265–2272.

[Parks et al., 2007] Parks, B. A., Jiang, L., Thomas, P. M., Wenger, C. D., Roth, M. J., Boyne, M. T., Burke, P. V., Kwast, K. E., and Kelleher, N. L. (2007). Top-down proteomics on a chromatographic time scale using linear ion trap Fourier transform hybrid mass spectrometers. *Anal. Chem.*, 79:7984–7991.

[Patel and Ahmed, 2015] Patel, S. and Ahmed, S. (2015). Emerging field of metabolomics: Big promise for cancer biomarker identification and drug discovery. *Journal of Pharmaceutical and Biomedical Analysis*, 107:63–64.

[Patterson et al., 2002] Patterson, G., Guymon, A., Riter, L., Everly, M., Griep-Raming, J., Laughlin, B., Ouyang, Z., and Cooks, R. (2002). Miniature cylindrical ion trap mass spectrometer. *Anal. Chem.*, 74 (24):6145.

[Paul et al., 1958] Paul, W., Reinhard, H. P., and von Zahn, U. (1958). Das elektrische massenfilter als massenspektrometer und isotopentrenner. *Zeitschrift für Physik*, 152:143–182.

[Paul and Steinwedel, 1953] Paul, W. and Steinwedel, H. (1953). Ein neues massenspektrometer ohne magnetfeld. *Z. Naturforschung*, 8a:448–451.

[Petrick, 2010] Petrick, M. (2006-2010). Fast high voltage switch.

[Petrie et al., 2015] Petrie, B., Barden, R., and Kasprzyk-Hordern, B. (2015). A review on emerging contaminants in wastewaters and the environment: Current knowledge, understudied areas and recommendations for future monitoring. *WATER RESEARCH*, 72:3–27.

[Pfeiffer Vacuum GmbH, 2013] Pfeiffer Vacuum GmbH (2013). *The Vacuum Technology Book*, volume 2. Pfeiffer Vacuum GmbH.

[Pikhtelev, 2015] Pikhtelev, A. (2010-2015). Mass analyzer control and daq software.

[Plass et al., 2016] Plass, W., Dickel, T., Ayet, S., Ebert, J., Greiner, F., Hornung, C., Jesch, C., Lang, J., Lippert, W., Maoros, T., Short, D., Geissel, H., Haettner, E., Reiter, M., Rink, A., Scheidenberger, C., and Yavor, M. (2016). High-performance multiple-reflection time-of-flight mass spectrometers for the research with exotic nuclei and for analytical mass spectrometry. *Physica Scripta*, T166:0140069.

[Plass et al., 2013a] Plass, W., Dickel, T., Purushothaman, S., Dendooven, P., Geisse, H., Ebert, J., Haettner, E., Jesch, C., Ranjan, M., Reiter, M., Weick, H., Amjad, F., Ayet, S., Diwisch, M., Estrade, A., Farinon, F., Greiner, F., Kalantar-Nayestanaki, N., Knbel, R., Kurcewicz, J., Lang, J., Moore, I., Mukha, I., Nociforo, C., Petrick, M., Pftzner, M., Pietri, S., Prochazka, A., Rink, A.-K., Rinta-Antila, S., Schfer, D., Scheidenberger, C., Takechi, M., Tanaka, Y., Winfield, J., and Yavor, M. (2013a). The frs ion catcher - a facility for high-precision experiments with stopped projectile and fission fragments. *NIM B*, 317:457–462.

[Plass, 1997] Plass, W. R. (1997). *Aufbau eines Flugzeitmassenspektrometers zur Analyse von flüchtigen organischen Verbindungen bei geringem Partialdruck*. Diploma thesis, Justus-Liebig-University Gießen.

[Plass et al., 2008] Plass, W. R., Dickel, T., Czok, U., Geissel, H., Petrick, M., Reinheimer, K., Scheidenberger, C., and Yavor, M. I. (2008). Isobar separation by time-of-flight mass spectrometry for low-energy radioactive ion beam facilities. *Nucl. Instrum. and Meth. in Phys. Res. B*, 266:4560–4564.

[Plass et al., 2007a] Plass, W. R., Dickel, T., Petrick, M., Boutin, D., Di, Z., Fleckenstein, T., Geissel, H., Jesch, C., Scheidenberger, C., and Whang, Z. (2007a). An RF quadrupole-time-of-flight system for isobar-separation and multiplexed low energy rare-isotope beam experiments. *Eur. Phys. J. Special Topics*, 150:367–368.

[Plass et al., 2007b] Plass, W. R., Dickel, T., Petrick, M., Czok, U., Geissel, H., Jesch, C., and Scheidenberger, C. (2007b). A multiple-reflection time-of-flight isobar separator. In *Proceedings of the 55th ASMS Conference on Mass Spectrometry and Allied Topics*, page TOF am 08:55, Indianapolis, IN.

[Plass et al., 2013b] Plass, W. R., Dickel, T., and Scheidenberger, C. (2013b). Multiple-reflection time-of-flight mass spectrometry. *Int J. Mass Spectrom*, in print.

[Plass et al., 2014] Plass, W. R., Lang, J., Dickel, T., and Scheidenberger (2014). Mobile hochauflösende multireflektor-flugzeitmassenspektrometrie. *AmbiProbe Schlussverwendungsnachweis 2013*.

[Poschenrieder, 1972] Poschenrieder, W. P. (1972). Multiple-focusing time-of-flight mass spectrometers part II. TOFMS with equal energy acceleration. *Int. J. Mass Spectrom. Ion Phys.*, 9:357–373.

[Purushothaman et al., 2013] Purushothaman, S., M.P.Reiter, Haettner, E., Dendooven, P., T.Dickel, Geissel, H., Ebert, J., C.Jesch, W.R.Plass, Ranjan, M., H.Weick, F.Amjad, S.Ayet, Diwisch, M., Estrade, A., F.Farinon, F.Greiner, Kalantar-Nayestanaki, N., R.Knoebel, Kurcewicz, J., Lang, J., Moore, I. D., Mukha, I., Nociforo, C., M.Petrick, M.Pfuetzner, S.Pietri, Prochazka, A., A.-K.Rink, Rinta-Antila, S., Scheidenberger, C., Takechi, M., Tanaka, Y. K., Winfiel, J. S., and Yavor, M. I. (2013). First experimental results of a cryogenic stopping cell with short-lived, heavy uranium fragments produced at 1000 mev/u. *EPL*, 104:42001.

[Rao et al., 2015] Rao, W., Pan, N., and Yang, Z. (2015). High resolution tissue imaging using the single-probe mass spectrometry under ambient conditions. *Journal of the American Society for Mass Spectrometry*, 26:986–993.

[Raznikov et al., 2001] Raznikov, V., Soulimenkov, I. V., Kozlovski, V. I., Pikhtelev, A. R., Raznikova, M. O., Horwath, T., A., K. A., Zhou, Z., Wollnik, H., and Dodonov, A. F. (2001). Ion rotating motion in a gas-filled radio-frequency quadrupole ion guide as a new technique for structural and kinetic investigations of ions. *Rapid Comm. Mass Spectrom.*, 15 (20):1912–1921.

[Reinheimer, 2008] Reinheimer, K. (2008). *Aufbau und Charakterisierung einer Ionenfalle für ein Multireflektions-Flugzeitmassenspektrometer*. Diploma thesis, Justus-Liebig-University Gießen.

[Reiter et al., 2015] Reiter, M., Rink, A.-K., Dickel, T., Haettner, E., Heie, F., Pla, W., Purushothaman, S., Amjad, F., Andrs, S. A. S., Bergmann, J., Blum, D., Dendooven, P., Diwisch, M., Ebert, J., Geissel, H., Greiner, F., Hornung, C., Jesch, C., Kalantar-Nayestanaki, N., Knbel, R., Lang, J., Lippert, W., Miskun, I., Moore, I., Nociforo, C., Petrick, M., Pietri, S., Pftzner, M., Pohjalainen, I., Prochazka, A., Scheidenberger, C., Takechi, M., Tanaka, Y., Weick, H., Winfield, J., and Xu, X. (2015). Rate capability of a cryogenic stopping cell for uranium projectile fragments produced at 1000 mev/u. *Nuclear Instruments and Methods in Physics Research Section B: Beam Interactions with Materials and Atoms*.

[Reuben et al., 1996] Reuben, A. J., Smith, G. B., Moses, P., Vagov, A. V., Woods, M. D., Gordon, D. B., and Munn, R. W. (1996). Ion trajectories in exactly determined quadrupole fields. *International Journal of Mass Spectrometry and Ion Processes*, 154(1-2):43 – 59.

[Reynolds, 1883] Reynolds, O. (1883). An experimental investigation of the circumstances which determine whether the motion of water shall be direct or sinuous, and of the law of resistance in parallel channels. *Philosophical Transactions of the Royal Society*, 174 ().

[Riedo et al., 2013] Riedo, A., Meyer, S., Heredia, B., Neuland, M., Bieler, A., Tulej, M., Leya, I., Iakovlevaa, M., Mezger, K., and Wurz, P. (2013). Highly accurate isotope composition measurements by a miniature laser ablation mass spectrometer designed for in situ investigations on planetary surfaces. *Planetary and Space Science*, 87:1–13.

[Ringle et al., 2013] Ringle, R., Schwarz, S., and Bollen, G. (2013). Penning trap mass spectrometry of rare isotopes produced via projectile fragmentation at the {LEBIT} facility. *International Journal of Mass Spectrometry*, 349-350:87 – 93.

[Robb et al., 2000] Robb, D., Covey, T., and Bruins, A. (2000). Atmospheric pressure photoionization: an ionization method for liquid chromatography-mass spectrometry. *Anal. Chem.*, 72:3653–3659.

[Roboz, 2002] Roboz, J. (2002). *Mass Spectrometry in Cancer Research*. CRC Press LLC.

[Rodgers et al., 2005] Rodgers, R. P., Schaub, T. M., and Marshall, A. G. (2005). Petroleomics: Ms returns to its roots. *Anal. Chem.*, 77:21A–27A.

[Roempp, 2014] Roempp, A. (2014). Sample of porcine brain.

[Roempp et al., 2015] Roempp, A., Both, J.-P., Brunelle, A., Heeren, R. M. A., Laprevote, O., Prideaux, B., Seyer, A., Spengler, B., Stoeckli, M., and Smith, D. F. (2015). Mass spectrometry imaging of biological tissue: an approach for multicenter studies. *Anal Bioanal Chem*, 407:2329–2335.

[Roempp and Karst, 2015] Roempp, A. and Karst, U. (2015). Current trends in mass spectrometry imaging. *Anal Bioanal Chem*, Anal Bioanal Chem:2323–2325.

[Roempp et al., 2013] Roempp, A., Schaefer, K.-C., Guenther, S., Wang, Z., Koestler, M., Leisner, A., Paschke, C., Schramm, T., and Spengler, B. (2013). High-resolution atmospheric pressure infrared laser desorption/ionization mass spectrometry imaging of biological tissue. *Anal Bioanal Chem*, 405:6959–6968.

[Roempp and Spengler, 2013] Roempp, A. and Spengler, B. (2013). Mass spectrometry imaging with high resolution in mass and space. *Histochem Cell Biol*, 139:759–783.

[Roennfeldt and Koenig, 2010] Roennfeldt, J. and Koenig, M. (2010). *Messtechnik im Feuerwehreinsatz*. Kohlhammer.

[Roussis, 2001] Roussis, S. G. (2001). Automated tandem mass spectrometry by orthogonal acceleration TOF data acquistion and simultaneous magnet sacnning for the characterization of petroleum mixtures. *Anal. Chem.*, 73:3611–3623.

[Sarbu et al., 2015] Sarbu, M., Ghiulai, R. M., and Zamfi, A. D. (2015). Recent developments

and applications of electron transfer dissociation mass spectrometry in proteomics. *Mass Spectrometry Reviews*, 34:43–63.

[Satoh et al., 2005] Satoh, T., Tsuno, H., Iwanaga, M., and Kammei, Y. (2005). The design and characteristic features of a new time-of-flight mass spectrometer with a spiral ion trajectory. *J. Am. Soc. Mass Spectrom.*, 16:1969–1975.

[Schaefer et al., 2011a] Schaefer, C., Lang, J., Takats, Z., and Spengler, B. (2011a). Test of continous inlet system applied for mini11.

[Schaefer et al., 2012] Schaefer, K.-C., Balog, J., Szaniszlo, T., Szalay, D., Mezey, G., Denes, J., Bognar, L., Oertel, M., and Takats, Z. (2012). Real timeanalysis of brain tissue bydirect combinationof ultrasonic surgical aspiration and sonic spray mass spectrometry. *Anal. Chem.*, 83:7729–7735.

[Schaefer et al., 2011b] Schaefer, K.-C., Szaniszlo, T., Guenther, S., Balog, J., Denes, J., Keser, M., Dezs, B., Toth, M., Spengler, B., and Takats, Z. (2011b). Insitu, real-time identificationof biological tissues by ultraviolet and infrared laser desorption ionization mass spectrometry. *Anal. Chem.*, 83:1632–1640.

[Schaefer, 2011] Schaefer, T. (2010-2011). Voltage control software for mr-tof-ms.

[Schatz, 2013] Schatz, H. (2013). Nuclear masses in astrophysics. *International Journal of Mass Spectrometry*, 349-350:181–186.

[Scheidenberger, 2005] Scheidenberger, C. (2005). The contribution of percision mass measurements to nuclear physics. *Nuclear Physics A*, 751:209c–225c.

[Scheidenberger et al., 2014] Scheidenberger, C., Plass, W., Dickel, T., and Lang, J. (2014). Nuclear physics for medicine: Mass spectrometry. *Nuclear Physics European Collaboration Committee (NuPECC)*, pages 89–91.

[Schmelzeisen-Redeker et al., 1989] Schmelzeisen-Redeker, G., Buetfering, L., and Roellgen, F. W. (1989). Desolvation of ions and molecules in thermospray mass spectrometry. *Mass Spectrom. Ion Proc.*, 90:139.

[Schmidt et al., 2008] Schmidt, A., Gehlenborg, N., Bodenmiller, B., Mueller, L. N., Campbell, D., Mueller, M., Aebersold, R., and Domon, B. (2008). An integrated, directed mass spectrometric approach for in-depth characterization of complex peptide mixtures. *Mol. Cell. Proteomics*, 7(11):2138–2150.

[Schober et al., 2011] Schober, Y., Schramm, T., Spengler, B., and Roempp, A. (2011). Protein identification by accurate mass matrix-assisted laser desorption/ionization imaging of tryptic peptides. *Rapid Commun. Mass Spectrom.*, 25:2475–2483.

[Schrittmatter et al., 2012] Schrittmatter, N., During, R.-A., and Takats, Z. (2012). Analysis of wastewater samples by direct combination of thin-film microextraction and desorption electrospray ionization mass spectrometry. *Analyst*, 137:4037.

[Schury et al., 2014a] Schury, P., Ito, Y., Wada, M., and Wollnik, H. (2014a). Wide-band mass measurements with a multi-reflection time-of-flight mass spectrograph. *International Journal of Mass Spectrometry*, 359:19–25.

[Schury et al., 2014b] Schury, P., Wada, M., Ito, Y., Arai, F., Naimi, S., Sonoda, T., Wollnik, H., Shchepunov, V., Smorra, C., and Yuan, C. (2014b). A high-resolution multi-reflection time-of-flight mass spectrograph for precision mass measurements at riken/slowri. *Nuclear Instruments and Methods in Physics Research B*, 335:39–53.

[Schwarz et al., 2003] Schwarz, S., Bollen, G., Lawton, D., Neudert, A., Ringle, R., Schury, P., and Sun, T. (2003). A second-generation ion beam buncher and cooler. *Nuclear Instruments and Methods in Physics Research Section B: Beam Interactions with Materials and Atoms*, 204:474 – 477. 14th International Conference on Electromagnetic Isotope Separators and Techniques Related to their Applications.

[Shimma et al., 2012] Shimma, S., Miki, S., and Toyoda, M. (2012). Polychlorinated biphenyls (PCBs) analysis using a miniaturized high-resolution time-of-flight mass spectrometer MULTUM-S II. *J. Environ. Monit.*, 14:1664–1670.

[Shimma et al., 2010] Shimma, S., Nagao, H., Aoki, J., Takahashi, K., Miki, S., and Toyoda, M. (2010). Miniaturized high-resolution time-of-flight mass spectrometer multum-s ii with an infinite flight path. *Anal. Chem.*, 82:8456–8463.

[Shubina et al., 2013] Shubina, D., Cakirli, R. B., Litvinov, Y. A., Blaum, K., Brandau, Bosch, F., Carroll, J. J., Casten, R. F., Cullen, D. M., Cullen, I. J., Deo, A. Y., Detwiler, B., Dimopoulou, C., Farinon, F., Geisse, H., Haettner, E., Heil, M., Kempley, R. S., Kozhuharov, C., Knbel, R., Kurcewicz, J., Kuzminchuk, N., Litvinov, S. A., Liu, Z., Mao, R., Nociforo, C., Nolden, F., Patyk, Z., Plass, W. R., Prochazka, A., Reed, M. W., Sanjari, M. S., Scheidenberger, C., Steck, M., Sthlker, T., Sun, B., Swan, T. P. D., Trees, G., Walker, P. M., Weick, H., Winckler, N., Winkler, M., Woods, P. J., Yamaguchi, T., , and Zhou, C. (2013). Schottky mass measurements of heavy neutron-rich nuclides in the element range $70 \leq z \geq 79$ at the gsi experimental storage ring. *PHYSICAL REVIEW C*, 88.

[Siebring, 2013] Siebring, J. (2013). Operating software for vacuum systems.

[Sinha and Wadsworth, 2005] Sinha, M. P. . and Wadsworth, M. (2005). Miniature focal plane mass spectrometer with 1000-pixel modified-ccd detector array for direct ion measurement. *Rev. Sci. Instrum.*, 76:103.

[Spengler, 2011] Spengler, B. (2011). Geschärfte Sinne für Gesundheit, Umwelt, Klima und Sicherheit. *Spiegel der Forschung. Wissenschaftsmagazin der Justus-Liebig-Universität Gießen*, 27:64–69.

[Stafford et al., 1984] Stafford, G. C., Kelley, P. E., Syka, J. E. P., Reynolds, W. E., and Todd, J. F. J. (1984). Recent improvements in and analytical applications of advanced ion trap technology. *Int.J. Mass Spec.*, 60(1):85–98.

[Standing and Vestal, 2015] Standing, K. and Vestal, M. L. (2015). Time-of-flight mass spectrometry (TOFMS): From niche to mainstream. *J Radioanal Nucl Chem*, 304:1201–1209.

[Stephens, 1946] Stephens, W. E. (1946). A pulsed mass spectrometer with time dispersion. *Phys. Rev.*, 69:691.

[Strathmann and Hoofnagle, 2011] Strathmann, F. G. and Hoofnagle, A. N. (2011). Current and

future applications of mass spectrometry to the clinical laboratory. *Am J Clin Pathol*, 136:609–616.

[Stresau et al., 2006] Stresau, D., Hunter, K., Shields, W., Raffin, P., and Benari, Y. (2006). A new class of robust sub-nanosecond TOF detectors with high dynamic range. In *54th ASMS Conference on mass spectrometry and applied topics*, Seattle, Washington.

[Su et al., 2012] Su, Y., Wang, H., Liu, J., Wei, P., Cooks, R. G., and Ouyang, Z. (2012). Quantitative paper spray mass spectrometry analysis of drugs of abuse. *Analyst*, 138:4443–4447.

[Syms, 2016] Syms, R. R. A. (2016). Advances in microfabricated mass spectrometers. *Journal of the American Society for Mass Spectrometry*, 27:4–21.

[Synal, 2013] Synal, H.-A. (2013). Developments in accelerator mass spectrometry. *International Journal of Mass Spectrometry*, 349-350:192–202.

[Szulejko and Solouki, 2002] Szulejko, J. E. and Solouki, T. (2002). Potential analytical applications of interfacing a GC to an FT-ICR MS: Fingerprinting complex sample matrixes. *Anal. Chem.*, 74:3434–3442.

[T. C. Rohner and Girault, 2004] T. C. Rohner, N. L. and Girault, H. H. (2004). Electrochemical and theoretical aspects of electrospray ionisation. *Phys.Chem.Chem.Phys.*, 6:3056–3068.

[T. Dickel and J. Lang et al., 2016] T. Dickel and J. Lang, M.Yavor, Plass, W., H.Geissel, Lippert, W., and Scheidenberger, C. (2016). Highly mass-selective retrapping in an MR-TOF-MS. *to be published*.

[Takamine et al., 2007] Takamine, A., Wada, M., Ishida, Y., Nakamura, T., Okada, K., Yamazaki, Y., Kanai, Y., Kojima, T. M., Yoshida, A., Kubo, T., Ohtani, S., Noda, K., Katayama, I., Lioubimov, V., Schuessler, H. A., Varentsov, V., and Wollink, H. (2007). Improvement of the slow ri beam transport using carbon-OPIG. *RIKEN Accel. Prog. Rep.*, 40.

[Takats, 2012] Takats, Z. (2010-2012). Atmospheric pressure ion inlet. private communication.

[Takats et al., 2012] Takats, Z., Denes, J., and Kinros, J. (2012). Identifying the margin: a new method to distinguish between cancerous and noncancerous tissue during surgery. *Future Oncol.*, 8 (2):113–116.

[Takats et al., 2004] Takats, Z., Wiseman, J. M., Gologan, B., and Cooks, R. G. (2004). Mass spectrometry sampling under ambient conditions with desorption electrospray ionization. *Science*, 306:471–473.

[Takatz, 2013] Takatz, Z. (2013). Gas chromatography coupled to atmospheric pressure ionization mass spectrometry (gc-api-ms): Review. *in Proceedings of the 61th ASMS Conference on Mass Spectrometry and Allied Topics, Minneapolis, MN*, page p. 16.

[Tang et al., 2007] Tang, X., Bruce, J. E., and Hill, H. H. (2007). Design and performance of an atmospheric pressure ion mobility Fourier transform ion cyclotron resonance mass spectrometer. *Rapid Commun. Mass Spectrom.*, 21:1115–1122.

[Teo et al., 2015] Teo, C. C., Chong, W. P. K., Tan, E., Basri, N. B., Low, Z. J., and Ho, Y. S. (2015). Advances in sample preparation and analytical techniques for lipidomics study of clinical samples. *Trends in Analytical Chemistry*, 66:1–18.

Bibliography

[Thermo Fischer Scientific, 2015] Thermo Fischer Scientific (2015). Ltq esi positive ion calibration solution.

[Thomson, 1913] Thomson, J. J. (1913). Bakerian Lecture: Rays of Positive Electricity. *Proc. R. Soc. Lond. A*, 89(607):1–20.

[Toker et al., 2009] Toker, Y., Altstein, N., Rappaport, O. A. M. L., Heber, O., Schwalm, D., Strasser, D., and Zajfman, D. (2009). The kick-out mass selection technique for ions stored in an electrostatic ion beam trap. *J. Instrum.*, 4:P09001.

[Tolmachev et al., 1997] Tolmachev, A. V., Chernushevich, I. V., Dodonov, A. F., and Standing, K. G. (1997). A collisional focusing ion guide for coupling an atmospheric pressure ion source to a mass spectrometer. *Nucl. Instr. and Meth. in Phys. Res. B*, 124:112–119.

[Tolmachev et al., 2000] Tolmachev, A. V., Udseth, H. R., and Smith, R. D. (2000). Charge capacity limitations of radio frequency ion guides in their use for improved ion accumulation and trapping in mass spectrometry. *Analytical Chemistry*, 72(5):970–978.

[Tominagaa et al., 2015] Tominagaa, M., Michiue, T., Inamori-Kawamoto, O., Hishmat, A. M., Oritani, S., Takama, M., Ishikawa, T., and Maeda, H. (2015). Efficacy of drug screening in forensic autopsy: Retrospective investigation of routine toxicological findings. *Legal Medicine*, 17:172–176.

[Toyoda et al., 2007] Toyoda, M., Giannakopulos, A. E., Colburn, A. W., and Derrick, P. J. (2007). High-energy collision induced dissociation fragmentaion pathways of peptides, probed using tandem time-of-flight mass spectrometer "MULTUM-TOF/TOF". *Rev. Sci. Instrum.*, 78:074101.

[Trimpin, 2016] Trimpin, S. (2016). "magic" ionization mass spectrometry. *Journal of the American Society for Mass Spectrometry*, 27:4–21.

[Turner et al., 2015] Turner, N. W., Bramhmbhatt, H., Szabo-Vezse, M., Poma, A., Coker, R., and Piletsky, S. A. (2015). Analytical methods for determination of mycotoxins: An update (2009-2014). *Analytica Chimica Acta*, 901:12–33.

[Urabe et al., 2014] Urabe, T., Takahashi, K., Kitagawa, M., Sato, T., Kondo, T., Enomoto, S., Kidera, M., and Seto, Y. (2014). Development of portable mass spectrometer with electron cyclotron resonance ion source for detection of chemical warfare agents in air. *Spectrochimica Acta Part A: Molecular and Biomolecular Spectroscopy*, 120:437–444.

[Vekey et al., 2008] Vekey, K., Telekes, A., and Vertes, A. (2008). *Medical Apllications of Mass Specrrometry*. Elsevier.

[Verentchikov et al., 2005] Verentchikov, A. N., Yavor, M. I., Hasin, Y. I., and Gavrik, M. A. (2005). Multireflection planar time-of-flight mass analyzer. I: An analyzer for a parallel tandem spectrometer. *Technical Physics*, 50(1):73–81.

[Wada et al., 2003] Wada, M., Ishida, Y., Nakamura, T., Yamazaki, Y., Kambara, T., Ohyama, H., Kanai, Y., Kojima, T. M., Nakai, Y., Ohshima, N., Yoshida, A., Kubo, T., Matsuo, Y., Fukuyama, Y., Okada, K., Sonoda, T., Ohtani, S., Noda, K., Kawakami, H., and Katayama, I. (2003). Slow RI-beams from projectile fragment separators. *Nucl. Instr. and Meth. in Phys. Res. B*, 204:570–581.

[Walker et al., 2013] Walker, P., Litvinov, Y. A., and Geissel, H. (2013). The {ILIMA} project at {FAIR}. *International Journal of Mass Spectrometry*, 349-350:247 – 254.

[Wang et al., 2015] Wang, C., Wang, M., and Han, X. (2015). Applications of mass spectrometry for cellular lipid analysis. *Mol. BioSyst.*, 11:698–713.

[Waters Corporation, 2014] Waters Corporation (2014). Xevo g2-xs tof instrument specification.

[Webb et al., 2013] Webb, I. K., Gao, Y., Londry, F. A., and McLuckey, S. A. (2013). Trapping mode dipolar dc collisional activation in the rf-only ion guide of a linear ion trap/time-of-flight instrument for gaseous bio-ion declustering. *J. Mass Spectrom.*, 48:1059–1065.

[Weizsäcker, 1935] Weizsäcker, C. F. v. (1935). Zur theorie der kernmassen. *Zeitschrift für Physik A Hadrons and Nuclei*, 96:431–458. 10.1007/BF01337700.

[Werner, 1972] Werner, H. W. (1972). Instrumental aspects of secondary ion mass spectrometry and secondary ion imaging mass spectrometry. *Vacuum*, 22(11):613–617.

[Whitehouse et al., 1985] Whitehouse, C. M., Yamashita, R. N. D. M., and Fenn, J. B. (1985). Electrospray interface for liquid chromatographs and mass spectrometers. *Anal. Chem.*, 57:675–679.

[Wienholtz et al., 2013] Wienholtz, F., Beck, D., Blaum, K., Borgmann, C., Breitenfeldt, M., Cakirli, R. B., George, S., Herfurth, F., Holt, J. D., Kowalska, M., Kreim, S., Lunney, D., Manea, V., Menendez, J., Neidherr, D., Rosenbusch, M., Schweikhard, L., Schwenk, A., Simonis, J., Stanja, J., Wolf, R. N., and Zuber, K. (2013). Masses of exotic calcium isotopes pin down nuclear forces. *Nature*, 498:346–349.

[Wiley et al., 2013a] Wiley, J., Lang, J., Lippert, W., Cooks, G., and Spengler, B. (2013a). Setup of a low-temperature plasma ion source. Research Visit.

[Wiley et al., 2013b] Wiley, J. S., Shelley, J. T., and Cooks, R. G. (2013b). Handheld low-temperature plasma probe for portable point-and-shoot ambient ionization mass spectrometry. *Anal. Chem.*, 85:6545–6552.

[Wiley and McLaren, 1955] Wiley, W. C. and McLaren, I. H. (1955). Time-of-flight mass spectrometer with improved resolution. *Rev. Sic. Instrum.*, 26(12):1150–1157.

[Wilkins et al., 1996] Wilkins, M. R., Pasquali, C., Appel, R. D., Ou, K., Golaz, O., Sanchez, J.-C., Yan, J. X., Gooley, A. A., Hughes, G., Humphery-Smith, I., Williams, K. L., and Hochstrasser, D. F. (1996). From proteins to proteomes: large scale protein identification by two-dimensional electrophoresis and amino acid analysis. *Bio-Technology*, 14:61–65.

[Wilson and GlaxoSmithKline, 2006] Wilson, M. A. and GlaxoSmithKline, R. J. D. (2006). Use of the ltq-orbitrap to investigate high resolution isotope patterns in ms and ms^n spectra of small molecules. *IMSC contribution*.

[Winfield et al., 2013] Winfield, J. S., Geissel, H., Gerl, J., unzenberg, G. M., Nociforo, C., Plass, W. R., Scheidenberger, C., Weick, H., Winkler, M., and Yavor, M. I. . (2013). A versatile high-resolution magnetic spectrometer for energy compression, reaction studies and nuclear spectroscopy. *Nucl. Instrum. Methods A*, 704:76–83.

[Wiza, 1979] Wiza, J. J. (1979). Microchannel plate detectors. *Nucl. Instrum. Meth.*, 162:582.

[Wohlfahrt, 2011] Wohlfahrt, B. (2011). *Simulation of a Beam Preparation System for a mobile Multiple-Reflection Time-of-Flight Mass Spectrometer*. Bachelor thesis, Justus-Liebig-University Gießen.

[Wolf et al., 2013] Wolf, R., Wienholtz, F., Atanasov, D., Beck, D., Blaum, K., Borgmann, C., Herfurth, F., Kowalska, M., Kreim, S., Litvinov, Y. A., Lunney, D., Manea, V., Neidherr, D., Rosenbusch, M., Schweikhard, L., Stanja, J., and Zuber, K. (2013). Isoltrap's multi-reflection time-of-flight mass separator/spectrometer. *International Journal of Mass Spectrometry*, 349-350(0):123–133.

[Wolf et al., 2012] Wolf, R. N., Beck, D., Blaum, K., ohm, C. B., Borgmann, C., Breitenfeldt, M., Herfurth, F., Kowalska, M., Kreim, S., Lunney, D., Naimi, S., Neidherr, D., Rosenbusch, M., Schweikhard, L., Stanja, J., Wienholtz, F., and Zuber, K. (2012). On-line separation of short-lived nuclei by a multi-reflection time-of-flight device. *Nucl. Instrum. Methods A*, 686:82–90.

[Wolf et al., 2011] Wolf, R. N., Errit, M., Marx, G., and Schweikhard, L. (2011). A multi-reflection time-of-flight mass separator for isobaric purification of radioactive ion beams. *Hyperfine Interact.*, 199:115–122.

[Wollnik, 1986] Wollnik, H. (1986). *Optics of charged particles*. Academic Press, Inc., San Diego / New York / Berkeley / Boston / London / Sydney / Tokyo / Toronto.

[Wollnik, 1993] Wollnik, H. (1993). Time-of-flight mass analyzers. *Mass Spec. Rev.*, 2:89–114.

[Wollnik, 2013] Wollnik, H. (2013). History of mass measurements in time-of-flight mass analyzers. *International Journal of Mass Spectrometry*, 349-350:38 – 46.

[Wollnik and Przewloka, 1990] Wollnik, H. and Przewloka, M. (1990). Time-of-flight mass spectrometers with multiply reflected ion trajectories. *Int. J. Mass Spectrom. Ion Processes*, 96:267–274.

[Wong et al., 2013] Wong, M. H., Atreya, S. K., Mahaffy, P. N., Franz, H. B., Malespin, C., Trainer, M. G., Stern, J. C., Conrad, P. G., Manning, H. L. K., Pepin, R. O., Becker, R. H., McKay, C. P., Owen, T. C., Jones, R. N.-G. J. H., Jakosky, B. M., and Steele, A. (2013). Isotopes of nitrogen on mars: Atmospheric measurements by curiosity's mass spectrometer. *GEOPHYSICAL RESEARCH LETTERS*, 40:6033–6037.

[Wozniak et al., 2008] Wozniak, A. S., Bauer, J. E., Sleighter, R. L., Dickhut, R. M., , and Hatcher, P. G. (2008). Technical note: Molecular characterization of aerosol-derived water soluble organic carbon using ultrahigh resolution electrospray ionization fourier transform ion cyclotron resonance mass spectrometry. *Atmos. Chem. Phys.*, 8:5099–5111.

[Wu et al., 2013] Wu, C., , Dill, A. L., Eberlin, L. S., Cooks, R. G., and Ifa, D. R. (2013). Mass spectrometry imaging under ambient conditions. *Mass Spectrometry Reviews*, 32:218.

[Wysocki et al., 2008] Wysocki, V. H., Joyce, K. E., Jones, C. M., and Beardsle, R. L. (2008). Surface-induced dissociation of small molecules, peptides, and non-covalent protein complexes. *J. Am. Soc. Mass Spectrom.*, 19:190–208.

[Yamashita and Fenn, 1984] Yamashita, M. and Fenn, J. B. (1984). Electrospray ion source. another variation on the free-jet theme. *The Journal of Physical Chemistry*, 88 (2):4451–4459.

[Yang and Gilmore, 2015] Yang, J. and Gilmore, I. (2015). Application of secondary ion mass spectrometry to biomaterials, proteins and cells: a concise review. *Materials Science and Technology*, 31(2):131–136.

[Yavor, 1996] Yavor, M. (1996). Progress in ion optics for mass-separator design. *NIM B*, 126:266–273.

[Yavor, 2009] Yavor, M. (2009). *Optics of charged particle analyzers*, volume 157 of *Advances in Imaging and Electron Physics*. Academic Press, Elsevier, San Diego / New York / Berkley / Boston / London / Sydney / Tokyo / Toronto.

[Yavor, 2011] Yavor, M. (2011). Optimization of a compacter MR-TOF analyzer. Internal report, Justus-Liebig-University Gießen.

[Yavor, 2012] Yavor, M. (2012). Note on optic axis alignment in mr-tof. Internal report, Justus-Liebig-University Gießen.

[Yavor, 2014a] Yavor, M. (2014a). Manuscript on retrapping. Internal report, Justus-Liebig-University Gießen.

[Yavor, 2014b] Yavor, M. (2014b). Manuscript on time focus shift. Internal report, Justus-Liebig-University Gießen.

[Yavor, 2014c] Yavor, M. (2014c). Space charge effects in shuttle-type mr tof analyzers with time focus shifts. Internal report, Justus-Liebig-University Gießen.

[Yavor et al., 2014] Yavor, M., Dickel, T., and Lang, J. (2011-2014). Private communication.

[Yavor et al., 2008a] Yavor, M., Verentchikov, A., Hasin, J., Kozlov, B., Gavrik, M., and Trufanov, A. (2008a). Planar multi-reflecting time-of-flight mass analyzer with a jig-saw ion path. *Physics Procedia*, 1:391–400.

[Yavor et al., 2008b] Yavor, M. I., Kirillov, S. N., and Verentchikov, A. N. (2008b). Interface for ion injection into a collision dissociation cell in a time-of-flight tandem with parallel analysis. *Nautchnoe priborostroenie (Scientific Instrumentation)*, 18(2):39–41.

[Yavor et al., 2015] Yavor, M. I., Plass, W. R., Dickel, T., Geissel, H., and Scheidenberger, C. (2015). Ion-optical design of a high-performance multiple-reflection time-of-flight mass spectrometer and isobar separator. *International Journal of Mass Spectrometry*, 381-382:1–9.

[Yost et al., 1979] Yost, R., Enke, C., McGilvery, D., Smith, D., and Morrison, J. (1979). High efficiency collision-induced dissociation in an rf-only quadrupole. *International Journal of Mass Spectrometry and Ion Physics*, 30(2):127–136.

[Young et al., 2011] Young, G. H., Loader, N. J., and McCarroll, D. (2011). A large scale comparative study of stable carbon isotope ratios determined using on-line combustion and low-temperature pyrolysis techniques. *Palaeogeography, Palaeoclimatology, Palaeoecology*, 300:23–28.

[Young-Pil et al., 2015] Young-Pil, K., HyunKyong, S., SeungKoo, S., and TaeGeol, L. (2015). Robing nanoparticles and nanoparticle-conjugated biomolecules using time-of-flight secondary ion mass spectrometry. *Mass Spectrometry Reviews*, 34:237–247.

[YunjuCho et al., 2015] YunjuCho, Ahmed, A., Islam, A., and Kim, S. (2015). Developments in FT-ICR MS instrumentation, ionization techniques, and data interpretation methods for petroleomics. *Mass Spectrometry Reviews*, 134(1-3).

[Zaia, 2004] Zaia, J. (2004). Mass spectrometry of oligosaccharides. *Mass Spectrometry Reviews*, 23:161–227.

[Zajfman et al., 2003] Zajfman, D., Rudich, Y., Sagi, I., Strasser, D., Savin, D., Goldberg, S., Rappaport, M., and Heber, O. (2003). High resolution mass spectrometry using a linear electrostatic ion beam trap. *International Journal of Mass Spectrometry*, 229:55–60.

[Zalewska et al., 2013] Zalewska, A., Pawlowski, W., and Tomaszewski, W. (2013). Limits of detection of explosives as determined with ims and field asymmetric ims vapour detectors. *Forensic Sci Int.*, 226:1–3.

[Zhai et al., 2015] Zhai, Y., Feng, Y., Wei, Y., Wang, Y., and Xu, W. (2015). Development of a miniature mass spectrometer with continuous atmospheric pressure interface. *Analyst*, 140:3406.

[Zhou and Wysock, 2014] Zhou, M. and Wysock, V. H. (2014). Surface induced dissociation: Dissecting noncovalent protein complexes in the gas phase. *Acc. Chem. Res.*, 47:1010–1018.

[Zubarev et al., 1998] Zubarev, R. A., Kelleher, N. L., and McLafferty, F. W. (1998). Electron capture dissociation of multiply charged protein cations. a nonergodic process. *J. Am. Chem. Soc.*, 120(13):3265–3266.

Eidestattliche Versicherung

Ich erkläre: Ich habe die vorgelegte Dissertation selbstständig und ohne unerlaubte fremde Hilfe und nur mit den Hilfen angefertigt, die ich in der Dissertation angegeben habe. Alle Textstellen, die wörtlich oder sinngemäß aus veröffentlichten Schriften entnommen sind, und alle Angaben, die auf mündlichen Auskünften beruhen, sind als solche kenntlich gemacht. Ich stimme einer evtl. Überprüfung meiner Dissertation durch eine Antiplagiat-Software zu. Bei den von mir durchgeführten und in der Dissertation erwähnten Untersuchungen habe ich die Grundsätze guter wissenschaftlicher Praxis, wie sie in der 'Satzung der Justus-Liebig-Universität Gießen zur Sicherung guter wissenschaftlicher Praxis' niedergelegt sind, eingehalten.

Acknowledgments